DESIGN AND SYNTHESIS OF NEW FUSED ARENE-CONTAINING CONJUGATED POLYMERS

A Dissertation
Presented to
The Academic Faculty

by

Chinmay Kulkarni

In Partial Fulfillment
of the Requirements for the Degree
Doctor of Philosophy in the
School of Chemistry and Biochemistry

Georgia Institute of Technology
December 2018

DESIGN AND SYNTHESIS OF NEW FUSED ARENE-CONTAINING CONJUGATED POLYMERS

Approved by:

Dr. David Collard, Advisor
School of Chemistry and Biochemistry
Georgia Institute of Technology

Dr. John Reynolds
School of Chemistry and Biochemistry
Georgia Institute of Technology

Dr. Stefan France
School of Chemistry and Biochemistry
Georgia Institute of Technology

Dr. Mohan Srinivasarao
School of Material Science and Engineering
Georgia Institute of Technology

Dr. Charles Liotta
School of Chemistry and Biochemistry
Georgia Institute of Technology

Date Approved: August 06, 2018

To my mother Medha, father Ravindra and my brother Mayank

ACKNOWLEDGEMENTS

I would like to express my gratitude towards Dr. David M. Collard for his invaluable support, encouragement throughout my graduate life. I want to specially thank him for developing me into an independent researcher, cultivating analytical thinking and communication of scientific ideas. Special thanks to Dr. Charles Liotta, Dr. Stefan France, Dr. John Reynolds and Dr. Mohan Srinivasarao for their participation in my committee and providing me with valuable insights in my research.

I would like to thank my collaborators Dr. Elsa Reichmanis and Mr. Yuan Zhiebo for their invaluable support in material characterization. I would also like to thank Dr. Seth Marder and Dr. Steve Barlow for their help in development of new functional materials. I want to thank Dr. John Reynolds for allowing me to use spin coating facility. I would also like to thank Dr. James Ponder, Dr. Michael Keersmaecker for helping with electrochemical measurements. I would like to extend my gratitude to Dr. Carlos Silva and Dr. Ilaria Bargigia for photoluminescence measurements, Dr. Leslie Gelbaum for NMR support, Dr. David Tavakoli for XRD and Mr. Walter Henderson for ultraviolet photoelectron spectroscopy. I want to express my gratitude to Dr. El Sayed and Dr. Sajan Lal for Raman spectroscopic measurements.

Finally, I want to thank my group members, Dr. Pranav Kalelkar, Bronson Cox, Ashley Johns, Elizabeth Henry, Jessie Berger for their friendship and invaluable support in solving synthetic problems.

TABLE OF CONTENTS

ACKNOWLEDGEMENTS **iv**

LIST OF TABLES **viii**

LIST OF FIGURES **ix**

LIST OF SYMBOLS AND ABBREVIATIONS **xiv**

SUMMARY **xvi**

CHAPTER 1. INTRODUCTION **1**
1.1 BACKGROUND 1
1.2 A PRIMER ON THE ELECTRONIC STRUCTURE OF CONJUGATED POLYMER 3
1.2.1 The Band Gap 3
1.2.2 The Effect of Bond Length Alternation 3
1.3 PHENYLENE AND FUSED ACENE CONTAINING CONJUGATED POLYMERS 7
1.3.1 Poly(phenylene ethynylene)s (PPE)s 7
1.3.2 Poly(phenylene vinylene)s 12
1.4 ACENE-CONTAINING CONJUGATED POLYMERS 15
1.4.1 Pentacene containing small molecules and conjugated polymers 15
1.4.2 Anthracene containing conjugated polymers 18
1.5 THESIS OUTLINE 20
1.6 REFERENCES 25

CHAPTER 2. EFFECT OF FUSED ARENE RPEAT UNITS ON ELECTRONIC STRUCUTRES OF POLY(ARYLENE ETHYNYLE)S **30**
2.1 INTRODUCTION 30
2.2 RESULTS AND DISCUSSION 31
2.2.1 Synthesis 31
2.2.2 ^{1}H NMR Analysis 36
2.2.3 Electrochemical Measurements 37
2.2.4 Absorption spectroscopy 38
2.2.5 Fluorescence spectroscopy 43
2.2.6 Thermal properties 46
2.2.7 Powder XRD of polymers 47
2.2.8 GIWAXS studies of thin films 50
2.2.9 Raman Spectroscopy 53
2.3 CONCLUSIONS 55
2.4 EXPERIMENTAL SECTION 56
2.4.1 Materials 56
2.4.2 Characterization 56
2.4.3 Synthetic procedures 58

2.4.3.1 1,4-Dihexylbenzene, **2** 58
2.3.3.2. 1,4-Dioctyloxybenzene, **5** 58
2.3.3.3. 1,4-Diiodo-2,5-dioctyloxy-benzene, **6** 59
2.3.3.4. 1,4-Dioctyloxy-2,5-bis(trimethylsilylethynyl)benzene, **7** 60
2.3.3.5. 1,4-Dihexyl-2,5-diiodobenzene, **3** 60
2.3.3.6. 1,4-Dihexyl-2,5-Bis(trimethylsilylethynyl) benzene 61
2.3.3.7. 3,4-Dibromothiophene-1,1-dioxide, **9** 62
2.3.3.8. 6,7-Dibromo-1,4-naphthaquinone, **10** 62
2.3.3.9. 6,7-Dibromo-1,4-bis(trimethylsilylethynyl)naphthalene,**12** 63
2.3.3.10. 6,7-Dihexyl-1,4-bis(trimethylsilylethynyl)naphthalene,**13** 66
2.3.3.11. 2,6-Dibromoanthraquinone, **14** 69
2.3.3.12. 2,6-Dibromo-9,10-bis(trimethylsilylethynyl)anthracene, **17** 70
2.3.3.13. 2,6-Dihexyl-9,10-bis(trimethylsilylethynyl)anthracene, **18a** 73
2.3.3.14. 2,6-Di(2-ethylhexyl)-9,10-bis(trimethylsilylethynyl)anthracene, **18b** 76
2.3.3.15. 2,6-Dibromo-9,10-dihydroanthracene,**19** 79
2.3.3.16. 2,6-Dibromoanthracene,**20** 79
2.3.3.17. 2,6-Di(2-ethylhexyl)anthracene, **21** 80
2.3.3.18. 9,10-dibromo-2,6-di-(2-ethylhexyl)anthracene,**22** 83
2.3.3.19. Poly (2,5-dihexyl-1,4-phenylenediyl ethynylene-alt-2,5-dioctyloxy phenylenediyl ethynylene), **PPPE** 86
2.3.3.20. Poly(6,7-dihexyl-1,4-naphthalene-alt-2,5-dioctyloxy-1,4-phenylene ethynylene), **PNPE** 89
2.3.3.21. Poly(2,6-dihexyl-9,10-anthracene ethynylene-alt-2,5-dioctyloxy-1,4-phenylene ethynylene), **PAPE** 91
2.3.3.22. Poly (2,6-di(2-ethylhexyl-9,10-anthralene ethynylene), **PAE** 94
2.5 REFERENCES 97

CHAPTER 3. THE ELECTRONIC STRUCUTRE OF ALTERNATING DONOR-ACCEPTOR COPOYLMERS OF NDI WITH PHENYLENE, NAPHTHALENE AND ANTHRACENE UNITS 99
3.1 INTRODUCTION 99
3.2 RESULTS AND DISCUSSION 106
3.2.1 Synthesis 106
3.2.2 Infrared spectroscopy 107
3.2.3 Ultraviolet-visible absorption spectroscopy 109
3.2.4 Fluorescence spectroscopy 113
3.2.5 Solvatochromism 114
3.2.6 Thermal properties 118
3.2.7 Electrochemical measurements 120
3.2.8 X-ray diffraction studies 122
3.3 CONCLUSION 124
3.4 EXPERIMENTAL 125
3.4.1 General methods 125
3.4.2 Synthesis 126
3.4.2.1 Poly(*N*,*N*'-di(2-decyltetradecyl)-2,6-naphthalene-1,4,5,8-bis(dicarboximide) ethynylene-*alt*-2,6-diethylhexyl-9,10-anthraceneethynylene),**NDIA.** 126
3.4.2.2 Poly(*N*,*N*'-bis(2-decyltetradecyl)-2,6-naphthalene-1,4,5,8-bis(dicarboximide) ethynylene-*alt*-6,7-dihexyl-1,4-naphthalene ethynylene), **NDIN.** 127
3.5 REFERENCES 129

CHAPTER 4. SYNTHETIC APPROACHES TO THE DEVELOPMENT OF ANTHRACENE MONOMERS FOR THE PREPARATION OF POLY(ARYLENE VINYLENE)S 132
4.1 INTRODUCTION 132
4.2 RESULTS AND DISCUSSION 135
4.2.1 Synthesis of 2,3,6,7-tetraoctyloxy-9,10-dicarbaldehyde, 9, by oxidation of 9,10-dimethyl anthracene intermediate 135
4.2.2 Synthesis of 2,3,6,7-tetramethoxy-9,10-dicarbaldehyde anthracene 137
4.3 Attempt to polymerize 2,3,6,7-tetraoctyloxy-9,10-bisbromomethyl anthracene 138
4.4 CONCLUSION 139
4.5 EXPERIMENTAL SECTION 140
4.5.1 2,3,6,7-Tetramethoxy-9,10- dimethylanthracene, **2** 140
4.5.2 2,3,6,7-Tetramethoxyanthracene-9,10-dione, **3** 141
4.5.3 4.4.3. 2,3,6,7-tetrahydroxy anthracene-9,10-dione, **4** 142
4.5.4 Synthesis of 2,3,6,7-tetraoctyloxyanthracene-9,10-dione, **5** 143
4.5.5 Synthesis of 2,3,6,7-tetraoctyloxyanthrone, **6** 145
4.5.6 Synthesis of 2,3,6,7- tetraoctyloxyanthracene, **7** 146
4.5.7 2,3,6,7-Tetraoctyloxy-9,10-dibromoanthracene, **8** 147
4.5.8 2,3,6,7-Tetrahydroxy-9,10-dimethylanthracene, **10** 148
4.5.9 2,3,6,7-Tetraoctyloxy-9,10-dimethylanthracene, **11** 149
4.5.10 2,3,6,7- Tetramethoxy-9,10-bis(bromomethyl) anthracene, **12** 150
4.5.11 2,3,6,7- Tetraoctyloxy-9,10-bisbromomethyl anthracene, **14** 151
4.6 REFERENCES 152

CHAPTER 5. CONCLUSION AND FUTURE PERSPECTIVE 153
5.1 CONCLUSIONS 153
5.2 FUTURE PERSPECTIVES 154
5.3 REFERENCES 155

APPENDIX. CRYSTAL STRUCUTRE DATA OF 2,6-(DI-2-ETHYLHEXYL-9,10-DITRIMETHYLSILYL) ANTHRACENE 156

LIST OF TABLES

Table 2.1	Electrochemical and photophysical properties of polymers.	32
Table 3.1	Electrochemical and photophysical properties of polymers.	122

LIST OF FIGURES

Figure 1.1. Examples of conjugated polymers. 2

Figure 1.2. Representative two-well energy diagrams of the electronic ground states of conjugated polymers: A, a segment of trans-polyacetylene; and B, poly(1,4-phenylene ethynylene). 4

Figure 1.3. A schematic plot of the variation of band gap with the extent of bond length alternation.[18] 5

Figure 1.4. Examples of the effect of ring fusion on the electronic structure of conjugated polymers containing fused arenes. 7

Figure 1.5. Sonogashira coupling: A, Overall reaction; and B, Pd-catalytic cycle.[29] 9

Figure 1.6. Solid state packing of PPEs: A, interdigitated side chains; and B, non-interdigitated side chains.[34] (Reprinted (adapted) with permission from (Bunz, U. H., Poly (aryleneethynylene) s: syntheses, properties, structures, and applications. *Chemical Reviews,* **2000,** *100* (4), 1605-1644). Copyright (2000) American Chemical Society. 10

Figure 1.7. The demonstration of PPE as molecular sensor.[34] (Reprinted (adapted) with permission from (Bunz, U. H., Poly (aryleneethynylene) s: syntheses, properties, structures, and applications. *Chemical Reviews,* **2000,** *100* (4), 1605-1644). Copyright (2000) American Chemical Society. 11

Figure 1.8. The synthesis scheme for PPVs.[11, 43] 14

Figure 1.9. Examples of PPV derivatives used in OPVs and OLEDs. 15

Figure 1.10. The crystal structure arrangement of pentacenes: A, herringbone arrangement of pentacene crystals; and B, stacked arrangement of TIPS-pentacene.[43-44] Figure 1.10 A. Reproduced from ref. 44 with permission from The Royal Society of Chemistry. Figure 1.10 B (Reprinted (adapted) with permission from (Anthony, J. E.;et.al.., Functionalized pentacene: improved electronic properties from control of solid-state order. *Journal of the American Chemical Society* **2001,** *123* (38), 9482-9483). Copyright (2001) American Chemical Society. 16

Figure 1.11. Pentacene containing polymers: A, pentacene-bithiophene copolymers; B, pentacene-cyclppentadithiophene; C, pentacene-diethynl benzene copolymers.[46] 17

Figure 1.12. Examples of anthracene-containing polymers.[47-51] 20
Figure 2.1. Poly(arylene ethynylene-*alt*-1,4-phenylene ethynylene)s with 1,4-phenylendiyl, 1,4- naphthalenediyl and 9,10-anthracenediyl units. (**PPPE**, **PNPE** and **PAPE** respectively), and poly(9,10-anthracene ethynylene) homopolymer (**PAE**). 31
Figure 2.2. Synthesis of phenylene monomers: A,1,4-dihexyl-2,5-diiodobenzene (**3**); and B, 1,4-dioctyloxy-2,5-bis(trimethylsilylethynyl)benzene (**7**). 32
Figure 2.3. Synthesis of 6,7-dihexyl-1,4-bis(trimethylsilylethynyl)naphthalene, **13**. 33
Figure 2.4. Synthesis of 2,6-dialkyl-9,10-bis(trimethylsilylethynyl)anthracene **18** and 2,6-di(2-ethylhexyl)-9,10-dibromoanthracene, **22**. 34
Figure 2.5. Synthesis of polymers by Sonogashira coupling: A, Alternating copolymers **PPPE**, **PNPE** and **PAPE**; and B, homopolymer, **PAE**. 36
Figure 2.6. Differential pulse voltammetry: A, **PPPE**; B, **PNPE**; C, **PAPE**; D, **PAE**. Step-size, 2mV; step time, 0.1 s. The measurements were performed using a Ag/Ag^+ reference electrode with a Pt counter electrode with 0.5 M (tetra-*n*-butylammonium hexafluorophosphate in propylene carbonate). 38
Figure 2.7. Normalized absorption (black) and fluorescence spectra (grey) of polymers in *o*-DCB: A, **PPPE** (λ_{ex} = 426 nm); B, **PNPE** (λ_{ex} = 472 nm); C, **PAPE** (λ_{ex} = 566 nm); and D, **PAE** (λ_{ex} = 623 nm). 40
Figure 2.8. Normalized solid state absorption (black) and fluorescence (grey) spectra of polymers: A, **PPPE** (λ_{ex} = 450 nm); B, **PNPE** (λ_{ex} = 495 nm); C, **PAPE** (λ_{ex} = 575 nm); and D, PAE (λ_{ex} = 620 nm). 42
Figure 2.9. Fluorescence life time decay of polymers in *o*-DCB: A, **PPPE** (λ_{ex} = 426 nm); B, **PNPE** (λ_{ex} = 472 nm); C, **PAPE** (λ_{ex} = 566 nm); and D, **PAE** (λ_{ex} = 623 nm). 44
Figure 2.10. Normalized emission spectrum: A; **PPPE** as a function of concentration in o-DCB(λ_{ex} = 428 nm); B, **PNPE** (λ_{ex} = 472 nm). 45
Figure 2.11. Differential Scanning Calorimetry of A. **PPPE**; B, **PNPE**; C, **PAPE**; and D, **PAE** (heating/cooling rate, 10 °C/min). 46
Figure 2.12. Thermogravimetric analysis of: A. PPPE; B, PNPE; C, PAPE; and D, PAE (heating rate, 10 °C/min). 47
Figure 2.13. Powder XRD spectrum of three polymers. A, PPPE; B, PNPE; C, PAPE and D, PAE. 49

Figure 2.14. Single crystal structure 2,6-di(2-ethylhexyl)-9,10-(bis(trimethylsilylethynyl)anthracene. 49
Figure 2.15. GIWAXS images of PPPE: A, pristine spin coated film; B, annealed spin coated film; C, pristine blade coated film (oriented perpendicular to blade coated direction); and D, pristine blade coated film (oriented parallel to blade coated direction) 51
Figure 2.16. GIWAXS of **PNPE**: A, pristine spin coated film; B, annealed spin coated film; C, pristine blade coated film (oriented parallel to blade coating direction); D, annealed blade coated film (oriented parallel to blade coating direction); E, pristine blade coated film (oriented perpendicular to blade coating direction) ; F,annealed blade coated film (oriented perpendicular to blade coating direction) 52
Figure 2.17. GIWAXS of **PAPE**: A, pristine spin coated film; B, annealed spin coated film 53
Figure 2.18. Raman spectroscopy: A, **PPPE**; B, **PNPE**; C, **PAPE**; and D, **PAE**. 54
Figure 2.19 Aromatic and quinoid forms of **PAPE**. 55
Figure 3.1. Donor-acceptor polymers of propylene dioxythiophene (ProDOT) and 2,1,3-benzothiadiazole.[4] 101
Figure 3.2. Alternating donor-acceptor polymers of cyclopentadithiophene and benzochalcogenodiazole units. 102
Figure 3.3. Thieno[3,4-b]thiophene (TT) and thiophene copolymers. 103
Figure 3.4. A, Fusion of benzene rings onto the phenylene ring in the conjugated backbone stabilizes the quinoidal form through retention of aromaticity in the fused rings. B, Quinoidal forms of the 2,6-naphthalenediyl [Ref.[14]], 2,6-anthracnediyl [ref.[16],[15]] and 2,6-pentacenediyl units [ref [19],[18]] are not stabilized in the same way. 104
Figure 3.5. NDI-acene donor-acceptor copolymers containing 1,4-phenylene, 1,4-naphthalene and 9,10-anthracene units (**NDIP**, **NDIN** and **NDIA**, respectively). R = 2-ethylhexyl. 105
Figure 3.6. The polymerization schemes for **NDIN** and **NDIA**. 107
Figure 3.7. IR spectra of thin films of polymers (transmission intensity). A, **NDIP**; B, **NDIN**; and C, **NDIA**. 108

Figure 3.8. UV-visible absorption spectra of three polymers in chlorobenzene: **NDIP**, **NDIN** and **NDIA**. 110
Figure 3.9. HOMO computed by semiempirical method of: A, 1,4-dipropyne-3,6-dimethyl phenylene; B, 1,4- dipropyne-6,7-dimethyl naphthalene; C, 2,6-dimethyl-9,10-dipropyne anthracene. 112
Figure 3.10. Normalized thin film spectra of three polymers: **NDIP, NDIN** and **NDIA** 112
Figure 3.11. Non-normalized fluorescence spectrum of three polymers: **NDIP**, **NDIN** **NDIA**. 113
Figure 3.12. Normalized absorption spectrum of **NDIP** in different solvents at concentration of 33 μg/mL. 115
Figure 3.13. Normalized absorption spectrum of **NDIA** in different solvents at concentration of 33 μg/mL. 115
Figure 3.14. Normalized fluorescence spectrum of **NDIP** at concentration 0.8 μg/mL (λ_{ex} 585 nm). 116
Figure 3.15. Absorption spectrum of **NDIP** in cyclohexane at two concentrations. 116
Figure 3.16. Normalized fluorescence spectrum of **NDIP** in cyclohexane at two concentrations (λ_{ex} 585 nm). 117
Figure 3.17. Normalized absorption (A) and fluorescence spectra (B) of **NDIN** in different solvents at concentration 33 μg/mL (λ_{ex} 372 nm) 117
Figure 3.18. TGA: A, **NDIN**; and B, **NDIA**. Heating rate 10°C/min from 25 to 480°C. 118
Figure 3.19. DSC curves for A, **NDIN**; and B, **NDIA.** Heating rate 10°C/min from -10 to 300°C for **NDIN** and -10 to 275°C for **NDIA** 119
Figure 3.20. DSC curve of **NDIN** after annealing for 6 h at 150 °C. 119
Figure 3.21. Differential pulse voltammetry analysis: A, **NDIP**; B, **NDIN**; C, **NDIA**. Stepsize: 2mV; step time 0.1 s. The measurements were performed using a Ag/Ag^+ reference electrode with a Pt counter electrode in 0.5 M (tetra-*n*-butylammonium hexafluorophosphate) in propylene carbonate. 121
Figure 3.22. Powder XRD of polymers; A, **NDIP**; B, **NDIN**; and C, **NDIA.** 123

Figure 4.1. A, Poly(9,10-anthracene-co-phenylene vinylene)s ; B,Poly(9,10-anthracene vinylene); and C, Poly(9,10-butadienylene vinylene) via Heck coupling. 133
Figure 4.2. Preparation of oligo(9,10-anthracene vinylene)s. 134
Figure 4.3. A, 2,3,6,7-Tetramethoxy-9,10-carbaldehyde anthracene; B, 2,3,6,7-tetramethoxy-9,10-bisbromomethyl anthracene; and C, 2,3,6,7-tetraoctyloxy-9,10-dibromo anthracene. 134
Figure 4.4. Synthesis of 9,10-dicarbaldehyde 136
Figure 4.5. Synthesis of 9,10-dicarbaldehyde **13**. 138
Figure 4.6. Synthesis scheme of Gilch reaction: A, polymerization raction of 14; B, mechanism of Gilch polymerization.[1] 139
Figure A.1. Images of the crystal on diffractometer 160

LIST OF SYMBOLS AND ABBREVIATIONS

BLA	Bond Length Alternation
dd	Doublet of doublet
d	doublet
FT-IR	Fourier transform Infra red spectroscopy
GIWAXS	Grazing- Incidence Wide angle Scattering
GPC	Gel Permeation Chromatography
J	Coupling constant of NMR peaks
M_n	Number average molecular weight
M_w	Weight Average molecular weight
NMR	Nuclear Magnetic Resonance
NDIA	poly(N,N'-bis(2-decyltetradecyl)-2,6-dibromonaphthalene-1,4,5,8-bis(dicarboximide) ethynylene-alt-2,6-diethylhexyl-9,10-anthracene ethynylene
NDIN	poly(N,N'-bis(2-decyltetradecyl)-2,6-dibromonaphthalene-1,4,5,8-bis(dicarboximide)ethynylene-alt-6,7-dihexyl-1,4-naphthalene ethynylene)
NDIP	poly(N,N'-bis(2-decyltetradecyl)-2,6-dibromonaphthalene-1,4,5,8-bis(dicarboximide)ethynylene-alt-2,5-di(2-ethylhexyl)-1,4-phenylene ethynylene)
o-DCB	o-dichloro benzene

PAE	poly(2,6-dihexyl-9,10-anthracene ethynylene)
PAPE	poly(2,6-dihexyl-9,10-anthracene ethynylene-*alt*-1,4- phenylene ethynylene)
PDI	Poly Dispersity Index
PNPE	Poly(6,7-dihexyl-1,4-naphthalene-*alt*-2,5-dioctyloxy-1,4-phenylene ethynylene), PNPE
PPPE	Poly (2,5-dihexyl-1,4-phenylenediyl ethynylene-*alt*-2,5-dioctyloxy phenylenediyl ethynylene), PPPE
XRD	X-ray diffraction
t	triplet
δ	NMR shifts
β	β-hydrogens in the alkyl groups attached to phenyl ring

SUMMARY

Conjugated polymer have attracted attention in the past two decades because of a range of advantages over inorganic – semiconductors. They can be solution processed, they offer flexibility, and their electronic structure can be tuned through molecular design. These characteristics make them applicable in solar cells, light-emitting diodes and transistors.

There are few examples of conjugated polymers that contain simple acenes (e.g., naphthalene, anthracene, pentacene). One of the key challenges to the incorporation of acene units is the need to retain solubility of the polymers. This requires the multistep synthesis of acene monomers bearing flexible alkyl or alkoxy groups.

Conjugated polymers containing aromatic units have two non-degenerate ground states that are referred to as the aromatic and quinoidal forms. The quinoidal form is higher in energy and can be stabilized by fusion of a benzene ring onto the aromatic unit of the conjugated backbone. The stabilization of the quinoidal form impacts the band gap of conjugated polymers, as demonstrated by the low band gap of polyisothianaphthalene, which is ~1 eV lower than that of polythiophene.

In chapter two, the effect of the incorporation of acenes into poly(arylene ethynylene)s is explored through the preparation and characterization of a series of copolymers shown in Figure 1 (X = 1,4-phenylene). It was found that the incorporation of a 9,10-anthracene unit significantly lowers the bandgap compared to analogs containing 1,4-phenylene and 1,4-naphthalene units. This can be understood in terms of the stabilization of the quinoidal form of the anthracene-containing polymers compared to the phenylene and naphthalene-containing analogs. The stabilization of quinoid form

Figure 1. Phenylene, naphthalene and anthracene containing poly(arylene ethynylenes): Alternating copolymers with 1,4-phenylene and naphthalenediimide units

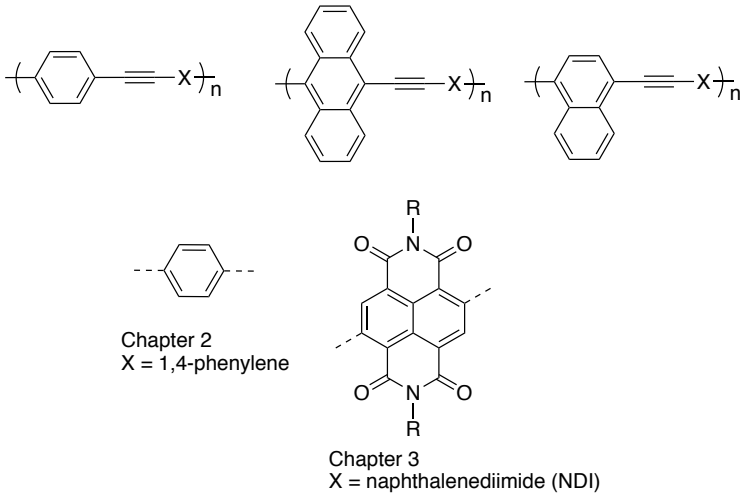

arises from the fusion of benzene rings onto the phenylene ring in the conjugated backbone.

In chapter three, the impact of in the incorporation of naphthalene and anthracene units on the electronic structure of alternating donor-acceptor polymers with *N,N*-disubstituted naphthalenediimide (NDI) units is explored (Figure 1, X = NDI). In this series of polymers it was observed that the anthracene-containing polymer displayed a significantly red-shifted charge transfer type transition compared to phenylene and naphthalene containing polymers. This may be understood to arise from the stabilization of quinoidal form of the anthracene-containing conjugated polymer.

In chapter four, approaches to the synthesis of tetraalkoxy-substituted anthracene monomers for synthesis of anthracene-containing (arylene vinylene) polymers are discussed.

CHAPTER 1. INTRODUCTION

1.1 BACKGROUND

The field of organic electronics has advanced over the last two decades in terms of new materials, new device architectures and optimization of device performance.[1] The idea that organic materials can conduct electricity took birth around 1930, however around that time it was graphite and carbon blacks that showed significant electrical conductivity. The achievement of electrical conductivity in *trans*-polyacetylene, Figure 1.1., on chemical doping by Heeger, MacDiarmid and Shirakawa really gave a boost to this field.[2] The characterization of the electronic structure of *trans*-polyacetylene led to a fundamental understanding of π electron delocalization in conjugated polymers and how it impacts the bandgap and charge transport in organic semiconductors.[3] Since then, numerous conjugated polymers have been prepared that contain aromatic units such as phenylene, heteroarenes (e.g., thiophene[4], pyrole,[5] furan[6]), acenes (e.g., anthracene,[7] pentacene[8]) and fused heteoaromatic systems (e.g., isothianaphthalene,[9] anthradithiophene, [10] benzothiadiazole,[9] fluorene,[9] thienopyranozine[9]).

The phenylene-containing polymers that were prepared were poly(phenylene vinylene)s (PPV)s shown in Figure 1.1., were mainly used in organic light-emitting diodes (OLED)s because of their fluorescent nature.[11] In conjugated polymers containing heteroarenes, poly(3-alkylthiophene)s (P3AT)s shown in Figure 1.1., have been widely studied as components of field effect transistors (FET)s.[12-13] Polymers such as PPVs and P3ATs have been used to acquire understanding of basic structure-property relationships

to gain better insights into the molecular level process that are important to the operation of these devices.

Organic semiconductors have advantages over their inorganic Si-based counterparts. In particular, they have the advantage of being solution processible and flexible, which makes them attractive materials for use in flexible displays, solar cells and transistors. However, limitations to their use include low charge mobility leading to low device efficiencies in case of solar cells. Average efficiency of solar cells based on conjugated polymers has been around 7%.[14] There are few conjugated polymers recently developed, such as poly(benzodithiophene-co-thieno[3,4-b]thiophene) (PBDTTT) materials, which have provided efficiency of conjugated polymer-based organic solar cells as high as ~10%.[15] Thus, the design of new molecular architectures to obtain desired electronic properties, morphology and optimization of device performance remains at the frontiers of research in organic electronics.

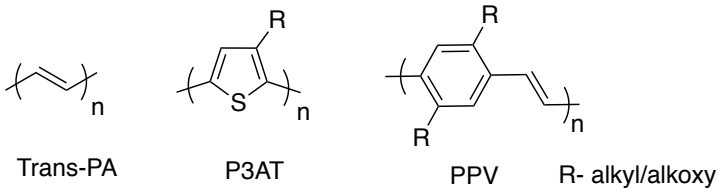

Figure 1.1. Examples of conjugated polymers.

1.2 A PRIMER ON THE ELECTRONIC STRUCTURE OF CONJUGATED POLYMER

1.2.1 The Band Gap

Conjugated polymers have delocalized π electrons along the polymer backbone which determine the electronic structure of the polymer. Controlling the extent of π electron delocalization is a key in optimizing the electronic properties of polymer. The bandgap (E_g) of a conjugated polymer is the energy difference between the top of the valence band edge and the bottom of the conduction band. The bandgap of a polymer is controlled by several factors, such as the conjugation length, presence of substituents on the aromatic rings in the polymer, degree of bond length alternation, and intermolecular interactions in the solid state. The polymers are typically characterized by photoelectron spectroscopy, electrochemistry, ultraviolet-visible spectroscopy, emission spectroscopy and X-ray diffraction to determine the ionization potential, HOMO-LUMO energy levels, and packing of molecules in solid state. These features give insights into the performance of the materials in devices such as FETs and OPVs.

1.2.2 The Effect of Bond Length Alternation

The potential energy of a one-dimensional chain of *trans*-polyacetylene as a function of the bond length alternation (BLA), which is the average difference between the lengths of adjacent bonds, as shown in Figure 2.2. This curve shows two degenerate ground states that arise as a consequence of Peierls distortion.[16-17] A BLA value of zero, at which the adjacent bond lengths are equal, corresponds to a maximum energy on the curve. As a result, alternation of single and multiple bond character is retained along the

chain.[16] In other conjugated polymers there are two non-degenerate minimum-energy geometries, as shown in Figure 1B for a poly(1,4-phenylene ethynylene) chain. These two minima correspond to the cases in which the rings in the backbone are either aromatic or quinoidal. The actual geometry of a conjugated polymer is usually a combination of these two extreme cases. Polymers such as polyparaphenylene, poly(phenylene vinylene), polypyridine and polythiophene (PT) possess a significant amount of aromatic character in their ground state. While other conjugated polymers, such as polyisothianaphthalene (PITN), polyisonaphthothiophene (PINT), display a significant amount of quinoidal character.[18-19]

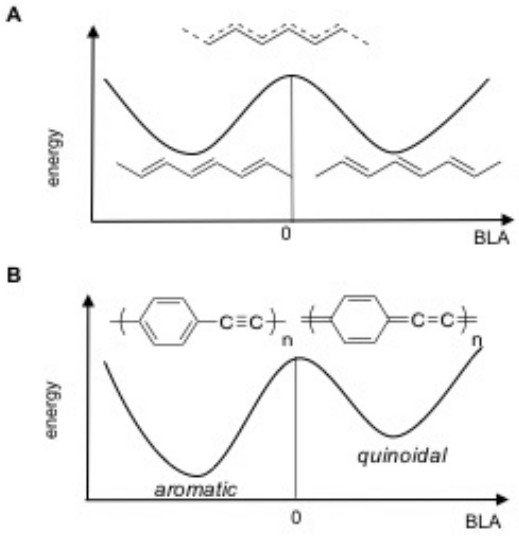

Figure 1.2. Representative two-well energy diagrams of the electronic ground states of conjugated polymers: A, a segment of trans-polyacetylene; and B, poly(1,4-phenylene ethynylene).

The band gap of a conjugated polymer can be related to the bond length alternation (BLA), as shown in Figure 1.3. This plot is divided into two regions - the aromatic side and the quinoidal side. It is evident from this curve that the band gap reaches a minimum when the bond length alternation (BLA) in the polymer is close to zero, and it increases

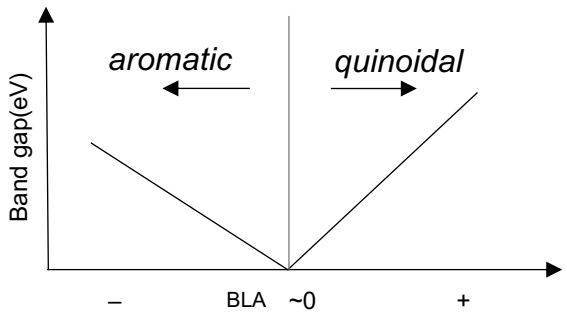

Figure 1.3. A schematic plot of the variation of band gap with the extent of bond length alternation.[18]

as the polymer takes on a predominantly aromatic or quinoindal geometry.[16] For example, the band gap of polyisothianaphthalene (**PITN**, $E_g \sim 1.0$ eV), in which a benzene ring is fused on each thiophene ring in the polymer backbone, is lower than that of polythiophene (**PT**, $E_g \sim 2.0$ eV), as shown Figure 3A.[20] This results from a stabilization of quiniodal character in the ground state of polyisothianaphthalene as a result of the aromaticity that is retained in the fused benzene rings.[18] However, fusion of a second benzene ring to give poly(naphtho[2,3-*c*]thiophene), **PNT**, leads to a higher bandgap (1.5 eV) (Figure 1.4A) by virtue of the transition to a more quinoidal type

structure.[21-22] This behavior is in contrast to the trend observed for **PT**, poly(isothianaphthalene-*alt*-bithiophene) (**P(ITN-T$_2$)**), and poly(naphtho[2,3-*c*]thiophene-*alt*-bithiophene) (**P(NT-T$_2$)**), as shown in Figure 1.4B. In this case, there is a monotonic decrease in the bandgap from ~2.1 eV to ~0.6 eV as the aromatic character of the polymer chain decreases without passing over into the quinoidal regime.[23]

A study of oligo(1,4-phenylene vinylene)s and oligo(9,10-anthracene vinylene)s by Müllen et al. showed that the anthracene analogs have a low HOMO-LUMO transition energy, as illustrated in Figure 1.4C.[24] The presence of two fused benzene rings in the structure of the 9,10-anthracenediyl units provide additional stability to the quinoidal form of the conjugated backbone, which isin accord with Clar's theory whereby a polycyclic aromatic hydrocarbon is stabilized by the presence of additional benzenoid sextets.[25-27]

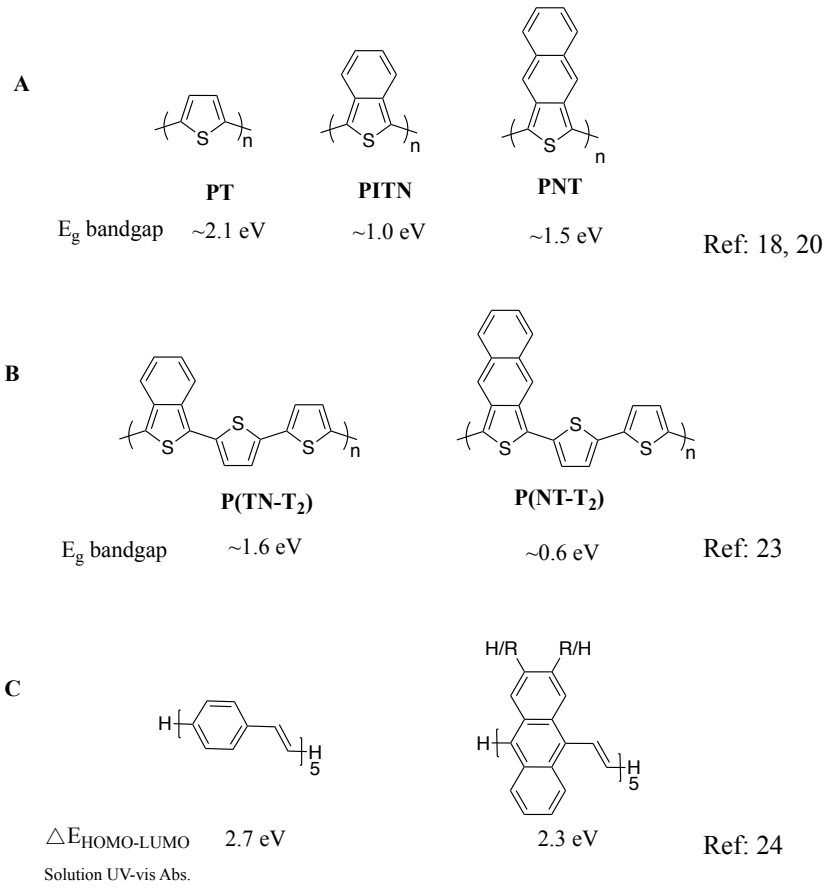

Figure 1.4. Examples of the effect of ring fusion on the electronic structure of conjugated polymers containing fused arenes.

1.3 PHENYLENE AND FUSED ACENE CONTAINING CONJUGATED POLYMERS

1.3.1 Poly(phenylene ethynylene)s (PPE)s

Poly(1,4-phenylene ethynylene) (PPE) have a linear structure containing ethynyl linkages between 1,4-phenylenediyl units. These materials have been applied in different areas such as explosive detection[28] and in polarizers for LC displays. [29] The polymers are typically synthesized using Pd-catalyzed Sonogashira coupling and tungsten-based

acyclic diyne metathesis.[29-30] The Pd-catalyzed Sonogashira couling is more commonly used and is feasible not only on phenylene monomers but also for non-phenylene monomers such as thiophene. The Pd-catalyzed coupling is between two dihalosubstituted arene and a diacetylene monomer (or coupling of a single monomer that contains both functionalities). The pathway for the reaction and for the catalytic cycle are shown in Figures 1.5A and B, respectively. The catalysts may be added with palladium present in its oxidized form (Pd^{+2}) or in neutral form (Pd^{0}). The oxidized form itself is inactive - it transmettalates with the cuprated form of the alkyne and reductive elimination then creates Pd^{0}. The oxidative addition of haloarene is the first step of the catalytic cycle. The nature of substituents on the haloarene influence the rate of oxidative addition: Electron-withdrawing groups increase the rate of oxidative addition to the electron-rich Pd^{0} species. This is followed by transmetallation with the cuprated alkyne, and reductive elimination to give the coupled product. The molecular weights obtained from this process are moderate. with a degree of polymerization in the range of between ten and twenty as determined by end group analysis by NMR.

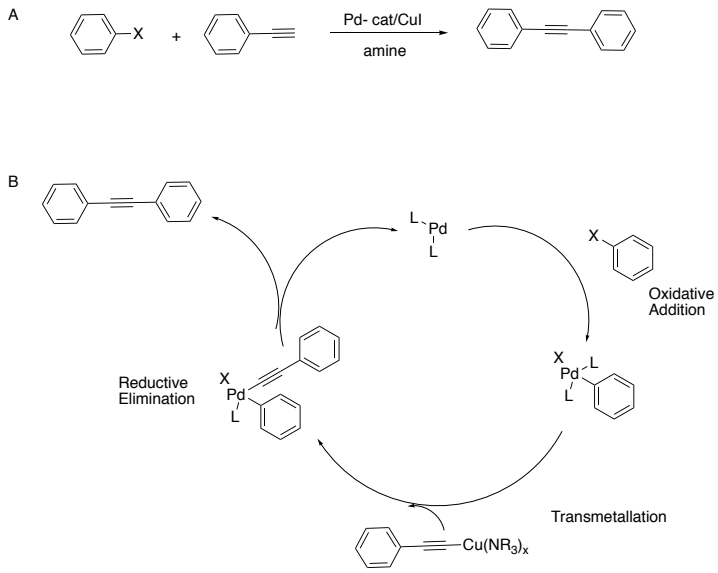

Figure 1.5. Sonogashira coupling: A, Overall reaction; and B, Pd-catalytic cycle.[29]

Dialkyl-substituted PPEs absorb in the range of 384-388 nm and dialkoxy-substituted PPEs absorb in the range of 410-414 nm. They form yellow colored solutions which strongly fluoresce. The efficient fluorescence of PPEs makes them attractive materials for optoelectronic applications.[28] It is important to understand the solid state morphology of PPEs. In the solid state, PPEs usually have lamellar order which can be interdigitated or non interdigitated depending on the number of side chains present on the repeat unit as shown in Figure 1.6.[29] For side-chains present on each repeat unit the side chains do not interdigitate, and for lower side-chain concentration an interdigitated morphology result. The π-π stacking distances are 3.7-3.8 Å for dialkyl PPEs substituted with 2-ethylhexyl side chains.[31] In order to avoid electrostatic repulsions between the π systems, the benzene unit of two adjacent chains do not stack directly on top of each other. While the solid state structures of PPE has been characterized in detail, there are fewer reports of the packing of other poly(arylene ethynylene)s (PAE)s.[32]

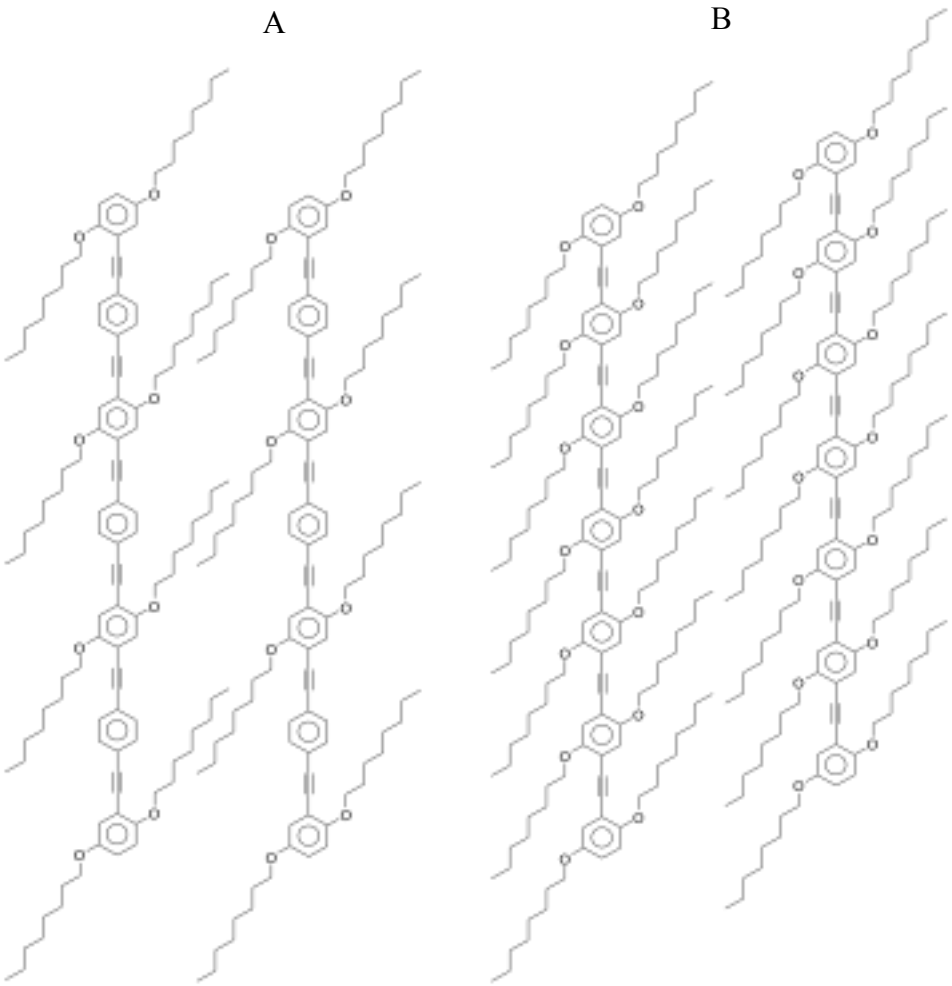

Figure 1.6. Solid state packing of PPEs: A, interdigitated side chains; and B, non-interdigitated side chains.[34] (Reprinted (adapted) with permission from (Bunz, U. H., Poly (aryleneethynylene) s: syntheses, properties, structures, and applications. *Chemical Reviews,* **2000,** *100* (4), 1605-1644). Copyright (2000) American Chemical Society.

Swager has reported extensive studies on the use of PPE derivatives in sensors. PPEs can be functionalized with binding sites which act as quenchers for analytes. For example, the PPE derivative shown in Figure1.7 has an electron-rich (ethylene glycol) cyclophane on each repeat unit which binds to paraquat (the analyte).[33-34] In dilute

solutions, these PPEs are highly fluorescent. When the analyte is bound to the binding site it creates a site of lower energy in the polymer chain, which creates a pathway for radiationless decay of the exciton, thereby leading to quenching of fluorescence. The exciton formed on the PPE backbone is delocalized over a number of repeat units so that it can locate the defect site even when only a small fraction of binding sites are bound to the analyte, leading to radiationless decay. This reveals the sensitivity of PPE systems to the concentration of analyte that can be detected using PPE systems as sensors. The fluorescent nature of PPEs can also be used in application such as OLEDs.

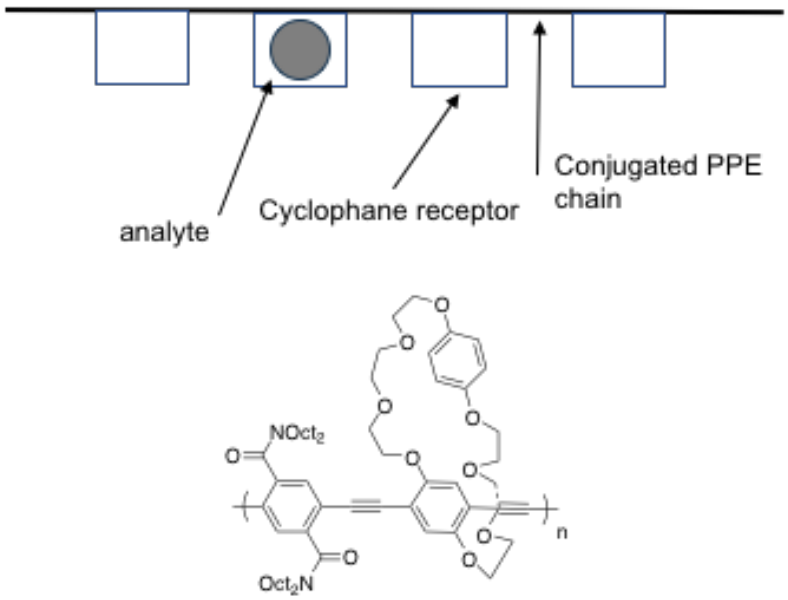

Figure 1.7. The demonstration of PPE as molecular sensor.[34] (Reprinted (adapted) with permission from (Bunz, U. H., Poly (aryleneethynylene) s: syntheses, properties, structures, and applications. *Chemical Reviews,* **2000,** *100* (4), 1605-1644). Copyright (2000) American Chemical Society.

The PPEs are also used in its use as light emitting polymer in LEDs and active layer in OPVs.[35-36] It was found that the presence of a triple bond in PPEs lowers the LUMO compared to poly(phenylene vinylene)s (PPV)s, thus making electron injection in the light emitting device efficient.[37] The efficiencies of the light emitting devices have been low for PPE derivatives possibly due to poor hole mobility. In order to improve hole mobility and processiblity of the material in the LED devices, research has been in developing hybrid materials which combine PPEs with poly(phenylene vinylene)s (PPV)s.[38] PPEs show high photoluminescence quantum yield, a high molar extinction coefficient in solution, and low lying LUMO for improved electron injection. While PPVs offer good solution processibility, higher photoluminsecene quantum yield in the solid state. This difference arisesfrom the lack of planarity of PPV compared toPPE, thereby resulting in less π- π interaction and improved hole injection.

1.3.2 Poly(phenylene vinylene)s

Poly(phenylene vinylene)s are conjugated polymers that contain vinylene linkages connecting the phenylene units.[11] They are not as coplanar as PPEs which gives them better solubility in the organic solvents. PPVs are often employed as electrolumiscent materials in light emitting diodes, and in OPVs.[39] They serve as model systems to understand the dynamics of electronic processes in the devices. The materials are accessible synthetically in good yields and with high molecular weights. Common synthetic pathways for PPVs make use of Wittig and Horner-Wadsworth-Emmons polycondensation reactions, and Pd-catalyzed cross coupling reactions (e.g., Heck, Stille and Suzuki couplings), as shown in Figure 1.??. All these synthetic pathways are step

growth polymerizations. There is also a chain growth polymerization pathway to PPVs that makes use of the ring-opening metathesis polymerization (ROMP) of paracyclophanedienes using Grubbs catalysts.[11] The ring-opening metathesis polymerization provides high molecular weight materials, but it is limited by the synthesis of complex monomers. Two other chain growth pathways make use of the Gilch and Wessling polymerizations that proceed through a p-quinodimethane intermediate that is generated *in situ*, as shown in Figure 1.8.[11]

PPVs have emission maxima between 521 and550 nm in the solid state, in the yellow-green region of the spectrum. Their attractive emission properties have led to their use as light emitting polymers.[39] In order for PPVs to be used in light emitting devices they need to be made solution processible. These polymers can be functionalized with alkoxy side chains, as shown in Figure 1.9, to enhance their solubility and also to tune their optoelectronic properties. The introduction of alkoxy side chains as in MEH-PPVs and MDMO-PPVs not only affords polymers that are solution-processible, but also improves the photoluminescence quantum yield in solid state.[39] These features result from the ability of the side chains to prevent interchain interactions. The external quantum efficiencies for PPV derivatives have been in the range of 0.1 to 5%. Substitution of the backbone with cyano groups, as shown in Figure 1.8 , lowers the LUMO levels of polymer so as to improve electron injection.

The PPV derivatives shown in Figure 1.8 have also been explored as active layers in photovoltaic devices.[40,41,42] The device efficiencies for PPV derivatives have been low. A primary reason for this is that the band gap of PPVs are typically in the range of ~2.1

to 2.3 eV. In order to harness maximum photons from the solar spectrum the band gap of the active layer in an OPV should typically be in the range of 1.4-1.7 eV.

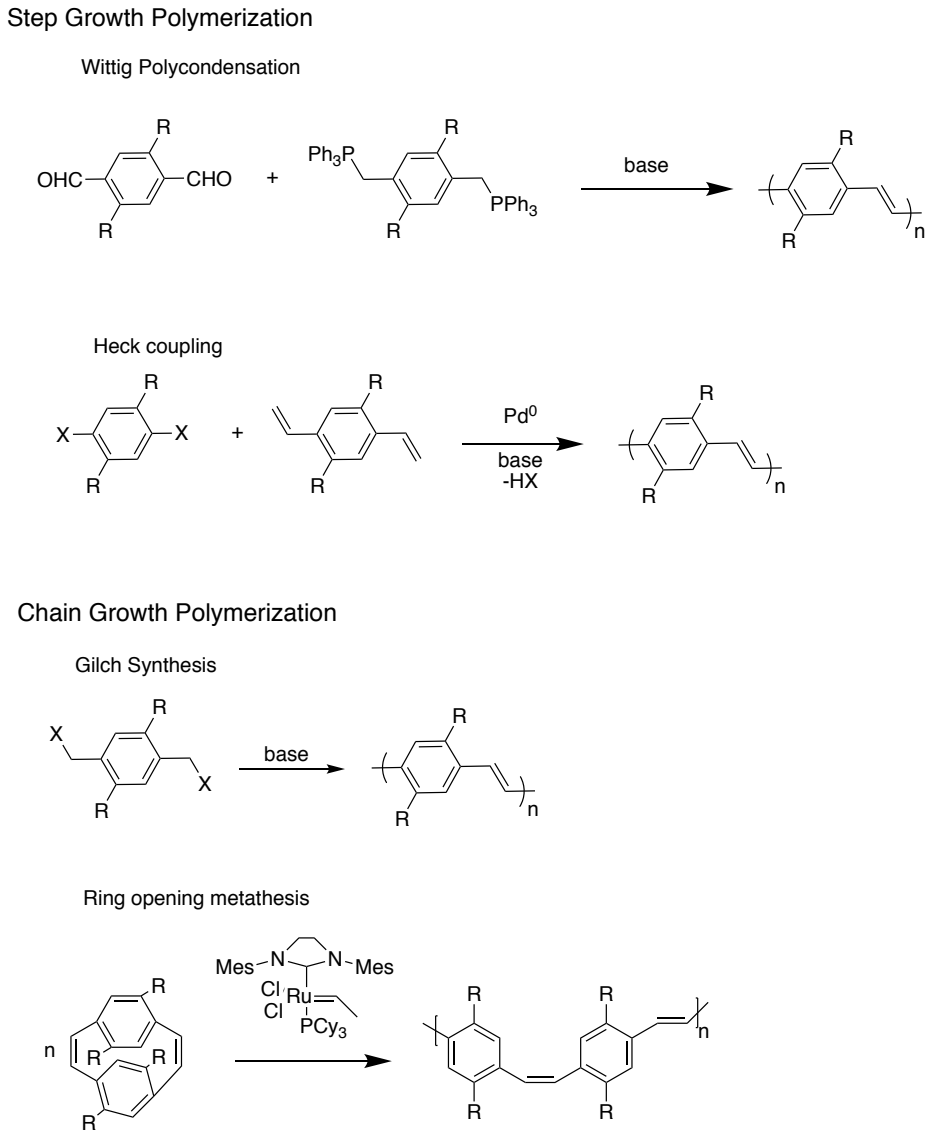

Figure 1.8. The synthesis scheme for PPVs.[11, 43]

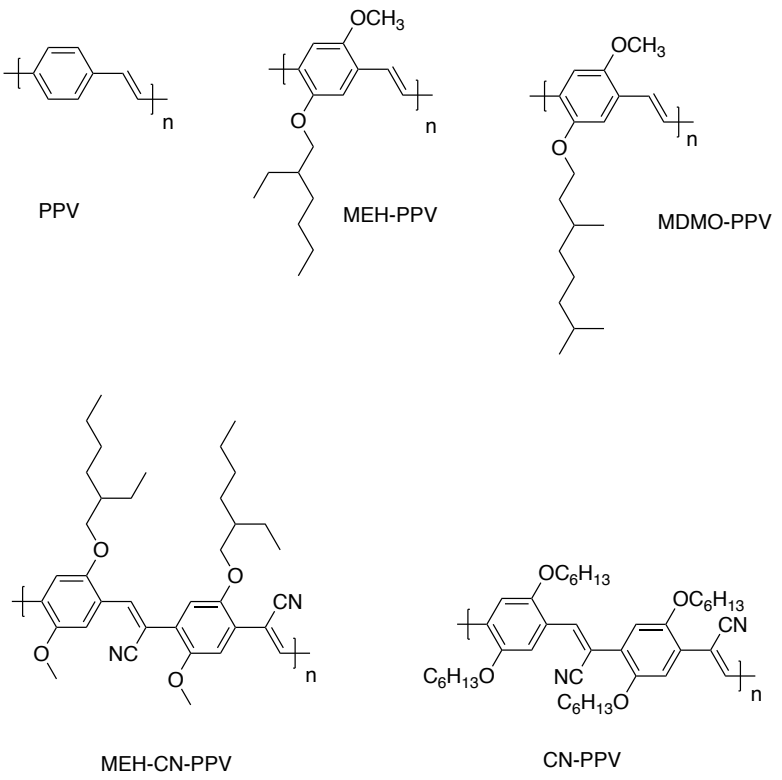

Figure 1.9. Examples of PPV derivatives used in OPVs and OLEDs.

1.4 ACENE-CONTAINING CONJUGATED POLYMERS

1.4.1 Pentacene containing small molecules and conjugated polymers

Pentacene has a bandgap of about 1.9 eV. Pentacene itself adopts a herringbone type packing in the solid state, as shown in Figure 1.10. It can be functionalized in different ways at 6,13- positions, 2,9-/2,10- positions. The substitution at 6,13- positions of pentacene by triisopropylacetylene groups (TIPS-pentacene)s as shown in Figure 1.9, leads to a brickwalled type packing and retains a relatively high mobility.[43] This type of arrangement reduces the interplanar spacing between aromatic rings from 6.27 Å for unsubstituted pentacene to 3.47 Å for substituted pentacene. This arrangement leads to a significant anisotropy in the resistivity of the crystals.[43] The resistivity along the π-π

stacking axis was found to be the lowest (2.5×10^6 Ω-cm), followed by the resistivity measured parallel to the long axis of the molecule (5×10^8 Ω-cm). The resistivity along the short axis which passes through the triple bond was the highest among all three axes (3×10^{10} Ω-cm).[43] This type of π-π stacking arrangement in the solid state is very beneficial to organic semiconductors in providing a pathway for intermolecular charge transport. However, there are few examples of pentacene-containing polymers. The main advantage of having conjugated polymers is solution processability leading to cost effective process to fabricate devices and considering electronic properties of pentacene, having polymers of pentacene can provide interesting properties.

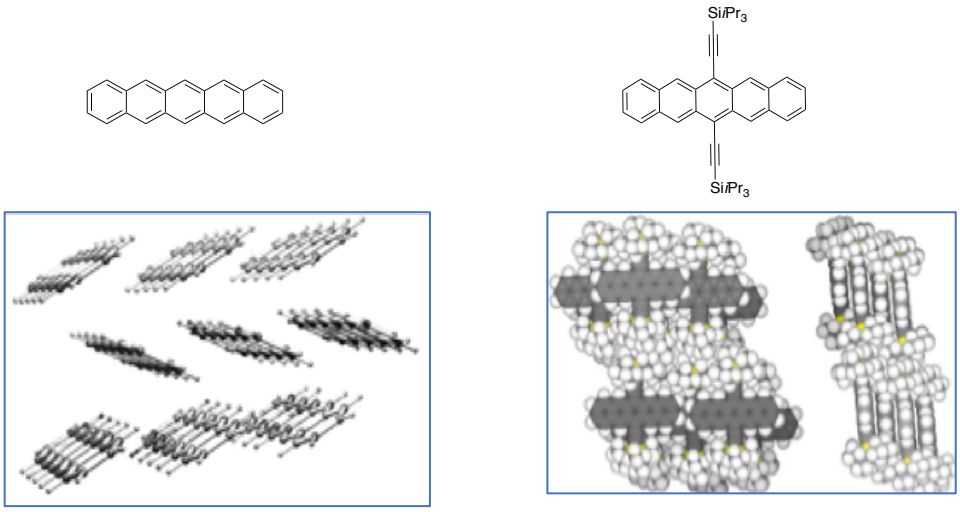

Figure 1.10. The crystal structure arrangement of pentacenes: A, herringbone arrangement of pentacene crystals; and B, stacked arrangement of TIPS-pentacene.[43-44] Figure 1.9 A. Reproduced from ref. 44 with permission from The Royal Society of Chemistry. Figure 1.9 B (Reprinted (adapted) with permission from (Anthony, J. E.;et.al.., Functionalized pentacene: improved electronic properties from control of solid-state order. *Journal of the American Chemical*

Society **2001,** *123* (38), 9482-9483). Copyright (2001) American Chemical Society.

Incorporating pentacene unit in conjugated polymers is synthetically challenging but work of Bao et al. presents a good starting point as shown in Figure 1.11.[45] The synthetic success in obtaining 2,9- and 2,10- substituted dibromo-6,13-triisopropylethynylpentacene as monomers has led to the development of series of alternating copolymers of 2,9-and 2,10- pentacendiyl unit with bithiophene, cyclopentadithiophene, and 1,4-diethynylbenzene. The polymers showed promising bandgap of ~1.5 to 1.6 eV. However, the power conversion efficiencies of the solar cells composed of the polymers with fullerene were low.

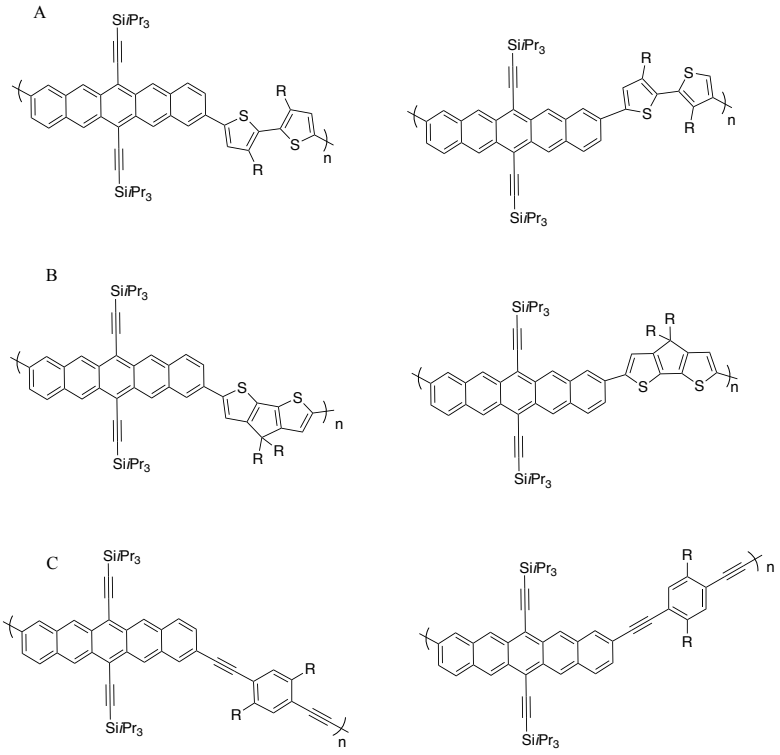

Figure 1.11. Pentacene containing polymers: A, pentacene-bithiophene copolymers; B, pentacene-cyclppentadithiophene; C, pentacene-diethynl benzene copolymers.[46]

1.4.2 Anthracene containing conjugated polymers

Similar to pentacene, the use of anthracene in conjugated polymers has been scarce. Anthracene has some advantage over pentacene as being more environmentally stable.[8] However, there are few reports that describe systematic studies of anthracene-containing polymers.

One study of anthracene-containing PPEs was conducted by Swager et.al.[47] The anthracene was coupled at 9,10-positions in poly(phenylene ethynylene-*co*-arylene ethynylene)s, as shown in Figure 1.12A). The study outlined a systematic variation of the ratio of 9,10-anthracenediyl units and 1,4-phenylenediyl units in the polymer. A progressive red-shift in the absorption maximum was observed with an increase in the amount of anthracene in the polymer. The fraction of anthracene units was varied from 7% to 17%,by varying the ratios of 1,4-diethynylbenzene, 1,4-diiodobenzene and 9,10-dibromoanthracene. A strictly alternating copolymer of 1,4-diethynyl phenylene and 9,10-dibromoanthracene yielded the most red-shifted spectrum compared to random copolymers that contained less of the anthracene units. The study outlined the potential of anthracene to provide the low energy traps that affect the absorption and emission characteristics of polymer.

Egbe et.al. developed anthracene-containing poly(1,4-phenylene ethynylene)-*alt*-(1,4- phneylene vinylene) polymers, as shown in Figure 1.12B).[48] The polymers were varied in their side chain structure to control the π-π stacking ability and correlate the photovoltaic response of the material. While the polymers displayed power conversion efficiency of ~ 3% , one limitation appears to be the band gaps of the polymers were little high for photovoltaic application (~ 2.0 eV).

Additional reports describe low band gap anthracene containing polymers in which the anthracene is used as a donor in donor-acceptor materials with diketopyrrolepyrole[49] and naphthalene diimide[50] serving as acceptors, as shown in Figure 1.12C and D).[51] The alternating copolymer of 9,10-diethynylanthracene with diketopyrrolopyrole (Figure 1.12D) showed a moderately low bandgap (~ 1.8 eV) and a good hole mobility in organic thin film transistor ~1.9 cm^2/Vs. The in-plane GIWAXS profile of thermally annealed thin film showed evidence of π-π stacking peak at 3.75Å, with the polymer chains having edge-on orientation relative to the substrate. The 9,10-diethynyl anthracene unit not only provided extended π- conjugation but also promoted interchain interactions leading to π-π stacking type morphology in the solid state. The alternating copolymer with naphthalene dimimde also provided a low bandgap of 1.4 eV. However, the copolymer had a relatively low molecular weight due to its low solubility and precipitation from the polymerization reaction.[50]

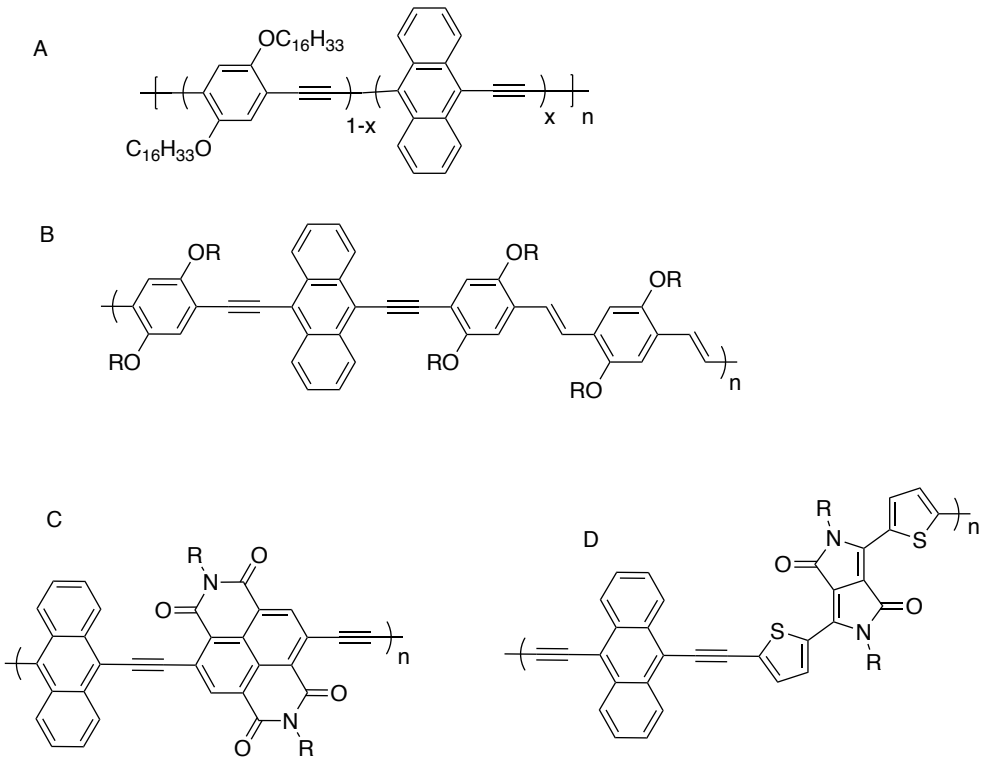

Figure 1.12. Examples of anthracene-containing polymers.[47-51]

1.5 THESIS OUTLINE

In Chapter 2, I describe the synthesis of 1,4-phenylene, 1,4-naphthalene and 9,10-anthracene-containing monomers and polymers, and compare the optical and electrochemical properties of the polymers. In addition to characterization of the electronic structure of the polymers by UV-visible and fluorescence spectroscopies and electrochemistry, I report on the Raman spectroscopy of the polymers to study the C≡C bond stretching frequency in the polymers. The C≡C bond stretching frequency reflects the extent of quinoid character in the polymer. In this chapter, I will also describe the synthesis and characterization of poly(2,6-diethylhexyl-9,10-anthracene ethynylene) homopolymer.

In Chapter 3, I describe the synthesis of alternating copolymers consisting of acene units (naphthalene and anthracene) with electron-poor naphthalene diimide units. The donor-acceptor polymers have a dual absorption spectrum which can be tuned by variation of electron donating strength of the acene. The objective of this study to tailor the optical characteristics of donor-acceptor polymers and to gain understanding of how the donor strength which is systematically varied by fusion of benzene rings onto the backbone of the polymer to promote quinoid character.

In Chapter 4, I describe synthetic approaches I have taken to develop tetraalkoxy-substituted anthracenes that could be further functionalized as potential monomers for poly(arylene vinylene)s, (PAV)s.

1.6 REFERENCES

1. Bundgaard, E.; Krebs, F. C., Low-band-gap conjugated polymers based on thiophene, benzothiadiazole, and benzobis (thiadiazole). *Macromolecules* **2006,** *39* (8), 2823-2831.

2. Rasmussen, S. C., The path to conductive polyactylene. *Bull. Hist. Chem* **2014,** *39* (6472.3).

3. Fincher Jr, C.; Chen, C.-E.; Heeger, A.; MacDiarmid, A.; Hastings, J., Structural Determination of the Symmetry-Breaking Parameter in trans-(CH) x. *Physical Review Letters* **1982,** *48* (2), 100.

4. McCullough, R. D., The chemistry of conducting polythiophenes. *Advanced Materials* **1998,** *10* (2), 93-116.

5. Diaz, A. F.; Castillo, J. I.; Logan, J.; Lee, W.-Y., Electrochemistry of conducting polypyrrole films. *Journal of Electroanalytical Chemistry and Interfacial Electrochemistry* **1981,** *129* (1-2), 115-132.

6. Woo, C. H.; Beaujuge, P. M.; Holcombe, T. W.; Lee, O. P.; Fréchet, J. M., Incorporation of furan into low band-gap polymers for efficient solar cells. *Journal of the American Chemical Society* **2010,** *132* (44), 15547-15549.

7. Yoshizawa, M.; Klosterman, J. K., Molecular architectures of multi-anthracene assemblies. *Chemical Society Reviews* **2014,** *43* (6), 1885-1898.

8. Dong, H.; Zhu, H.; Meng, Q.; Gong, X.; Hu, W., Organic photoresponse materials and devices. *Chemical Society Reviews* **2012,** *41* (5), 1754-1808.

9. Bundgaard, E.; Krebs, F. C., Low band gap polymers for organic photovoltaics. *Solar Energy Materials and Solar Cells* **2007,** *91* (11), 954-985.

10. Jiang, Y.; Mei, J.; Ayzner, A. L.; Toney, M. F.; Bao, Z., 5,11-Conjugation-extended low-bandgap anthradithiophene-containing polymer exhibiting enhanced thin-film order and field-effect mobility. *Chemical Communications* **2012,** *48* (58), 7286-7288.

11. Junkers, T.; Vandenbergh, J.; Adriaensens, P.; Lutsen, L.; Vanderzande, D., Synthesis of poly (p-phenylene vinylene) materials via the precursor routes. *Polymer Chemistry* **2012,** *3* (2), 275-285.

12. Mehmood, U.; Al-Ahmed, A.; Hussein, I. A., Review on recent advances in polythiophene based photovoltaic devices. *Renewable and Sustainable Energy Reviews* **2016,** *57*, 550-561.

13. Prosa, T.; Winokur, M.; McCullough, R., Evidence of a novel side chain structure in regioregular poly (3-alkylthiophenes). *Macromolecules* **1996,** *29* (10), 3654-3656.

14. Scharber, M. C.; Mühlbacher, D.; Koppe, M.; Denk, P.; Waldauf, C.; Heeger, A. J.; Brabec, C. J., Design rules for donors in bulk-heterojunction solar cells—Towards 10% energy-conversion efficiency. *Advanced materials* **2006,** *18* (6), 789-794.

15. Zhang, S.; Ye, L.; Hou, J., Breaking the 10% Efficiency Barrier in Organic Photovoltaics: Morphology and Device Optimization of Well-Known PBDTTT Polymers. *Advanced Energy Materials* **2016,** *6* (11), 1502529.

16. Burrezo, P. M.; Zafra, J. L.; López Navarrete, J. T.; Casado, J., Quinoidal/Aromatic Transformations in π-Conjugated Oligomers: Vibrational Raman studies on the Limits of Rupture for π-Bonds. *Angewandte Chemie International Edition* **2017,** *56* (9), 2250-2259.

17. Heeger, A. J.; Kivelson, S.; Schrieffer, J. R.; Su, W. P., Solitons in conducting polymers. *Reviews of Modern Physics* **1988,** *60* (3), 781-850.

18. Brédas, J., Relationship between band gap and bond length alternation in organic conjugated polymers. *The Journal of chemical physics* **1985,** *82* (8), 3808-3811.

19. Kertesz, M., The aromatic-quinonoid transition in conducting polymers. *Synthetic Metals* **1995,** *69* (1), 641-644.

20. Wudl, F.; Kobayashi, M.; Heeger, A., Poly (isothianaphthene). *The Journal of Organic Chemistry* **1984,** *49* (18), 3382-3384.

21. Lee, Y. S.; Kertesz, M., The effect of additional fused rings on the stabilities and the band gaps of heteroconjugated polymers. *International Journal of Quantum Chemistry* **1987,** *32* (S21), 163-170.

22. Ikenoue, Y., Synthesis and characteristic properties of poly (naphtho)[2, 3-c] thiophene) as a series of fused-ring conducting polymers analogous to poly (isothianaphthene. *Synthetic Metals* **1990,** *35* (3), 263-270.

23. Lakshmikantham, M.; Lorcy, D.; Scordilis-Kelley, C.; Wu, X. L.; Parakka, J. P.; Metzger, R. M.; Cava, M. P., Poly (naphtho [2, 3-c] thiophene-alt-bithiophene): A novel low band gap polymer. *Advanced Materials* **1993,** *5* (10), 723-726.

24. Ohlemacher, A.; Schenk, R.; Weitzel, H. P.; Tyutyulkov, N.; Tasseva, M.; Müllen, K., Energy spectra of poly (arylenevinylene) s containing different aromatic units. *Macromolecular Chemistry and Physics* **1992,** *193* (1), 81-93.

25. Clar, E.; McCallum, A., The significance of benzenoid rings for the stability of aromatic hydrocarbons. *Tetrahedron* **1960,** *10* (3-4), 171-174.

26. Zhang, L.; Fonari, A.; Liu, Y.; Hoyt, A.-L. M.; Lee, H.; Granger, D.; Parkin, S.; Russell, T. P.; Anthony, J. E.; Brédas, J.-L., Bistetracene: an air-stable, high-mobility organic semiconductor with extended conjugation. *Journal of the American Chemical Society* **2014,** *136* (26), 9248-9251.

27. Suresh, C.; Gadre, S. R., Clar's aromatic sextet theory revisited via molecular electrostatic potential topography. *The Journal of Organic Chemistry* **1999,** *64* (7), 2505-2512.

28. Swager, T. M., The molecular wire approach to sensory signal amplification. *Accounts of Chemical Research* **1998,** *31* (5), 201-207.

29. Bunz, U. H., Poly (aryleneethynylene) s: syntheses, properties, structures, and applications. *Chemical reviews* **2000,** *100* (4), 1605-1644.

30. Kloppenburg, L.; Song, D.; Bunz, U. H., Alkyne metathesis with simple catalyst systems: poly (p-phenyleneethynylene) s. *Journal of the American Chemical Society* **1998,** *120* (31), 7973-7974.

31. Bunz, U. H.; Enkelmann, V.; Kloppenburg, L.; Jones, D.; Shimizu, K. D.; Claridge, J. B.; zur Loye, H.-C.; Lieser, G., Solid-state structures of phenyleneethynylenes: Comparison of monomers and polymers. *Chemistry of Materials* **1999,** *11* (6), 1416-1424.

32. Ofer, D.; Swager, T. M.; Wrighton, M. S., Solid-state ordering and potential dependence of conductivity in poly (2, 5-dialkoxy-p-phenyleneethynylene). *Chemistry of Materials* **1995,** *7* (2), 418-425.

33. Yang, J.-S.; Swager, T. M., Fluorescent porous polymer films as TNT chemosensors: electronic and structural effects. *Journal of the American Chemical Society* **1998,** *120* (46), 11864-11873.

34. Zhou, Q.; Swager, T. M., Fluorescent chemosensors based on energy migration in conjugated polymers: the molecular wire approach to increased sensitivity. *Journal of the American Chemical Society* **1995,** *117* (50), 12593-12602.

35. Silvestri, F.; Marrocchi, A., Acetylene-Based materials in organic photovoltaics. *International Journal of Molecular Sciences* **2010,** *11* (4), 1471-1508.

36. Campbell, K.; Zappas, A.; Bunz, U.; Thio, Y. S.; Bucknall, D. G., Fluorescence quenching of a poly (para-phenylene ethynylenes) by C 60 fullerenes. *Journal of Photochemistry and Photobiology A: Chemistry* **2012,** *249*, 41-46.

37. Montali, A.; Smith, P.; Weder, C., Poly (p-phenylene ethynylene)-based light-emitting devices. *Synthetic metals* **1998,** *97* (2), 123-126.

38. Egbe, D. A.; Neugebauer, H.; Sariciftci, N. S., Alkoxy-substituted poly (arylene-ethynylene)-alt-poly (arylene-vinylene) s: synthesis, electroluminescence and photovoltaic applications. *Journal of Materials Chemistry* **2011,** *21* (5), 1338-1349.

39. Kraft, A.; Grimsdale, A. C.; Holmes, A. B., Electroluminescent conjugated polymersÐseeing polymers in a new light. *Angew. Chem. Int. End Engl* **1998,** *37*, 402-428.

40. Marks, R.; Halls, J.; Bradley, D.; Friend, R.; Holmes, A., The photovoltaic response in poly (p-phenylene vinylene) thin-film devices. *Journal of Physics: Condensed Matter* **1994,** *6* (7), 1379.

41. Gao, J.; Yu, G.; Heeger, A. J., Polymer p-i-n Junction Photovoltaic Cells. *Advanced Materials* **1998,** *10* (9), 692-695.

42. Brabec, C. J.; Sariciftci, N. S.; Hummelen, J. C., Plastic solar cells. *Advanced Functional Materials* **2001,** *11* (1), 15-26.

43. Yu, C. Y.; Turner, M. L., Soluble Poly (p-phenylenevinylene) s through Ring-Opening Metathesis Polymerization. *Angewandte Chemie* **2006,** *118* (46), 7961-7964.

44. Anthony, J. E.; Brooks, J. S.; Eaton, D. L.; Parkin, S. R., Functionalized pentacene: improved electronic properties from control of solid-state order. *Journal of the American Chemical Society* **2001,** *123* (38), 9482-9483.

45. MacGillivray, L. R., On substituents, steering, and stacking to control properties of the organic solid state. *CrystEngComm* **2004,** *6* (16), 77-78.

46. Okamoto, T.; Bao, Z., Synthesis of solution-soluble pentacene-containing conjugated copolymers. *Journal of the American Chemical Society* **2007,** *129* (34), 10308-10309.

47. Jiang, Y.; Hong, S.; Oh, J. H.; Mondal, R.; Okamoto, T.; Verploegen, E.; Toney, M. F.; McGehee, M. D.; Bao, Z., Impact of regioregularity on thin-film transistor and photovoltaic cell performances of pentacene-containing polymers. *Journal of Materials Chemistry* **2012,** *22* (10), 4356-4363.

48. Swager, T. M.; Gil, C. J.; Wrighton, M. S., Fluorescence studies of poly (p-phenyleneethynylene) s: the effect of anthracene substitution. *The Journal of Physical Chemistry* **1995,** *99* (14), 4886-4893.

49. Egbe, D. A.; Turk, S.; Rathgeber, S.; Kuhnlenz, F.; Jadhav, R.; Wild, A.; Birckner, E.; Adam, G.; Pivrikas, A.; Cimrova, V., Anthracene based conjugated polymers: correlation between π− π-stacking ability, photophysical properties, charge carrier mobility, and photovoltaic performance. *Macromolecules* **2010,** *43* (3), 1261-1269.

50. Lee, D. H.; Shin, J.; Cho, M. J.; Choi, D. H., High-performance low-bandgap conjugated polymers bearing diethynylanthracene units for thin-film transistors. *Chemical Communications* **2013,** *49* (37), 3896-3898.

51. Alvey, P. M.; Ono, R. J.; Bielawski, C. W.; Iverson, B. L., Conjugated NDI–Donor Polymers: Exploration of Donor Size and Electrostatic Complementarity. *Macromolecules* **2013,** *46* (3), 718-726.

52. Liu, C.; Cai, W.; Guan, X.; Duan, C.; Xue, Q.; Ying, L.; Huang, F.; Cao, Y., Synthesis of donor–acceptor copolymers based on anthracene derivatives for polymer solar cells. *Polymer Chemistry* **2013,** *4* (14), 3949-3958.

CHAPTER 2. EFFECT OF FUSED ARENE RPEAT UNITS ON ELECTRONIC STRUCUTRES OF POLY(ARYLENE ETHYNYLE)S

2.1 INTRODUCTION

In this chapter, we report on a series of poly(arylene ethynylene)s that contain 1,4-naphthalenediyl and 9,10-anthracenediyl units to explore how stabilization of the quinoid form of conjugated polymers effects their electronic and optical properties. A series of alternating copolymers was synthesized by Sonogashira coupling of 1,4-diiodo-2,5-dioctyloxybenzene with three comonomers: 1,4-dihexyl-2,5-bis(trimethylsilylethynyl) benzene, 6,7-dihexyl-1,4-bis(trimethylsilylethynyl)naphthalene and 2,6-dihexyl-9,10-bis(trimethylsilylethynyl)anthracene. The resulting alternating copolymers, poly(arylene ethynylene-*alt*-phenylene ethynylene)s, which are abbreviated as **PPPE**, **PNPE** and **PAPE** respectively as shown in Figure 2.1. Along with these copolymers, a homopolymer containing 9,10-anthracenediyl units, poly(2,6-dihexyl-9,10-anthracene ethynylene) (**PAE**) is reported. The electronic structures of the polymers were characterized by UV-visible spectroscopy, photoluminescence and cyclic voltammetry. The hypothesis for this study was that fusing one ring in naphthalene and two rings in anthracene will stabilize the quinoid form of polymer by retaining the aromaticity of the fused rings in the backbone.

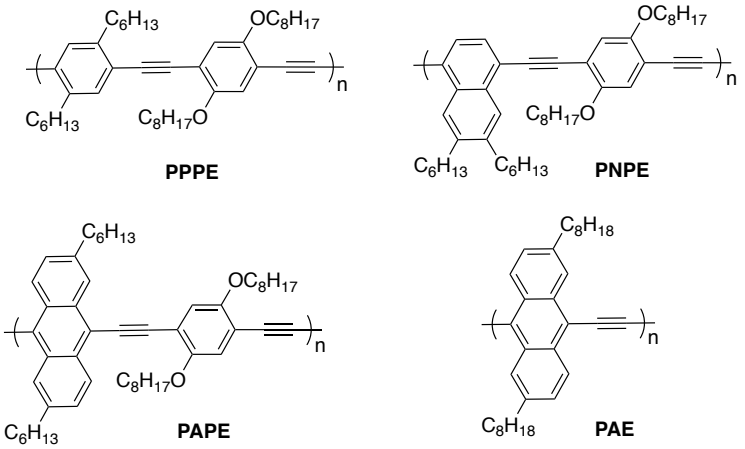

Figure 2.1. Poly(arylene ethynylene-*alt*-1,4-phenylene ethynylene)s with 1,4-phenylendiyl, 1,4- naphthalenediyl and 9,10-anthracenediyl units. (**PPPE**, **PNPE** and **PAPE** respectively), and poly(9,10-anthracene ethynylene) homopolymer (**PAE**).

2.2 RESULTS AND DISCUSSION

2.2.1 Synthesis

The diiodophenylene monomer **3** was synthesized in three steps according to the route shown in Figure 2.2. 1,4-Dichlorobenzene, **1**, was treated with 1-hexylmagnesium bromide in the presence of $Ni(dppp)Cl_2$ to prepare 1,4-dihexylbenzene, **2**. Electrophilic aromatic iodination provided the monomer, 1,4-dihexyl-2,5-diiodo-benzene **3**.[1] The diyne monomer 1,4-dioctyloxy-2,5-bis(trimethylsilylethynyl)benzene, **7,** was prepared from 1,4-dihydroxybenzene **4** by Williamson ether synthesis followed by iodination and Sonogashira coupling with trimethylsilylacetylene.

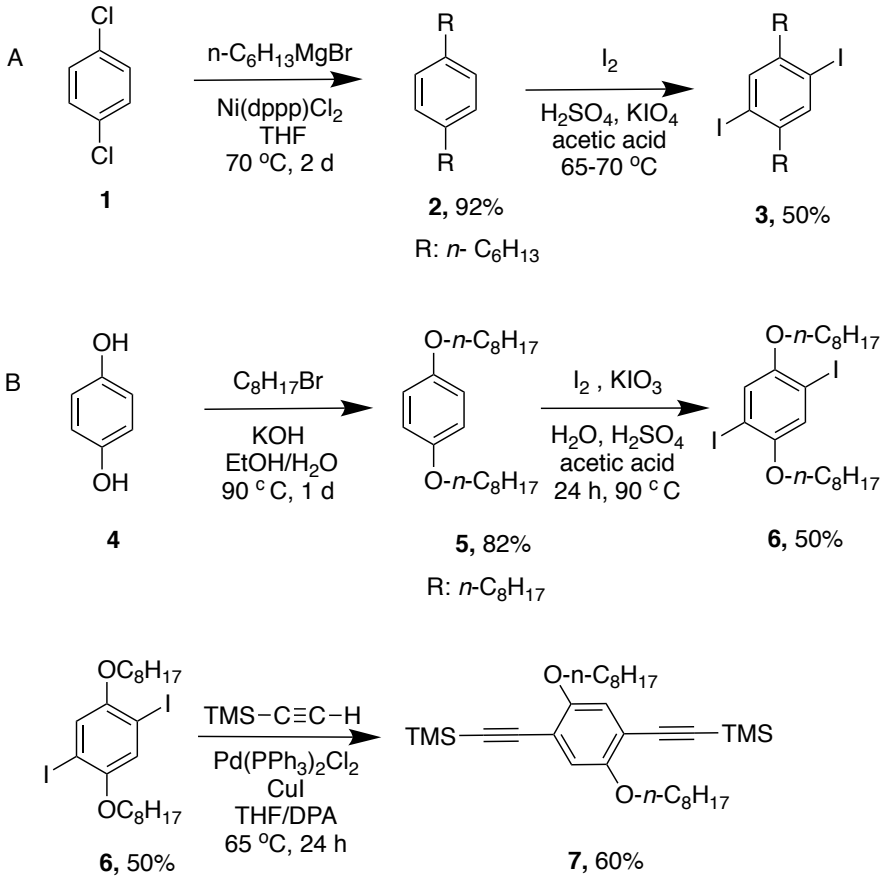

Figure 2.2. Synthesis of phenylene monomers: A,1,4-dihexyl-2,5-diiodobenzene (**3**); and B, 1,4-dioctyloxy-2,5-bis(trimethylsilylethynyl)benzene (**7**).

The 1,4-diethynylnaphthalene monomer **13** was synthesized in five steps by the preparation of 6,7-disubstituted 1,4-naphthaquinone core followed by the installation of trimethylsilylethynyl and alkyl groups, as shown in Figure 2.3. 3,4-Dibromothiophene, **8**, was oxidized by treatment with hydrogen peroxide in trifluoroacetic anhydride to afford 3,4-dibromothiophene-1,1-dioxide, **9**.[2] A Diels-Alder reaction between **9** and benzoquinone, with subsequent loss of sulfur dioxide, gave 6,7-dibromo-1,4-naphthaquinone, **10**.[3] Nucleophilic addition of trimethylsilylacetylide to **10** afforded a mixture of cis and trans diol **11**. Reduction of the mixture of distereoisomers with tin(II)

chloride provided 6,7-dibromo-1,4-di(trimethylsilylethynyl)naphthalene, **12**, in 50% yield. Monomer **13** was obtained by Negishi coupling of **12** with 1-hexylzinc chloride.

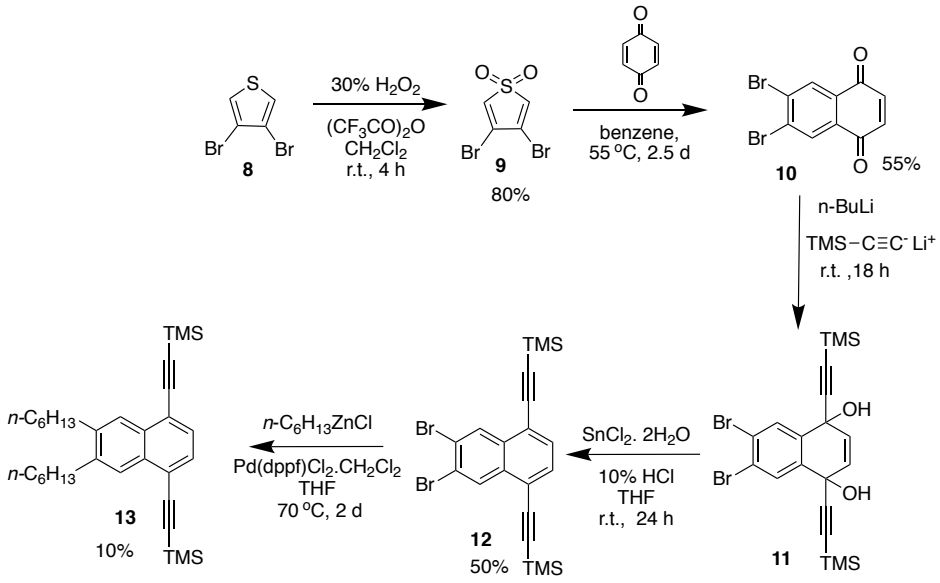

Figure 2.3. Synthesis of 6,7-dihexyl-1,4-bis(trimethylsilylethynyl)naphthalene, **13**.

The anthracene monomer, 2,6-dihexyl-9,10-bis(trimethylsilylethynyl) anthracene, **18**, was synthesized starting from commercially available 2,6-diamino-9,10-anthraquinone, **14**, as shown in Figure 2.4. Conversion of **14** to 2,6-dibromo-9,10-anthraquinone, **15**, was conducted using a standard Sandmeyer reaction.[4] The trimethylsilylethynyl groups were installed at the 9- and 10-positions by treatment of **15** with lithium trimethylsilylacetylide followed by reductive aromatization using tin(II) chloride dihydrate to give 2,6-dibromo-9,10-diethynylanthracene, **17**.[5] Negishi coupling with 1-hexylzinc(II) chloride was used to install alkyl groups at the 2- and 6- positions of the anthracene to afford monomer **18**.

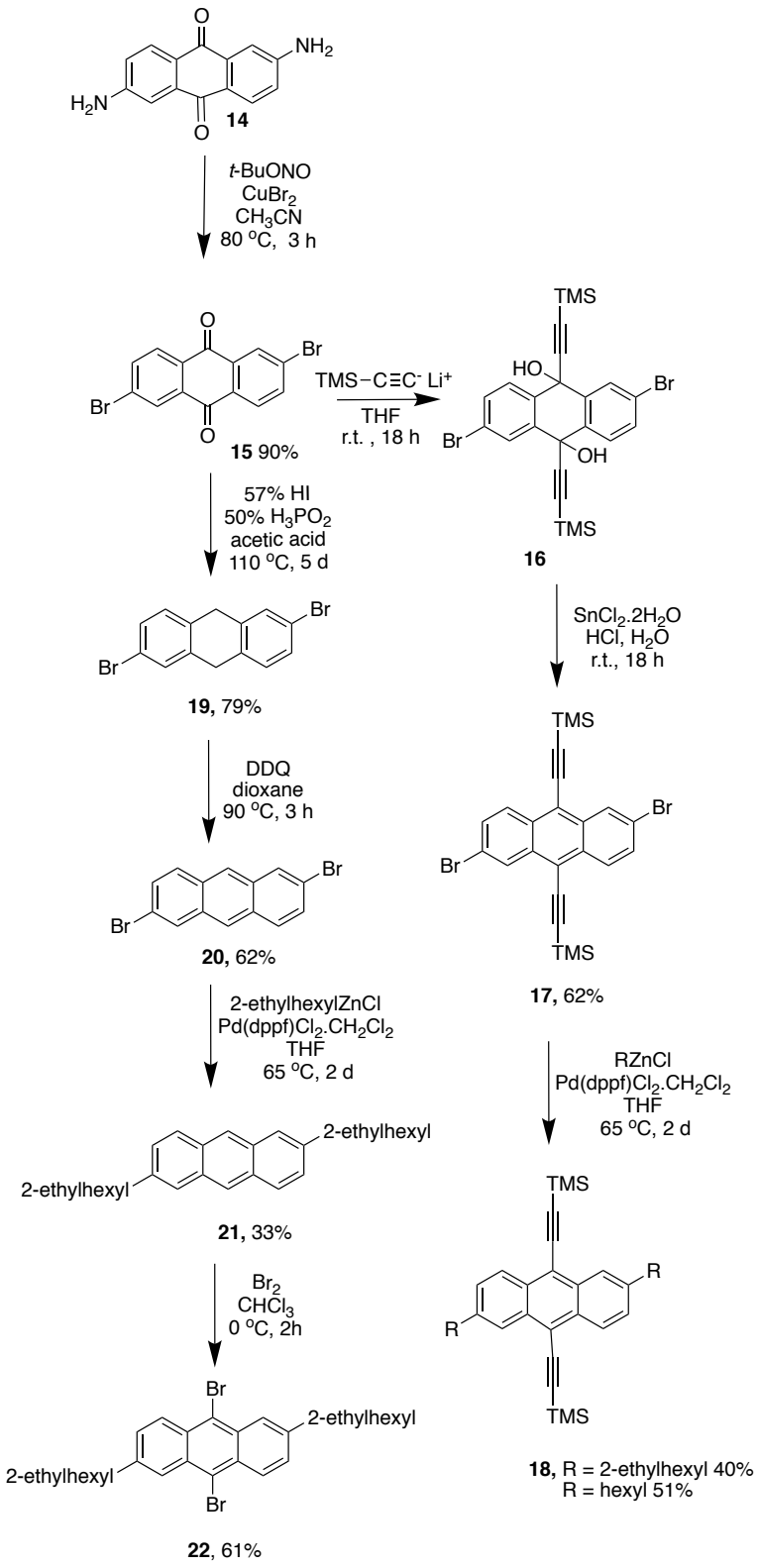

Figure 2.4. Synthesis of 2,6-dialkyl-9,10-bis(trimethylsilylethynyl)anthracene **18** and 2,6-di(2-ethylhexyl)-9,10-dibromoanthracene, **22**.

The synthesis of a 9,10-dibromoanthracene monomer, 9,10-dibromo-2,6-di(2-ethylhexyl) anthracene, **22**, is shown in Figure 2.4. The conversion of anthraquinone **15** to anthracene **20** was carried out in a two-step process. Reduction of **15** by treatment with HI/H_3PO_2 yielded 2,6-dibromo-9,10-dihydroanthracene, **19**.[6] Mild oxidation of **19** by treatment with DDQ afforded 2,6-dibromoanthracene **20**. Negishi coupling with 1-hexylzinc(II) chloride was used to install alkyl groups at the 2- and 6- positions of the anthracene to afford 2,6-di(2-ethylhexyl)anthracene, **21**. The bromination of **21** with a small excess of molecular bromine at 0 °C gave 9,10-dibromo-2,6-di(2-ethylhexyl)anthracene, **22**.

The polymers **PPPE**, **PNPE** and **PAPE** were synthesized by *in situ* desilation and Sonogashira coupling of diyne monomers **7**, **13** and **18** with diiodophenylene monomer, **6** as shown in Figure 2.5.[7] The **PAE** homopolymer was prepared by reaction of diethynylanthracene monomer, **18** and dibromoanthracene monomer, **22**.[7]

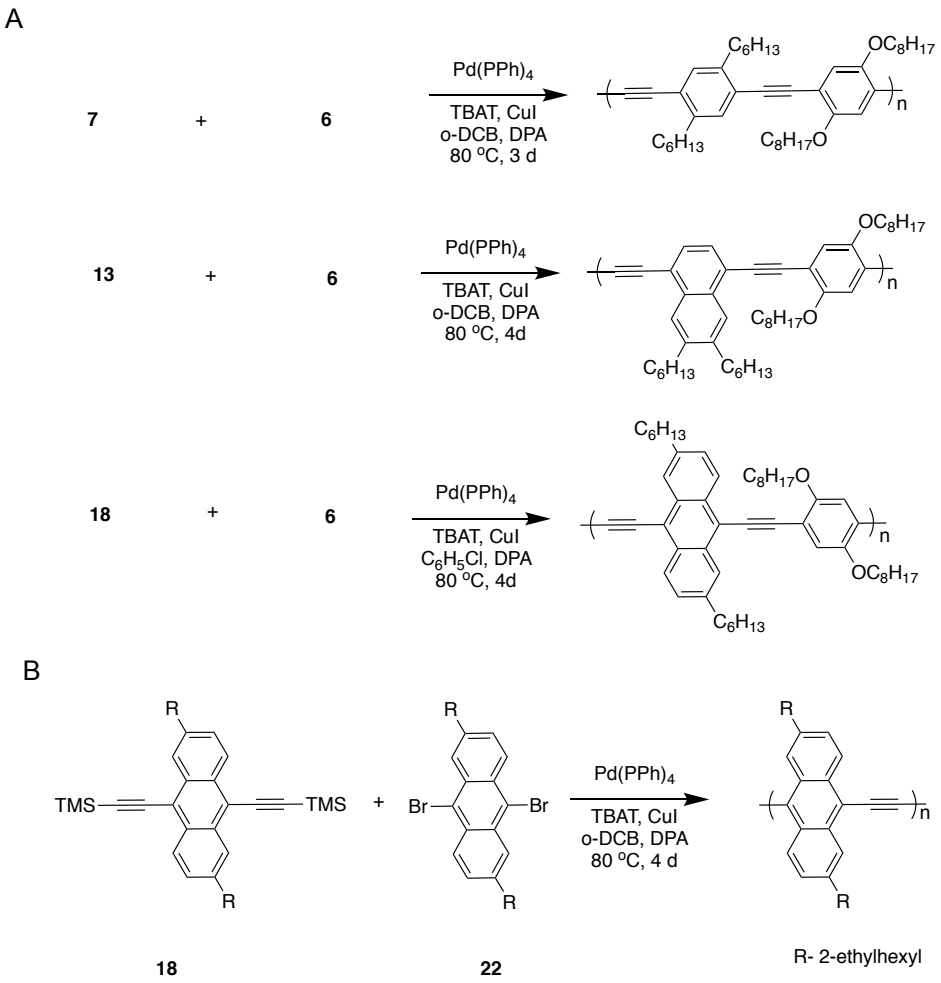

Figure 2.5. Synthesis of polymers by Sonogashira coupling: A, Alternating copolymers **PPPE**, **PNPE** and **PAPE**; and B, homopolymer, **PAE**.

2.2.2 ^{1}H NMR Analysis

In the ^{1}H NMR spectrum of the phenylene-containing alternating copolymer, **PPPE**, singlets at 6.90 ppm and 7.32 ppm correspond to the hydrogen atoms of the rings which are substituted with octyloxy and hexyl side chains, respectively. The upfield part of the spectrum consists of signals for the two alkyl groups, with a broad triplet at 4.10 ppm for the α-methylene units of the alkoxy groups and a broad triplet at 2.80 ppm for the benzylic α-methylene units of the hexyl side chains. The spectrum of the

naphthalene-containing analog, **PNPE**, shows three signals in the aromatic region, at 7.10 ppm for the hydrogen atoms of the phenylene unit, at δ 7.60 for the protons ortho to alkyl groups, and at 8.22 ppm for the peri-hydrogens of the naphthalene unit. The hydrogen atoms in the 5- and 8-positions appears downfield by virtue of the ring currents associated with the ethynylene units in the peri positions. For anthracene containing copolymer, **PAPE**, three broad signals for the 2,6,9,10-tetrasubstitiuted anthracene unit at δ 9.25 (d, J = 9 Hz), 9.00 (s) and 7.74 (d, J = 9 Hz) are observed consistent with the substitution pattern of the anthracene ring. The ^{1}H NMR analysis of the anthracene-containing homopolymer **PAE** shows three sets of protons in the aromatic region at 9.00 (m), 8.82 (s) and 7.61 (m), ppm.

2.2.3 Electrochemical Measurements

The electrochemical properties of thin films of polymers were investigated on a polymer-coated glassy carbon button electrode. The cyclic voltammograms of the copolymers exhibited an irreversible oxidation wave. This is consistent with the oxidative degradation of the polymers, which has previously been observed for dialkoxy-substituted PPEs.[8] Differential pulse voltammetry (DPV) was used to determine the potential for the onset of oxidation. The oxidation potential shows a decrease when proceeding from **PPPE** to **PNPE** and to **PAPE**, as shown in Figure 2.6 and Table 1. The decrease proceeding from **PNPE** to **PAPE** ($\Delta E_{ox} \sim 0.3$ V) is significantly larger than the difference in oxidation potential of **PPPE** and **PNPE** ($\Delta E_{ox} \sim 0.1$ V). This suggests that anthracene, with benzene rings fused on to both sides of the phenylene ring in the conjugated backbone of the polymer, has a more destabilizing effect on the HOMO level relative to **PPPE** and **PNPE**. The onset of oxidation of **PAE** is higher than that of **PAPE** ($\Delta E_{ox} \sim 0.2$ V) despite having solely anthracene units in the polymer. We ascribe this

difference to the absence of electron-rich dioctyloxyphenylene units in the copolymer **PAPE**.

Table2.1. Electrochemical and photophysical properties of polymers

	UV-Vis absorption, λ_{max} (nm)						Fluorescence λ_{max} (nm)			
	solution[a]	solid state	bandgap (eV)-[b]	V_{ox} (V)[c]	E_{HOMO} (eV)	E_{LUMO} (eV)	solution	solid state	Quantum yield	I.P. (eV)[d]
PPPE	428	457	2.56	+0.88	–5.94	–3.38	458	545	0.48	–5.70
PNPE	456	456	2.34	+0.76	–5.82	–3.48	499	575	0.55	–5.46
PAPE	575	614	1.86	+0.42	–5.48	–3.62	594	670	0.31	–5.55
PAE	621	621	1.58	+0.65	–5.71	–4.13	674	-	0.10	–5.85

[a]measured in *o*-dichlorobenzene; [b]determined from onset of absorption; [c]DPV measurements of polymer films deposited on glassy carbon button electrode in 0.5 M tetra-*n*-butylammonium hexaflourophosphate ($TBAPF_6$) in propylene carbonate against standard electrode Ag/Ag^+; $E_{HOMO} = (E_{ox} + 5.06)$ eV; [d]determined by ultraviolet photoelectron spectroscopy (UPS).

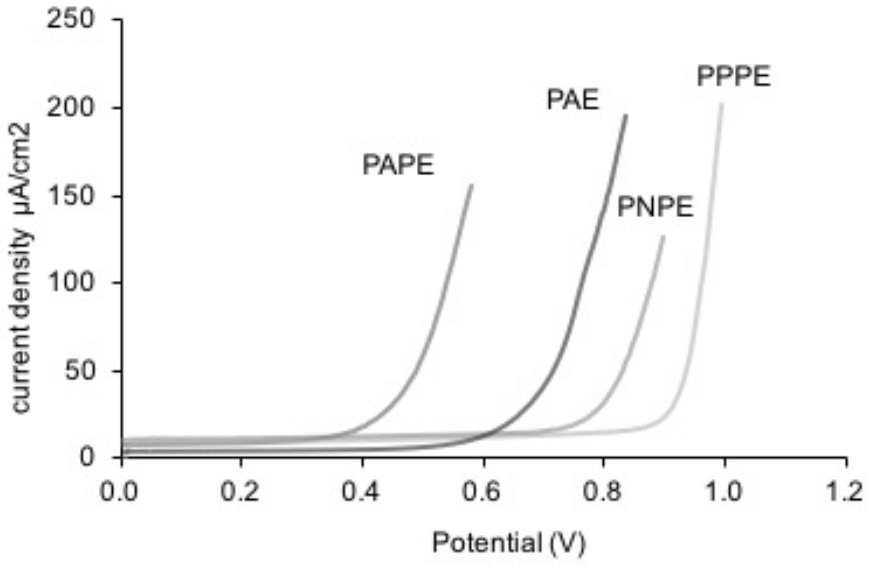

Figure 2.6. Differential pulse voltammetry: A, **PPPE**; B, **PNPE**; C, **PAPE**; D, **PAE**. Step-size, 2mV; step time, 0.1 s. The measurements were performed using a Ag/Ag^+ reference electrode with a Pt counter electrode with 0.5 M (tetra-*n*-butylammonium hexafluorophosphate in propylene carbonate).

2.2.4 Absorption spectroscopy

The UV-visible spectra of the polymers recorded in o-dichlorobenzene solution are shown in Figure 2.7. The absorption maximum observed for **PPPE**, which consists of alternating dialkyl and dialkoxy-substituted phenylene ethynylene units, is intermediate in value between that of dialkyl substituted PPEs which generally fall in the range at 384 to 388 nm,[9] and dialkoxy-substituted PPEs which are typically in the range of 442 to 452 nm.[10] The absorption maximum (λ_{max}) follows the trend: **PPPE** (427 nm) < **PNPE** (456 nm) << **PAPE** (569 nm), as shown in Table 1. Thus, the red shift that results from fusion of benzene rings onto the phenylene ring of the conjugated backbone is consistent with the trend observed in the onset of oxidation in electrochemical measurement of the **PPPE**, **PNPE** and **PAPE** copolymers. The absorption of the **PAE** homopolymer is further red shifted, with an absorption maximum of 621 nm. This is consistent with a further decrease in the aromatic nature of the conjugated backbone.

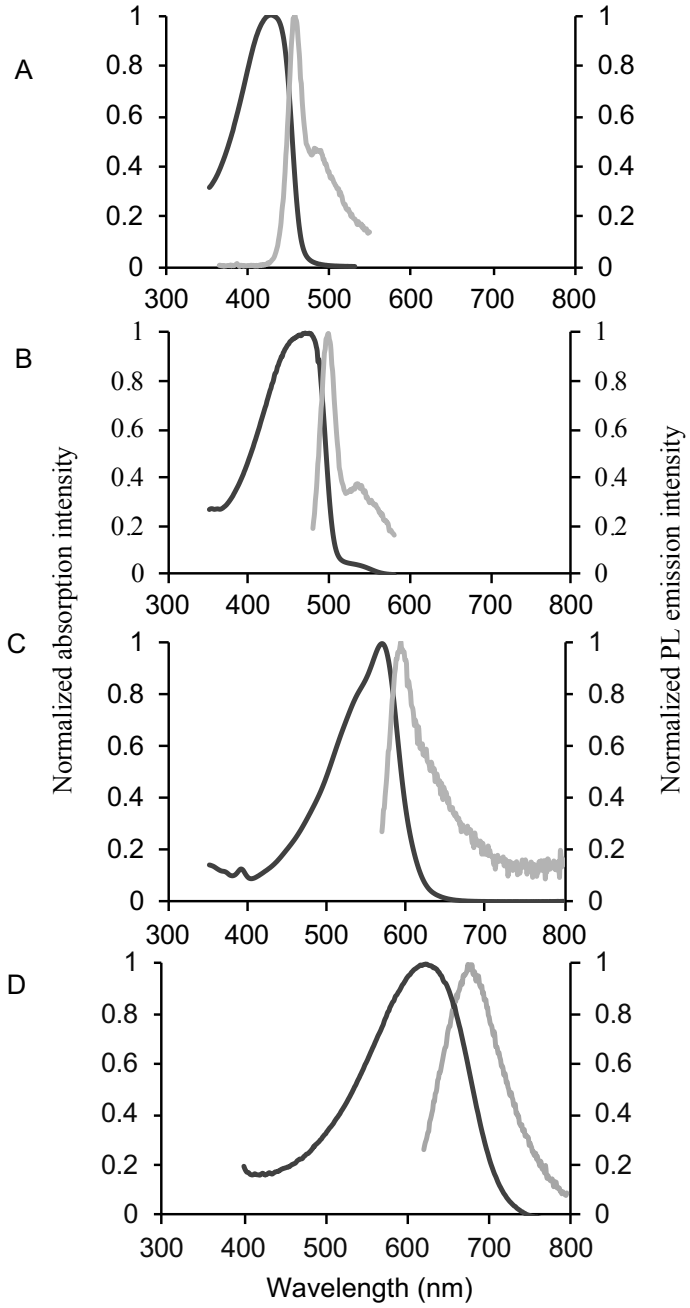

Figure 2.7. Normalized absorption (black) and fluorescence spectra (grey) of polymers in *o*-DCB: A, **PPPE** (λ_{ex} = 426 nm); B, **PNPE** (λ_{ex} = 472 nm); C, **PAPE** (λ_{ex} = 566 nm); and D, **PAE** (λ_{ex} = 623 nm).

The absorption spectra of **PPPE**, **PNPE** and **PAPE** in the solid state, as shown in Figure 2.8. The films were annealed for 15 min at 120 ^{o}C. For **PPPE** the maximum is red shifted by 32 nm relative to solution, for **PNPE** the maximum similar to solution but a

shoulder is observed at 493 nm and for **PAPE** the maximum is red shifted by 29 nm, relative to the absorption maxima in solution. The red shift in the maximum for **PPPE** and **PAPE** and the shoulder for **PNPE** is consistent with both an increase in conjugation that results from planarization of the backbone, and with the presence of interchain interactions in the solid state that are absent in solution.[11] In the solid state, interchain interactions between the molecular orbitals of the chromophores interact giving rise to new set of molecular orbitals which has destabilized HOMO and stabilizes LUMO, thus producing red shifted spectrum. The solid state absorption spectrum of **PAE** has a maximum at 621 nm, similar to the maximum in solution and a shoulder at 710 nm. The shoulder at 710 nm could be due to planarization of polymer backbone and interchain interactions. Overall, the absorption spectra of thin films of all polymers were broad. This suggests that the polymers are not highly ordered in solid state. The optical band gaps of the four polymers were determined from the onset of absorption in the UV-visible spectra of thin films. The band gaps fall in the range of 1.9 to 2.5 eV as shown in Table 2, decreasing in the order **PPPE** > **PNPE** >> **PAPE** > **PAE**.

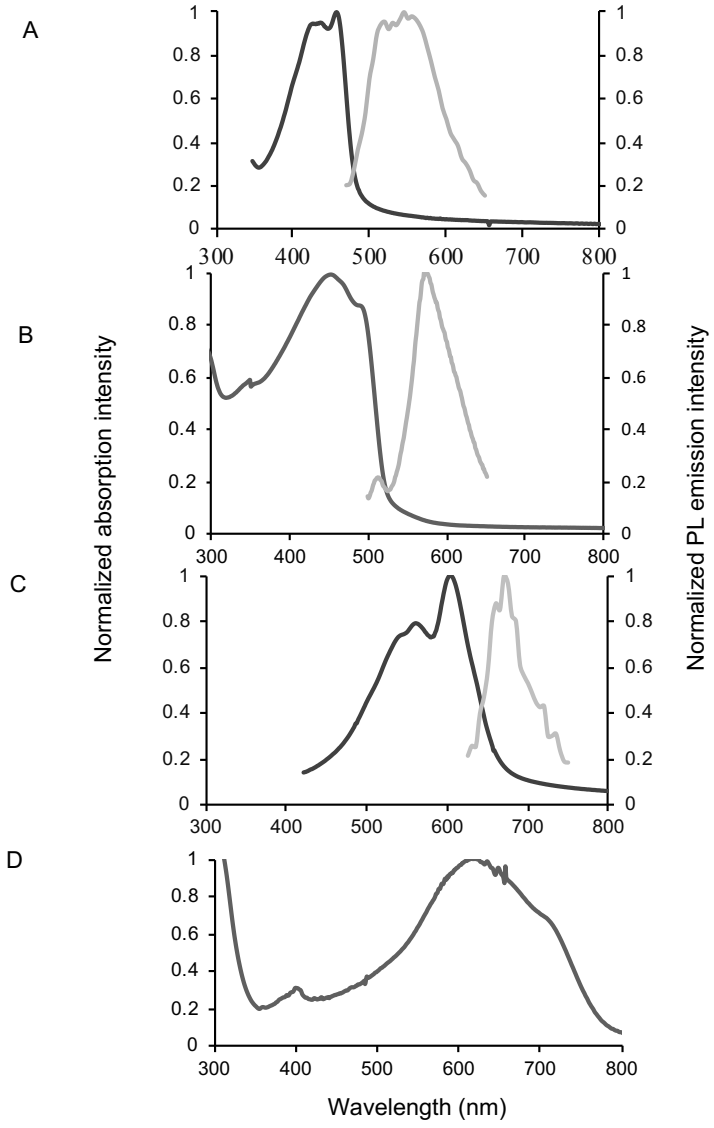

Figure 2.8. Normalized solid state absorption (black) and fluorescence (grey) spectra of polymers: A, **PPPE** (λ_{ex} = 450 nm); B, **PNPE** (λ_{ex} = 495 nm); C, **PAPE** (λ_{ex} = 575 nm); and D, PAE (λ_{ex} = 620 nm).

2.2.5 Fluorescence spectroscopy

The emission spectra of solutions of the polymers in *o*-dichlorobenzene were recorded. Upon excitation at the absorption maximum of the individual polymers, the emission maxima of the polymers shifted to lower energy in progressing from **PPPE** (458 nm), to **PNPE** (499 nm), and to **PAPE** (594 nm). The emission of **PAE** was further red shifted to 674 nm as shown in Figure 2.7. The absolute quantum yields for the four polymers were measured and are reported in Table 1. Notably, the homopolymer **PAE** emits at longer wavelengths (lower energy) of the electromagnetic spectrum indicating that the excited state of the polymer is relatively more stable than the excited state of other three polymers. The fluorescence lifetimes of polymers in solution showed single exponential decay suggesting only one type of specie in excited state as shown in Figure 2.9. For **PPPE** the lifetime was 0.7 ns, for **PNPE** 0.8 ns, for **PAPE** 0.84 ns and for **PAE** it was low 0.2 ns. The low quantum yield and the lifetime of PAE relative to other three polymers, points out that the non-radiative decay rate is relatively more strong than the other three polymers. This is consistent with the energy gap law which states increase in non-radiative decay rate as the energy difference between ground and excited state decreases.

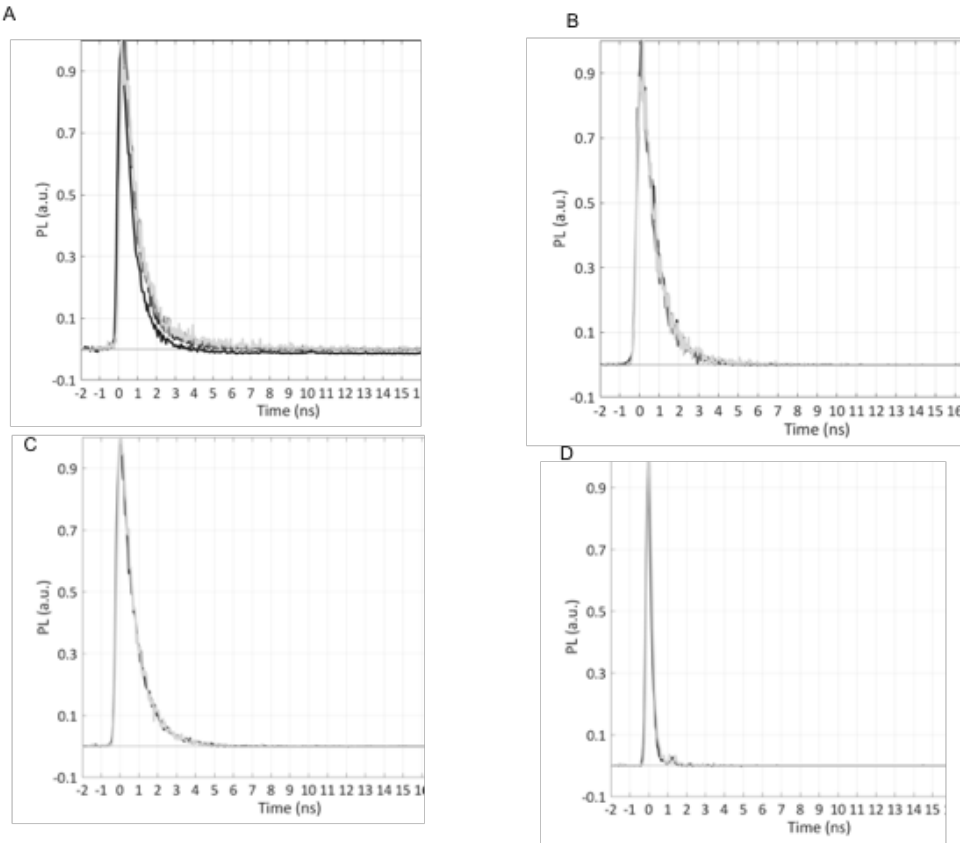

Figure 2.9. Fluorescence life time decay of polymers in *o*-DCB: A, **PPPE** (λ_{ex} = 426 nm); B, **PNPE** (λ_{ex} = 472 nm); C, **PAPE** (λ_{ex} = 566 nm); and D, **PAE** (λ_{ex} = 623 nm).

Solid-state fluorescence spectra were recorded on drop-cast films after they were annealed at 120 ^{o}C for 15 min. As expected, the emission spectra of the copolymers **PPPE** (545 nm), **PNPE** (575 nm) and **PAPE** (670 nm) were all red-shifted compared to their emission in solution, as shown in Figure 2.8 and Table 1. The red shift results from excimer formation in the solid state due to interchain interactions.[12] The emission spectrum of **PPPE** is broad with a maximum at 545 nm, corresponding to a Stokes shift of 88 nm. The lack of sharp features in this emission spectrum suggests a lack of long range order in the solid state, and is consistent with previous report of the emission spectra of films of dialkyl-substituted PPEs.[13] The spectrum of **PNPE** is broad suggesting

amorphous type of morphology , with a maximum at 575 nm and has a small feature at 511 nm. Films of **PAPE** exhibited very weak fluorescence, which can be ascribed to strong interchain interactions that leads to quenching of the excited state. Films of the **PAE** homopolymer did not fluoresce. It is consistent with the observed behavior in solution where the quantum yields and lifetime were significantly low compared to other polymers. In solid state, the non radiative pathways could be more enhanced compared to solution due to interchain interactions. Evidence of aggregation of polymer chains is commonly observed in the solution fluorescence spectra of PPEs. [11, 14] In the fluorescence spectra of **PPPE** and **PNPE** the presence of peaks at 486 nm and 557 nm, respectively, as shown in Figure 2.10, provided preliminary evidence for aggregation. These peaks become more intense upon increasing the concentration of the polymer. We did not observe any long wavelength shoulder in fluorescence spectra **PAPE** and **PAE** suggesting lack of aggregation of these polymers in solution.

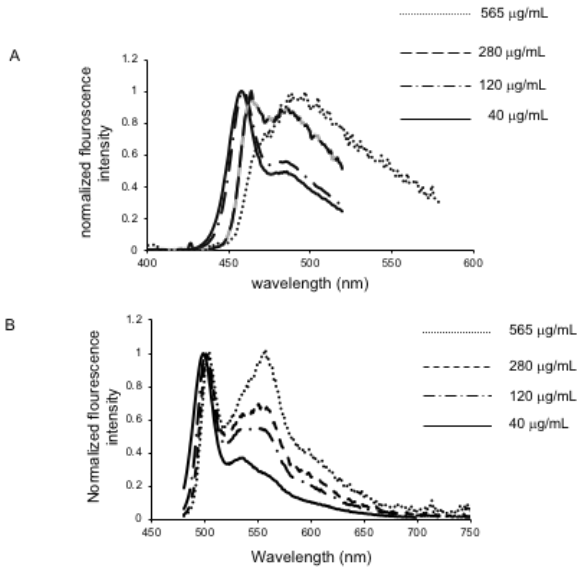

Figure 2.10. Normalized emission spectrum: A; **PPPE** as a function of concentration in o-DCB(λ_{ex} = 428 nm); B, **PNPE** (λ_{ex} = 472 nm).

2.2.6 Thermal properties

The thermal transition of polymers was analyzed by Differential Scanning Calorimetry (DSC). **PPPE** showed a melt transition at 120 °C as shown in Figure 2.11. The other polymers, **PNPE**, **PAPE** and **PAE** showed no melt transition in the DSC. All of the polymers are stable up to 320 °C, as demonstrated by Thermal Gravimetrtic Analysis (TGA), as shown in Figure 2.12.

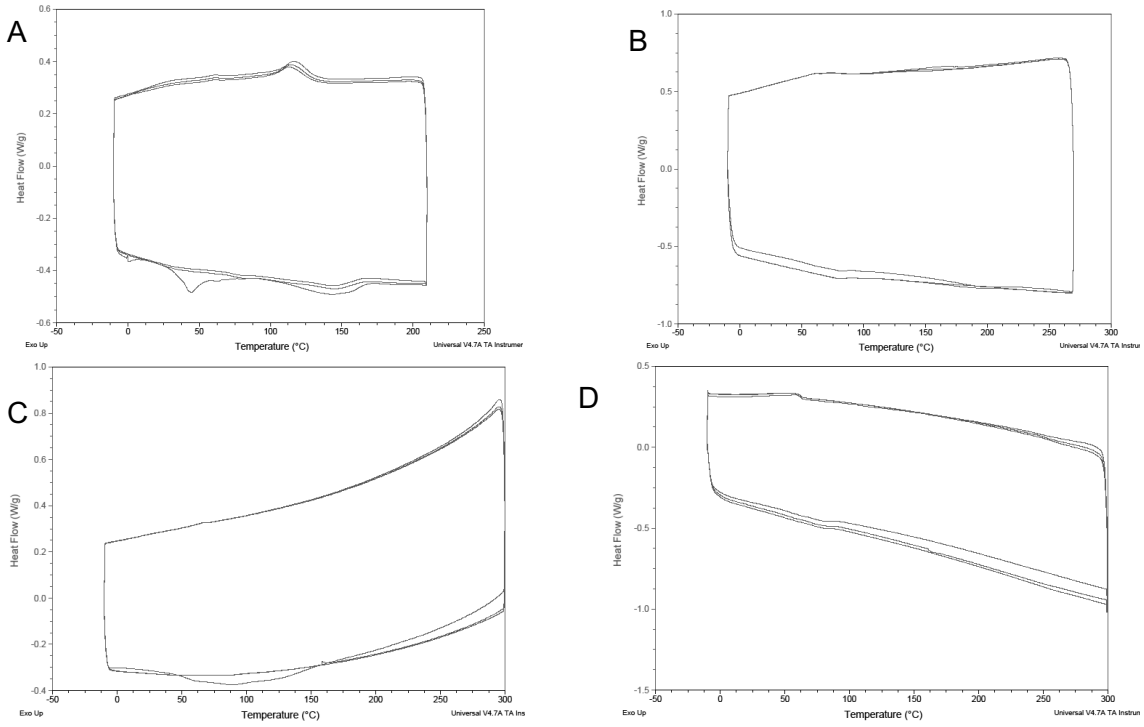

Figure 2.11. Differential Scanning Calorimetry of A. **PPPE**; B, **PNPE**; C, **PAPE**; and D, **PAE** (heating/cooling rate, 10 °C/min).

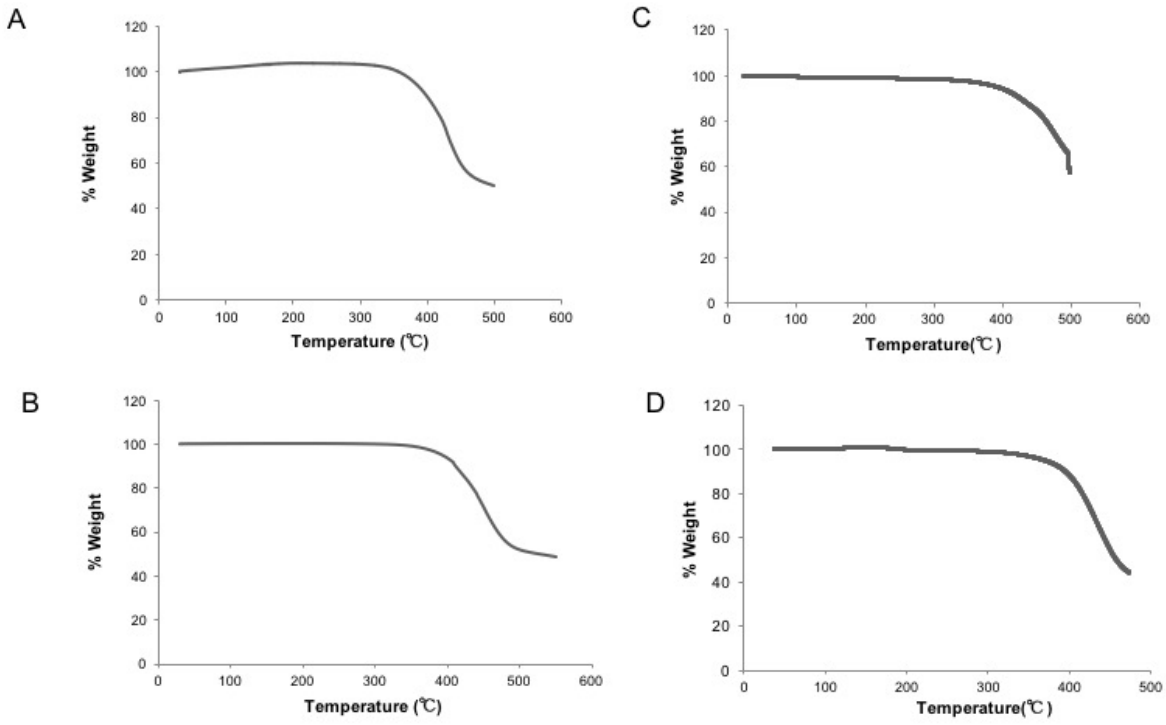

Figure 2.12. Thermogravimetric analysis of: A. PPPE; B, PNPE; C, PAPE; and D, PAE (heating rate, 10 °C/min).

2.2.7 Powder XRD of polymers

The powder x-ray diffractogams of powders of **PAE** and **PPPE** that had been annealed at 100 °C for 12 h are shown in Figure 2.13. The reason for choosing 100 °C is that PPPE has melt transition around 130 °C. Dialkyl PPEs are reported to form films with lamellar order.[15] In all of the polymers mentioned here the 2θ values observed in the range of 2 to 6° corresponds to distances in the range of 25 to 13 Å. These distances correspond to the spacing between adjacent polymer chains separated by linear alkyl chains attached to the backbone, giving rise to lamellar type arrangement. Hence the distances vary with the length of alkyl side chains. **PPPE** showed sharp peak at 2θ of 20.8 ° which correspond to distances of ~4.3 Å. This is amorphous halo corresponds to

close packing of alkyl side chains. These distances ususally lie in the range ~ 4.3 – 5.2 Å depending on the tilt angle of akyl groups with respect to the polymer backbone.[16]

PNPE also showed lamellar stacking peak around 2θ of 5.7° corresponding to the lamellar distance is ~ 21 Å. The broad hump around 18°to 26° is amorphous halo due to presence of alkyl side chains, however it is not as sharp as observed for PPPE. This could be because PPPE melted during annealing which helped in increasing the side chain order in solid state compared to PNPE.

PAPE and PAE showed peaks at 2θ of 5° and 5.7°, coresponding to a *d*-spacing of 17 Å and 15 Å respectively. This is consistent with a lamellar type of packing arrangement described above. The broad peak ranging from 2θ of 19° to 23° is amorphous halo similar to observed for other two polymers.The lack of π-π stacking peaks in the polymers could be because the polymers may not be adopting a planar conformation in the solid state. This is because there is free rotation of aromatic groups around the triple bond resulting in all possible conormations in solution. In solid state it seems that the polymers do not planarize, which could prevent good π-π interactions. If we were to expect π-π stacking peaks it would be in the 3.3-3.5 Å as observed for other conjugated polymers and also for 2,6-di(2-ethylhexyl)-9,10-(bis(trimethylsilylethynyl)anthracene in single crystal strucutre analysis which reveals a π-π stacking distance of 3.363 Å as shown in figure 2.13.

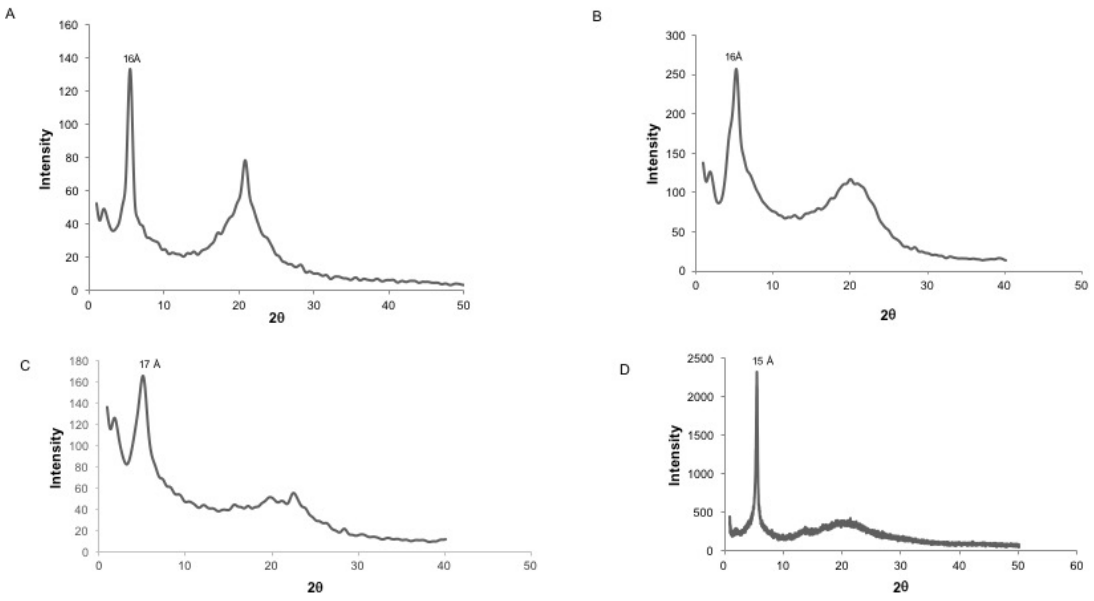

Figure 2.13. Powder XRD spectrum of three polymers. A, PPPE; B, PNPE; C, PAPE and D, PAE.

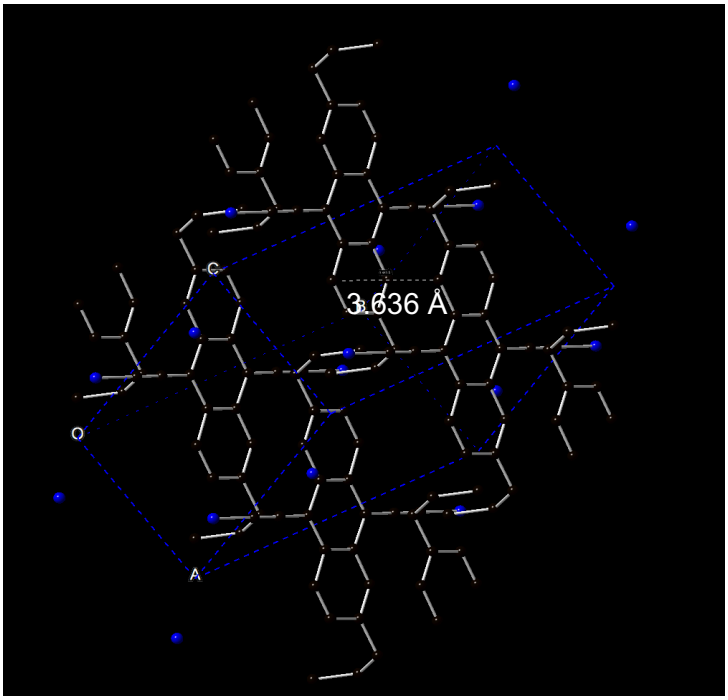

Figure 2.14. Single crystal structure 2,6-di(2-ethylhexyl)-9,10-(bis(trimethylsilylethynyl)anthracene.

2.2.8 GIWAXS studies of thin films

GIWAXS was performed on **PPPE**, **PNPE** and **PAPE** thin films that were spin coated or blade coated. The annealing was done on films to explore the presence of any π-π stacking. GIWAXS pristine of **PPPE** as shown in Figure 2.15 A, consists of only one peak denoted as (100), with a d-spacing of 15.7 Å. This is consistent with the lamellar structure formed by the polymer chains of poly(2,5-dihexyl-1,4-phenylene ethynylene) which has a d-spacing of about 16.2 Å.[15] Annealing did not improve the long range order of the polymer as no higher order peaks appeared in the (h00) direction or (0h0) direction, as evident from Figure 2.15 B. Blade coating of films enhanced the order in polymer chains (Figure 2.15 C and D) as evident from the appearance of higher order (200) and (300) peaks on the z-axis and the presence of a (010) peak at Q_{xy} of 1.6 $Å^{-1}$ which corresponds to a π-π stacking with a d-spacing of 4.2 Å. The π-stacking in phenylene ethynlene type of polymers does not involve direct face to face stacking of two benzene rings. Rather the rings are offset.The direct face to face stacking creates repulsion beween the π- faces of the two benzene rings when stacked on top of each other.[15] The off axis peaks at Q_{xy} 1.5 $Å^{-1}$ in pristine blade coated samples,may be due to the order in the alkyl side chains on the polymer backbone, which are also observed for donor-acceptor polymer of cyclopentadithiophene and benzothiadiazole.[16]

In the case of **PNPE**, spin coating only showed the presence of lamellar stacking (Figure 2.16 B). The spin-coated films of **PNPE** were all thermally annealed at 150 ^{o}C in a glove box for 5 h. Such thermal annealing treatment did not show enhancement of the film order. Blade coating of **PNPE** films showed some success in orienting polymer chains along the blade coating direction. This can be seen by an increase in the intensity o

of higher order of peaks (200) and (300) and disappearance of isotropic halo contributed from side chains, when the sample is viewed perpendicular to the blade coating direction. The side chains do not seem to form diffraction planes when viewed perpendicular to blade coating direction. (Figure 2.16 E,F).

PAPE spin coated films showed a faint (200) peak in addition to a strong (100) peak in both the pristine and annealed films as shown in Figure 2.17. This indicates that the thermal annealing treatment slightly improved the order in **PAPE** polymer. The films showed some lamellar order on blade coating. The lack of long range order is also evident from the DSC which shows lack of melt transition peak.

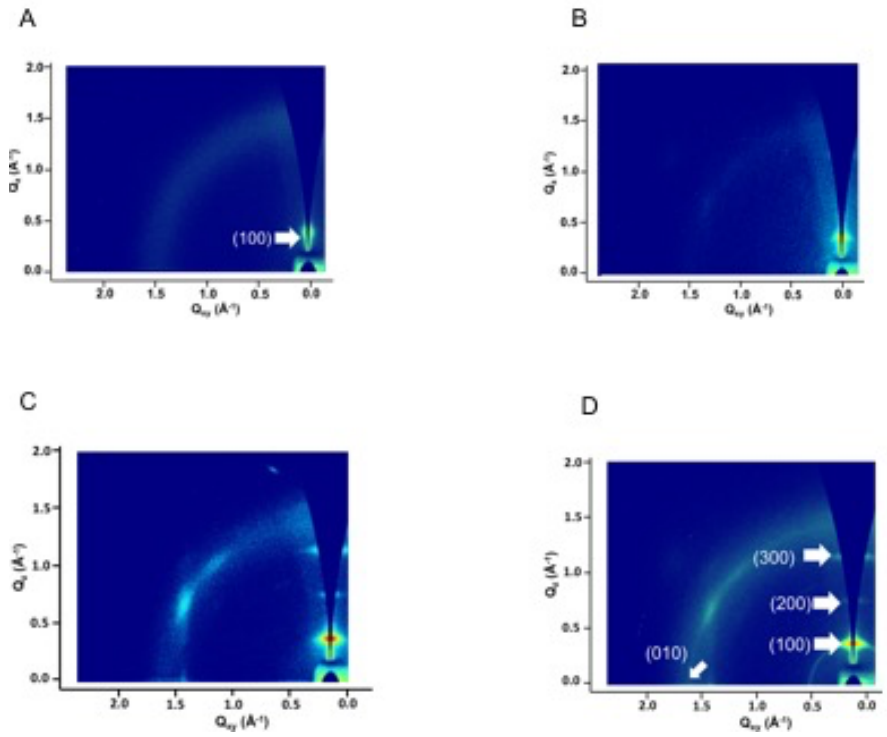

Figure 2.15. GIWAXS images of PPPE: A, pristine spin coated film; B, annealed spin coated film; C, pristine blade coated film (oriented perpendicular to blade coated direction); and D, pristine blade coated film (oriented parallel to blade coated direction)

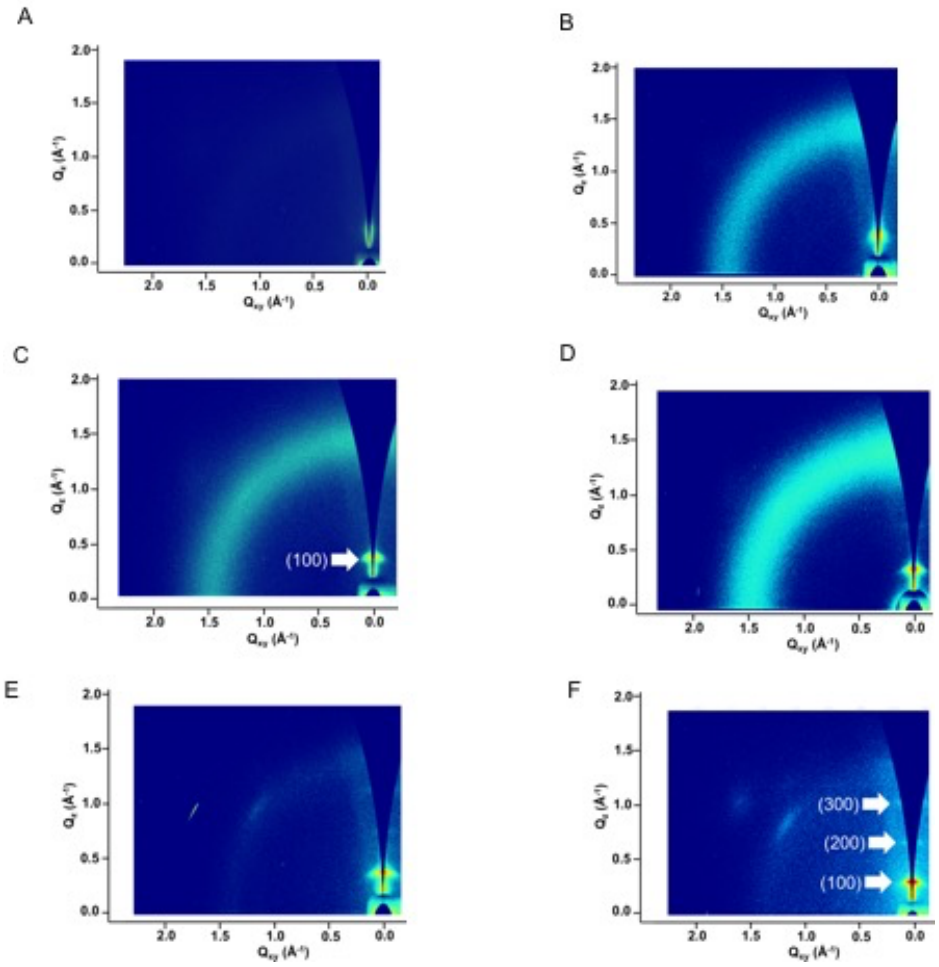

Figure 2.16. GIWAXS of **PNPE**: A, pristine spin coated film; B, annealed spin coated film; C, pristine blade coated film (oriented parallel to blade coating direction); D, annealed blade coated film (oriented parallel to blade coating direction); E, pristine blade coated film (oriented perpendicular to blade coating direction) ; F,annealed blade coated film (oriented perpendicular to blade coating direction)

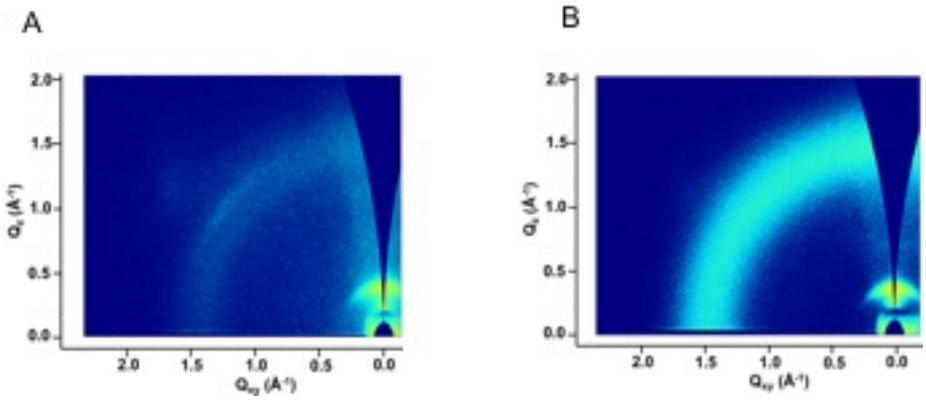

Figure 2.17. GIWAXS of **PAPE**: A, pristine spin coated film; B, annealed spin coated film

2.2.9 Raman Spectroscopy

Raman spectroscopy has a significant role in demonstrating the nature of bonding in the backbone of conjugated polymers by virtue of its sensitivity to vibrations associated with non-polar bonds.[17] For example, in the case of poly(2,5-dodecyloxy-1,4-phenylene ethynylene)s the carbon-carbon triple bond stretching frequency varies with conjugation length.[18] The C≡C stretching frequency of the polymer (2196 cm^{-1}) is lower than the corresponding trimer (2207 cm^{-1}). This shift to lower frequency in the polymer suggests weakening of the acetylenic bond with increasing conjugation length. This may be accounted for by a greater extent of double bond character by virtue of contributions from the quinoid form of the conjugated backbone.

The C≡C bond stretching frequency decreaseed upon proceeding from **PPPE** (2192 cm^{-1}) to **PNPE** (2188 cm^{-1}) and **PAPE** (2170 cm^{-1}) upon the introduction of flanking benzene rings fused onto one side, and then both sides, of the conjugated backbone (Figure 2.18). The significant decrease in the C≡C stretching frequency for **PAPE** suggests that the conjugated backbone of the 9,10-anthracenediyl containing

polymer possess significantly more quinoid character by virtue of the presence of two fused benzene rings which retain their aromaticity in the quinoid form, as shown in Figure 2.19. This provides the C≡C bond with more double bond character and a lower stretching frequency. The homopolymer **PAE** shows a further decrease in the C≡C stretching frequency to 2140 cm^{-1}.

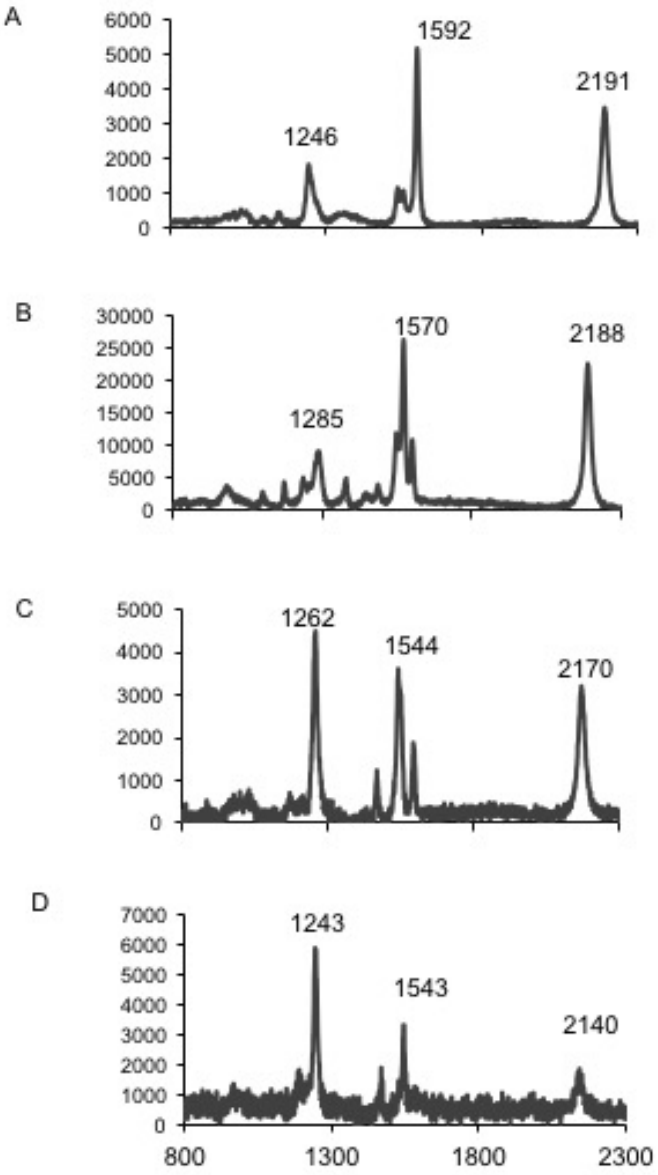

Figure 2.18. Raman spectroscopy: A, **PPPE**; B, **PNPE**; C, **PAPE**; and D, **PAE**.

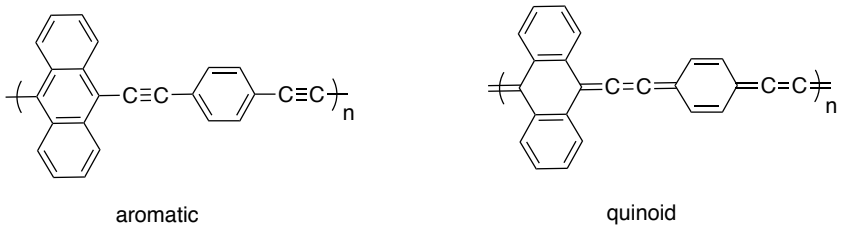

Figure 2.19 Aromatic and quinoid forms of **PAPE**.

2.3 CONCLUSIONS

We have synthesized a series of poly(arylene ethynelene)s that contain 1,4-phenylene, 1,4-naphthalene and 9,10-anthracene units. The incorporation of naphthalene and anthracene led to the promotion of quinoid character in the conjugated polymer. The UV-visible spectroscopy shows the decrease in the optical band gap upon the fusion of one benzene ring to the phenylene ring in the conjugated backbone (i.e., in **PNPE**), and a greater decrease upon fusion of a second ring (i.e., **PAPE)**. Raman spectroscopy suggests that fusion of rings on the backbone lowers the C≡C bond order. A decrease in bond order, with promotion of double bond character reflects an increase of quinoidal character to the electronic structure of the polymer backbone.

2.4 EXPERIMENTAL SECTION

2.4.1 Materials

[1,3-Bis(diphenylphosphino)propane]dichloronickel(II), $[(C_6H_5)_2P(CH_2)_3P(C_6H_5)_2]NiCl_2$, bis(triphenylphosphine)palladium(II) dichloride $[(C_6H_5)_3P]_2PdCl_2$, copper iodide (CuI), iodine, potassium periodate (KIO_4), trimethylsilylacetylene, *n*-hexylmagnesium bromide (2 M in Et_2O), *n*-butyllithium (2.5 M in hexane), triflouroacetic anhydride, *tert*-butyl nitrite, anhydrous zinc(II) chloride ($ZnCl_2$), tetra-*n*-butylammonium difluorotriphenylsilicate (TBAT), tin(II) chloride dihydrate, copper (II) bromide, 1,4-dichlorobenzene, *p*-benzoquinone and anhydrous diisopropylamine (DPA) were purchased from Sigma Aldrich. 3,4-Dibromothiophene was purchased from Accela ChemBio. All the reagents were used as purchased without further purification.

2.4.2 Characterization

The molecular weights of polymers were determined by size exclusion chromatography (SEC) using 1,3,4-trichlorobenzene as the eluent and refractive index (RI) detector at 130 °C, against polystyrene standard. UV-Vis measurements were recorded on an Agilent 8510 instrument. Electrochemical measurements were done in a three -electrode cell with a Pt flag as the counter electrode, a Ag/Ag^+ standard electrode which had $E_{1/2}$ vs ferrocene ~ 58 mV and a polymer-coated glassy carbon button as a working electrode. The electrolyte was 10 mM $AgNO_3$ in 0.5 M $TBAPF_6$ in acetonitrile. The films were dropcast from a solution in chlorobenzene. NMR

spectra were recorded in chloroform for all the compounds except PAPE which was in chlorobenzene using a Varian Mercury spectrometer (^{1}H NMR, 300 MHz, ^{13}C, 75 MHz). IR spectra were recorded using a Bruker ALPHA FT-IR spectrometer. Fluorescence measurements of thin films were measured using a QuantaMaster 40 fluorimeter on solutions of the polymers having an absorbance of less than 0.1. The thin films were spin coated from a solution if chlorobenzene with a concentration of about 5 mg/mL for all the three polymers. The solution fluorescence and quantum yield measurements were performed on Hamamatsu absolute PL quantum yield spectrometer C11347. Time-resolved Photoluminescence spectroscopy measurements were performed using an ultrafast laser system (Pharos - Model PH1-20-0200-02-10, Light Conversion, Lithuania) emitting 1030-nm pulses at 100 KHz, with an output power of 20W and pulse duration of around 220 fs. A commercial optical parametric amplifier (Orpheus, Light Conversion, Lithuania) was used to generate pump wavelengths in the visible range. PL emitted by the sample was collected in reflectance geometry using a silver parabolic mirror. Detection was achieved through imaging spectrograph (Shamrock 193i, Andor Technology Ltd., UK) in combination with a photomultiplier tube (Becker&Hickl DCC-100, Germany) and with time-correlated single-photon counting electronic board (Becker&Hickl SPC-130, Germany). Differential Scanning Calorimetry (DSC) measurements were performed on Q200 TA instrument with 10°C/min scan rate. Thermogravimetric measurements. (TGA) were performed on Perkin Elmer Pyris 1 TGA, with scan rate of 10°C/min.

2.4.3 Synthetic procedures

2.4.3.1 1,4-Dihexylbenzene, 2[1]

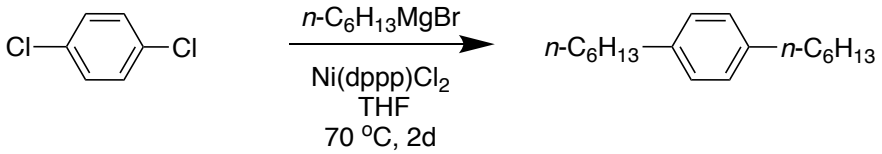

1-Hexylmagnesium bromide (75 mL of a 2 M solution in Et_2O, 150 mmol) was added dropwise to the solution of 1,4-dichlorobenzene (10.0 g, 68.0 mmol) in THF (170 mL) under N_2. $Ni(dppp)Cl_2$ (368 mg, 680 μmol) was added and the mixture was heated at 50 °C for 48 h. H_2O (100 mL) was added and the mixture was extracted with CH_2Cl_2 (4 × 100 mL). The solvent was removed under reduced pressure and the residue was dried under vacuum to afford the product as a colorless oil which was used without further purification (15.42 g, 92%). ^1H NMR (300 MHz, $CDCl_3$): δ 7.10 (s, 4H, Ar–H), 2.60 (t, J = 6 Hz, 4H, Ar–CH_2) , 1.60 (p, J = 6 Hz, 4H, β-CH_2), 1.30 (m, 12H), 0.90 (t, J = 6 Hz, 6H, –CH_3). The spectral data matches that present in reference 1

2.3.3.2. 1,4-Dioctyloxybenzene, 5[19]

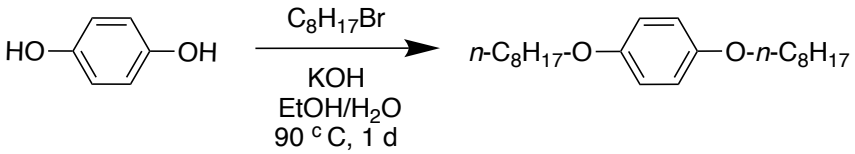

Hydroquinone (6.0 g, 54 mmol) was added to the solution of 1-bromooctane (23.5 mL, 136 mmol) and potassium hydroxide (9.22 g, 164 mmol) in a mixture of EtOH (182 mL) and H_2O (20 mL). The mixture was heated at reflux for 24 h. Upon cooling, an off-white solid precipitated that was isolated by filtration. Recrystallization from EtOH (60

mL) gave the product as a colorless solid (15.0 g, 82% yield). ^{1}H NMR (300 MHz, $CDCl_3$): δ 6.75 (s, 4H, Ar–H), 3.96 (t, *J* = 6Hz, 4H, Ar–CH_2), 1.75 (p, *J* = 6Hz, 4H, β-CH_2), 1.4-1.2 (m, alkyl, 20 H), 0.80 (t, *J* = 6 Hz, 6H, –CH_3). The spectral data matches that present in reference 1

2.3.3.3. 1,4-Diiodo-2,5-dioctyloxy-benzene, 6[19]

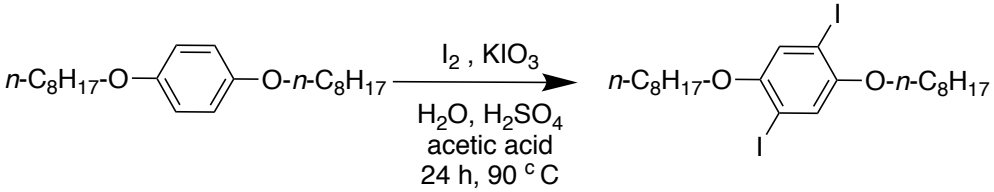

1,4-Dioctyloxybenzene (1.0 g, 3.0 mmol), iodine (636 mg, 2.50 mmol), KIO_3 (266 mg, 1.20 mmol), H_2SO_4 (0.3 mL) and H_2O (3 mL) were added to acetic acid (10 mL) and the mixture was heated at 65-70 °C for 24 h under air. The solution was poured into 10% m/v aqueous $Na_2S_2O_3$ (60 mL) and the mixture was stirred for 15 min. The mixture was extracted with CH_2Cl_2 (4 ×10 mL) and the solvent was removed under reduced pressure. The residue was recrystallized from EtOH to afford 1,4-dioctyloxy-2,5-diiodobenzene as a colorless solid (1.0 g, 50% yield). ^{1}H NMR (300 MHz, $CDCl_3$): δ 7.60 (s, 2H, Ar–H), 2.58 (t, *J* = 6 Hz, 4H, Ar–CH_2), 1.60 (p, *J* = 6 Hz, 4H, β-CH_2), 1.4-1.2 (m,12H), 0.80 (t, *J* = 6 Hz, 6H, -CH_3). The spectral data matches that present in the reference 19.

2.3.3.4. 1,4-Dioctyloxy-2,5-bis(trimethylsilylethynyl)benzene, 7[19]

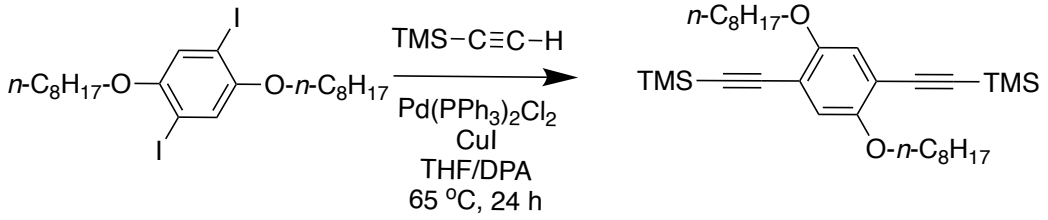

A mixture of 1,4-diiodo-2,5-dioctyloxy benzene (1.00 g, 1.71 mmol), $Pd(PPh_3)_2Cl_2$ (60 mg, 85 μmol), CuI (32 mg, 0.17 mmol) anhydrous THF (35 mL) and anhydrous diisopropyl amine (87 mL) was stirred under Ar at room temperature for 40 min. Trimethylsilylacetylene (0.52 mL, 3.7 mmol) was added dropwise and the mixture was heated at reflux for 2 d. Distilled water (75 mL) was added and the organic phase was extracted with CH_2Cl_2 (75 mL). The solvent was removed under reduced pressure and the residue was recrystallized from acetone to afford 1,4-dihexyl-2,5-bis(trimethylsilylethynyl)benzene as a solid brown in color (0.540 g, 60 % yield). ^{1}H NMR (300 MHz, $CDCl_3$): δ 6.90 (s, 2H, Ar–H), 3.94 (t, J = 6 Hz, 4H, OCH_2), 1.80 (p, J = 6 Hz, 4H, β-CH_2), 1.5-0.9 (m, 26 H), 0.30 (s, 18H, $SiCH_3$). The spectral data matches that present in reference 21

2.3.3.5. 1,4-Dihexyl-2,5-diiodobenzene, 3[1]

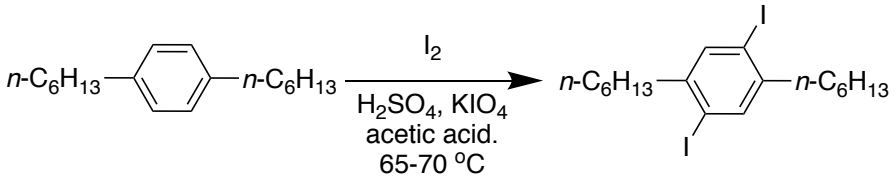

1,4-Dihexylbenzene (1.0 g, 4.0 mmol), iodine (1.2 g, 4.9 mmol), KIO_4 (560 mg, 2.40 mmol), H_2SO_4 (0.4 mL) and H_2O (0.4 mL) were added to acetic acid (8 mL) and the mixture was heated at 65-70 °C for 24 h under air. The solution was poured into 10% m/v aqueous $Na_2S_2O_3$ (60 mL) and the mixture was stirred for 15 min. The mixture was

extracted with CH_2Cl_2 (4 × 10 mL) and the solvent was removed under reduced pressure. The residue was recrystallized from EtOH to afford 1,4-dihexyl-2,5-diiodobenzene as a colorless solid (1.0 g, 50% yield). ^{1}H NMR (300 MHz, $CDCl_3$): δ 7.60 (s, 2H, Ar–H), 2.58 (t, J = 6 Hz, 4H, Ar–CH_2), 1.60 (p, J = 6 Hz, 4H, β-CH_2), 1.4-1.2 (m, 12H), 0.80 (t, J = 6 Hz, 6H, –CH_3). m.p.: 49-50 °C (lit:[1] 50 °C). The spectral data matches that present in reference 1.

2.3.3.6. 1,4-Dihexyl-2,5-Bis(trimethylsilylethynyl) benzene[1]

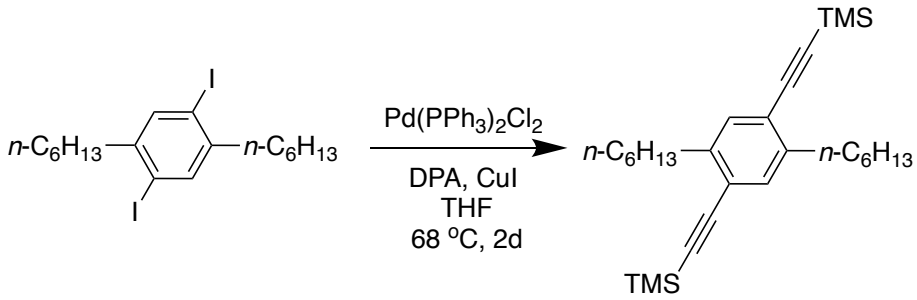

A mixture of 1,4-dihexyl-2,5-diiodobenzene (2.00 g, 3.83 mmol), $Pd(PPh_3)_2Cl_2$ (81 mg, 0.11 mmol), CuI (36 mg, 0.19 mmol) and triphenylphosphine (80 mg, 0.30mmol) in anhydrous THF (14 mL) and anhydrous *N*,*N*-diisopropylamine (41 mL) was stirred under Ar at room temperature for 40 min. Trimethylsilylacetylene (1.2 mL, 8.4 mmol) was added dropwise and the mixture was heated at reflux for 2 d. Distilled water (75 mL) was added and the organic phase was extracted with CH_2Cl_2 (3 × 50 mL). The solvent was removed under reduced pressure and the residue was recrystallized from acetone to afford 1,4-bis(trimethylsilylethynyl)-2,5-dihexylbenzene as a pale yellow solid (0.744 g, 45 % yield). ^{1}H NMR (300 MHz, $CDCl_3$): δ 7.22 (s, 2H, Ar–H), 2.84 (t, J = 6 Hz, 4H, Ar-CH_2), 1.80 (p, J = 6 Hz, 4H, β-CH_2), 1.5-0.9 (m, 26 H), 0.30 (s, 18H, $SiCH_3$). m.p.: 46-47 °C (lit:[1] 44 °C). The spectral data matches that present in reference 1.

2.3.3.7. 3,4-Dibromothiophene-1,1-dioxide, 9[2]

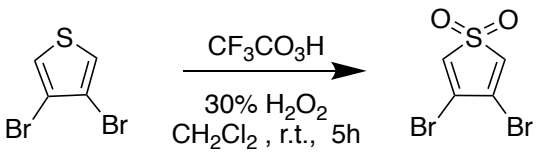

Trifluoroacetic anhydride (30.0 mL, 248 mmol) was added dropwise to a solution of H_2O_2 (30% w/w in H_2O) (11.3 mL, 124 mmol) at −10 °C. After 10 min at 0 °C, a solution of 3,4-dibromothiophene (3.00 g, 12.4 mmol) in CH_2Cl_2 (50 mL) was added. The mixture was allowed to warm to room temperature and it was stirred for 5 h. The reaction mixture was poured into aqueous 5% (w/v) $NaHCO_3$ (80 mL). The mixture was extracted with CH_2Cl_2 (3 × 60 mL) and the solvent was removed under reduced pressure to afford an orange residue. Recrystallization from a 1:1 v/v mixture of $CHCl_3$ and ethanol gave 3,4-dibromothiophene-1,1-dioxide as a yellow solid(1.70 g, 50% yield). ^1H NMR ($CDCl_3$, 300 MHz): δ 6.84 (s). m.p.: 99-100 °C (lit.[2] 103-104 °C). The spectral data matches that present in reference 2

2.3.3.8. 6,7-Dibromo-1,4-naphthaquinone, 10[3]

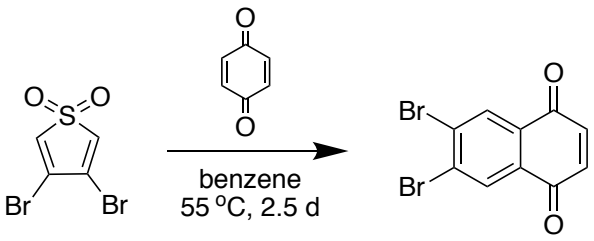

A solution of 3,4-dibromothiophene-1,1-dioxide (500 mg, 2.00 mmol) and benzoquinone (99 mg, 10 mmol) in benzene (2.3 mL) was heated at 55 °C for 68 h. The solvent was removed under reduced pressure and the residue was stirred with a 1:1 v/v mixture of methanol and 30% H_2O_2 (35 mL) for 90 min. The mixture was filtered to give

a pale brown solid (176 mg). Recrystallization of 135 mg of the solid from MeOH/$CHCl_3$ (12 mL of MeOH and 5 mL of $CHCl_3$) afforded 6,7-dibromo-1,4-naphthaquinone as a pale orange solid (80 mg, 13 % yield). ^{1}H NMR ($CDCl_3$, 300 MHz): δ 8.30 (s, 2H, Ar–$H_{5,8}$), 7.00 (s, 2H, Ar-$H_{2,3}$). m.p.: 180-182 °C (lit:[3] 171-173 °C). The spectral data matches that present in reference 3

2.3.3.9. 6,7-Dibromo-1,4-bis(trimethylsilylethynyl)naphthalene, 12

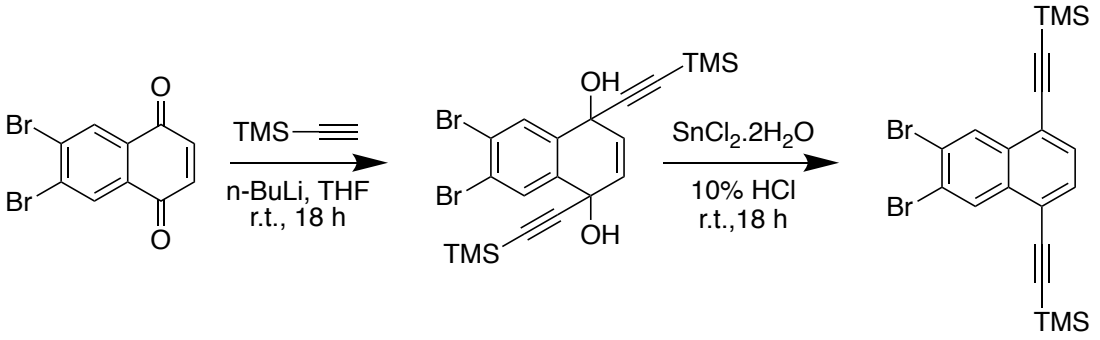

A solution of *n*-butyllithium (1.7 mL of a 2.5 M solution in Et_2O, 4.4 mmol) was added to a solution of trimethylsilylacetylene (0.80 mL, 5.5 mmol) in THF (16 mL) and the mixture was stirred for 90 min under Ar. 6,7-Dibromo-1,4-naphthaquinone (500 mg, 1.58 mmol) was added and the mixture was stirred for 18 h. A saturated solution of $SnCl_2.2H_2O$ in 10% aqueous HCl solution (10 mL) was added and the mixture was stirred at room temperature for 24 h. Water (75 mL) was added and the mixture was extracted with CH_2Cl_2 (3 × 25 mL). The solvent was removed under reduced pressure and the residue was triturated in hot CH_2Cl_2 (50 mL) to afford the product as dark brown powder (315 mg, 50% yield). ^{1}H NMR (300 MHz, $CDCl_3$): δ 8.60 (s, 2H, Ar–$H_{5,8}$) ,7.60 (s, 2H, Ar–$H_{2,3}$), 0.40 (s, 18H, TMS). ^{13}C NMR (75 MHz, $CDCl_3$): 132.85, 131.38, 131, 124.19, 120.67 (aromatic), 102.91, 101.61 (C≡C), o (TMS group); (FT-IR (neat): 2150

(C≡C str.), 1460 cm^{-1} (aromatic C=C str.). GC-MS (EI): 477 (M^+), 479 (M+2), 475 (M-2), 73 (trimethylsilyl). m.p.: 174-176 °C.

^{1}H NMR of 6,7-Dibromo-1,4-bis(trimethylsilylethynyl)naphthalene, ***12***

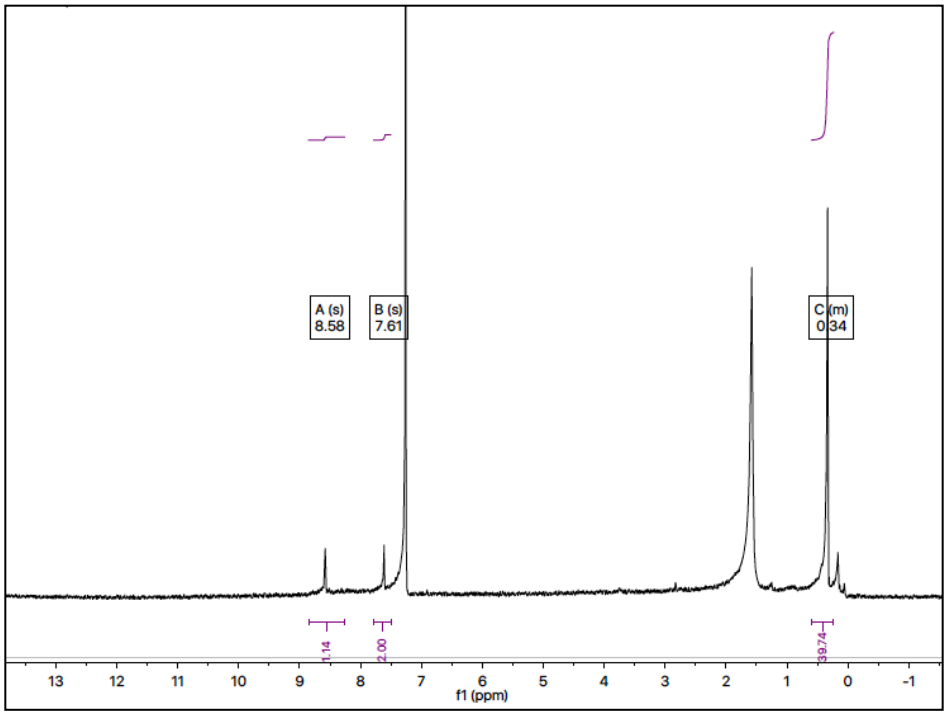

^{13}C NMR of 6,7-Dibromo-1,4-bis(trimethylsilylethynyl)naphthalene, ***12***

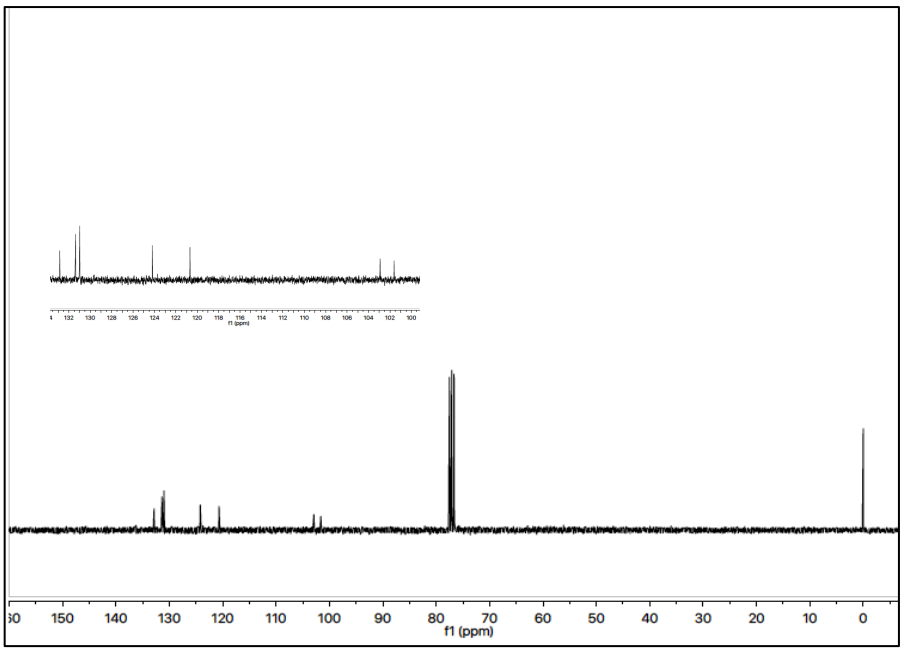

IR spectrum of 6,7-Dibromo-1,4-bis(trimethylsilylethynyl)naphthalene, ***12***

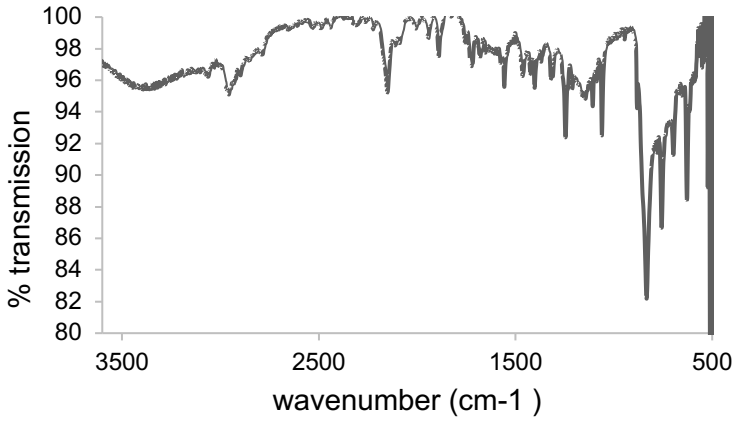

MS spectrum (inset: simulation of molecular ion cluster) of ***12***

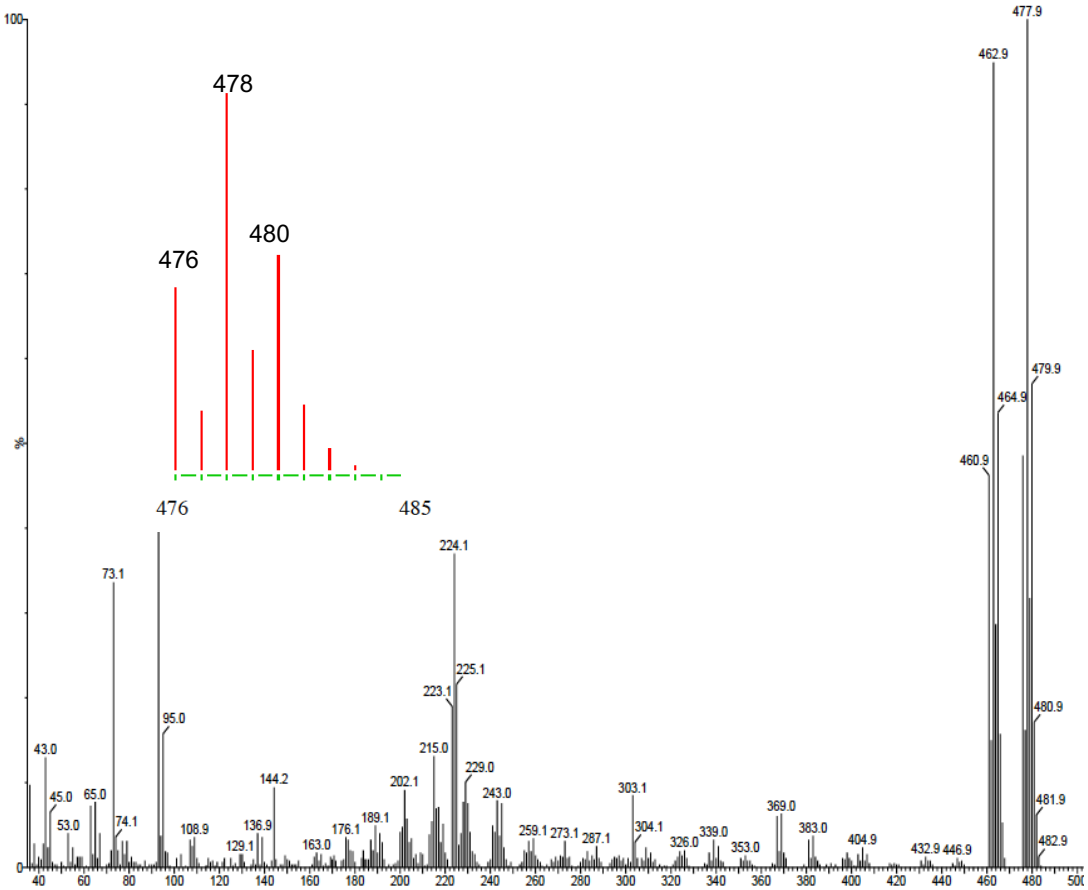

2.3.3.10. 6,7-Dihexyl-1,4-bis(trimethylsilylethynyl)naphthalene, 13

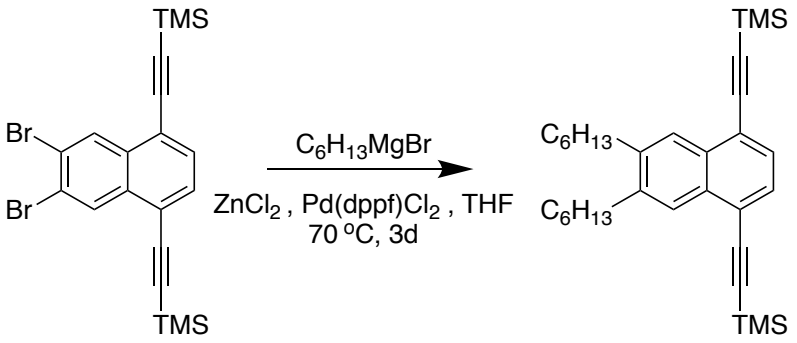

Anhydrous zinc(II) chloride (2.56 g, 18.8 mmol) and *n*-hexylmagnesium bromide (8.40 mL of a 2M solution in Et_2O, 16.8 mmol) were added to dry THF (52 mL) under Ar and the mixture was stirred for 1.5 h. 6,7-Dibromo-1,4-bis(trimethylsilylethynyl)naphthalene (2.0 g, 4.2 mmol) and $Pd(dppf)Cl_2$ (103 mg, 42.0 μmol), were added and the mixture was stirred for 48 h at 55-60 °C. Distilled H_2O (120 mL) was added and the mixture was extracted with CH_2Cl_2 (100 mL). The solvent was removed under reduced pressure and the residue was subjected to column chromatography (hexane, silica gel). The product was recrystallized from acetone to afford the title compound as a yellow solid (116 mg, 5.6% yield). ^{1}H NMR (300 MHz, $CDCl_3$): δ 8.00 (s, 2H, Ar–$H_{5,8}$), 7.44 (s, 2H, Ar–$H_{2,3}$), 2.80 (t, *J* = 6 Hz, 4H, Ar–CH_2), 1.70 (t, *J* = 6 Hz, 4H, β-CH_2), 1.20-1.40 (m, 18H, –CH_2), 0.80 (t, J = 6Hz, –CH_3), 0.30 (18H, TMS) ; FT-IR (neat): 2139 (C≡C str.), 2910 (cm^{-1}) (sp^3 C–H str.), 1436 cm^{-1} (aromatic C=C str.). ^{13}C (75 MHz, $CDCl_3$): 140, 132, 130, 126, 120 (Ar), 114, 112 (C≡C), 34, 32, 30, 29, 23, 14 (hexyl), 0 (TMS group). MS (EI): *m*/*z* 488 (M^+), 347 (M-C_5H_{11})$^+$. m.p.: 45-47 °C. Anal. Calcd. ($C_{32}H_{48}Si_2$): C, 78.61; H, 9.90. Found C, 78.73; H, 10.05.

[1]H NMR 6,7-Dihexyl-1,4-bis(trimethylsilylethynyl)naphthalene, ***13***

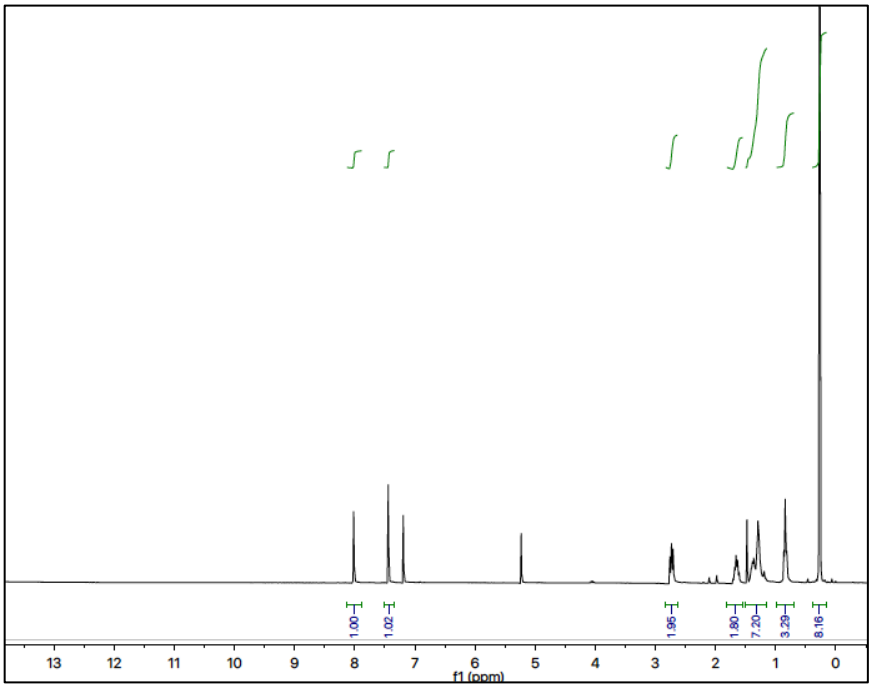

[13]C NMR of 6,7-Dihexyl-1,4-bis(trimethylsilylethynyl)naphthalene, ***13***

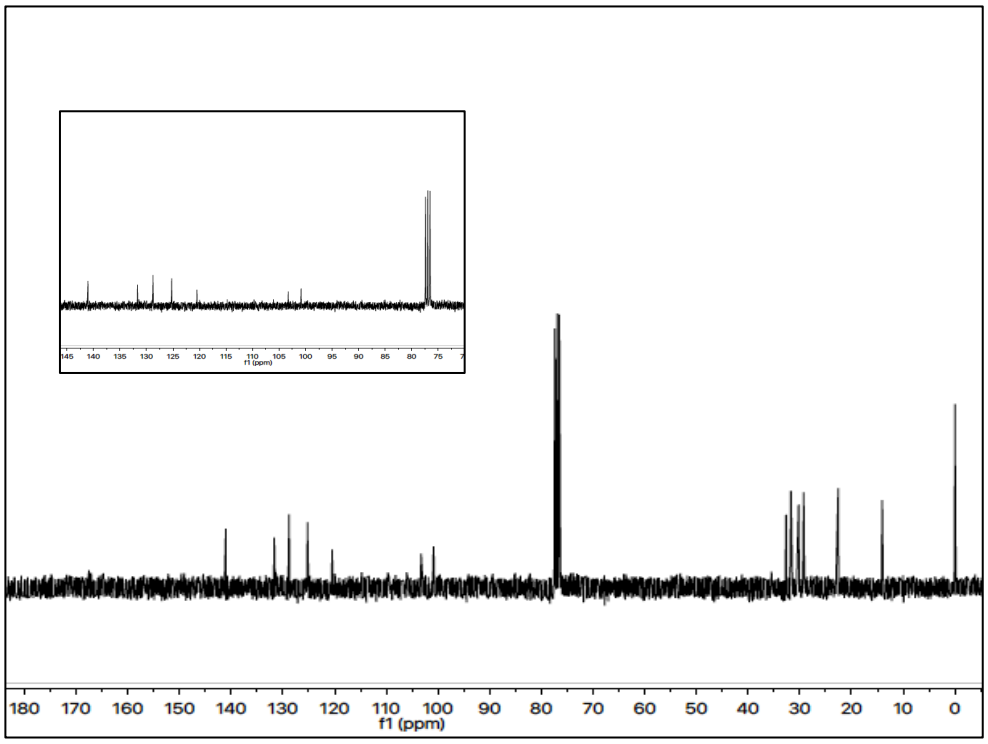

IR spectrum of 6,7-Dihexyl-1,4-bis(trimethylsilylethynyl)naphthalene, ***13***

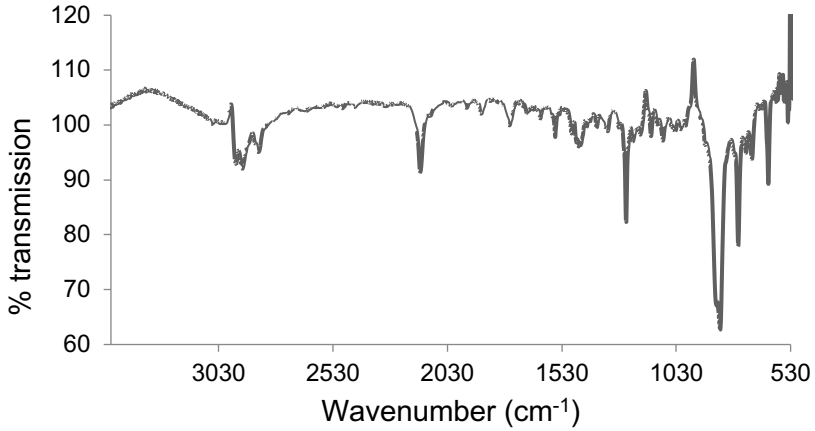

MS spectrum (inset: simulation of molecular ion cluster) of ***13***

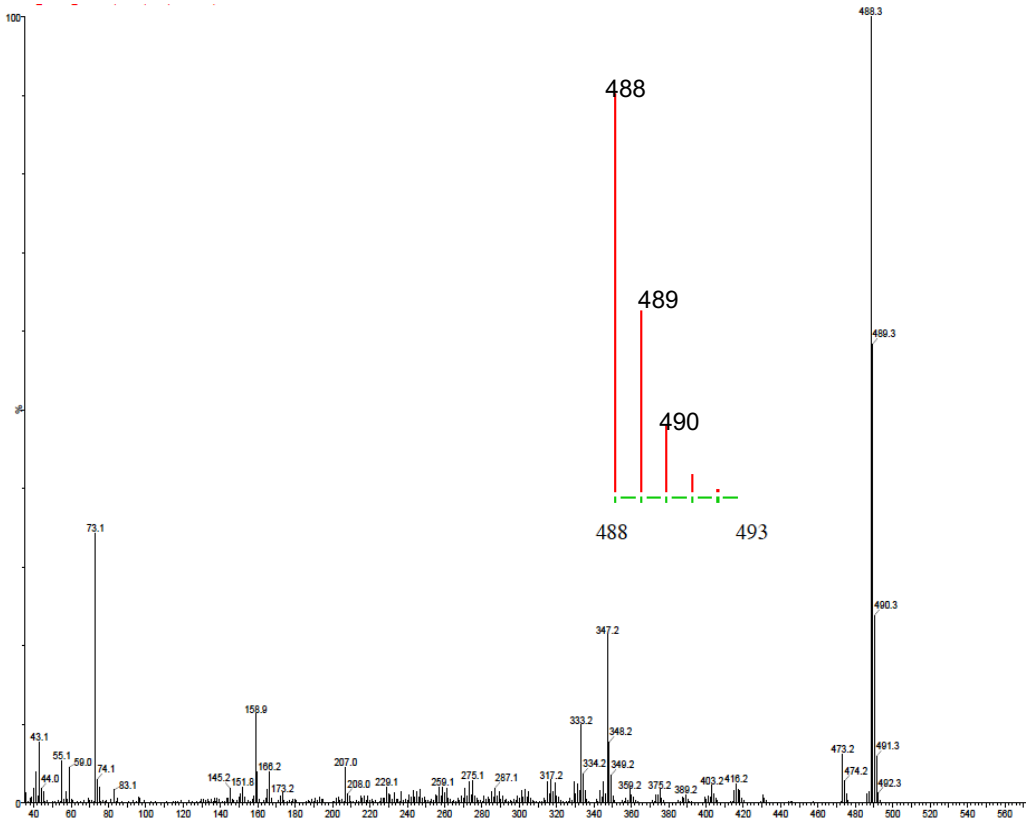

2.3.3.11. 2,6-Dibromoanthraquinone, 14[4]

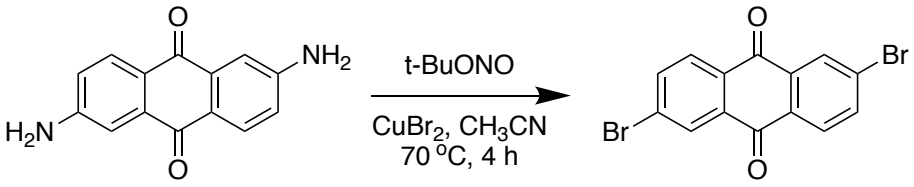

2,6-Diamino-9,10-anthraquinone (300 mg, 1.20 mmol) was added to a solution of *tert*-butyl nitrite (0.32 g, 3.1mmol) and copper(II) bromide (700 mg, 3.10 mmol) in acetonitrile (6.0 mL) under Ar. The solution was heated at 65 °C for 2 h. Aqueous HCl (2M, 6.0 mL) was added and a pale brown solid precipitated. The solid was collected by filtration and washed with cold MeOH to afford the product as a pale brown solid that was used without further purification (0.41 g, 90 % yield). ^{1}H NMR (300 MHz, $CDCl_3$): δ 8.42 (d, J = 2 Hz, 2H, Ar–$H_{1,5}$) 8.16 (d, J = 9 Hz, 2H, Ar–$H_{4,8}$) ,7.94 (dd, J = 9, 2 Hz, 2H, Ar–$H_{3,7}$); FT-IR (neat): 1573 (Ar C=C str.1678 cm^{-1} (C=O str.), MS (EI): m/z 365.9 (M^+), 367.9 (M+2), 363.9 (M-2), 285 (M-Br). m.p.: 286-288 °C. The spectral data matches that present in reference 4.

2.3.3.12. 2,6-Dibromo-9,10-bis(trimethylsilylethynyl)anthracene, 17[5]

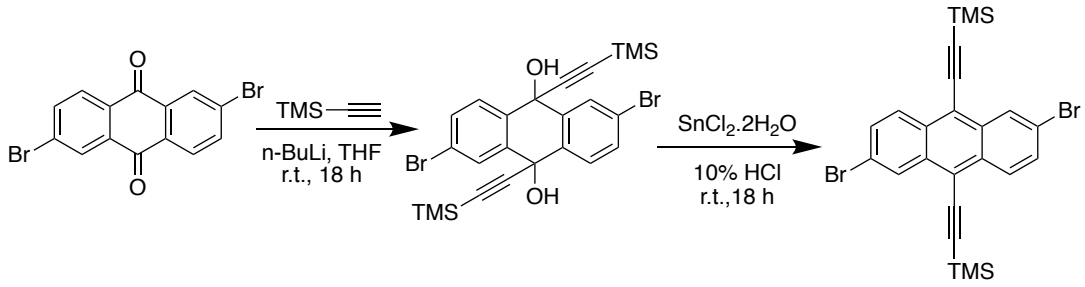

n-BuLi (50 mL of a 1.6 M solution in hexane, 80 mmol) was added to a solution of trimethylsilylacetylene (16.2 mL, 117 mmol) in dry THF (231 mL) at 0 °C under Ar and the mixture was stirred for 2 h. 2,6-Dibromo-9,10-anthraquinone (6.0 g, 16 mmol) was added and the mixture was stirred for 18 h to afford a maroon solution. $SnCl_2 \bullet 2H_2O$ (14.2 g, 62.9 mmol) and 10% H_2SO_4 (28 mL) were added and the solution was stirred for 24 h. H_2O (100 mL) was added and the mixture was extracted with CH_2Cl_2 (50 × 2 mL). The solvent was removed under reduced pressure and the residue was recrystallized from acetone to afford the 2,6-dibromo-9,10-bis(trimethylsilylethynyl)anthracene as an orange solid (3.0 g, 35%, yield). ^{1}H NMR (300 MHz, $CDCl_3$): δ 8.57 (d, J = 3 Hz, 2H, Ar–$H_{1,5}$), 8.30 (d, J = 9 Hz, 2H, Ar–$H_{4,8}$), 7.58 (dd, J = 9,3 Hz, 2H, Ar–$H_{3,7}$); ^{13}C NMR (75 MHz, $CDCl_3$): (132.8, 130.8, 130.8, 129.1, 128.9, 122, 117.8) (aromatic), 109.4, 100.2 (ethynylene), 0 (TMS). FT-IR (neat): 2148 (C≡C str), 1436 (aromatic C=C str), 688 cm^{-1} (C–Br str.). MS (EI): m/z = 527.9 (M^+). m.p.: > 250 °C.

[1]H NMR 2,6-Dibromo-9,10-bis(trimethylsilylethynyl)anthracene, ***17***

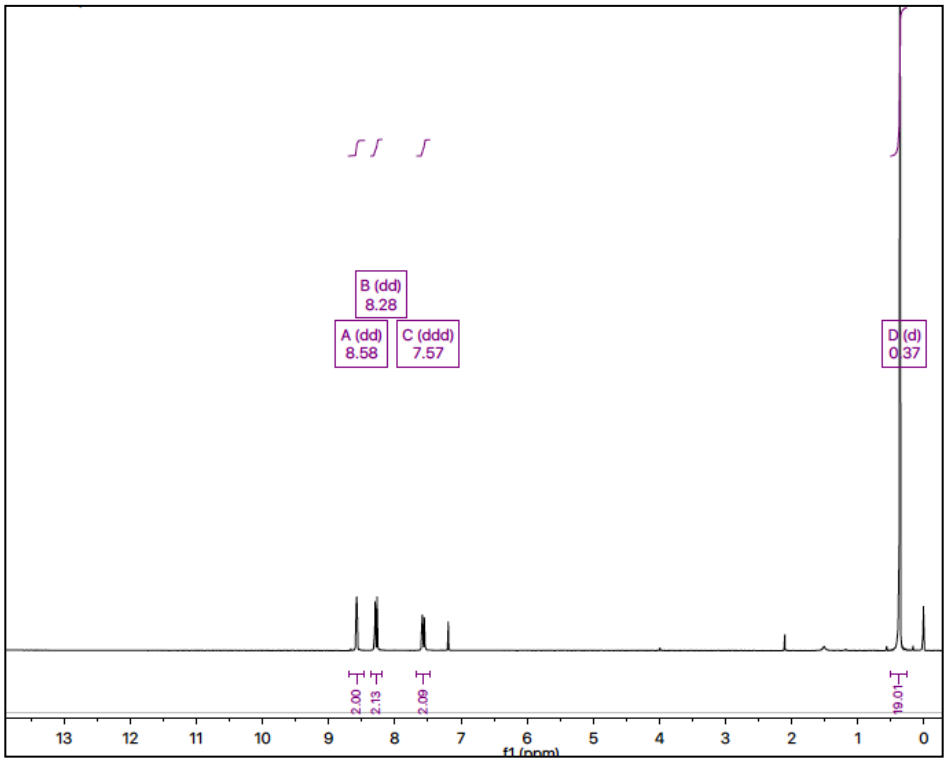

[13] C NMR of 2,6-Dibromo-9,10-bis(trimethylsilylethynyl)anthracene, ***17***

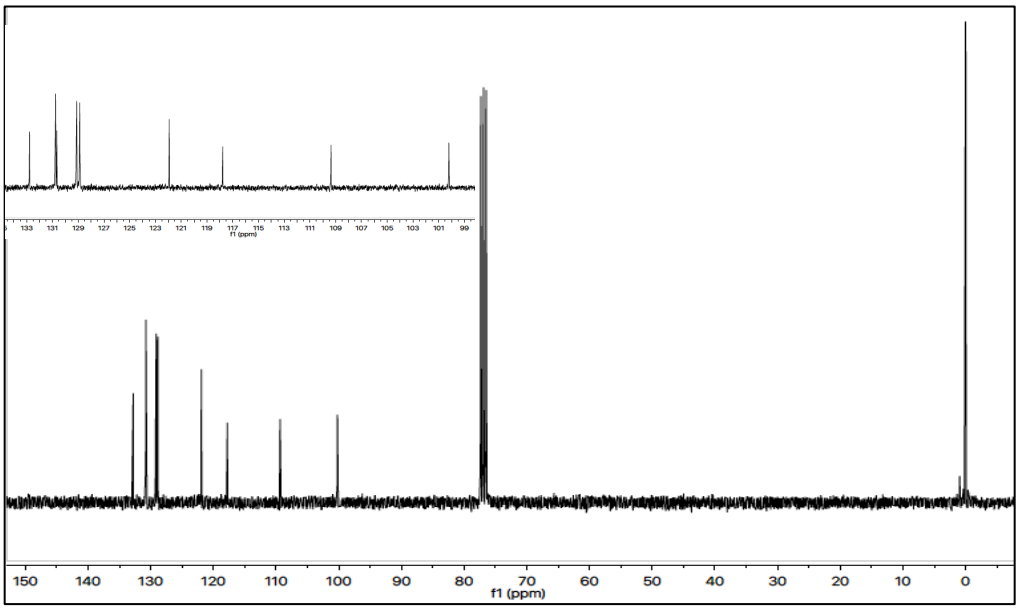

*IR spectrum of 2,6-Dibromo-9,10-bis(trimethylsilylethynyl)anthracene,**17***

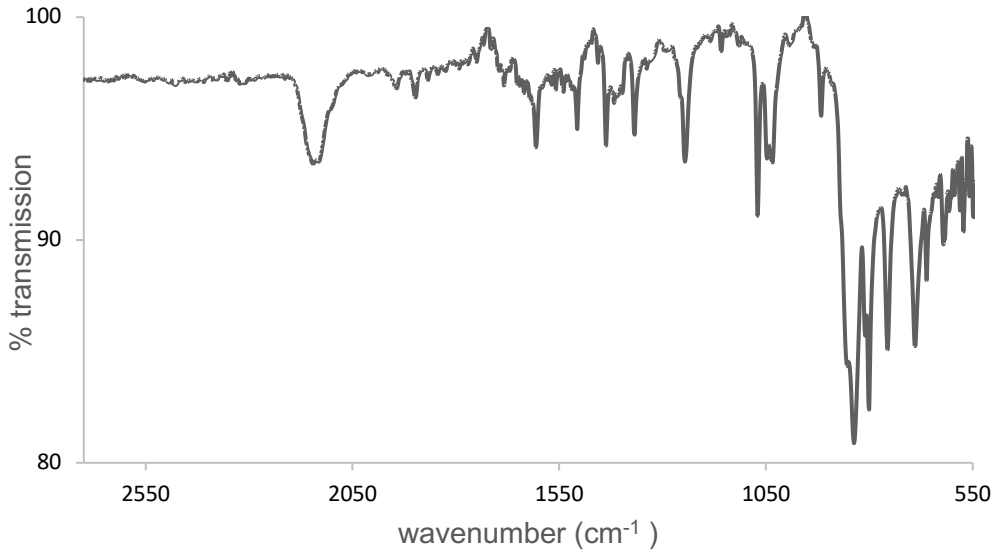

*MS spectrum ((inset: simulation of molecular ion cluster) of **17***

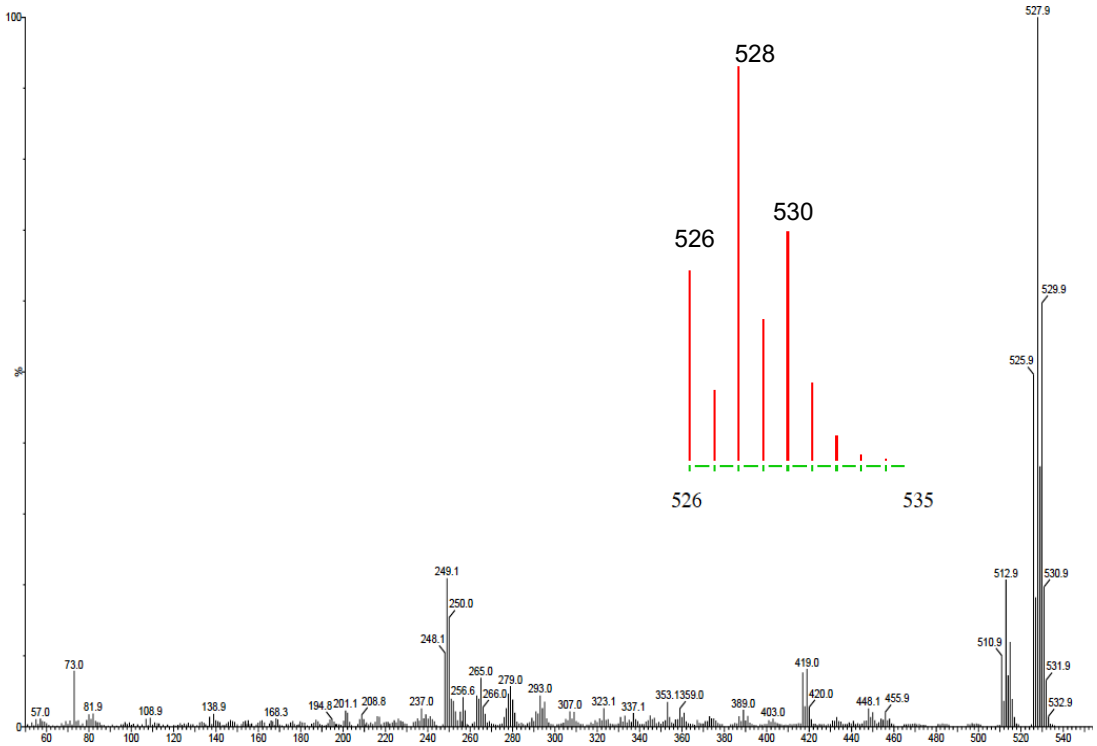

2.3.3.13. 2,6-Dihexyl-9,10-bis(trimethylsilylethynyl)anthracene, 18a[20]

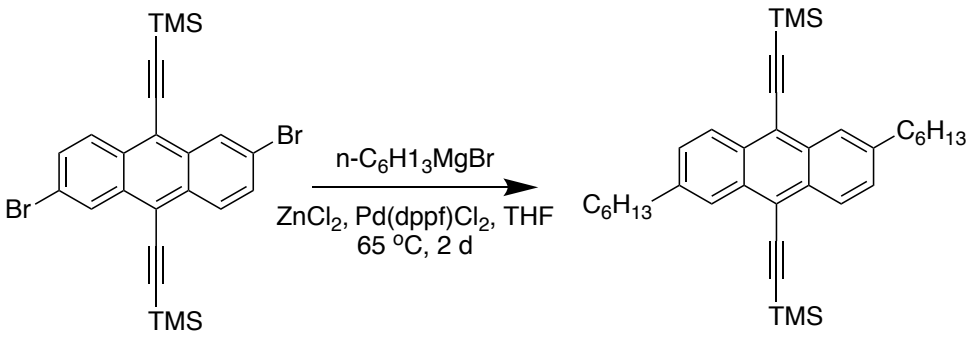

Anhydrous $ZnCl_2$ (1.81 g, 13.3 mmol) was added to a solution of *n*-hexylmagnesium bromide (5.67 mL of a 2M solution in Et_2O, 11.3 mmol) in dry THF (50 mL). The mixture was stirred for 1 h. $Pd(dppf)Cl_2$ (154 mg, 188 μmol) and 2,6-dibromo-9,10-bis(trimethylsilylethynyl)anthracene (2.0 g, 0.40 mmol) were added and the solution was heated at reflux for 72 h. H_2O (20 mL) was added and the mixture was extracted with CH_2Cl_2 (40 mL). The solvent was removed under reduced pressure and the residue was recrystallized twice from acetone to afford 2,6-dihexyl-9,10-bis(trimethylsilylethynyl)anthracene as an orange solid (0.9 g, 45% yield). ^{1}H NMR (300 MHz, $CDCl_3$): δ 8.47 (d, J = 9 Hz, 2H, Ar-$H_{4,8}$), 8.29 (s, 2H, Ar–$H_{1,5}$), 7.45 (dd, J = 9, 3 Hz, 2H, Ar–$H_{3,7}$), 2.85 (t, J = 6 Hz, 4H, Ar–CH_2), 1.78 (p, J = 6 Hz, β–CH_2 , 4H), 1.32-0.87 (18H), 0.90 (t, J = 6Hz, 6H), 0.52 (18H, TMS); FT-IR (neat): 2917 (sp^3 C–H str.), 2127 (C≡C str.), 1467 cm^{-1} (aromatic C=C str.); ^{13}C NMR (75 MHz, $CDCl_3$): 140.84, 131.83, 130.95, 128.58, 126.69, 124.63 (aromatic), 116.98, 107.23,101.74, (ethynylene) 36.0, 31.53, 30.37, 28.72, 22.38, 13.90 (sp^3), 0 (TMS). MS (EI): m/z = 538 (M^+). m.p.: 145-147 °C. Anal. calcd. for ($C_{36}H_{50}Si_2$): C, 80.23; H, 9.35. Found: C, 74.09; H, 8.80.

[1]H NMR of 2,6-dihexyl-9,10-bis(trimethylsilylethynyl)anthracene, ***18a***

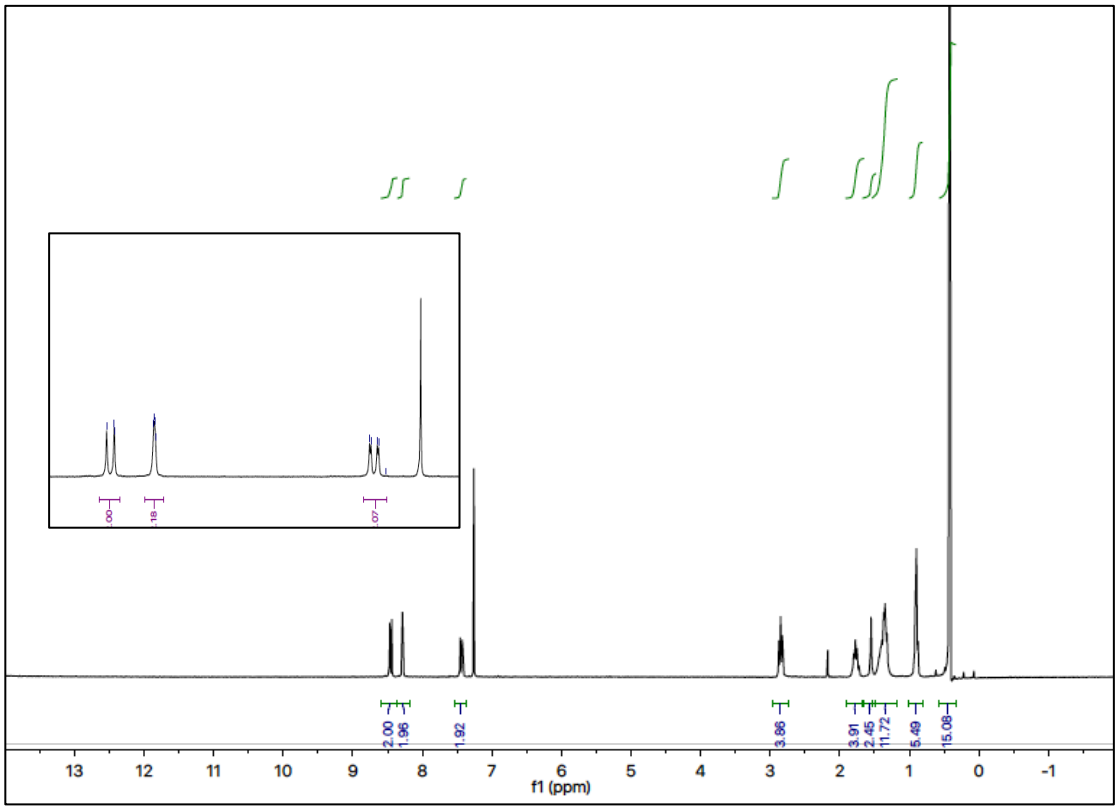

[13] C NMR of 2,6-dihexyl-9,10-bis(trimethylsilylethynyl)anthracene, ***18a***

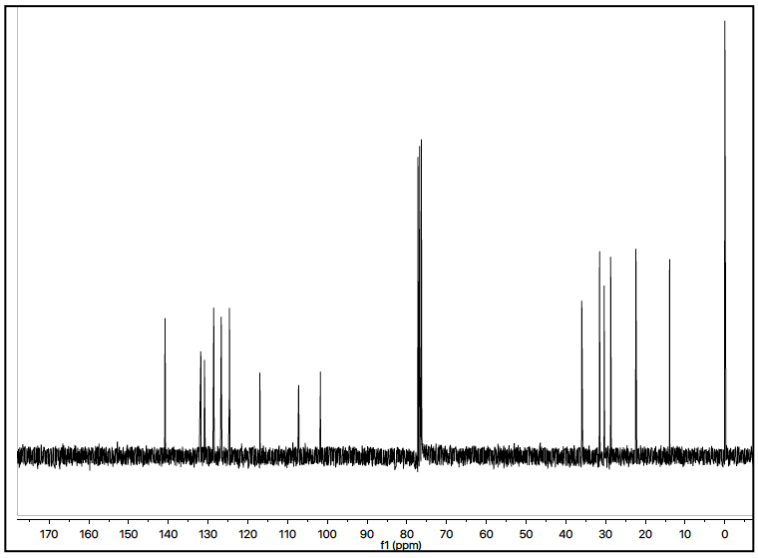

IR spectrum 2,6-dihexyl-9,10-bis(trimethylsilylethynyl)anthracene, ***18a***

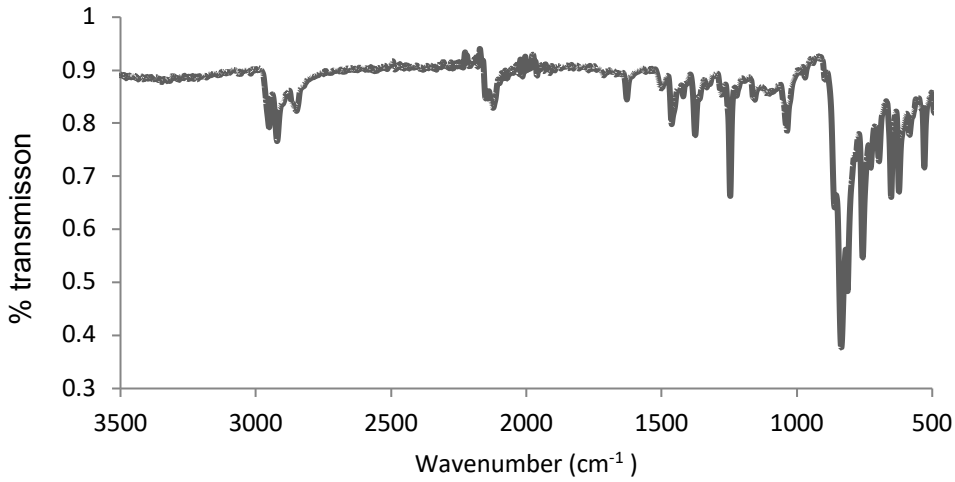

MS spectrum ((inset: simulation of molecular ion cluster **)** *of* ***18a***

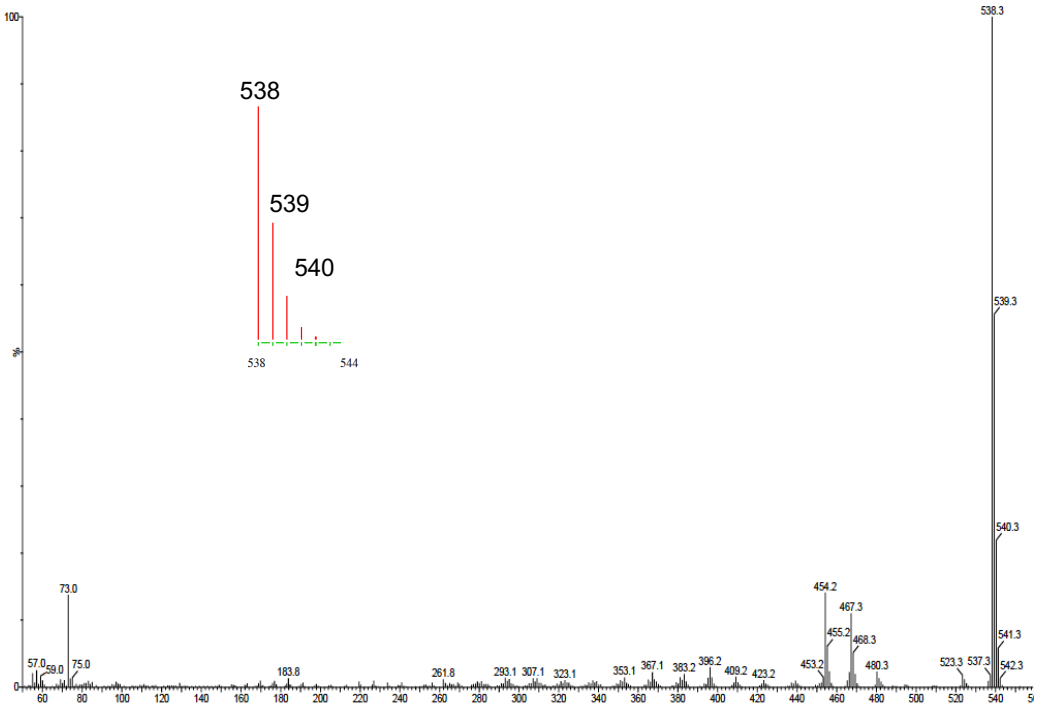

2.3.3.14. 2,6-Di(2-ethylhexyl)-9,10-bis(trimethylsilylethynyl)anthracene, 18b[20]

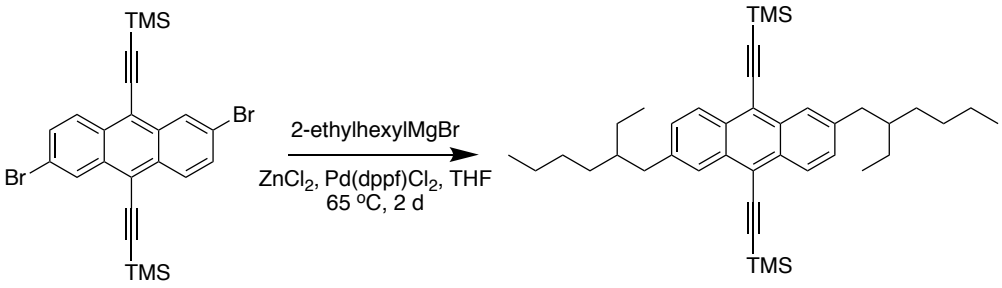

Anhydrous $ZnCl_2$ (1.70g, 12.5 mmol), was added in a solution of 2-ethylhexylmagnesium bromide (11.3 mL of a 1M solution in Et_2O, 11.3 mmol), in dry THF (37 mL) and the mixture was stirred for 1 h. $Pd(dppf)Cl_2$ (37 mg, 45 μmol) followed by 2,6-dibromo-9,10-bis(trimethylsilyl) ethynyl anthracene (1.2 g, 2.3 mmol) were added and the solution was heated at reflux for 72 h. Water (100 mL) was added and the mixture was filtered to afford an orange solid which was purified with column chromatography (eluent hexane) followed by recrystallization in acetone to afford orange colored product (0.43 g, 32% yield). ^{1}H NMR (300 MHz, $CDCl_3$): δ 8.40 (d, J = 9 Hz, 2H, Ar-H), 8.20 (s, 2H, Ar-H), 7.36 (dd, J = 6 Hz, 3 Hz, 2H, Ar-H), 2.69 (d, J = 6 Hz,4H, Ar-CH_2), 1.78 (septet, J = 6 Hz, Ar-CH_2CH_2 , 4H), 1.32-0.87 (18H), 0.5 (TMSi-, 18H); ^{13}C NMR (75 MHz, $CDCl_3$): 140.12, 132.00, 131.10, 129.33, 126.73, 126.00, 117.12 (aromatic), 107.43, 101.95 (ethynylene), 40.76, 40.34, 32.42, 28.86, 25.50, 23.00, 14.15, 10.85 (sp^3), 0 (TMS); FT-IR (neat): 2924 (sp^3 C–H str.), 2125 (C≡C str.), 1462 cm^{-1} (aromatic C=C str.); MS (EI): *m*/*z* = 595 (M^+), m.p. 90 - 92 °C. Anal. calcd. for ($C_{40}H_{58}Si_2$): C, 80.74; H, 9.82. Found: C, 80.60; H, 10.01.

[1]H NMR of 2,6-Di(2-ethylhexyl)-9,10-bis(trimethylsilylethynyl)anthracene, ***18b***

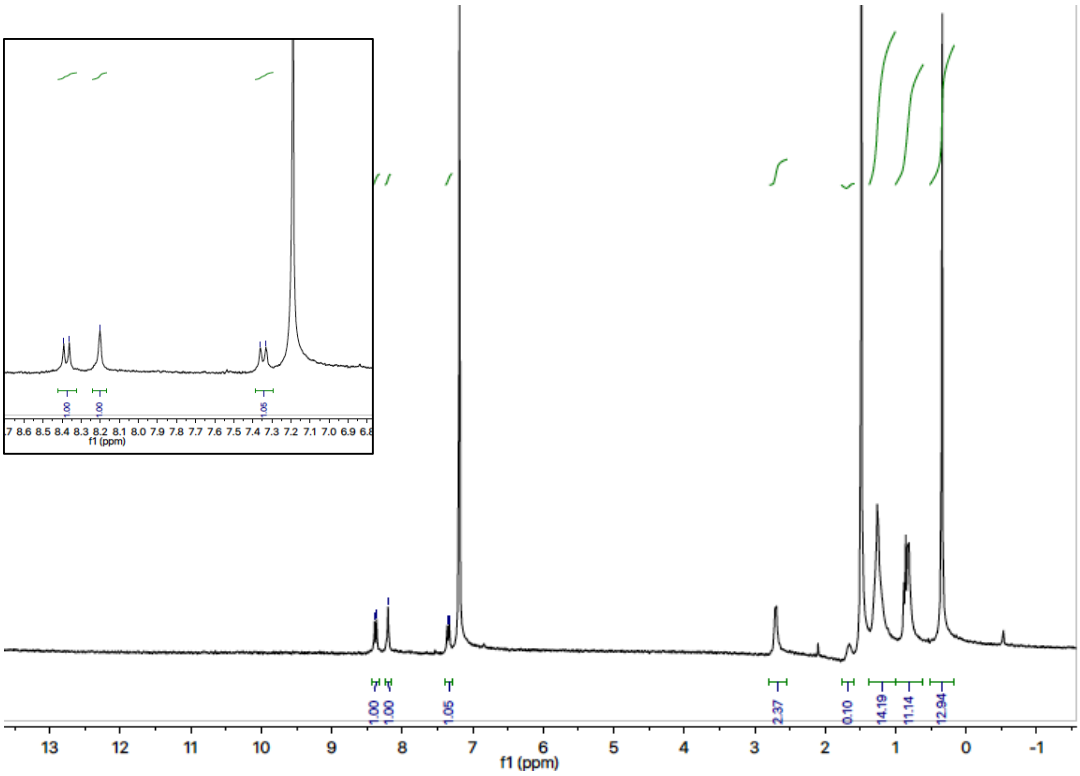

[13]C NMR of 2,6-Di(2-ethylhexyl)-9,10-bis(trimethylsilylethynyl)anthracene, ***18b***

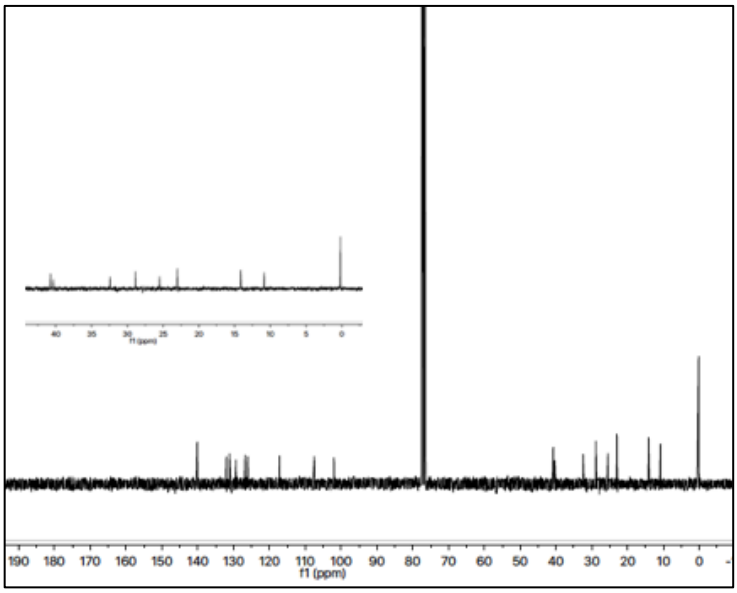

IR of 2,6-Di(2-ethylhexyl)-9,10-bis(trimethylsilylethynyl)anthracene, ***18b***

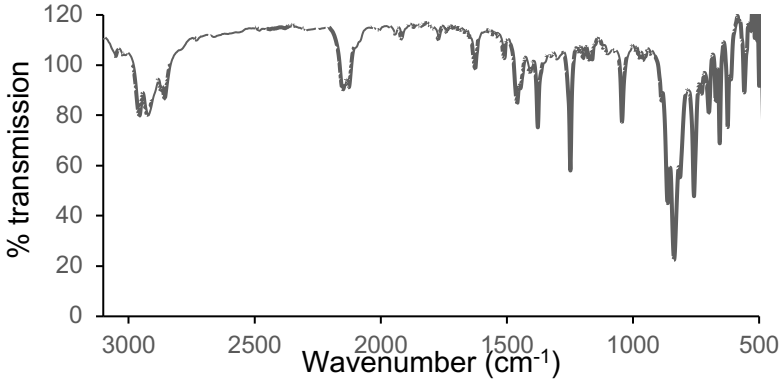

MS spectrum ((inset: simulation of molecular ion cluster **)** *of* ***18b***

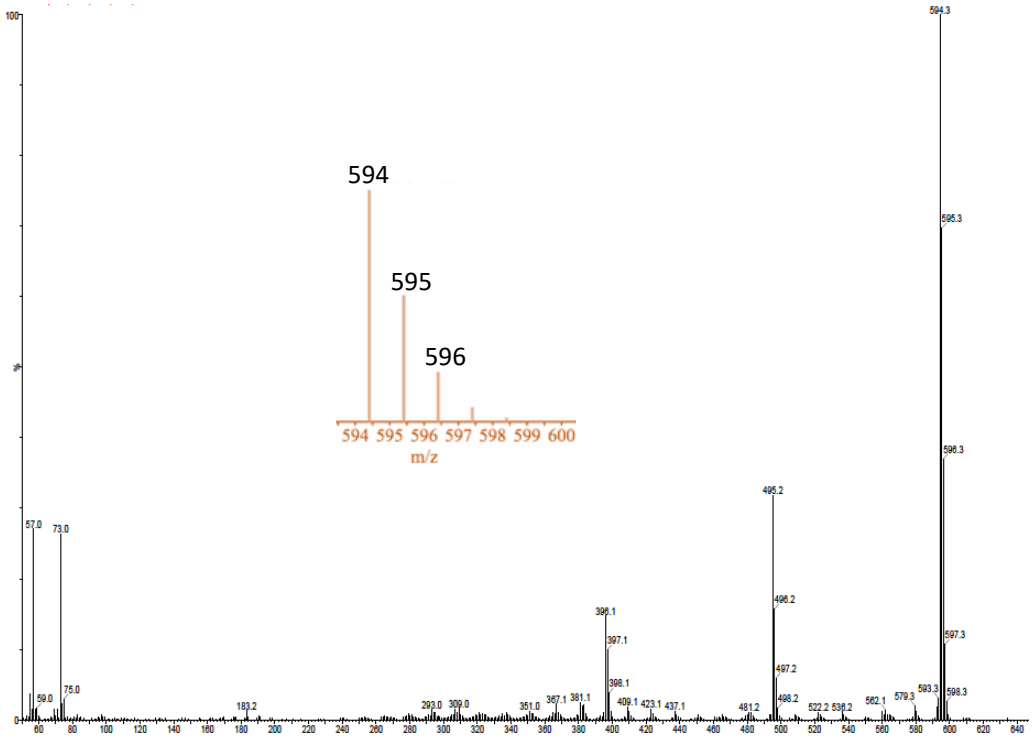

2.3.3.15. 2,6-Dibromo-9,10-dihydroanthracene, 19

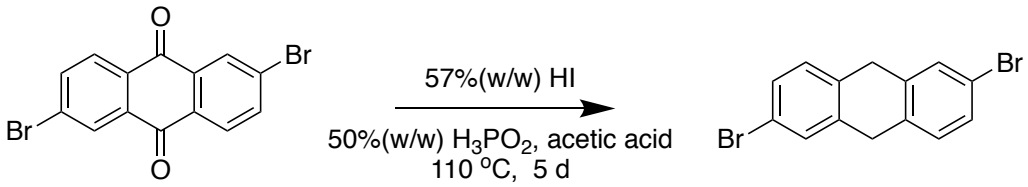

2,6-Dibromo-9,10-anthraquinone (7.0 g, 19 mmol), was added to the solution of HI (37.0 mL of 57% (w/w) solution in water, 285 mmol) and H_3PO_2 (19.0 mL of 50% w/w solution in water, 171 mmol) in acetic acid (380 mL) and the mixture was heated at 115 °C for 5 d. H_2O (300 mL) was added and the mixture was filtered to afford the title compound as an off-white powder that was dried under vacuum (5.1 g, 79%). The product was used without further purification. ^{1}H NMR (300 MHz, $CDCl_3$): δ 7.42 (d, J = 3 Hz, 2H, Ar-H $_{1,5}$), 7.32 (dd, J = 9, 3 Hz, 2H, Ar-H $_{3,7}$), 7.14 (d, J = 9 Hz, Ar-$H_{4,8}$), 3.90 (s, 4H, CH_2).

2.3.3.16. 2,6-Dibromoanthracene, 20[20, 22]

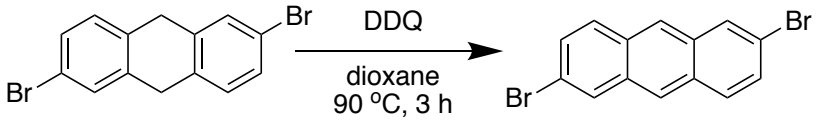

2,6-Dibromoanthracene (5.1 g, 15 mmol) was added to the solution of DDQ (5.1 g, 22 mmol) in dioxane (150 mL) under Ar. The mixture was heated to reflux for 4 h. Upon cooling a solid precipitated which was collected by filtration and washed with a 0.1 M solution of NaOH (4 × 100 mL) to afford 2,6-dibromoanthracene as an off-white powder (3.1 g, 62 %). ^{1}H NMR (300 MHz, DMSO-d_6): δ 8.60 (s, 2H, Ar-$H_{9,10}$), 8.40 (s, 2H, Ar-H $_{1,5}$), 8.13 (d, J = 9Hz, 2H, Ar-H $_{4,8}$), 7.63 (d, J = 9 Hz, 2H, Ar-H $_{3,7}$). FT-IR (neat): 1440 (aromatic C=C str), 790 cm^{-1} (C-Br stretch).

The spectral data matches that of the reference 22.

2.3.3.17. 2,6-Di(2-ethylhexyl)anthracene, 21

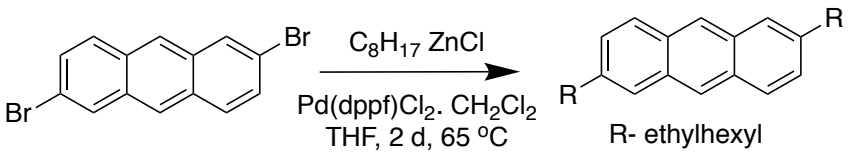

Anhydrous $ZnCl_2$ (7.3 g, 53 mmol) was added under Ar to the solution of 2-ethylhexyl-1-magnesium bromide (49 mL of 1M solution in Et_2O, 49 mmol) and the mixture was stirred for 1h. $Pd(dppf)Cl_2$ (218 mg, 268 μmol) and 2,6-dibromoanthracene (3.0 g, 9.0 mmol) were added and the mixture was heated at reflux for 48 h. Water (150 mL) was added and the mixture was extracted with CH_2Cl_2 (150 mL). The solvent was removed under reduced pressure and the residue was purified by column chromatography (eluent: hexane, R_f : 0.58) to afford 2,6-di(2-ethylhexyl)anthracene as an off white solid (1.2 g, 33% yield). ^{1}H NMR (300 MHz, $CDCl_3$): δ 8.30 (s, 2H, Ar-$H_{9,10}$), 7.90 (d, J = 9Hz, 2H, Ar-$H_{4,8}$), 7.68 (d, J = 3 Hz, 2H, Ar-$H_{1,5}$), 7.30 (dd, J = 9, 3 Hz, 2H, Ar-$H_{3,7}$), 2.68 (d, J = 6 Hz, Ar–CH_2, 4H), 1.68 (septet, J = 6 Hz, β–CH , 2H), 1.32-1.20 (m,16H), 0.60-0.90 (m,12H), 0.5 (18H, TMSi); ^{13}C NMR ($CDCl_3$): 138.4, 131.6, 130.8, 127.8, 127.6, 126.8, 125 (sp^2 aromatic), 40, 31, 28, 23, 22, 12,10 (sp^3). FT-IR (neat): 1469 (Ar CC str.), 2929 cm^{-1} (sp^3 C–H str.); MS (EI): m/z = 403 (M^+).; m.p.: 56-58 °C.

[1]H NMR of 2,6-D(2-ethylhexyl) anthracene, ***21***

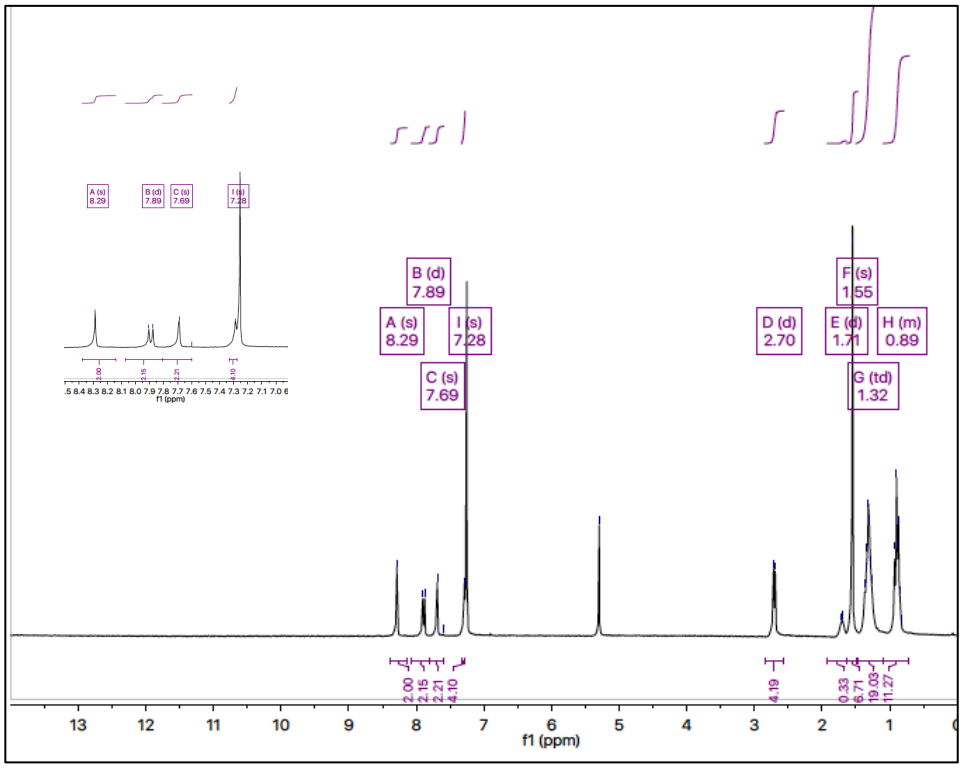

[13]C NMR of 2,6-D(2-ethylhexyl) anthracene, ***21***

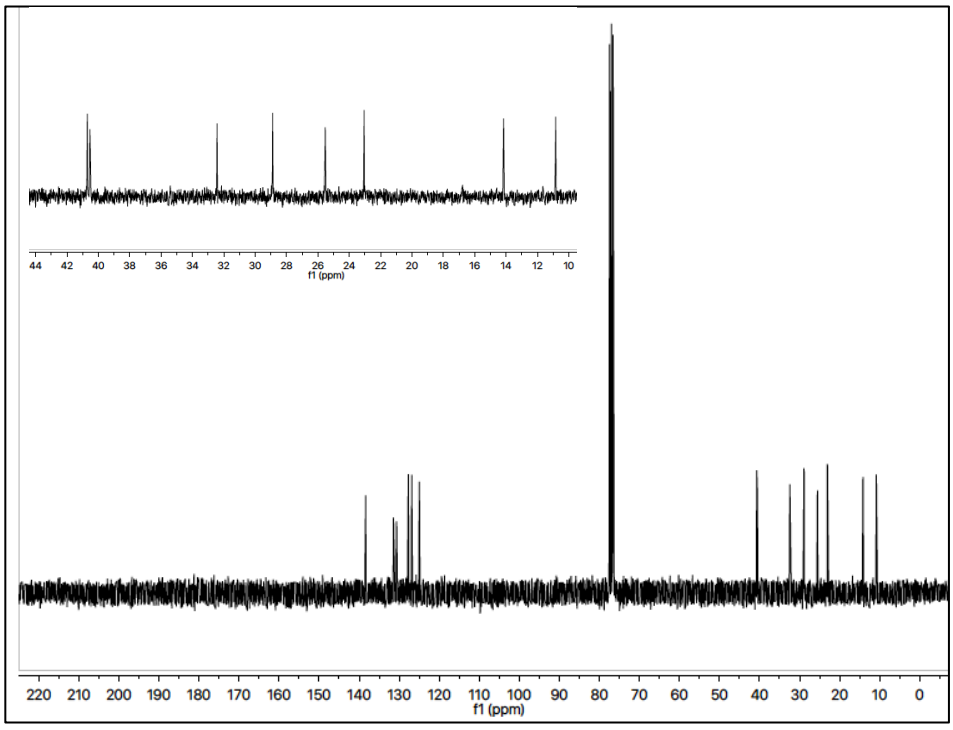

IR Spectrum of 2,6-D(2-ethylhexyl) anthracene, ***21***

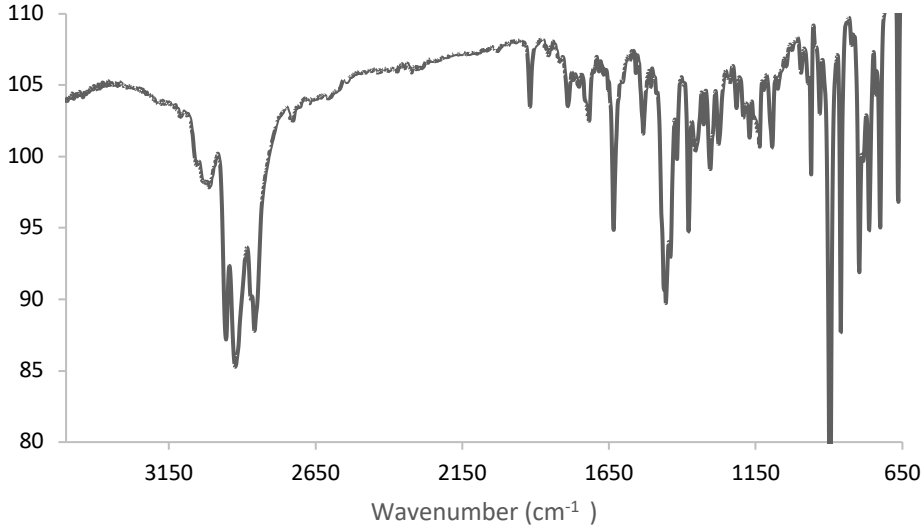

MS Spectrum ((inset: simulation of molecular ion cluster) of ***21***

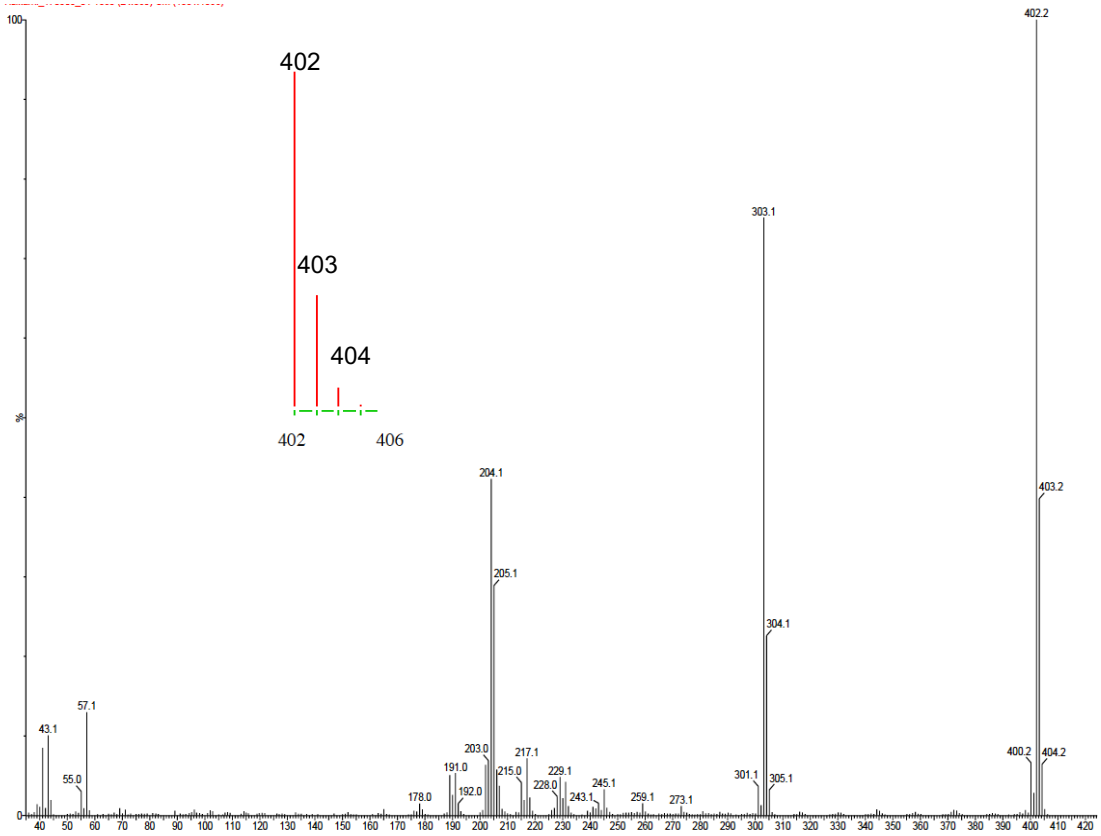

2.3.3.18. 9,10-dibromo-2,6-di-(2-ethylhexyl)anthracene, 22

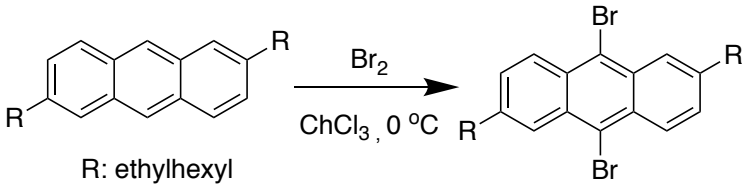

Bromine (35 μL 6. 83 μmol) was added dropwise over the period of 30 min to a solution of 2,6-di(2-ethylhexyl)anthracene (250 mg, 620 μmol), at 0°C. Aqeous $Na_2S_2O_3$ solution (10% w/v,15 mL) was added to the reaction mixture. The mixture was extracted in CH_2Cl_2 (10 mL). The solvent was removed under reduced pressure and the residue was recrystallized from EtOH (4 mL) to afford the product as a yellow solid (214 mg, 61% yield). ^{1}H NMR (300 MHz, $CDCl_3$): δ 8.50 (d, J = 6 Hz, 2H, Ar-$H_{4,8}$), 8.30 (d, J = 3 Hz, 2H, Ar-$H_{1,5}$), 7.44 (dd, J = 6, 3 Hz, 2H, Ar-$H_{3,7}$), 2.80 (d, J = 6 Hz, Ar–CH_2), 1.80 (septet, J = 6 Hz, β–CH_2, 2H), 1.3-1.2 (m, 16H) (m, 16H), 0.60 - 0.90 (m, 12H), 0.5 (18H, TMS). ^{13}C NMR ($CDCl_3$): 140.88, 130.6, 130.02, 129.83, 127.91, 126.90, 122.32, 40.64, 32.35, 28.80, 25.58, 23.03, 14.15, 10.85; IR (neat): 1458 (Ar CC str.) . MS (EI): m/z = 560 (M^+); m.p. 60-62°C. Anal. calcd. for ($C_{30}H_{41}Br_2$): C, 64.29; H, 7.19; Br, 28.51. Found: C, 64.40; H, 7.15; Br, 28.46.

[1]H NMR 9,10-dibromo-2,6-di-(2-ethylhexyl)anthracene, ***22***

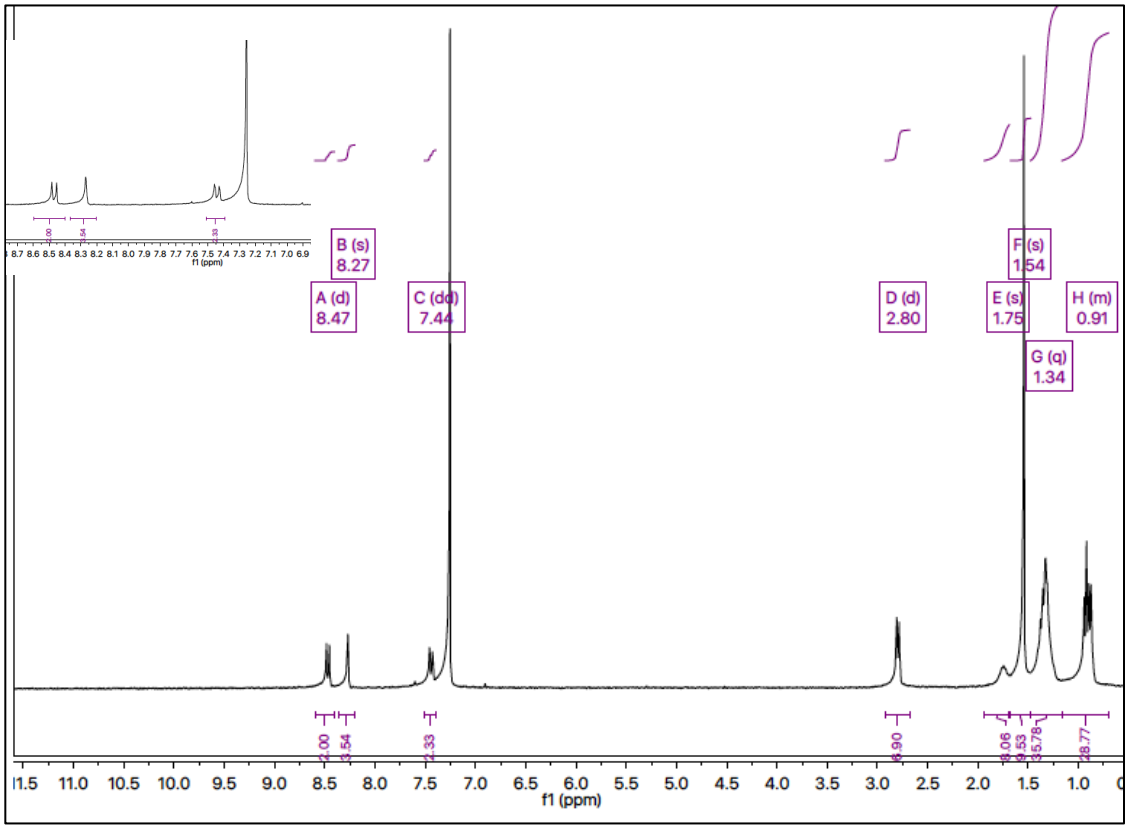

[13]C NMR of 9,10-dibromo-2,6-di-(2-ethylhexyl)anthracene, ***22***

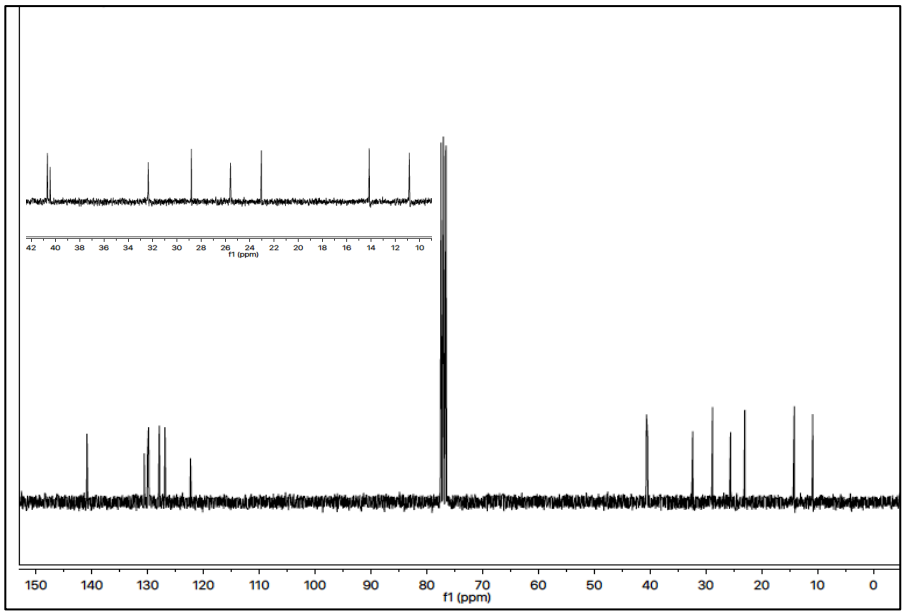

IR Spectrum of 9,10-dibromo-2,6-di-(2-ethylhexyl)anthracene, ***22***

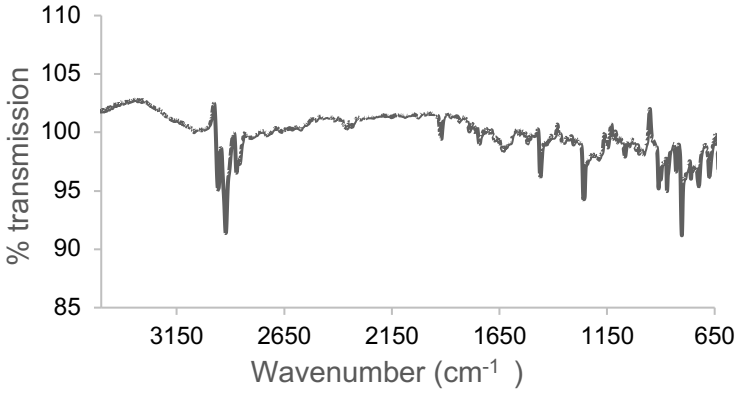

MS Spectrum (inset: simulation of molecular ion cluster) of ***22***

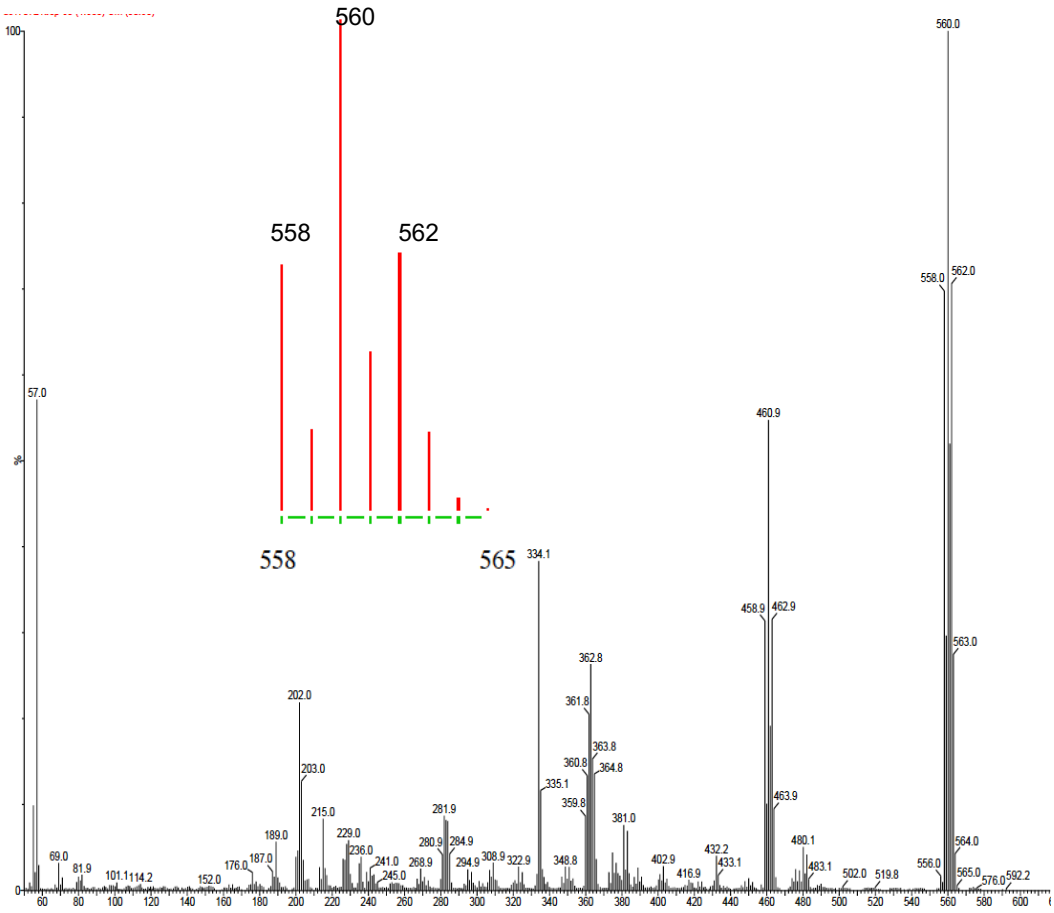

2.3.3.19. Poly (2,5-dihexyl-1,4-phenylenediyl ethynylene-alt-2,5-dioctyloxy phenylenediyl ethynylene), PPPE

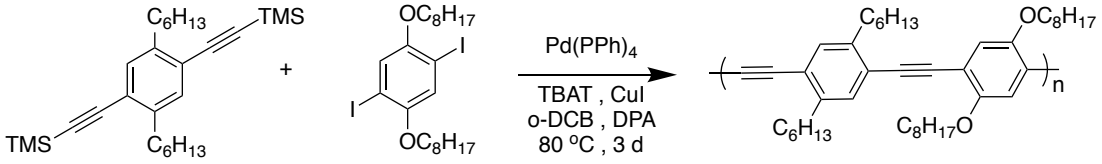

2,5-Dioctyloxy-1,4-bis(trimethylsilylethynyl) benzene (272 mg, 516 μmol), 1,4-dihexyl- 2,5-diiodo-benzene (250 mg, 502 μmol), $Pd(PPh_3)_4$ (6.0 mg, 5.0 μmol) and CuI (14.3 mg, 75.0 μmol) were added to mixture of o-DCB (5 mL) and *N,N*-diisopropylamine (DPA) (2.7 mL). The mixture was heated under Ar to 80 °C for 3 d. The reaction mixture was cooled to room temperature, added to acetone (40 mL) and filtered to provide a yellow solid. The solid was subjected to extraction in a Soxhlet extractor with MeOH, followed by acetonitrile, hexane and chloroform. The orange colored material in the hexane fraction (70 mg) was characterized.

^{1}H NMR (300 MHz, $CDCl_3$): δ 7.38 (s, 2H, dialkyl- Ar–H), 7.02 (s, 2H, dialkoxy- Ar–H), 4.35 (t, J = 6Hz, 4H, Ar–OCH_2), 3.11 (t, J = 6Hz, 4H, Ar–CH_2), 1.9-1.8 (m, 4H, β–CH_2), 1.7-1.1 (m, 32H), 0.92 (t, *J* = 6 Hz, 12H, CH_3). GPC (1,3,5-trichlorobenzene): M_n 10.4 kDa, PDI 1.7. Anal.calcd. for $(C_{44}H_{64}O_2)_n$ C: 84.56; H: 10.32; Found C: 83.88; H:9.91.

^{1}H –NMR of PPPE

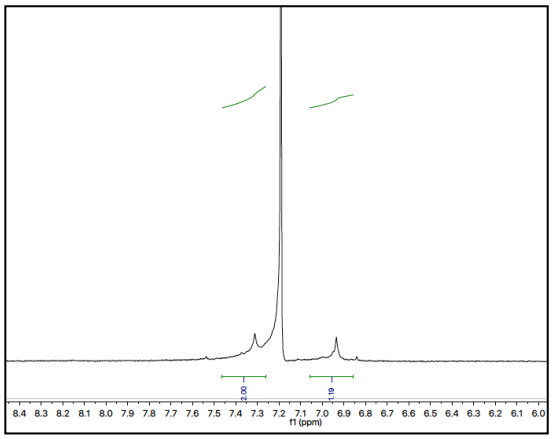

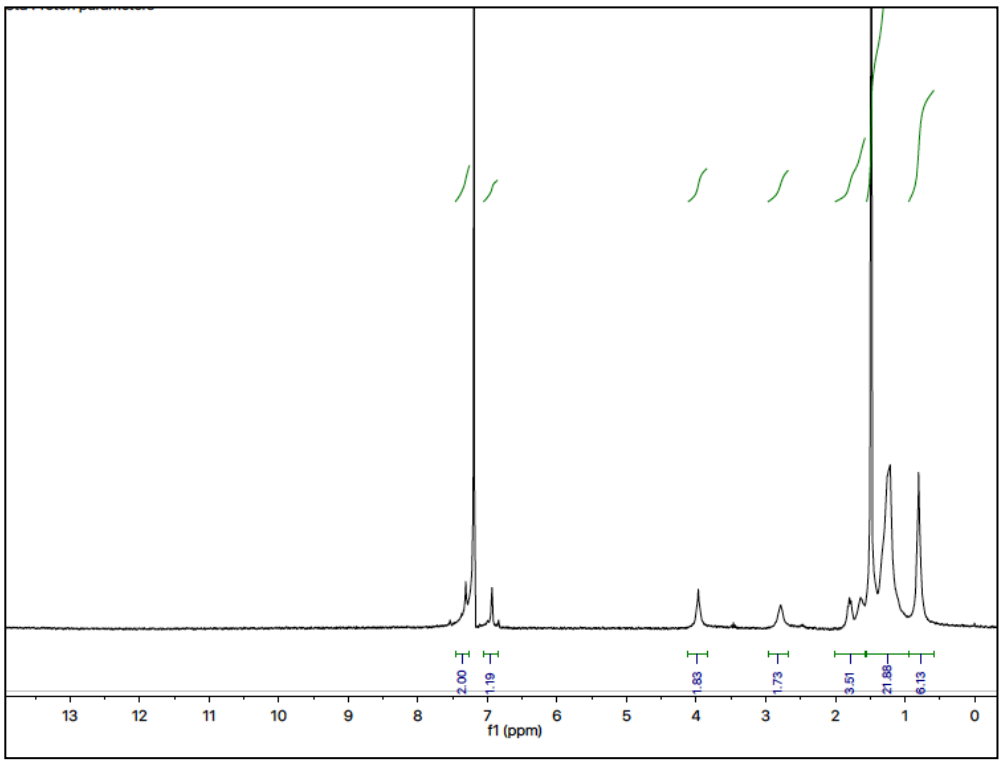

GPC of PPPE

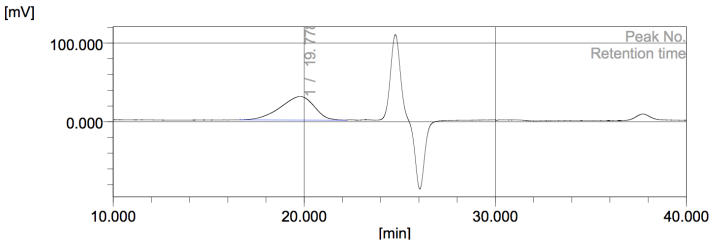

Molecular mass calculation result (RI)

Peak 1 Valley Peak

	[min]	[mV]	[mol]		
Peak start	16.595	2.374	303,567	Mn	13,364
Peak top	19.778	32.124	14,513	Mw	25,406
Peak end	22.243	2.143	1,378	Mz	52,653
				Mz+1	97,493
				Mv	25,406
Height [mV]			30.055	Mp	14,514
Area [mV*s]			3718.014	Mz/Mw	2.072
Height% [%]			100.000	Mw/Mn	1.901
[eta]			25406.44827	Mz+1/Mw	3.837

Ultraviolet photoelectron spectroscopy (UPS) of PPPE

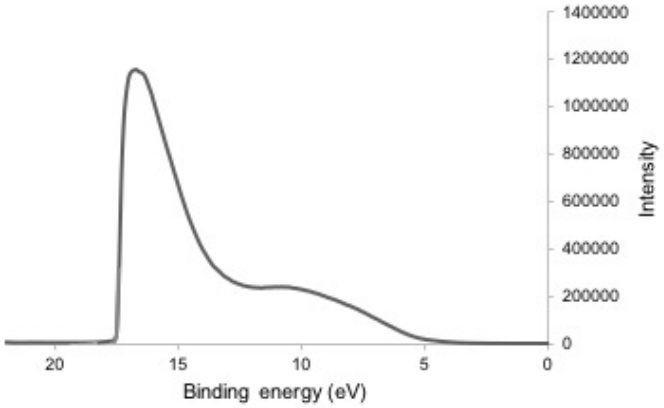

2.3.3.20. Poly(6,7-dihexyl-1,4-naphthalene-alt-2,5-dioctyloxy-1,4-phenylene ethynylene), PNPE

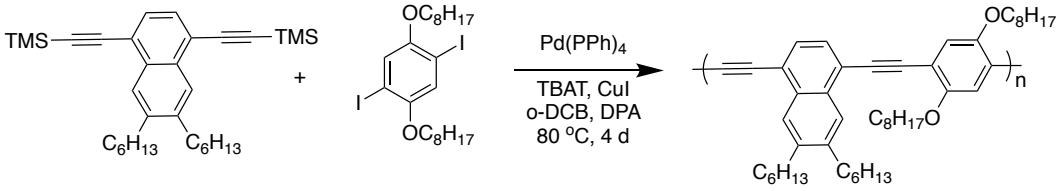

6,7-Dihexyl-1,4-bis(trimethylsilylethynyl)naphthalene (110 mg, 225 μmol) and 1,4-diiodo-2,5-dioctyloxybenzene (128 mg, 218 μmol) were added to a mixture of $Pd(PPh_3)_4$ (2.6 mg, 2.2 μmol), CuI (6.4 mg, 33.7 μmol) and TBAT (485 mg, 900 μmol) in anhydrous o-DCB (4.2 mL) and *N,N*-diisopropyl amine (1.2 mL). The reaction mixture was heated to 80 °C for 4 d. The mixture was cooled and added to methanol (35 mL). The dark orange precipitated colored solid was collected by filtration (142 mg). The solid was subjected to extraction in a Soxhlet extractor with acetone followed by hexane, acetonitrile and then chloroform. The orange material in the chloroform fraction (66 mg) was characterized. ^{1}H NMR (500 MHz, $CDCl_3$): δ 8.32 (s, 2H, Ar–H $_{2,3}$), 7.62 (s, 2H, Ar–H $_{6,7}$), 7.23(s, 2H, Ar–$H_{5,8}$) 4.11 (t, J = 6Hz, 4H, O–CH_2), 2.8-2.6 (br.s., Ar–CH_2), 2.0-1.9 (m, 4H, alkoxy β-CH_2), 1.8-1.7 (m, alkyl β-CH_2), 1.5-1.2 (32H), 0.8-0.9 (m, 12H, CH_3). GPC (1,3,5-trichlorobenzene): M_n 22 kDa, PDI 2. Anal.calcd. for $(C_{48}H_{66}O_2)_n$ C: 84.99; H: 9.81; Found C: 85.24; H:9.80.

^{1}H –NMR of PNPE

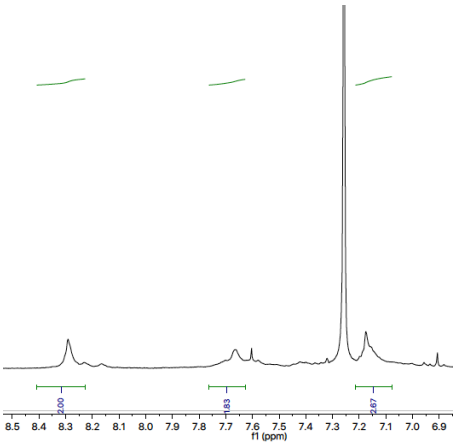

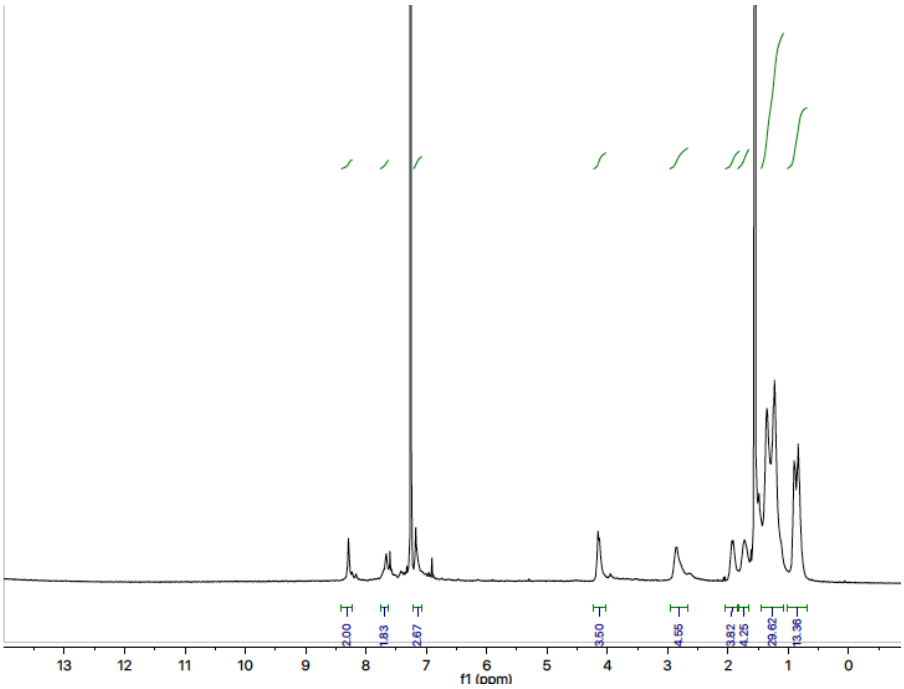

GPC of PNPE

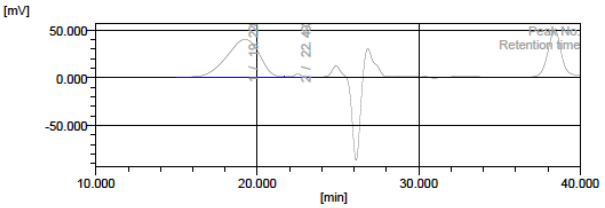

Molecular mass calculation result (RI)
Peak 1 Base Peak

	[min]	[mV]	[mol]
Peak start	15.000	0.893	1,389,939
Peak top	19.228	40.548	26,277
Peak end	21.648	1.531	2,711
Height [mV]			39.649
Area [mV*s]			5574.341
Height% [%]			92.591
[eta]			46634.05446

Mn	22,139
Mw	46,634
Mz	109,133
Mz+1	244,232
Mv	46,634
Mp	26,278
Mz/Mw	2.340
Mw/Mn	2.106
Mz+1/Mw	5.237

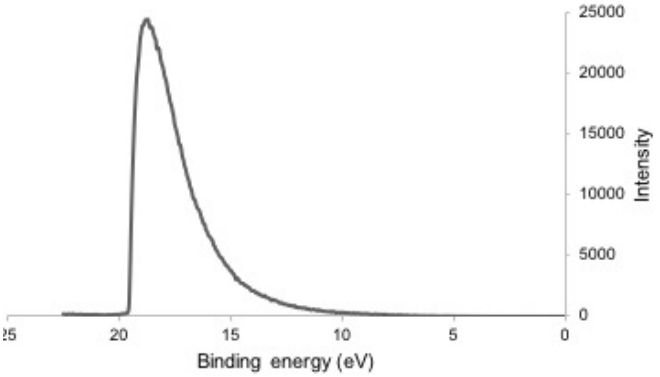

2.3.3.21. Poly(2,6-dihexyl-9,10-anthracene ethynylene-alt-2,5-dioctyloxy-1,4-phenylene ethynylene), PAPE

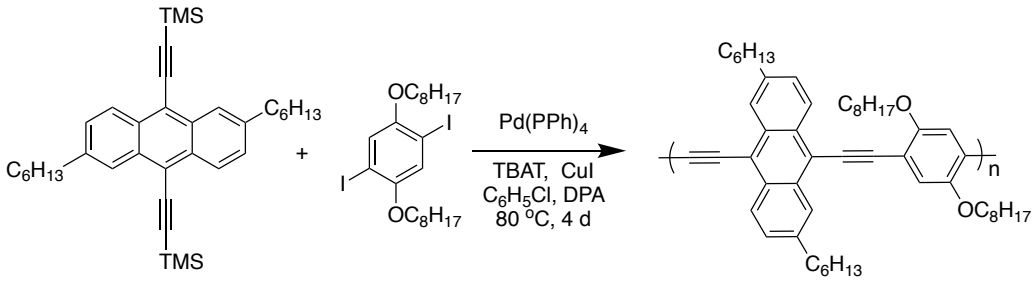

2,6-Dihexyl-9,10-bis(trimethylsilylethynyl)anthracene (190 mg, 351 μmol) and 1,4-diiodo-2,5-dioctyloxybenzene (200 mg, 341μmol) were added to a mixture of $Pd(PPh_3)_4$ (3.90 mg, 3.41 μmol), CuI (10 mg, 7.2 μmol), and TBAT (760 mg, 71.7 μmol) in a mixture of anhydrous chlorobenzene (5.20 mL) and *N,N*-diisopropyl amine (3.10 mL). The mixture was heated to 80 ˚C for 4 d over which a purple solid precipitated from the solution. The mixture was cooled and added to methanol (35 mL). The precipitated solid was collected by filtration and subjected to extraction in a Soxhlet extractor with acetone followed by hexane and then chloroform. The material remaining in the thimble (63 mg) was characterized. ^{1}H NMR (300 MHz, $CDCl_3$): δ 9.20 (d, J = 9 Hz, 2H, Ar–H $_{4,8}$), 8.94 (s, 2H, Ar–H $_{1,5}$), 7.70 (d, J = 9 Hz, 2H, Ar–H $_{3,7}$), 7.62 (s, 2H, phenylene), 4.40 (t, J = 6 Hz, 4H, Ar–OCH_2), 3.10 (t, J = 6 Hz, 4H, Ar–CH_2), 2.10–2.20 (m, 4H, alkoxy β-

CH_2,), 2.00-2.10 (m, 4H, alkyl β-CH_2), 1.4-1.7 (m, 19 H), 1.10 (s, 6H, CH_3), 1.00 (s, 6H, CH_3). GPC (trichlorobenzene) M_n: 11 kDa, PDI 2.7. Anal.calcd. for $(C_{52}H_{68}O_2)_n$ C: 84.93; H: 9.77; Found C: 69.81; H: 8.13. Although the elemental analysis does not match with theory, the ratio of C to H is very close to theory. The difference between the theoretical and actual values my arise from incomplete combustion of sample.

^1H –NMR of PAPE

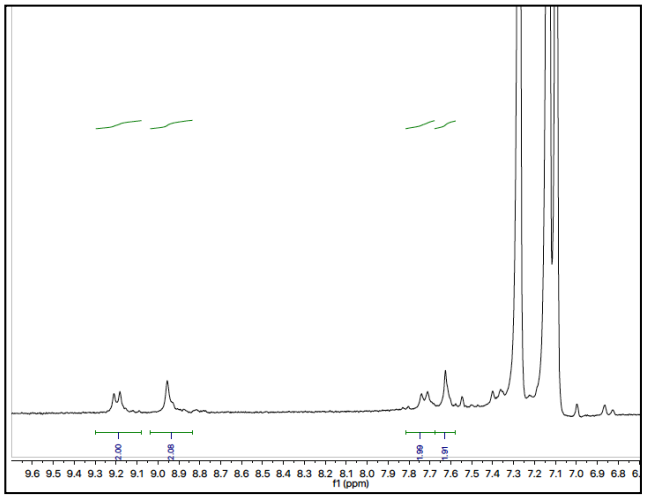

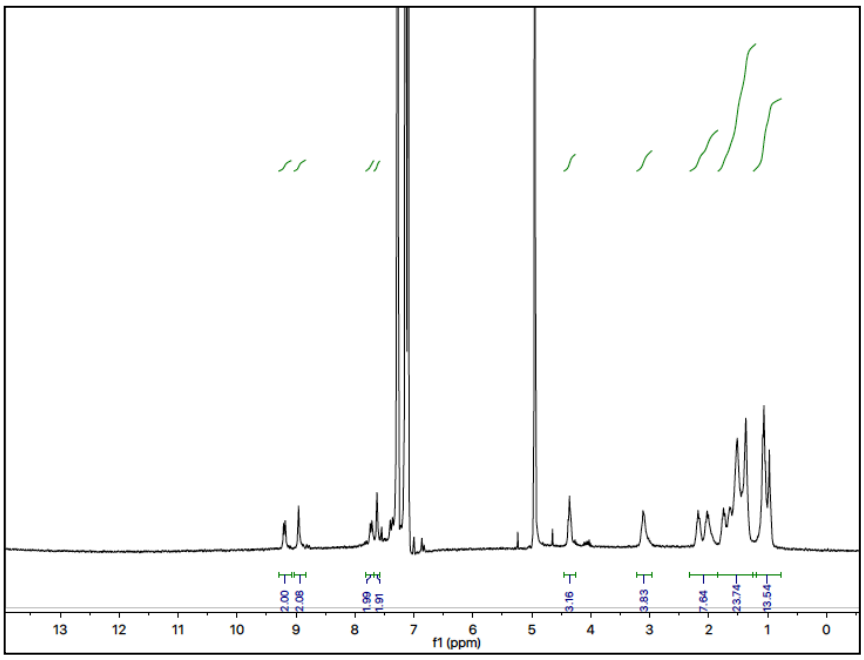

GPC of PAPE

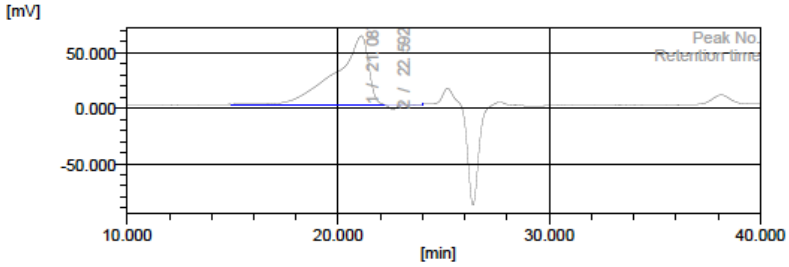

Molecular mass calculation result (RI)

Peak 1 Valley Peak

	[min]	[mV]	[mol]
Peak start	14.930	3.486	2,283,536
Peak top	21.087	65.227	7,579
Peak end	22.163	3.278	2,793
Height [mV]			61.967
Area [mV*s]			6671.169
Height% [%]			93.571
[eta]			32513.51740

Mn	11,698
Mw	32,514
Mz	278,101
Mz+1	1,105,240
Mv	32,514
Mp	7,580
Mz/Mw	8.553
Mw/Mn	2.779
Mz+1/Mw	33.993

Ultraviolet photoelectron spectroscopy (UPS) of PAPE

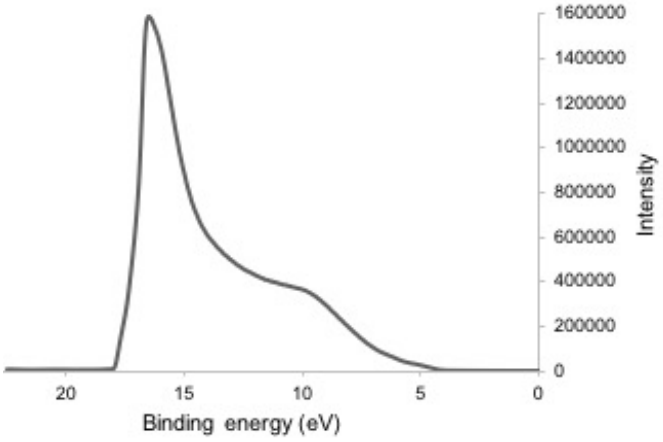

2.3.3.22. Poly (2,6-di(2-ethylhexyl-9,10-anthralene ethynylene), PAE

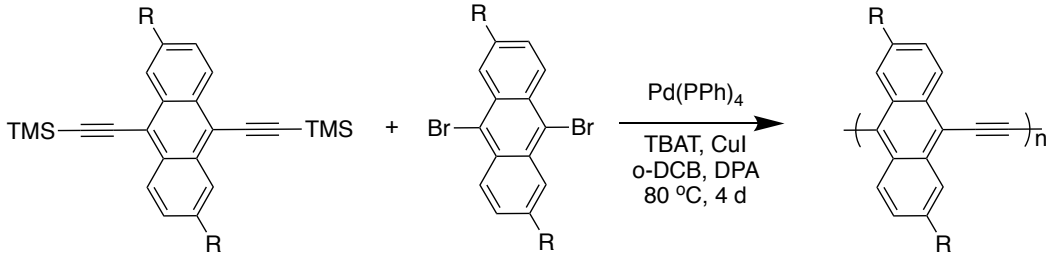

2,6-Di(2-ethylhexyl)-9,10-bis(trimethylsilylethynylene)anthracene (70.0 mg, 118 μmol), 9,10-dibromo-2,6-bis(2-ethylhexyl)anthracene (60.0 mg, 107 μmol), $Pd(PPh_3)_4$ (1.3 mg , 1.2 μmol), CuI (3.4 mg, 18 μmol), were added to mixture of o-dichlorobenzene (3 mL) and *N,N*-diisopropyl-*N*-ethylamine (DPA) (1 mL). The mixture was heated to 80 °C for 4 d under Ar. The reaction mixture was cooled to room temperature, added to MeOH (40 mL) and filtered to obtain a red-brown solid. The solid was subjected to extraction in a Soxhlet extractor with MeOH, followed by acetonitrile, acetone, hexane and chloroform. The red-brown material in the chloroform fraction (10 mg) was characterized. ^{1}H NMR (300 MHz, $CDCl_3$): δ 8.90-9.04 (m, 2H, Ar–H $_{4,8}$), 8.78-8.88 (m, 2H, Ar–H $_{1,5}$), 7.62-7.56 (m, 2H, Ar-H $_{3,7}$), 2.80 (m, 4H, Ar–CH_2), 1.9-1.8 (m, 4H, β-CH_2), 1.7-1.1 (m, 32H), 0.92 (t, J = 6 Hz, 12H, CH_3).;. GPC (1,3,5-trichlorobenzene): M_n 13.4 kDa, PDI 1.9.Anal.calcd. for $(C_{32}H_{40})_n$ C: 88.25; H: 10.03; Found C: 87.97; H:9.06.

^{1}H –NMR of PAE

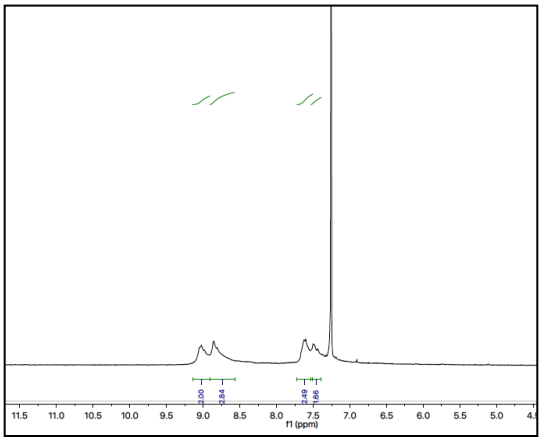
11.5 11.0 10.5 10.0 9.5 9.0 8.5 8.0 7.5 7.0 6.5 6.0 5.5 5.0
f1 (ppm)

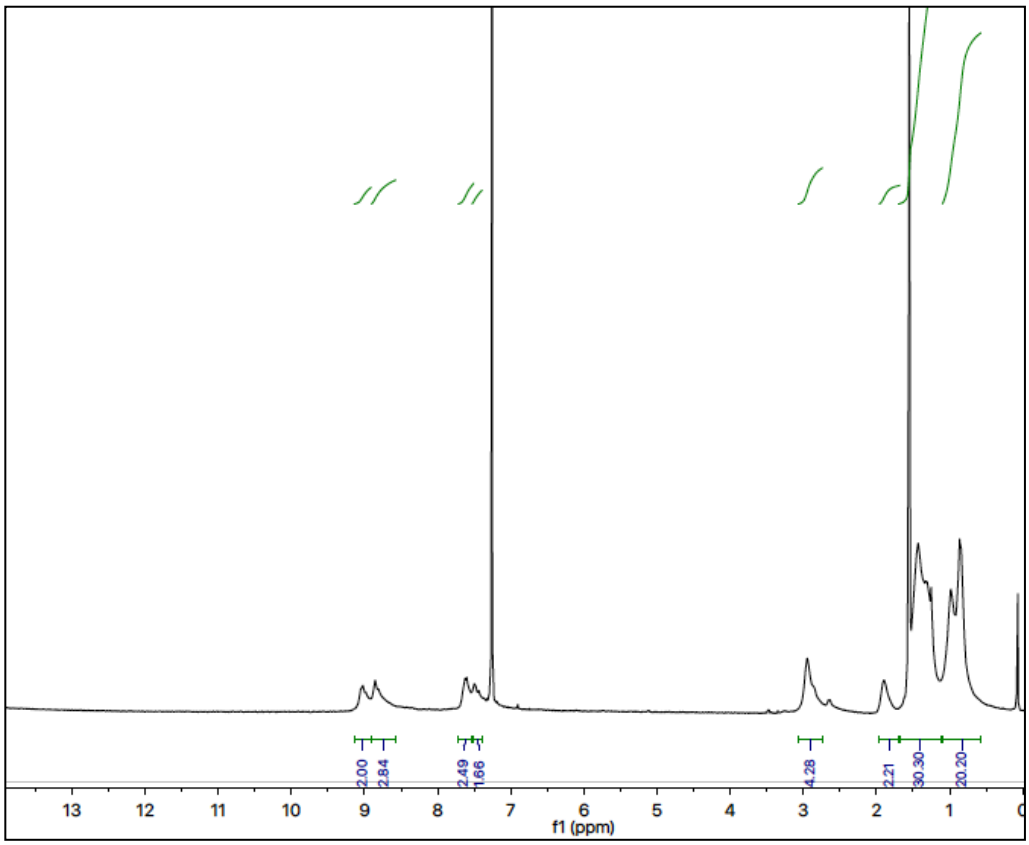
2.00
2.84
2.49
1.66
4.28
2.21
30.30
20.20
13 12 11 10 9 8 7 6 5 4 3 2 1
f1 (ppm)

GPC of PAE

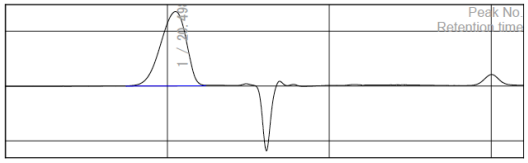

Molecular mass calculation result (RI)

Peak 1 Valley Peak

	[min]	[mV]	[mol]		
Peak start	17.442	0.122	138,419	Mn	7,388
Peak top	20.498	67.752	7,675	Mw	11,667
Peak end	22.353	0.783	1,326	Mz	20,183
				Mz+1	35,799
				Mv	11,667
Height [mV]			67.590	Mp	7,676
Area [mV*s]			7477.405	Mz/Mw	1.730
Height% [%]			100.000	Mw/Mn	1.579
[eta]			11667.01601	Mz+1/Mw	3.068

Molecular mass calculation result (RI)

Total

	[min]	[mV]	[mol]		
Peak start	17.442	0.122	138,419	Mn	7,388
Peak top	20.498	67.752	7,675	Mw	11,667
Peak end	22.353	0.783	1,326	Mz	20,183
				Mz+1	35,799
				Mv	11,667
Height [mV]			67.590	Mp	7,676
Area [mV*s]			7477.405	Mz/Mw	1.730
Height% [%]			100.000	Mw/Mn	1.579
[eta]			11667.01601	Mz+1/Mw	3.068

Ultraviolet photoelectron spectroscopy (UPS) of PAE

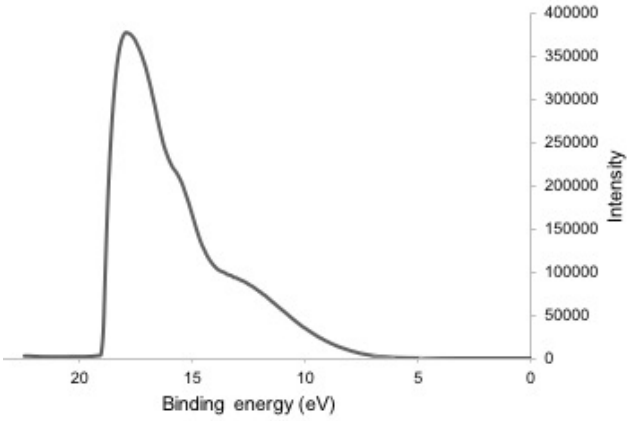

2.5 REFERENCES

1. Mössinger, D.; Jester, S.-S.; Sigmund, E.; Müller, U.; Höger, S., Defined Oligo (p-phenylene− butadiynylene) Rods. *Macromolecules* **2009,** *42* (20), 7974-7978.
2. Kim, R.; Yoo, S.-J.; Kim, E.-K.; Yu, H. S.; Shin, S. C.; Lee, S.-K.; Kwon, S.-K.; Kim, Y.-H., New limb structured blue light emitting materials for OLEDs. *Dyes and Pigments* **2012,** *95* (2), 384-391.
3. Bailey, D.; Williams, V. E., An efficient synthesis of substituted anthraquinones and naphthoquinones. *Tetrahedron Letters* **2004,** *45* (12), 2511-2513.
4. Santra, D. C.; Bera, M. K.; Sukul, P. K.; Malik, S., Charge-Transfer-Induced Fluorescence Quenching of Anthracene Derivatives and Selective Detection of Picric Acid. *Chemistry–A European Journal* **2016,** *22* (6), 2012-2019.
5. Park, J.-H.; Chung, D. S.; Park, J.-W.; Ahn, T.; Kong, H.; Jung, Y. K.; Lee, J.; Yi, M. H.; Park, C. E.; Kwon, S.-K., Soluble and easily crystallized anthracene derivatives: precursors of solution-processable semiconducting molecules. *Organic Letters* **2007,** *9* (13), 2573-2576.
6. Konieczny, M.; Harvey, R. G., Efficient reduction of polycyclic quinones, hydroquinones, and phenols with hydriodic acid. *The Journal of Organic Chemistry* **1979,** *44* (26), 4813-4816.
7. Jiang, Y.; Mei, J.; Ayzner, A. L.; Toney, M. F.; Bao, Z., 5,11-Conjugation-extended low-bandgap anthradithiophene-containing polymer exhibiting enhanced thin-film order and field-effect mobility. *Chemical Communications* **2012,** *48* (58), 7286-7288.
8. Ofer, D.; Swager, T. M.; Wrighton, M. S., Solid-state ordering and potential dependence of conductivity in poly (2, 5-dialkoxy-p-phenyleneethynylene). *Chemistry of materials* **1995,** *7* (2), 418-425.
9. Bunz, U. H., Poly (aryleneethynylene) s. *Macromolecular Rapid Communications* **2009,** *30* (9-10), 772-805.
10. Swager, T. M.; Gil, C. J.; Wrighton, M. S., Fluorescence studies of poly (p-phenyleneethynylene) s: the effect of anthracene substitution. *The Journal of Physical Chemistry* **1995,** *99* (14), 4886-4893.
11. Halkyard, C. E.; Rampey, M. E.; Kloppenburg, L.; Studer-Martinez, S. L.; Bunz, U. H., Evidence of aggregate formation for 2, 5-dialkylpoly (p-phenyleneethynylenes) in solution and thin films. *Macromolecules* **1998,** *31* (25), 8655-8659.
12. Jenekhe, S. A.; Osaheni, J. A., Excimers and exciplexes of conjugated polymers. *Science* **1994,** *265* (5173), 765-768.
13. Bunz, U. H.; Imhof, J. M.; Bly, R. K.; Bangcuyo, C. G.; Rozanski, L.; Vanden Bout, D. A., Photophysics of Poly [p-(2, 5-didodecylphenylene) ethynylene] in Thin Films. *Macromolecules* **2005,** *38* (14), 5892-5896.

14. Mohanakrishnan, A.; Lakshmikantham, M.; Cava, M. P.; Rogers, R. D.; Rogers, L. M., o-Quinonoid heterocyclic compounds: Naphtho [2, 3-c] thiophene revisited. *Tetrahedron* **1998,** *54* (25), 7075-7080.

15. Bunz, U. H.; Enkelmann, V.; Kloppenburg, L.; Jones, D.; Shimizu, K. D.; Claridge, J. B.; zur Loye, H.-C.; Lieser, G., Solid-state structures of phenyleneethynylenes: Comparison of monomers and polymers. *Chemistry of Materials* **1999,** *11* (6), 1416-1424.

16. Niedzialek, D.; Lemaur, V.; Dudenko, D.; Shu, J.; Hansen, M. R.; Andreasen, J. W.; Pisula, W.; Müllen, K.; Cornil, J.; Beljonne, D., Probing the Relation Between Charge Transport and Supramolecular Organization Down to Ångström Resolution in a Benzothiadiazole-Cyclopentadithiophene Copolymer. *Advanced Materials* **2013,** *25* (13), 1939-1947.

17. Castiglioni, C.; Navarrete, J. L.; Zerbi, G.; Gussoni, M., A simple interpretation of the vibrational spectra of undoped, doped and photoexcited polyacetylene: amplitude mode theory in the GF formalism. *Solid State Communications* **1988,** *65* (7), 625-630.

18. Moroni, M.; Le Moigne, J.; Luzzati, S., Rigid rod conjugated polymers for nonlinear optics: 1. Characterization and linear optical properties of poly (aryleneethynylene) derivatives. *Macromolecules* **1994,** *27* (2), 562-571.

19. Hou, J.; Song, F.; Wang, L.; Wei, G.; Cheng, Y.; Zhu, C., In Situ Generated 1: 1 Zn (II)-Containing Polymer Complex Sensor for Highly Enantioselective Recognition of N-Boc-Protected Alanine. *Macromolecules* **2012,** *45* (19), 7835-7842.

20. Liu, C.; Cai, W.; Guan, X.; Duan, C.; Xue, Q.; Ying, L.; Huang, F.; Cao, Y., Synthesis of donor–acceptor copolymers based on anthracene derivatives for polymer solar cells. *Polymer Chemistry* **2013,** *4* (14), 3949-3958.

21. Susumu K; Fisher J.K.; Zheng J.; Beratan D.N.; Yodh A.G.; Therien M.J.; Two-Photon Absorption Properties of Proquinoidal D-A-D and A-D-A Quadrapolar Chromophores. *The Journal of Physical Chemistry A*, **2011**, *115*, 5525-5539.

22. Ito K.; Suzuki T.; Sakamoto Y.; Kubota D.; Inoue Y.; Fumio S.; Tokito S.; Oligo(2,6-Anthylene)s: Acene-Oligomer Approach for Organic Field-Effect Transistors. *Angew. Chem. Int. Ed.*, **2003**, *42* (10), 1159-1162.

CHAPTER 3. THE ELECTRONIC STRUCUTRE OF ALTERNATING DONOR-ACCEPTOR COPOYLMERS OF NDI WITH PHENYLENE, NAPHTHALENE AND ANTHRACENE UNITS

3.1 INTRODUCTION

In Chapter 2, I discussed how the incorporation of 9,10-anthracenediyl units impacts the electronic structure of poly(arylene ethynylene)s. Characterization of the electronic structure by electrochemistry, UV-visible absorption, fluorescence, and ultraviolet photoelectron spectroscopies and Raman, indicate that the anthracene unit imparts significant quinoid character to the polymer. This motivated me to study how the 9,10-anthracenediyl unit might serve as a donor in donor-acceptor conjugated polymers. In this chapter, I explore how incorporation of anthracene influences the electronic structure of donor-acceptor polymers with naphthalene diimide.

One approach to gain control over the bandgap of conjugated polymers is to combine in a single chain both an electron-rich donor unit that has a high ionization potential, corresponding to a high-energy HOMO, and an electron-poor acceptor unit that has high electron affinity by virtue of having a low lying LUMO. The combination of these units in a single donor-acceptor (D-A) copolymer leads to a new set of molecular orbitals in which the HOMO is raised relative to that of the isolated donor unit and the LUMO will be lower than that of the acceptor unit. The electronic structure of the copolymers depends on the contribution of the molecular orbitals of the donor and

acceptor units which is determined by their relative energies, the degree of mixing of the constituent wave functions for example through the influence of torsional angle between the units.

An important characteristic of donor-acceptor copolymers is the appearance of two absorption bands in the UV-visible-near IR region of the electromagnetic spectrum. The low energy transition band is usually assigned to a HOMO-LUMO transition.[1-2] This transition may have a significant amount of charge transfer character that arises from contributions of the donor unit to the HOMO and of the acceptor unit to the LUMO, which give rise to a polar excited state. The high-energy transitions can be centered on either the donor unit or acceptor unit.[1-2]The energy and intensity of the optical transitions is affected by the degree of interaction between the donor and acceptor units at the molecular orbital level.[3]

Three case studies illustrate the interplay between the polymer structure and electronic properties. A homologous series of alternating copolymers of 3,4-propylene dioxythiophene and 2,1, 3-benzothiadiazole (BTD) acceptor units shown in Figure 3.1 was synthesized to probe how the energy and intensity of optical transitions is affected by the variation of the molecular backbone. The length of the donor unit was controlled by the number of 3,4-propylene dioxythiophene units. It was observed that increasing the length of the donor unit gave rise to a small blue shift and a reduction in the intensity of the low-energy charge transfer type transition. The reason for the trend was discerned from molecular orbital calculations, which revealed that the energy of the LUMO of the polymer, although localized on the acceptor, has some contribution from the donor. As the length of the donor shortens, the degree of interaction between donor and acceptor

orbitals is enhanced resulting in overall lowering of LUMO of polymer. As the donor length increases, the overall concentration of acceptors is reduced in the polymer backbone making the acceptor unit act like 'dopants'. This results in lesser donor-acceptor contribution in the LUMO of polymer resulting in increase in energy of LUMO.

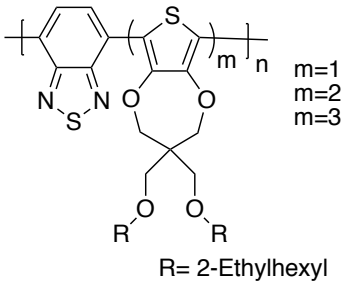

Figure 3.1. Donor-acceptor polymers of propylene dioxythiophene (ProDOT) and 2,1,3-benzothiadiazole.[4]

The degree of interaction of frontier molecular orbitals between donor and acceptor units in a polymer backbone is affected by the variation of the quinoid character in the polymer. A study of the effect of the structure of the acceptor unit on the optical properties of a series of D-A polymers was made by variation of the heteroatom (X = S, Se, Te) in a series of polymers consisting of alternating cyclopentadithiophene and benzochalcogenodiazole units as shown in Figure 3.2. Among the three polymers, the polymer containing Te gave the lowest bandgap and the most red-shifted low - energy transition. The longer X-N bond length in Te affected the conjugation within the benzene ring and the bond alternation along the conjugated backbone. Calculations of the bond lengths showed that the degree of bond length alternation in the benzene ring increases in

the order of S to Se to Te. This leads to more quinoid type geometry within the polymer backbone for the Te containing acceptor, resulting in destabilization of the HOMO and stabilization of the LUMO that gives rise to lower band gap.[2]

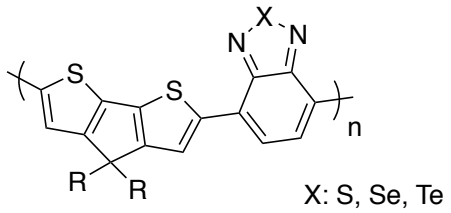

Figure 3.2. Alternating donor-acceptor polymers of cyclopentadithiophene and benzochalcogenodiazole units.

The variation of quinoid character in donor-acceptor copolymers is also explored by Yu et.al in series of copolymers containing thieno[3,4-*b*]thiophene-2,5-diyl units (TT) and 2,5-thiophenediyl units by varying the ratio of dibromo derivative of TT to 2, 5-dibromo-3-hexylthiophene and 2,5-bis(tributylstannyl thiophene) in the monomer feed for Stille polymerization as shown in Figure 3.3. It was observed that the band gap of the polymers decreased from ~ 1.7 eV to 1.2 eV with increase in the content of thieno[3,4-b]thiophene because TT enhances the quinoid character in the polymer by aromatization of thiophene ring fused to the thiophene in the polymer backbone.[5]

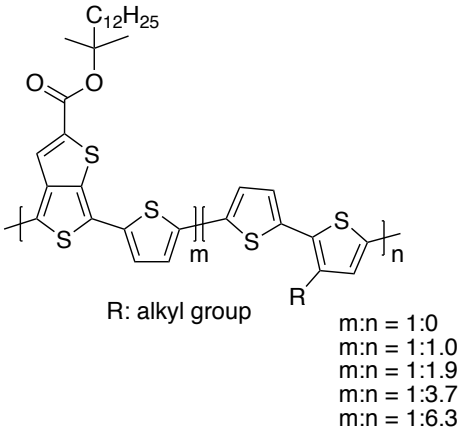

Figure 3.3. Thieno[3,4-b]thiophene (TT) and thiophene copolymers.

The many possible combinations of donors and acceptors allows one to tune the band gap of a material to meet the demands of particular application.[6-7,8,3] Some commonly used donor units in these polymers include fluorene, cyclopenta[2,1-*b*:3,4-*b'*] bithiophene, oligothiophenes, benzo[1,2-*b*:4,5-*b'*]dithiophene, and indacenodithiophene (IDT).[9] These donor units are used with a range of acceptors units such as thieno[3,4-*b*]thiophene (TT), 2,1,3-benzothiadiazole (BT), thieno[3,4-*c*]pyrrole-4,6-dione (TPD), isoindigo, diketopyrrolopyrrole (DPP), and *N*,*N*'-di(2-decyltetradecyl)-2,6-naphthalene-1,4,5,8-bis(dicarboximide) (NDI).[10]

Naphthalene diimide has recently received attention for developing electron transport polymers.[10] The incorporation of naphthalene diimide as an acceptor unit in conjugated polymers has been pursued with numerous donors including thiophene[11-12] cyclopentadithazole[13] and cyclopenta[2,1-*b*:3,4-*b'*]dithiophene. However, there have been few studies of conjugated polymers of naphthalene diimde with simple acene donors.[1] Here I set out to compare the electronic structures of naphthalene diimide-containing donor-acceptor polymers that contain alkyl-substituted 1,4-phenylenediyl, 1,4-

naphthalenediyl and 9,10-anthracenediyl units. In the naphthalene and anthracene analogs, I posit that the fusion of benzene rings onto the phenylene unit in the conjugated backbone stabilizes the quinoid form of the polymer and have a potentially strong influence on the electronic structure of the materials, as shown in Figure 3.4A. While acenes (e.g., naphthalenes,[14] anthracenes,[15-16] pentacenes,[17-18]) have previously been explored as units within conjugated copolymers, the most common substitution patterns do not support the stabilization of the quinoid form, as shown in Figure 3.4 B.

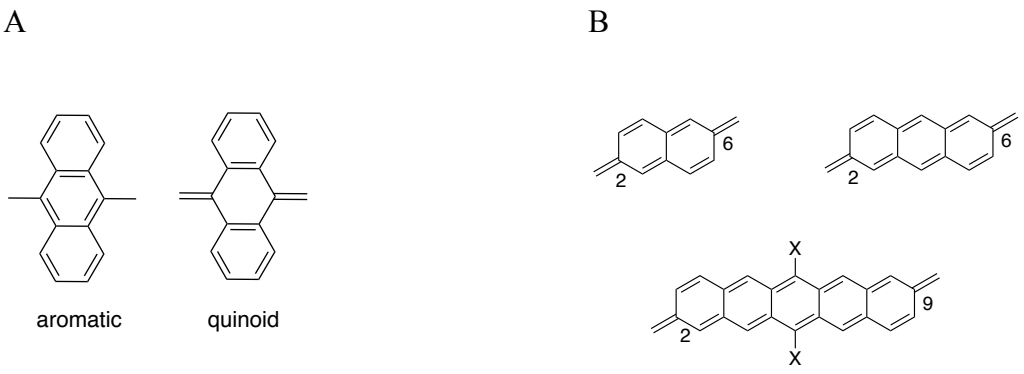

Figure 3.4. A, Fusion of benzene rings onto the phenylene ring in the conjugated backbone stabilizes the quinoidal form through retention of aromaticity in the fused rings. B, Quinoidal forms of the 2,6-naphthalenediyl [Ref.[14]], 2,6-anthracnediyl [ref.[16],[15]] and 2,6-pentacenediyl units [ref [19],[18]] are not stabilized in the same way.

Iverson et. al., previously reported on the solid state packing of an alternating oligomers of naphthalene dimmide and 9,10-diethynylanthracene.[14] However, the polymers were limited in molecular weight, possibly due to their low solubility which

leads to precipitation during the polymerization before the reaction proceeds to high conversion. Here we chose to substitute both the donor and acceptor units with alkyl chains to improve the solubility of the materials. We compare the electronic structure of alternating donor-acceptor polymers of N,N- disubstituted NDI units with 1,4-bis(2-ethylhexyl)-2,5-diethynylbenzene (**NDIP**),[1] 6,7-dihexyl-1,4-bis(trimethylsilylethynyl)naphthalene (**NDIN**), 2,6-dialkyl-9,10-bis(trimethylsilylethynyl)lanthracene (**NDIA**) shown in Figure 3.5. UV-visible, fluorescence and infrared spectroscopies, along with differential pulse voltammetry were used to explore the quinoidal character in the polymer and to study its influence on the bandgap of D-A polymers.

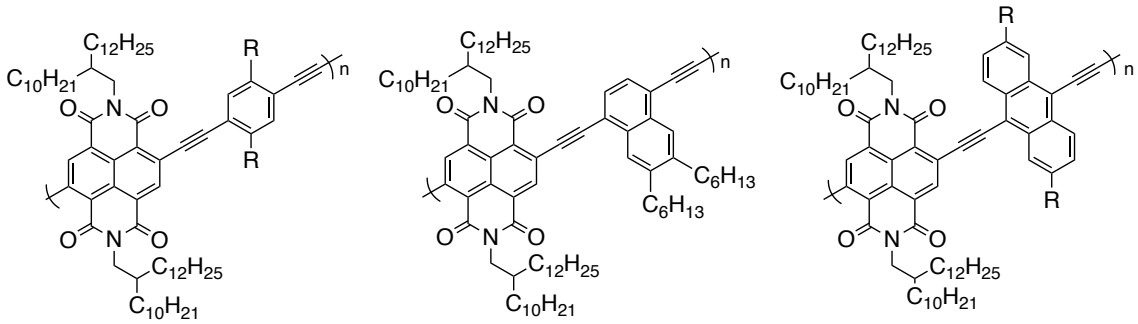

Figure 3.5. NDI-acene donor-acceptor copolymers containing 1,4-phenylene, 1,4-naphthalene and 9,10-anthracene units (**NDIP**, **NDIN** and **NDIA**, respectively). R = 2-ethylhexyl.

3.2 RESULTS AND DISCUSSION

3.2.1 Synthesis

The alternating conjugated polymers of **NDI** with anthracene and naphthalene units were synthesized by Pd-catalyzed Sonogashira coupling of *N*,*N*'-di(2-decyltetradecyl)-2,6-dibromonaphthalene-1,4,5,8-bis(dicarboximide) monomer and the appropriate diethynylarene monomer. The synthesis of 6,7-dihexyl-1,4-bis(trimethylsilyl ethynylene) naphthalene (**1)**, and 2,6-bis(2-ethylhexyl)-9,10- bis(trimethylsilyl ethynylene) anthracene (**2)** are reported in chapter 2. Attempts to purify the 9,10-diethynylanthracene monomer were unsuccessful due to its instability in air. Accordingly, we chose to carry out the polymerizations by *insitu* desilylation of the bis(trimethylsilylethynyl) substituted monomers **1** and **2** using tetra-*n*-butylammonium difluorotriphenylsilicate (TBAT) as source of flouride, as shown in Figure 3.6. At the end of polymerization, the polymers were precipitated in methanol and purified by Soxhlet extraction with acetonitrile, acetone, hexane and chloroform. The molecular weights of polymer fraction extracted into chloroform were determined by high temperature GPC in 1,2,4-trichlorobenzene to be 10 kDa for the NDI-naphthalene polymer **NDIN** and 31 kDa for **NDIA**. Thus, the molecular weight of **NDIA**, which has alkyl substitutents on both the donor and acceptor units, was higher than for the analog with alkyl groups only on the acceptor unit that has been reported previously (~3 kDa).[14] We could not obtain well resolved NMR signals for the polymers, possibly due to aggregation, as has been suggested by others for NDI- and PMDI-containing D-A conjugated polymers.[14]

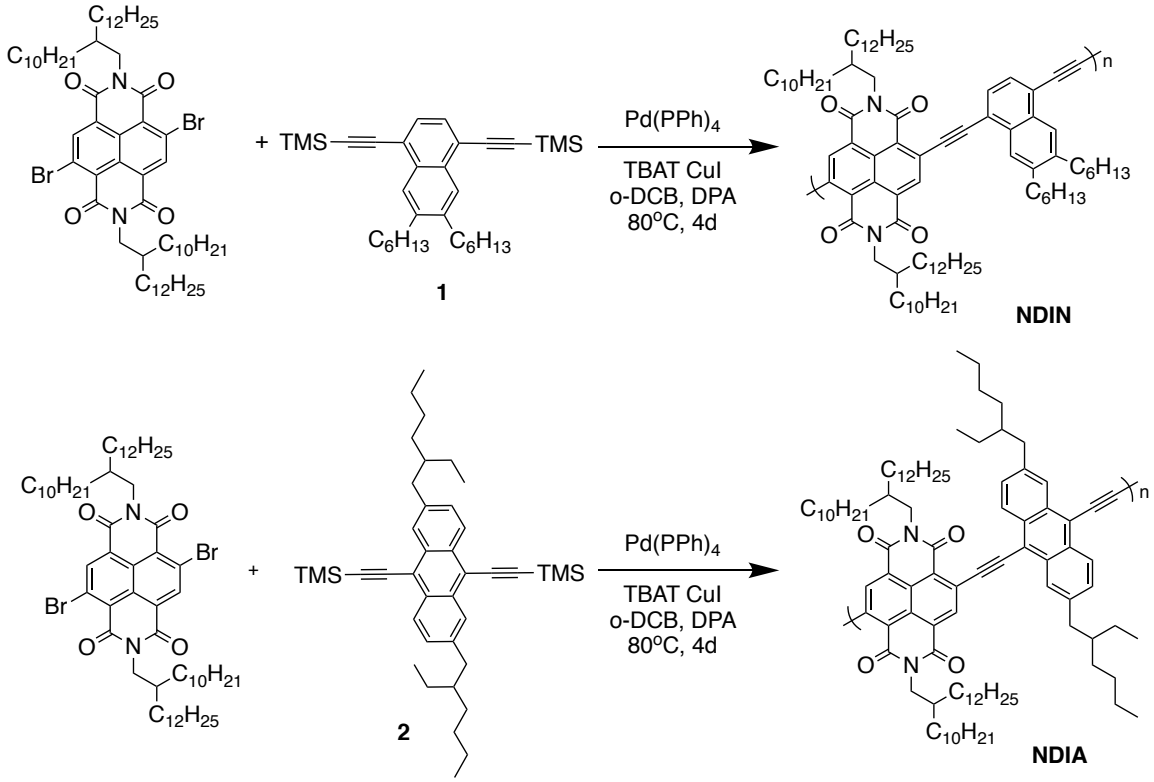

Figure 3.6. The polymerization schemes for **NDIN** and **NDIA**.

3.2.2 Infrared spectroscopy

Infrared spectra were recorded for solid samples of the polymers as shown in Figure 3.7. All of the polymers displayed a medium-strength bond stretching band for the unsymmetrically substituted C≡C bond. The C≡C bond stretching frequency of **NDIA** (2169 cm^{-1}) was lower than that of **NDIN** (2183 cm^{-1}) and **NDIP** (2188 cm^{-1})**.** The lower bond stretching frequency of the triple bond for **NDIA** corresponds to a lower bond order than in the other two polymers. This is consistent with the suggestion that the presence of the 9.10-anthracenediyl unit in the conjugated backbone enhances the quinoidal character of the of the polymer by maintain the aromaticity of the fused benzene rings.

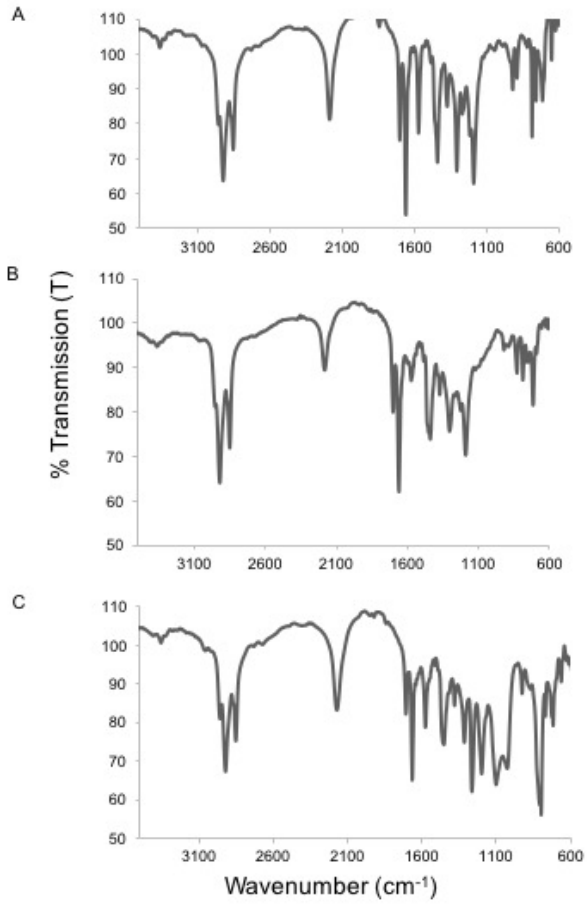

Figure 3.7. IR spectra of thin films of polymers (transmission intensity). A, **NDIP**; B, **NDIN**; and C, **NDIA**.

3.2.3 Ultraviolet-visible absorption spectroscopy

The UV-visible spectra of the polymers were recorded in chlorobenzene, as shown in Figure 3.8. Solution spectra of **NDIN** and **NDIP** showed two optical transitions while **NDIA** had a strong low energy transition but a weak high- energy transition. The low-energy transitions of the phenylene and naphthalene analogs were in the range of 500-780 nm and probably correspond to a HOMO-LUMO transition which has some donor-to-NDI charge transfer character.[1] The **NDIA** and **NDIP** both have a vibronic feature slightly at lower wavelength from the maxima of low energy transition at 546 nm for NDIP and at 698 nm for NDIA respectively. The energy of the vibronic transition is about 0.17 eV and it corresponds to wavenumber of about 1350 cm^{-1} . In the infra red of solid samples there are peaks around 1375 cm^{-1} which correspond to C-N stretches.[20] The appearance of vibronic feature in **NDIP** and **NDIA** and not in **NDIN** is possibly because **NDIP** and **NDIA** have more restricted rotation compared to **NDIN** leading to a lesser conformational inhomogeneity, which tend make the absorption spectrum broad. The high-energy transitions were around 372 nm for **NDIN** and **NDIP**, and correspond to a π-π^* transition that may be localized on NDI, since the spectrum of NDI itself displays a strong adsorption at 372 nm [1]. For **NDIA** the high energy transitions are weak and slightly red shifted compared to **NDIP** and **NDIN**. This could be because of electron richness of the anthracene unit, which leads to destabilization in the energy of the valence band.

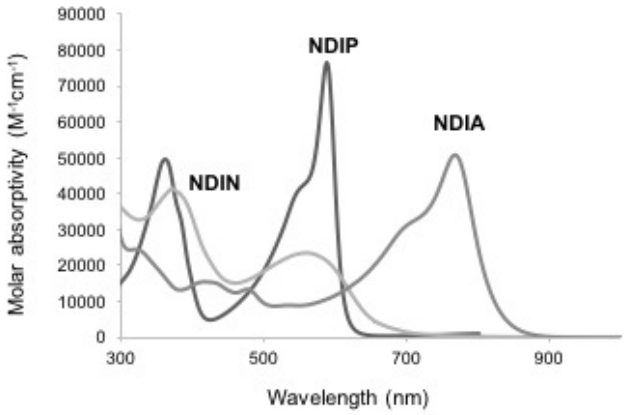

Figure 3.8. UV-visible absorption spectra of three polymers in chlorobenzene: **NDIP**, **NDIN** and **NDIA**.

The relative energies of the low- energy absorptions can be also understood in terms of electron richness of the donor, with anthracene being a stronger donor compared to phenylene and naphthalene. As a result anthracene destabilizes the HOMO of the polymer more than phenylene and naphthalene. This leads to significant red-shift in the low energy absorption by about 190 nm. The absorption spectra of three polymers is shown in the Figure 3.8. **NDIP** has the highest molar absorptivity for the low energy transition, followed by **NDIA** and **NDIN,** respectively. These features could be ascribed to a better spatial overlap of ground and excited state wavefunctions in **NDIP** which determines the oscillator strength of the transition.[3] Despite of delocalization along the polymer backbone, the HOMO might be relatively more localized on the donors in the case of **NDIA** and **NDIN** compared to the phenylene in **NDIP**. This is evident from the electrostatic potential maps for tetramers similar in molecular structure to **NDIP** and **NDIA**. The electron density is higher in the anthracene of **NDIA** compared to phenylene with **NDIP**.[14] Detailed analysis of the HOMO and LUMO wavefunctions of oligomeric

models of the polymers is necessary to confirm this conjecture. **NDIN** showed lowest absorptivity for low energy transition, this shows relatively lesser spatial overlap of ground and excited states. The possible reason could be that the HOMO is relatively more localized on the phenyl ring bearing alkyl groups. Preliminary semi empirical calculations on model compounds shown in Figure 3.9. The presence of node in the HOMO of 1,4- dipropyne naphthalene on carbons fusing the two benzene rings, suggest that the peripheral π- electrons on the fused benzene ring does not participate in the main conjugation which is through the 1,4-positions. This probably lead to slight blue shift in charge transfer transition and low absorptivity of the transition. Detailed theoretical investigation of ground and excited states of **NDIN** would be necessary. The other possible reason could be an inherent twist along the backbone, which could be giving rise to broad spectrum lacking any vibronic structure. It could be either of these or both contributing.

The absorption spectra of the three polymers in the solid state were similar to those obtained in in solution as shown in Figure 3.10. This shows that the polymers adopt the same structure in solution and solid state. The band gaps were measured from the solid-state absorption onsets and monotonically decease with the fusion of benzene rings onto the conjugated backbone, ranging from **NDIP** ~ 2.0 eV for **NDIP**, to 1.76 eV for **NDIN,** to 1.42 eV for **NDIA.**

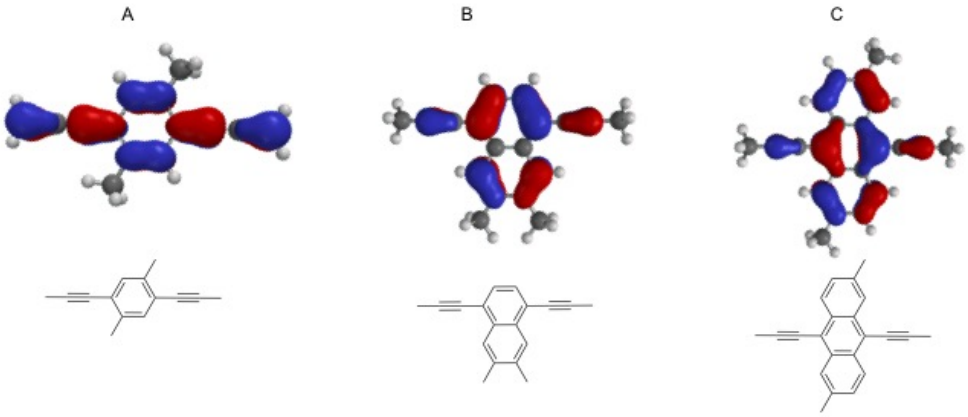

Figure 3.9. HOMO computed by semiempirical method of: A, 1,4-dipropyne-3,6-dimethyl phenylene; B, 1,4- dipropyne-6,7-dimethyl naphthalene; C, 2,6-dimethyl-9,10-dipropyne anthracene.

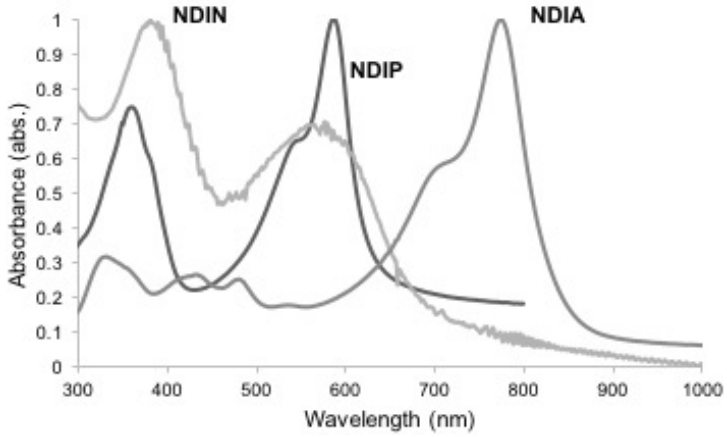

Figure 3.10. Normalized thin film spectra of three polymers: **NDIP, NDIN** and **NDIA**

3.2.4 Fluorescence spectroscopy

The photoluminescence spectra were recorded for the three polymers in chloroform (Figure 3.11). **NDIP** showed fluorescence maximum at 694 nm, for **NDIN** it was at 666 nm and **NDIA** showed very weak fluorescence at 822 nm. The weak fluorescence in **NDIA** is because of higher rate of non - radiative pathways compared to the radiative decay. The increase in non-radiative decay rate can be attributed to the lesser energy difference between ground electronic state and excited electronic state for **NDIA** than for **NDIP** and **NDIN**, thus making non radiative pathways more efficient compared to the radiative pathways.[21]

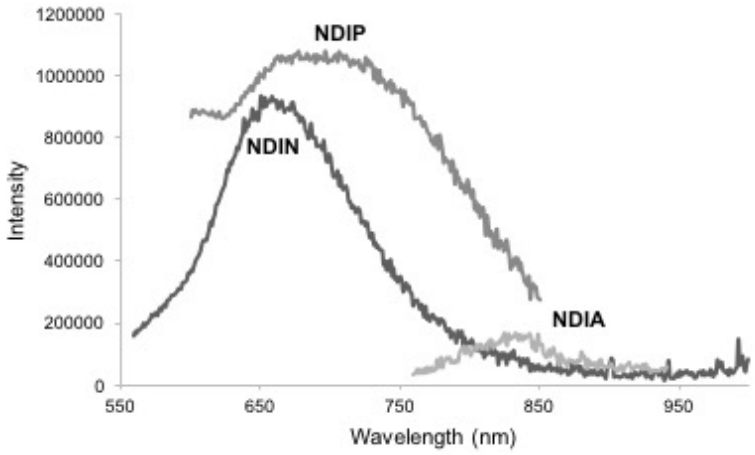

Figure 3.11. Non-normalized fluorescence spectrum of three polymers: **NDIP**, **NDIN** **NDIA**.

3.2.5 Solvatochromism

The solvatochromism in three different solvents of varying polarity was performed to understand the charge separated state in the polymers. The solvents used, in the order of increasing dielectric constant were cyclohexane (ε = 2.0), chloroform (ε =4.8), and chlorobenzene (ε = 9.2). The absorption spectrum of **NDIP**, **NDIN** and **NDIA** showed only small changes in absorbance upon changing the solvents as shown in Figures 3.12 and 3.13.

NDIP shows some solvatochromic effect in its fluorescence as shown in Figure 3.13. The emission maxima progressively red – shifted upon increase in solvent dielectric from cyclohexane (~678 nm) to chloroform (~694 nm) to chlorobenzene (~718 nm). This indicates that the presence of a polar excited state that is stabilized by more polar solvent. Another feature worth noting is that **NDIP** has a shoulder at 745 nm in the emission spectrum which could be due to intermolecular aggregation. This is evident from the increase in intensity of the shoulder when the concentration is increased from 0.8 μg/mL to 33μg/mL as shown in Figure 3.15 and 3.16, the absorption spectrum, however, is weakly changed upon changing the concentration. The lack of red shifted peak in the absorption spectrum upon changing the concentration suggest that the aggregate is possibly an excimer.

The absorption spectrum was of **NDIN** shows only a small change in absorption spectrum in the three solvents as shown in Figure 3.17. The emission spectra of **NDIN** shows a maximum approximately at 667 nm in chlorobenzene, cyclohexane and chloroform. The lack of a red shift in the emission spectrum in chlorobenzene suggests that the excited state of **NDIN** is not very polar**.** The increased electron density due to

fusion of benzene ring within the naphthalene seems to diminish the charge separation in the excited state.

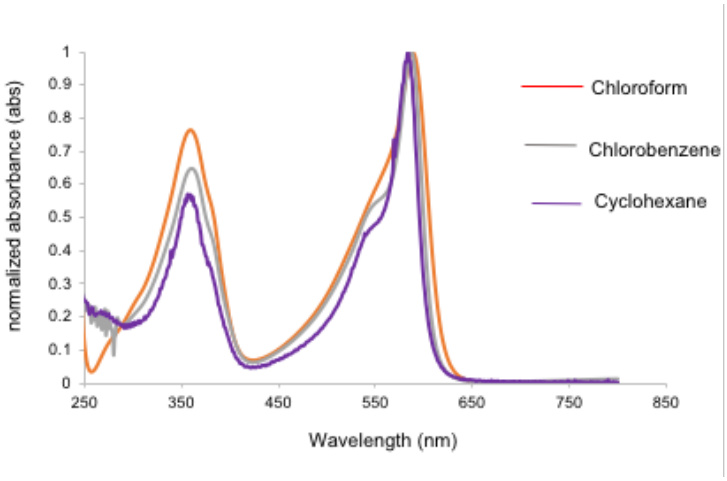

Figure 3.12. Normalized absorption spectrum of **NDIP** in different solvents at concentration of 33 µg/mL.

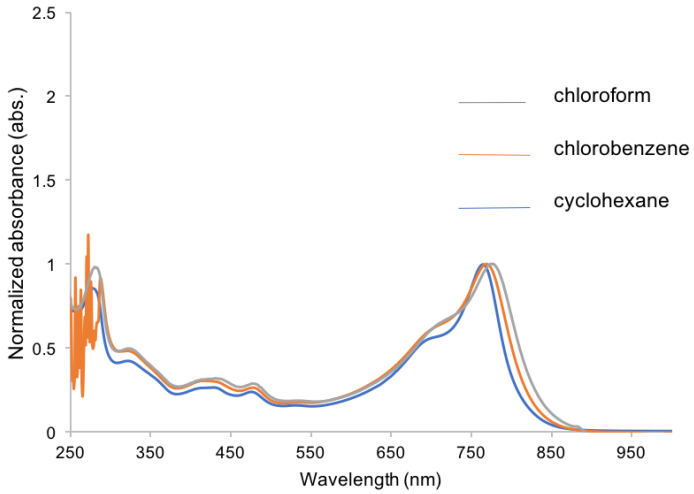

Figure 3.13. Normalized absorption spectrum of **NDIA** in different solvents at concentration of 33 µg/mL.

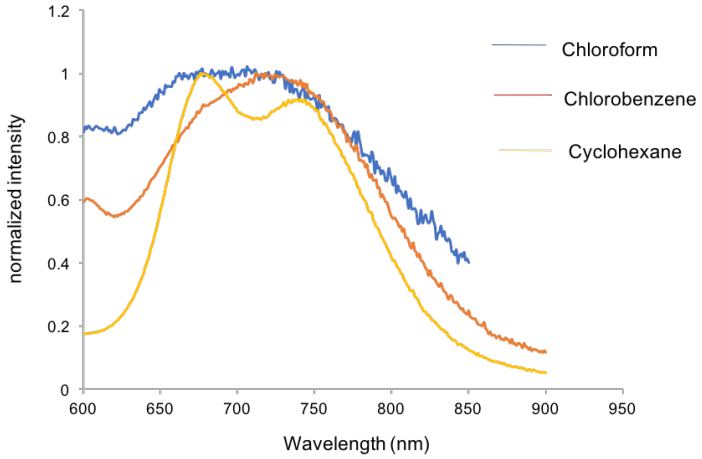

Figure 3.14. Normalized fluorescence spectrum of **NDIP** at concentration 0.8 µg/mL (λ_{ex} 585 nm).

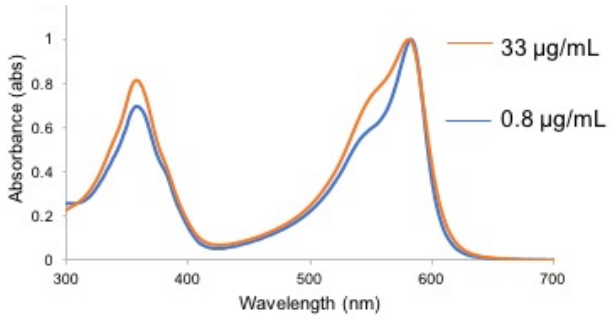

Figure 3.15. Absorption spectrum of **NDIP** in cyclohexane at two concentrations.

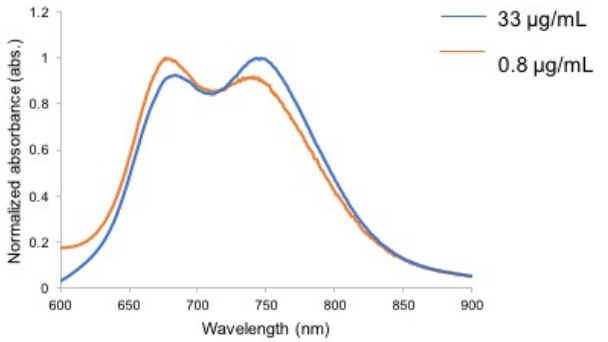

Figure 3.16. Normalized fluorescence spectrum of **NDIP** in cyclohexane at two concentrations (λ_{ex} 585 nm).

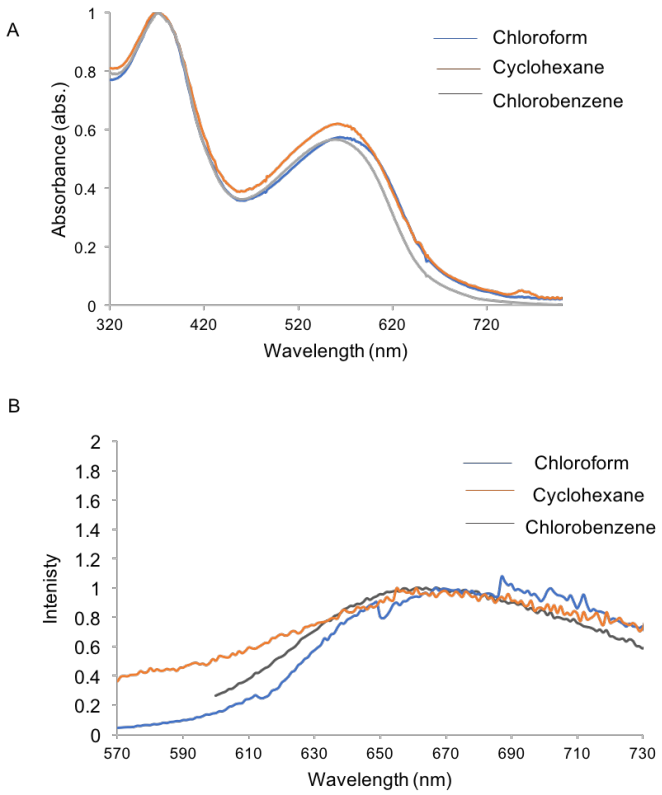

Figure 3.17. Normalized absorption (A) and fluorescence spectra (B) of **NDIN** in different solvents at concentration 33 µg/mL (λ_{ex} 372 nm)

3.2.6 Thermal properties

The decomposition temperatures of the two polymers **NDIN** and **NDIA** were found to be above 360°C in thermogravimetric analysis (TGA) (Figure 3.18). The thermal transitions of two polymers **NDIN** and **NDIA** were investigated by differential scanning calorimetry (DSC) which demonstrated no evidence of phase transitions in the temperature range examined (0-300°C), as shown in Figure 3.19. The annealing of **NDIN** at 150 °C did not induce any crystallinity as shown in Figure 3.20.

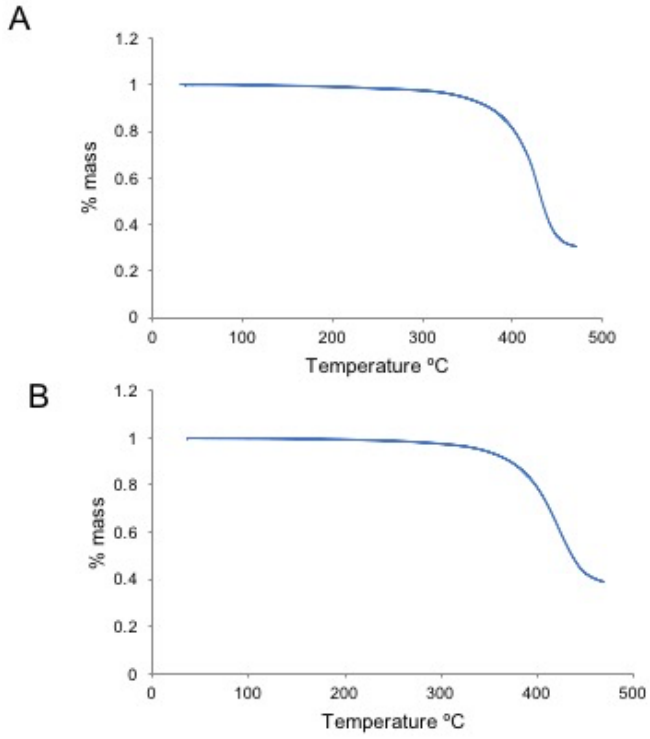

Figure 3.18. TGA: A, **NDIN**; and B, **NDIA**. Heating rate 10°C/min from 25 to 480°C.

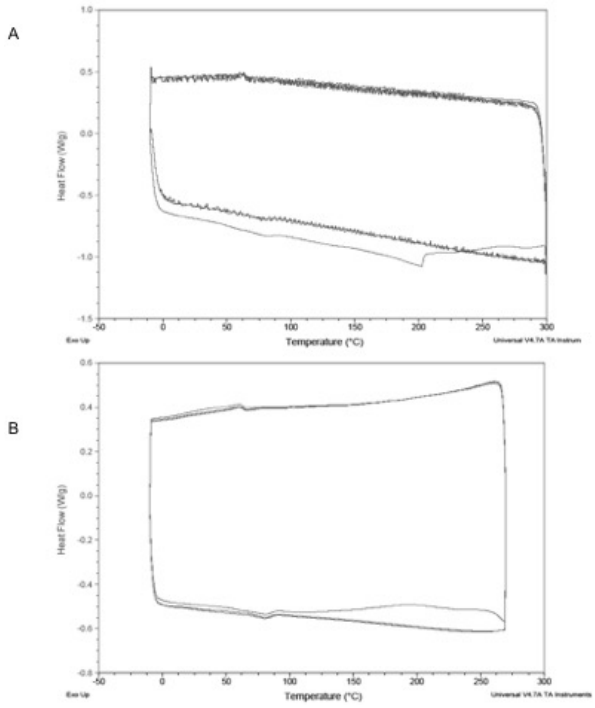

Figure 3.19. DSC curves for A, **NDIN**; and B, **NDIA.** Heating rate 10°C/min from -10 to 300°C for **NDIN** and -10 to 275°C for **NDIA**

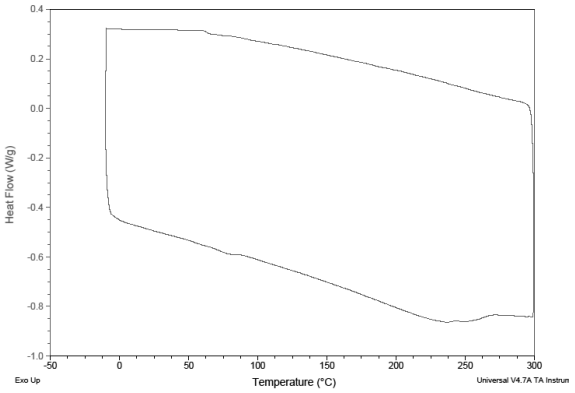

Figure 3.20. DSC curve of **NDIN** after annealing for 6 h at 150 °C.

3.2.7 Electrochemical measurements

Electrochemical measurements were made on polymer films deposited on glassy carbon button electrode using differential pulse voltammetry (DPV) (Figure 3.21). The reduction potentials of the polymer were measured in 0.5 M tetra-n-butylammonium hexafluorophosphate ($TBAPF_6$) in propylene carbonate against Ag/Ag^+ reference electrode. The three polymers show two reductive peaks, which is characteristic of NDI-containing polymers. The first reduction peak potential appears at ~1.01 V for **NDIP** and ~ 0.95 V and ~0.97 V for **NDIN** and **NDIA** respectively as shown in Table 2. The values of the reduction potential reflects domination of NDI in making contributions to the LUMO. The reduction potential for NDI is ~ (1.0-1.1 V).[14] Incorporation of naphthalene and anthracene lowers the LUMO level slightly as evident from the potential of the first reduction peaks.

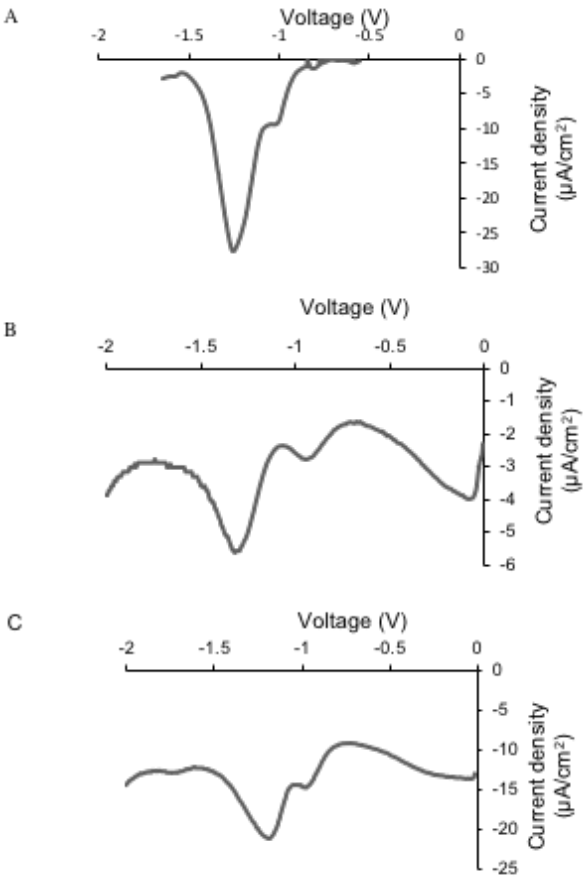

Figure 3.21. Differential pulse voltammetry analysis: A, **NDIP**; B, **NDIN**; C, **NDIA**. Stepsize: 2mV; step time 0.1 s. The measurements were performed using a Ag/Ag^+ reference electrode with a Pt counter electrode in 0.5 M (tetra-*n*-butylammonium hexafluorophosphate) in propylene carbonate.

Table3.1. Electrochemical and photophysical properties of polymers.

Polymer	UV-Vis, λ_{max} (nm)		$E_{red,1}$ (V)[b]	$E_{red,2}$ (2) (V)	E_{HOMO} (eV)[b]	E_{LUMO} (eV)[b]	Optical bandgap, E_g^{opt} (eV)[c]
	solution[a]	solid state					
NDIP	365, 587	365, 585	-1.01	-1.26	-5.84	-3.79	1.99
NDIN	373, 565	373, 575	-0.95	-1.29	-5.49	-3.85	1.61
NDIA	763	768	-0.97	-1.21	-5.25	-3.83	1.42

[a]Measured in THF; [b]Onset for reduction wave from DPV measurements of polymer films deposited on glassy carbon button electrode in 0.5 M tetra-*n*-butylammonium hexafluorophosphate ($TBAPF_6$) in propylene carbonate. LUMO = -(E_{red} (1) + 4.8) eV. HOMO = LUMO - E_g^{opt} ; [c]Optical bandgap measured from absorption spectroscopy of thin films.

3.2.8 X-ray diffraction studies

The powder XRD of all three polymers are shown in Figure 3.22. All the three polymers showed a broad peak in the range of 18° to 22°. This corresponds to an amorphous halo that usually appears in alkyl substituted conjugated polymers. The origin of the amorphous halo is the distance between the alkyl side groups which can vary in the range of (4.3–5.1 Å) depending on the tilt angle with respect to the polymer backbone.[22] The **NDIN** and **NDIA** showed two additional broad peaks at ~ 4.3° and ~ 3.9°, respectively, which correspond to the distances of ~21 Å and ~22 Å. These distances correspond to the distance between two parallel polymer chains in a lamellar structure.

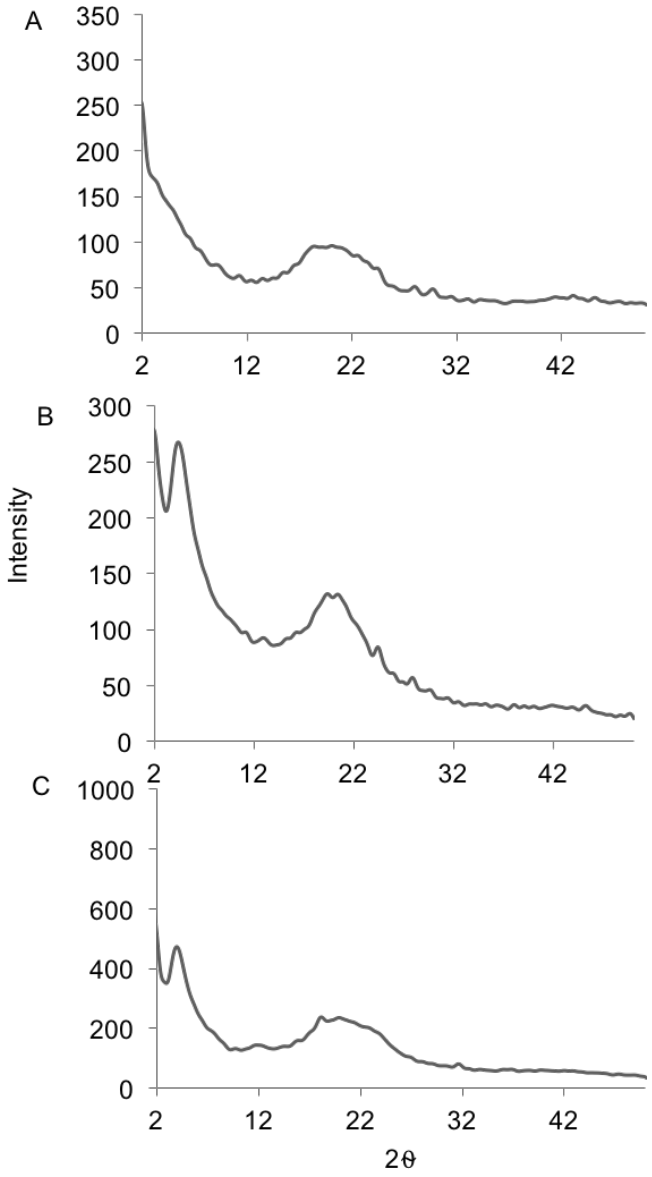

Figure 3.22. Powder XRD of polymers; A, **NDIP**; B, **NDIN**; and C, **NDIA.**

3.3 CONCLUSION

In conclusion, the optical band gap of a series of NDI-acene containing polymers decreases in the order of **NDIP** > **NDIN** > **NDIA**, because the extended π- electron conjugation offered by the fusion of benzene rings to the phenylene unit in the conjugated backbone of the polymer enhances the quinoidal character of the polymer. The molar absorptivity values for low energy transition however, is maximum for **NDIP** followed by **NDIA** and least for **NDIN**. The reason for low oscillator strength of low energy transition for NDIN is possibly due to poor spatial overlap of ground and excited states. The reasons for this possibly be that the HOMO could be more localized on the phenyl ring bearing alkyl groups and/or inherent twist in the polymer backbone. The fluorescence of **NDIP** does shows a solvatochromic effect, suggesting the presence of a polar excited state. Considering the low bandgap offered by **NDIA**, it is a potential material for application for OPV.

3.4 EXPERIMENTAL

3.4.1 General methods

Materials. [1,3-Bis(diphenylphosphino)propane]dichloronickel(II) dichloride, ($[Ph_2P(CH_2)_3P\ Ph_2]NiCl_2$), bis(triphenylphosphine)palladium(II) dichloride ($[(Ph_3P]_2PdCl_2$), copper iodide (CuI), trimethylsilylacetylene, tetra-*n*-butylammonium difluorotriphenylsilicate (TBAT), and anhydrous diisopropylamine (DPA), were purchased from Sigma Aldrich. *N*,*N*'-di(2-decyltetradecyl)-2,6-dibromonaphthalene-1,4,5,8-bis(dicarboximide) (**NDI**) and Poly(*N*,*N*'-bis(2-octyldodecyl)-2,6-naphthalene-1,4,5,8-bis(dicarboximide) ethynylene-*alt*-1,4-bis(2-ethylhexyl)-2,5-diethynyl benzene) (**NDIP**) were synthesized by Reichmannis lab and Marder lab respectively. All the reagents were used as purchased without further purification.

Characterization. The molecular weights of polymers were determined by size exclusion chromatography (SEC) using polystyrene standard and 1,3,4-trichlorobenzene as the eluent at 130 °C. UV-Vis measurements were recorded on an Agilent 8510 instrument. Electrochemical measurements were done in a three-electrode cell with a Pt flag as the counter electrode, a Ag/Ag^+ standard electrode ($E_{1/2}$ vs ferrocene = +58 mV) and a polymer-coated glassy carbon button as a working electrode with electrolyte consisting 10 mM $AgNO_3$ in 0.5 M $TBAPF_6$ in acetonitrile. NMR spectra were recorded using a Varian Mercury spectrometer (^1H NMR, 300 MHz). IR spectra were recorded using a Bruker ALPHA FT-IR spectrometer. Fluorescence measurements of solutions were measured using a QuantaMaster 40 fluorimeter on solutions of the polymers having an absorbance of less than 0.1. Thin films were spin coated from a solution if chlorobenzene with a concentration of about 5 mg/mL for all the three polymers. Powder

XRD was measured by X'Pert Pro Alpha-1 diffraction system which uses Kα1 radiation for Cu or Co.

3.4.2 Synthesis

3.4.2.1 Poly(*N*,*N*'-di(2-decyltetradecyl)-2,6-naphthalene-1,4,5,8-bis(dicarboximide) ethynylene-*alt*-2,6-diethylhexyl-9,10-anthraceneethynylene),NDIA.

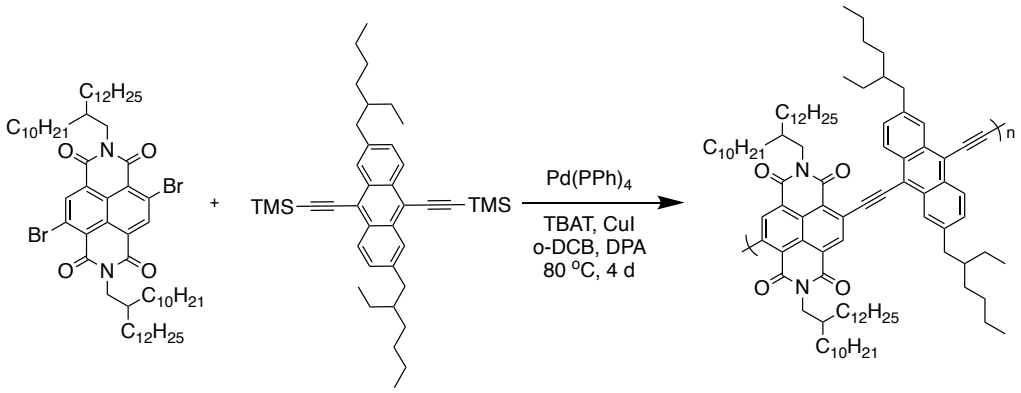

2,6-Di(2-ethylhexyl)-9,10-bis(trimethylsilylethynyl)anthracene (123 mg, 206 μmol) and *N*,*N*'-di(2-decyltetradecyl)-2,6-dibromonaphthalene-1,4,5,8-bis(dicarboximide) (220 mg, 200 μmol) were added to a solution of $Pd(PPh_3)_4$ (2.3 mg, 2.0 μmol), CuI (5.9 mg, 31 μmol) and TBAT (446 mg, 826 μmol) in a mixture of anhydrous 1,2-dichlorobenzene (7.0 mL) and *N*,*N*'-diisopropylamine (2.3 mL) The mixture was heated to 80°C for 4 d. The mixture was cooled and added to methanol (50 mL). The precipitated solid was collected by filtration to afford a green solid. The solid was subjected to extraction in a Soxhlet extractor with acetonitrile followed by acetone, hexane, and then chloroform. The material isolated by removal of solvent from the chloroform fraction (50 mg) was characterized further. GPC (in trichlorobenzene): M_n, 31

kDa (PDI, 4.4). Anal. calcd. for $C_{98}H_{146}N_2O_4$: C, 82.90; H, 10.37; N, 1.97. Found: C, 81.65; H, 9.79; N, 1.99.

GPC of NDIA

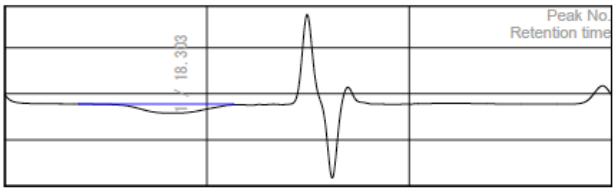

Molecular mass calculation result (RI)
Peak 1 Valley Peak

	[min]	[mV]	[mol]		
Peak start	13.625	138.845	5,081,341	Mn	31,482
Peak top	18.303	128.884	62,694	Mw	139,644
Peak end	21.325	138.066	3,667	Mz	755,379
				Mz+1	2,173,281
				Mv	139,644
Height [mV]			10.017	Mp	62,694
Area [mV*s]			2162.844	Mz/Mw	5.409
Height% [%]			100.000	Mw/Mn	4.436
[eta]			139643.94480	Mz+1/Mw	15.563

3.4.2.2 Poly(*N*,*N*'-bis(2-decyltetradecyl)-2,6-naphthalene-1,4,5,8-bis(dicarboximide) ethynylene-*alt*-6,7-dihexyl-1,4-naphthalene ethynylene), NDIN.

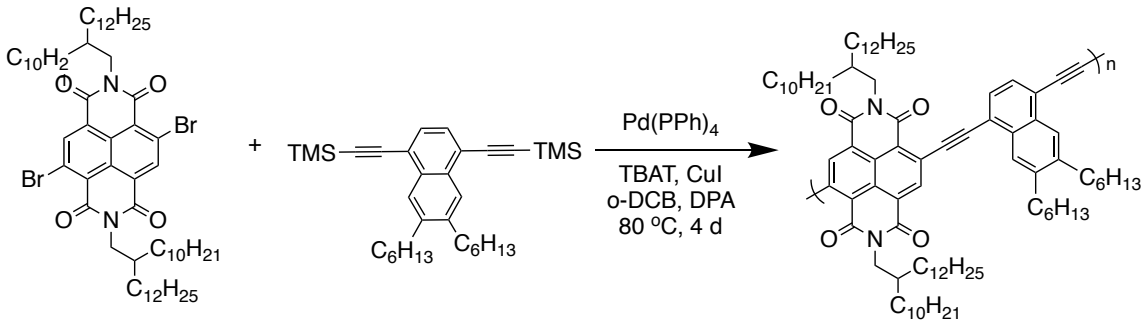

6,7-Dihexyl-1,4-bis(trimethylsilylethynyl)naphthalene (79.0mg, 161 μmol) and *N*,*N*'-bis(2-decyltetradecyl)-2,6-dibromonaphthalene-1,4,5,8-bis(dicarboximide) (172 mg, 157 μmol) were added to a mixture of $Pd(PPh_3)_4$ (1.86 mg, 1.61 μmol), CuI (4.4 mg,

23 μmol), TBAT (338 mg, 627 μmol) in a mixture of anhydrous 1,2-dichlorobenzene (2.6 mL) and *N*,*N*-diisopropyl amine (1.0 mL). The mixture was heated to 80 °C for 4 d. The mixture was cooled and added to methanol (75 mL), and the precipitated solid was collected by filtration to yield a purple solid. The solid was subjected to extraction in a Soxhlet extractor with acetonitrile, and acetone, followed by hexane, and then chloroform. The material isolated by removal of solvent from the chloroform fraction (10 mg) was characterized further. GPC (in trichlorobenzene): M_n, 10 kDa (PDI, 2.5). Anal. calcd. for $C_{90}H_{136}N_2O_4$: C, 82.57; H, 10.24; N, 2.19. Found: C, 82.14; H, 9.98; N, 2.38.

GPC of NDIN

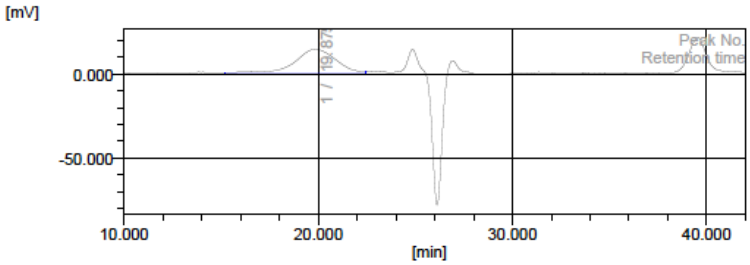

Molecular mass calculation result (RI)
Peak 1 Valley Peak

	[min]	[mV]	[mol]
Peak start	15.227	0.912	1,174,050
Peak top	19.875	14.715	14,603
Peak end	22.453	1.335	1,281
Height [mV]			13.794
Area [mV*s]			1925.057
Height% [%]			100.000
[eta]			26449.36158

Mn	10,264
Mw	26,449
Mz	126,884
Mz+1	406,902
Mv	26,449
Mp	14,581
Mz/Mw	4.797
Mw/Mn	2.577
Mz+1/Mw	15.384

3.5 REFERENCES

1. Sajoto, T.; Tiwari, S. P.; Li, H.; Risko, C.; Barlow, S.; Zhang, Q.; Cho, J.-Y.; Brédas, J.-L.; Kippelen, B.; Marder, S. R., Synthesis and characterization of naphthalene diimide/diethynylbenzene copolymers. *Polymer* **2012,** *53* (5), 1072-1078.

2. Gibson, G. L.; McCormick, T. M.; Seferos, D. S., Atomistic band gap engineering in donor–acceptor polymers. *Journal of the American Chemical Society* **2011,** *134* (1), 539-547.

3. Pandey, L.; Risko, C.; Norton, J. E.; Brédas, J.-L., Donor–acceptor copolymers of relevance for organic photovoltaics: a theoretical investigation of the impact of chemical structure modifications on the electronic and optical properties. *Macromolecules* **2012,** *45* (16), 6405-6414.

4. Beaujuge, P. M.; Amb, C. M.; Reynolds, J. R., Spectral engineering in π-conjugated polymers with intramolecular donor− acceptor interactions. *Accounts of Chemical Research* **2010,** *43* (11), 1396-1407.

5. Liang, Y.; Xiao, S.; Feng, D.; Yu, L., Control in energy levels of conjugated polymers for photovoltaic application. *The Journal of Physical Chemistry C* **2008,** *112* (21), 7866-7871.

6. Cheng, Y.-J.; Yang, S.-H.; Hsu, C.-S., Synthesis of conjugated polymers for organic solar cell applications. *Chemical Reviews* **2009,** *109* (11), 5868-5923.

7. Chen, J.; Cao, Y., Development of novel conjugated donor polymers for high-efficiency bulk-heterojunction photovoltaic devices. *Accounts of Chemical Research* **2009,** *42* (11), 1709-1718.

8. Anthony, J. E.; Facchetti, A.; Heeney, M.; Marder, S. R.; Zhan, X., n-Type Organic Semiconductors in Organic Electronics. *Advanced Materials* **2010,** *22* (34), 3876-3892.

9. Lu, L.; Zheng, T.; Wu, Q.; Schneider, A. M.; Zhao, D.; Yu, L., Recent advances in bulk heterojunction polymer solar cells. *Chemical Reviews* **2015,** *115* (23), 12666-12731.

10. Sommer, M., Conjugated polymers based on naphthalene diimide for organic electronics. *Journal of Materials Chemistry C* **2014,** *2* (17), 3088-3098.

11. Yan, H.; Chen, Z.; Zheng, Y.; Newman, C.; Quinn, J. R.; Dötz, F.; Kastler, M.; Facchetti, A., A high-mobility electron-transporting polymer for printed transistors. *Nature* **2009,** *457* (7230), 679-686.

12. Jung, J. W.; Jo, J. W.; Chueh, C. C.; Liu, F.; Jo, W. H.; Russell, T. P.; Jen, A. K. Y., Fluoro-Substituted n-Type Conjugated Polymers for Additive-Free All-Polymer Bulk Heterojunction Solar Cells with High Power Conversion Efficiency of 6.71%. *Advanced Materials* **2015,** *27* (21), 3310-3317.

13. Kudla, C. J.; Dolfen, D.; Schottler, K. J.; Koenen, J.-M.; Breusov, D.; Allard, S.; Scherf, U., Cyclopentadithiazole-based monomers and alternating copolymers. *Macromolecules* **2010,** *43* (18), 7864-7867.

14. Alvey, P. M.; Ono, R. J.; Bielawski, C. W.; Iverson, B. L., Conjugated NDI–Donor Polymers: Exploration of Donor Size and Electrostatic Complementarity. *Macromolecules* **2013,** *46* (3), 718-726.

15. Ito, K.; Suzuki, T.; Sakamoto, Y.; Kubota, D.; Inoue, Y.; Sato, F.; Tokito, S., Oligo (2, 6-anthrylene) s: Acene–Oligomer Approach for Organic Field-Effect Transistors. *Angewandte Chemie International Edition* **2003,** *42* (10), 1159-1162.

16. Liu, C.; Cai, W.; Guan, X.; Duan, C.; Xue, Q.; Ying, L.; Huang, F.; Cao, Y., Synthesis of donor–acceptor copolymers based on anthracene derivatives for polymer solar cells. *Polymer Chemistry* **2013,** *4* (14), 3949-3958.

17. Jiang, Y.; Mei, J.; Ayzner, A. L.; Toney, M. F.; Bao, Z., 5, 11-Conjugation-extended low-bandgap anthradithiophene-containing polymer exhibiting enhanced thin-film order and field-effect mobility. *Chemical Communications* **2012,** *48* (58), 7286-7288.

18. Okamoto, T.; Bao, Z., Synthesis of solution-soluble pentacene-containing conjugated copolymers. *Journal of the American Chemical Society* **2007,** *129* (34), 10308-10309.

19. Jiang, Y.; Hong, S.; Oh, J. H.; Mondal, R.; Okamoto, T.; Verploegen, E.; Toney, M. F.; McGehee, M. D.; Bao, Z., Impact of regioregularity on thin-film transistor and photovoltaic cell performances of pentacene-containing polymers. *Journal of Materials Chemistry* **2012,** *22* (10), 4356-4363.

20. Mallakpour, S.; Zadehnazari, A., Molten salt-supported polycondensation of optically active diacid monomers with an aromatic thiazole-bearing diamine using microwave irradiation. *Journal of Advanced Research* **2014,** *5* (3), 311-318.

21. Englman, R.; Jortner, J., The energy gap law for radiationless transitions in large molecules. *Molecular Physics* **1970,** *18* (2), 145-164.

22. Niedzialek, D.; Lemaur, V.; Dudenko, D.; Shu, J.; Hansen, M. R.; Andreasen, J. W.; Pisula, W.; Müllen, K.; Cornil, J.; Beljonne, D., Probing the Relation Between Charge Transport and Supramolecular Organization Down to Ångström

Resolution in a Benzothiadiazole-Cyclopentadithiophene Copolymer. *Advanced Materials* **2013,** *25* (13), 1939-1947.

CHAPTER 4. SYNTHETIC APPROACHES TO THE DEVELOPMENT OF ANTHRACENE MONOMERS FOR THE PREPARATION OF POLY(ARYLENE VINYLENE)S

4.1 INTRODUCTION

Poly(arylene vinylene)s are a class of conjugated polymers that consist of a;ternating arylene and vinylene linkages. These polymers find major application in organic light emitting diodes (OLEDs) and organic photovoltaics OPVs.[1] There has been a significant amount of research towards the development of poly(phenylene vinylene)s (PPV) derivatives that are solution processible. While the first few solution-processible PPV derivatives had long alkoxy side chains on the backbone, polymers with methoxy side chains such as Poly(2-methoxy-5-(3,7-dimethyloctyloxy)-1,4-phenylene-vinylene) (MDMO PPV) and poly(2-methoxy-5-(2-ethylhexyloxy)-1,4-phenylene-vinylene) (MEH PPV) are two examples that have received a significant amount of attention.[2]

The poly(arylene vinylene)s that containing acenes are less common. It is known from the literature that the incorporation of fused arenes into conjugated polymers can lead to stabilization of quinoidal forms of the polymer, which give rise to a low HOMO-LUMO gap.[3-4] Hence acenes incorporation of acenes can lead to lower band gap of the material as observed in chapter 2 and 3. There are few reports of the incorporation of anthracene into conjugated polymers to improve their optical and electrical properties.[5-6] One reason could be the difficulty in synthesizing alkoxy or alkyl substituted anthracene monomers which add solution processibility to the polymer.

The previous attempts to develop alternating copolymers that contain 9,10-anthrcenediyl and 1,4-phenylene diyl units were made by Heck coupling of 1,4-divinyl benzene and 9,10-dibromoanthracene, as shown in Figure 4.1 A. Low molecular weight materials were obtained due to lack of solubility of the polymer. Attempts to develop poly(9,10-anthrylene vinylene) via Heck coupling, as shown in Figure 4.1B failed.[7] This might be ascribed to the steric hindrance at the 9,10-positions of the 9,10-divinylanthracene monomer, or to insolubility of oligomers that precipitate from solution. The peri hydrogens of the divinylanthracene monomer (i.e., ones at 1,4- and 5,8-positions) offer steric hindrance to the addition of organometallic intermediate to the ethylene bond. In order to avoid this steric hindrance, the distance between the anthrylene units was increased by synthesizing 9,10-substituted butadienylene group.[7]

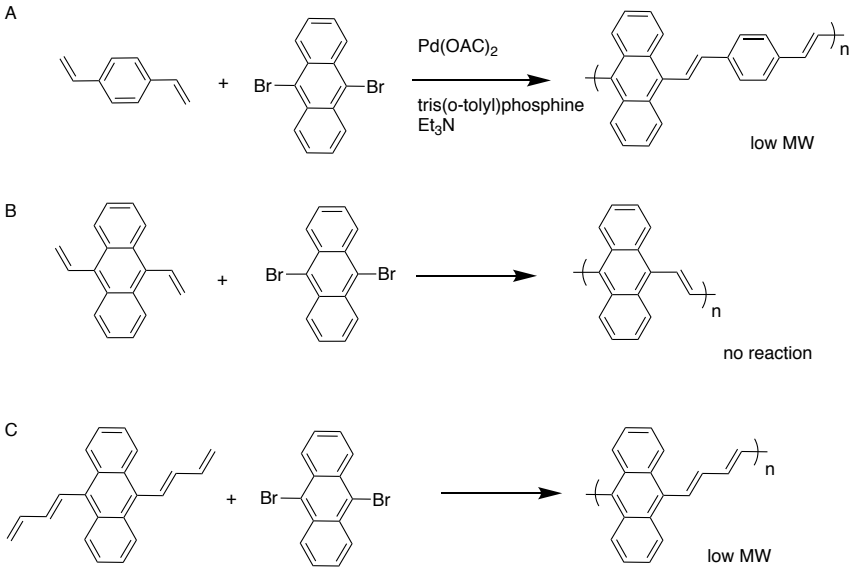

Figure 4.1. A, Poly(9,10-anthracene-co-phenylene vinylene)s ; B,Poly(9,10-anthracene vinylene); and C, Poly(9,10-butadienylene vinylene) via Heck coupling.

Despite failures to synthesize poly(9,10-anthralyne vinylene) via Heck coupling, small oligomers of 9,10-anthrylene vinylene units were obtained by Horner-Emmons type carbonyl olefinations (Figure 4.2). The degree of polymerization was really low, only trimers and tetramers were isolated.

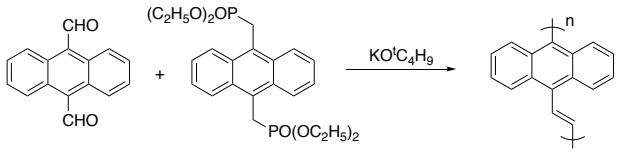

Figure 4.2. Preparation of oligo(9,10-anthracene vinylene)s.

In this chapter I discuss synthetic approaches to the tetra-alkoxy substituted anthracene monomers shown in Figure 4.3. We envisioned that the use of alkoxy side chains would provide solubility to the polymers. The 9,10-substitution by carbaldehyde and bromo methyl was planned to explore the polymerization via Wittig and Gilch methods, respectively.

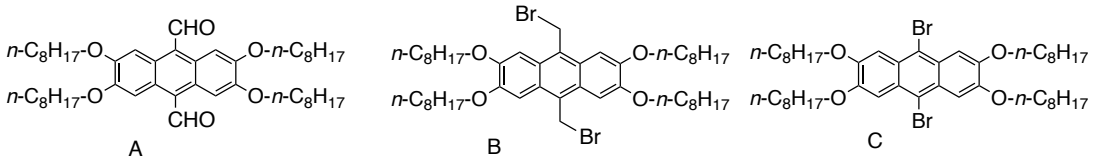

Figure 4.3. A, 2,3,6,7-Tetramethoxy-9,10-carbaldehyde anthracene; B, 2,3,6,7-tetramethoxy-9,10-bisbromomethyl anthracene; and C, 2,3,6,7-tetraoctyloxy-9,10-dibromo anthracene.

4.2 RESULTS AND DISCUSSION

4.2.1 Synthesis of 2,3,6,7-tetraoctyloxy-9,10-dicarbaldehyde, 9, by oxidation of 9,10-dimethyl anthracene intermediate

The synthesis of 2,3,6,7-tetraoctyloxy-9,10-carbaldehyde anthracene, **11**, was attempted from commercially available 1,2-dimethoxybenzene (veratrole, **1**), as shown in Figure 4.4. 2,3,6,7-Tetramethoxy-9,10-dimethyl anthracene, **2**, was synthesized from veratrole by condensation of acetaldehyde and veratrole. The oxidation of **2** with sodium chromate gave 2,3,6,7-tetramethoxy-9,10-anthraquinone, **3**. The demethylation of **3** was attempted by exposure to hydrobromic acid (48% HBr V/V) but the reaction was slow and did not facilitate complete demethylation of all four methoxy groups. However, reaction with boron tribromide followired by aqueous workup successfully yielded 2,3,6,7-tetrahydroxyanthracene-9,10-dione, **4**. The alkylation of **4** was achieved by Williamson ether synthesis by treating **4** with 1-bromooctane and potassium carbonate in *N,N*-dimethylformamide to yield **5**.

The reduction of **5** was achieved in two steps. In the first step, treatment of **5** with zinc in acetic acid provided anthrone **6**. Hydride reduction of **6** gave anthracene **7**. Reduction with sodium borohydride was sensitive to the choice of solvent. A first attempt in methanol resulted in a slow reaction. However, use of isopropanol as the solvent gave the desired product in approximately 50% yield. 2,3,6,7-Tetraoctyloxyanthracene **7** was treated with molecular bromine at 0°C to the yield dibromo compound **8**.

The formation of aldehyde **9** from **8** by dilithiation followed by formylation with DMF did not proceed as expected. The dilithiation was slow, requiring 4-5 hours to

proceed to completion. However, the nucleophilic addition to the carbonyl of DMF did not take place, instead we always obtained the debrominated anthracene after aqueous work-up. The reason for the low reactivity of aryllithium of anthracene derivative is not clear. It is known from the literature that the reactivity of organolithium reagents depends on the aggregates that it forms in the solution. The disaggregation can be induced by introducing chelating agents like TMEDA.[8] Use of TMEDA did not facilitate the reaction.

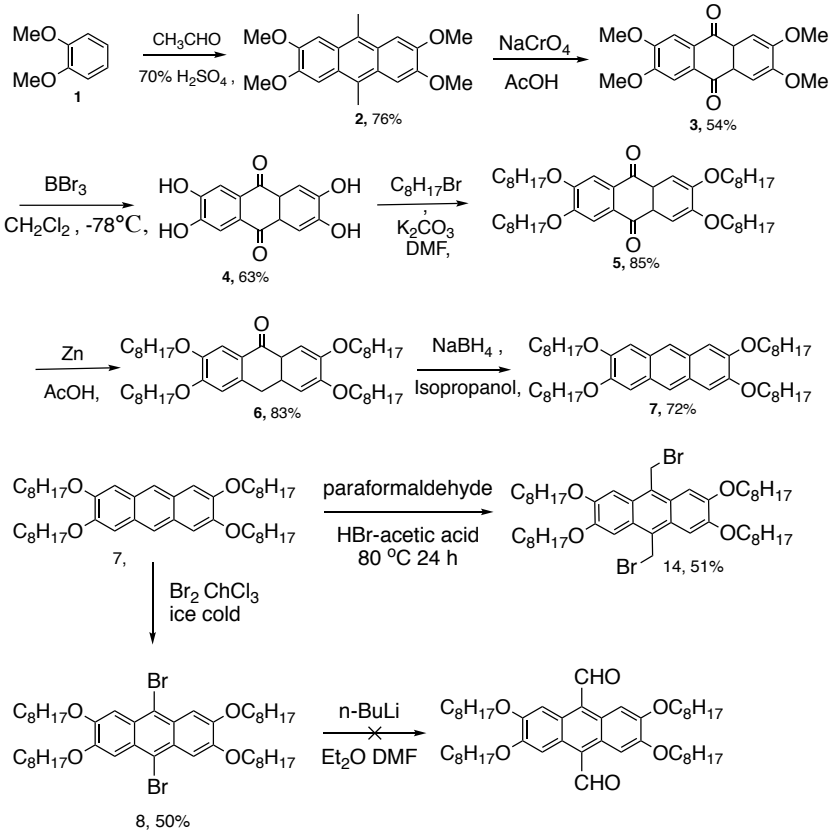

Figure 4.4. Synthesis of 9,10-dicarbaldehyde

4.2.2 Synthesis of 2,3,6,7-tetramethoxy-9,10-dicarbaldehyde anthracene

In a separate approach, we attempted to synthesize 2,3,6,7-tetramethoxy-9,10-anthracene dicarbaldehyde **13** without the need to oxidize **2** to the quinnone and reduction back to anthracene, as shown in Figure 4.5**.** Unlike the approach to prepare **9**, this approach functionalizes the methyl substituents at the 9,10-positions by bromination followed by oxidation. The aromaticity of the central ring of compound **2** is maintained in this approach. Initial success in radical bromination of the methyl groups of **2** to form 2,3,6,7-tetramethoxy-9,10-bis(bromomenthyl)anthracene, **12,** led us to pursue sodium nitrate oxidation of **12** to dialdehyde **13** in the presence of a base.[9] Multiple attempts made to conduct this reaction. However, the desired product was obtained in only trace amounts. This reaction is reported to proceed in quantative yields for benzylic bromides but with bis(bromomenthyl)anthracene derivative, **12,** it provided a number of side products which included anthraquinone **3**, based on the ^{1}H- NMR spectra of reaction products. The formation of the anthraquinone suggests that the 9- and 10- positions of tetramethoxy substituted anthracene derivative, **12** are very electron rich which makes sodium nitrate too harsh as an oxidant**,** to selectively oxidize it to dialdehyde, **13**. The installation of alkyl groups to improve solubility was achieved by demethylation of **2** by BBr_3 to obtain tetrahydroxy anthracene **10**, which underwent alkylation with primary alkyl halides in the presence of base to give tetraoctyloxy-substituted anthracene, **11**. The routes to the tetraalkoxy- substituted dicarboxaldehyde and bis(bromomethyl) anthracene monomer from **11** was further pursued by my colleague Jessie Sandridge.

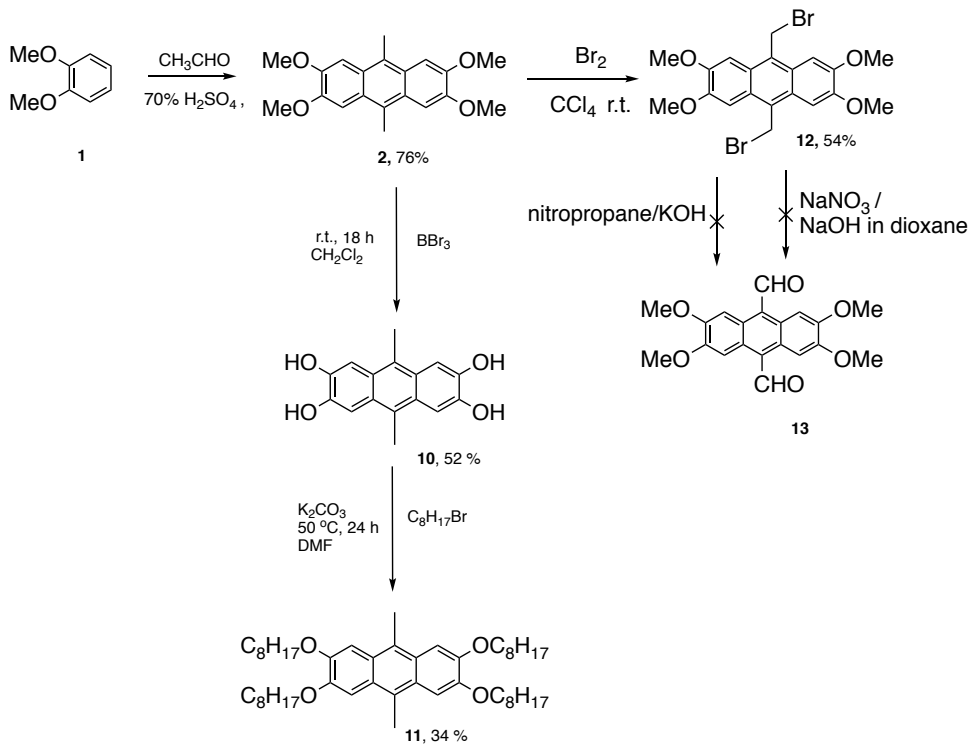

Figure 4.5. Synthesis of 9,10-dicarbaldehyde **13**.

4.3 Attempt to polymerize 2,3,6,7-tetraoctyloxy-9,10-bisbromomethyl anthracene, 14.

The polymerization of monomer **14**, via Gilch method as shown in Figure 4.6 did not proceed to give a polymer. The NMR of the material isolated from the reaction was complex. A possible reason for the lack of polymerization could lie in the mechanistic pathway of the Gilch reaction. In PPV syntheses, the propagating species for polymerization is p-quinodimethane formed by base-promoted 1,6-dehydrohalogentation of monomer.[1] In case of anthracene monomer **14,** this p-quinodimethane intermediate is stabilized by virtue of two fused benzene rings which may influence the rate of the propagation step.

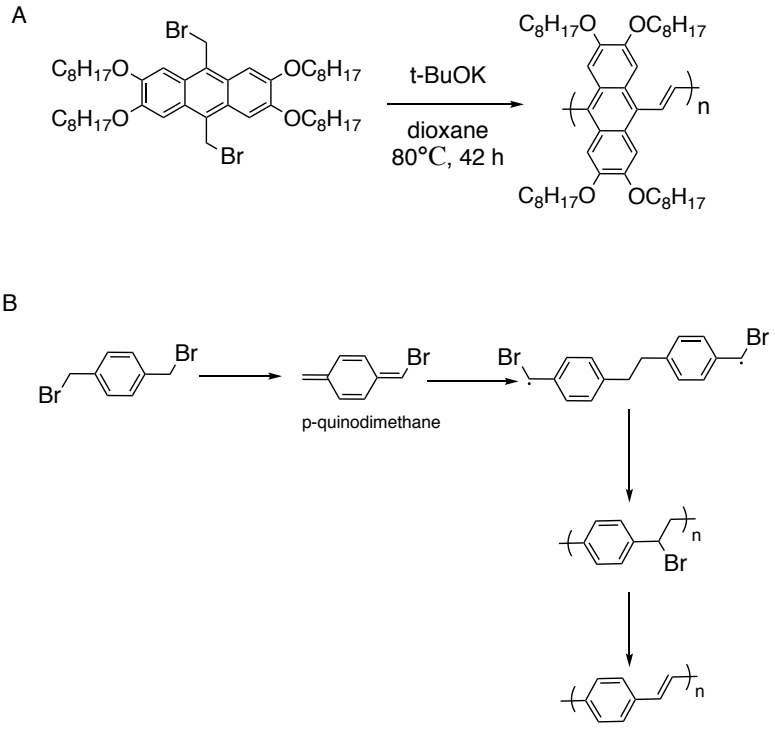

Figure 4.6. Synthesis scheme of Gilch reaction: A, polymerization raction of 14; B, mechanism of Gilch polymerization.[1]

4.4 CONCLUSION

Synthetic routes to prepare 2,3,6,7-tetraoctyloxy-9,10-dicarbaldehyde were explored. Two routes to 9,10-difunctionalized anthracenes we based on the reactivity of readily-available 2,3,6,7-Tetramethoxy-9,10-dimethyl anthracene, **2**. One approach made use of oxidative demethylation followed by conversion of the resulting anthraquinone to 9,10-disubstited anthracenes. The other involved reduced bromination of the methyl groups of **2** without effecting the oxidation state of the anthacene core. The success in preparing bis(bromomethyl)anthracene compounds might lead to the potential for Gilch polymerization to afford new PPV derivatives.

4.5 EXPERIMENTAL SECTION

4.5.1 2,3,6,7-Tetramethoxy-9,10- dimethylanthracene, 2[10]

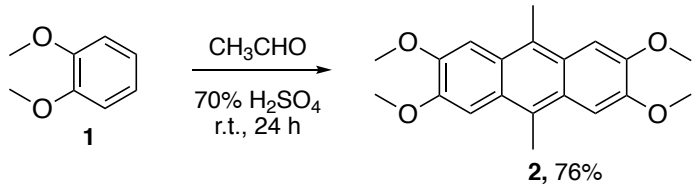

Veratrol (18 mL, 0.14 mol) was added to 500 mL of 70% H_2SO_4 solution at room temperature. The reaction mixture was cooled to 0°C and acetaldehyde (15 mL, 0.26 mol) was added in aliquots (1.5 mL over 20 min). The reaction mixture turned dark pink. After the addition was complete, the reaction mixture was warmed to room temperature and stirred for 24 h. The solution became viscous and additional 70% sulfuric acid was added to keep the solution stirring. After 24 h, the reaction vessel was cooled to 0°C, methanol (250 mL) and the mixture was stirred for 1 h. The mixture was filtered and the collected solid was washed with ice cold methanol (4 × 250 mL), and triturated with hot hexane. The solid was filtered and air dried to afford the product as a purple powder (18g, 76%). ^{1}H NMR (300 MHz, $CDCl_3$): δ 2.94 (s, 6H, Ar-CH_3), 4.08 (s, 12H, Ar-OCH_3), 7.40 (s, 4H, Ar-H). Spectral data matches with reference 10.

[1]H NMR of 2,3,6,7-tetramethoxy-9,10-dimethy anthracene, ***2***

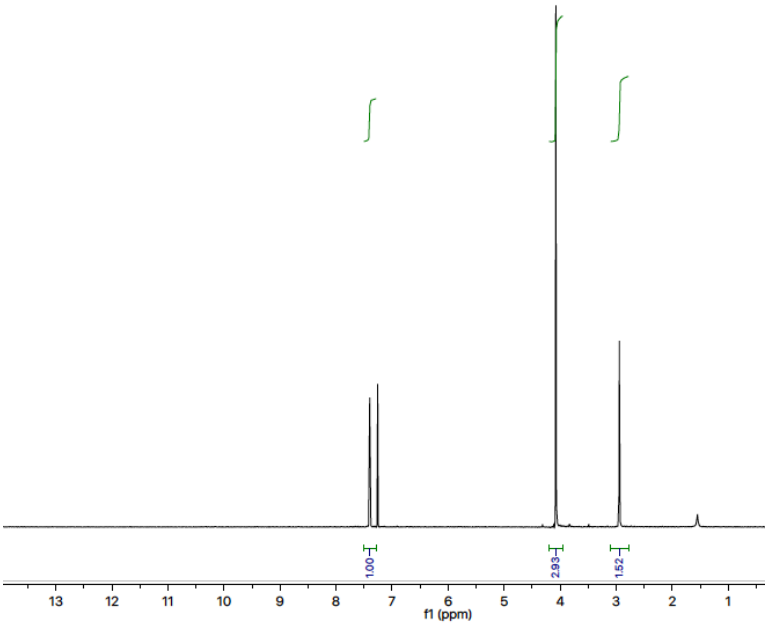

4.5.2 2,3,6,7-Tetramethoxyanthracene-9,10-dione, 3[10]

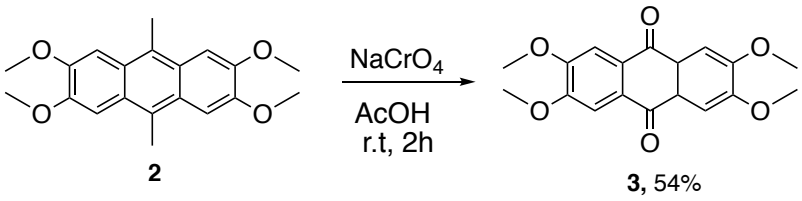

2,3,6,7-Tetramethoxy-9,10-dimethylanthracene, 2 (29 g, 89 mmol), and sodium chromate (79.2 g, 489 mmol) were dissolved in acetic acid (807 mL) and the mixture was stirred for 2 h. The solution was cooled to 0°C, filtered and washed with cold methanol to afford the product 3 as a yellow solid (15g, 53 %). ^{1}H NMR (300 MHz, $CDCl_3$): δ 4.06 (s, 12H, Ar-OCH_3), 7.68 (s, 4H, Ar-H). Spectral data matches with reference 10.

[1]H NMR of 2,3,6,7-tetramethoxyanthracene-9,10-dione, ***3***

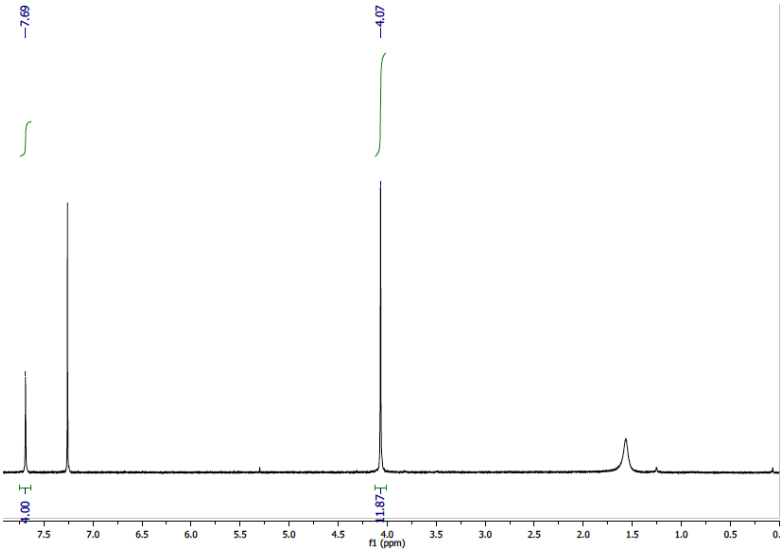

4.5.3 2,3,6,7-tetrahydroxy anthracene-9,10-dione, 4[10]

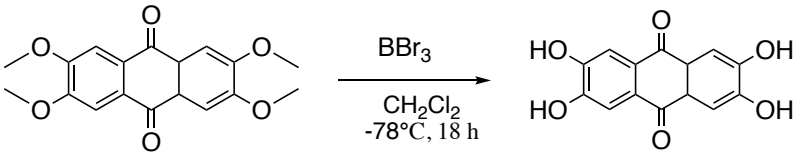

3 **4,** 63%

2,3,6,7-Tetramethoxy-9,10-dimethylanthracene, 3 (2.0 g, 6.0 mmol) was dissolved in 61 mL of dry dichloromethane and the solution was cooled to -78°C in a dry ice/isopropanol bath. Boron tribromide (17 mL of a 1 M solution in dichloromethane, 17 mmol) was added to the solution. The reaction mixture was allowed to warm to room temperature and stirred for 90 min. Ice-cold water (25 mL) was added and the reaction mixture was stirred for another 40 min. The mixture was filtered to afford 4 as a brown solid that was used immediately without further purification. ^{1}H NMR (300MHz,

DMSO-d_6): δ 7.3 (s, 4H, Ar-H), δ 2.7 (s, 6H, Ar-CH_3), δ 9.3 (s, 4H, Ar-OH). Spectral data matches reference 10.

^{1}H NMR of 2,3,6,7-tetrahydroxy anthracene-9,10-dione, ***4***

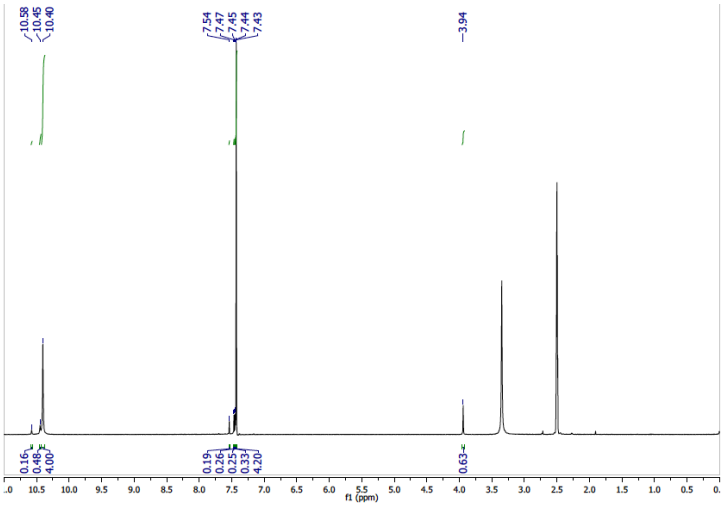

4.5.4 Synthesis of 2,3,6,7-tetraoctyloxyanthracene-9,10-dione, 5[10]

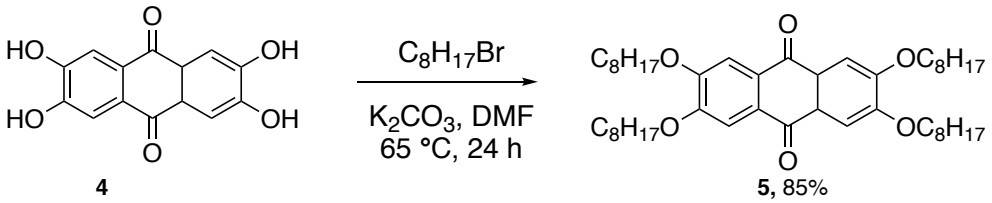

A mixture of crude 2,3,6,7-tetrahydroxy-9,10-anthracenedione, 4 (8.0g, 29 mmol), 1-bromooctane (38mL, 0.19 mol) and anhydrous potassium carbonate (29 g, 0.20 mol) in dimethyl formamide (250 mL) was stirred at room temperature for 90 min and then heated to 60°C for 24 h. Distilled water (250 mL) was added to the reaction mixture

and the solution was cooled to 0˚C. The precipitate was collected by filtration and washed with 50% methanol/water (300 mL) to afford 5 as a dark brown solid (18 g, 85% yield). ^{1}H-NMR (300 MHz, $CDCl_3$) 300 MHz: δ 7.63 (s, 4H, Ar-H), δ 4.1 (t, J = 6 Hz, 8H, Ar-OCH_2), δ 1.9(t, J = 6 Hz, 8H, Ar-OCH_2CH_2), δ 1.3-1.5(m, 40H), δ 0.9 (t, J = 6 Hz, 12H, -CH_3).

^{1}H NMR of 2,3,6,7-tetraoctyloxyanthracene-9,10-dione, ***5***

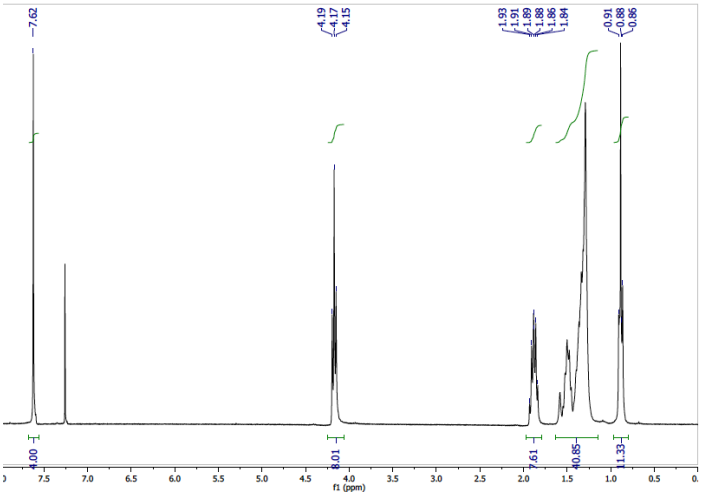

4.5.5 Synthesis of 2,3,6,7-tetraoctyloxyanthrone, 6[10]

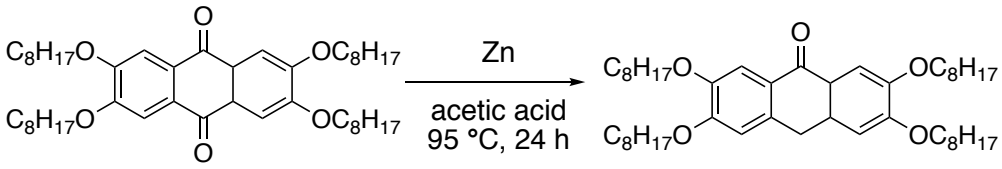

5 **6**

A mixture of 2,3,6,7-tetraoctyloxy-9,10-anthraquinone (0.5 g, 0.7 mmol) and zinc (1.15 g, 17.6 mmol) in acetic acid (30.0 mL) was heated to 95°C for 24 h. Deionized water (30.0 mL) was added and the resulting precipitate was collected by filtration and dried to afford 6 as off white powder (411 mg, 83% yield).

^{1}H NMR (300 MHz, $CDCl_3$): δ 7.80 (s, 2H, Ar-$H_{4,5}$), 6.80 (s, 2H, Ar-$H_{1,8}$), 4.11 (t, *J*= 6Hz, 8H, Ar-OCH_2), 4.14 (s, 2H, Ar-CH_2), 1.85 (p, *J* = 6 Hz, 8H, β-CH_2), 1.5-1.2 (m, 40 H), 0.95 (t, *J* = 6 Hz, 12 H, -CH_3).

^{1}H NMR of 2,3,6,7-tetraoctyloxyanthrone, ***6***

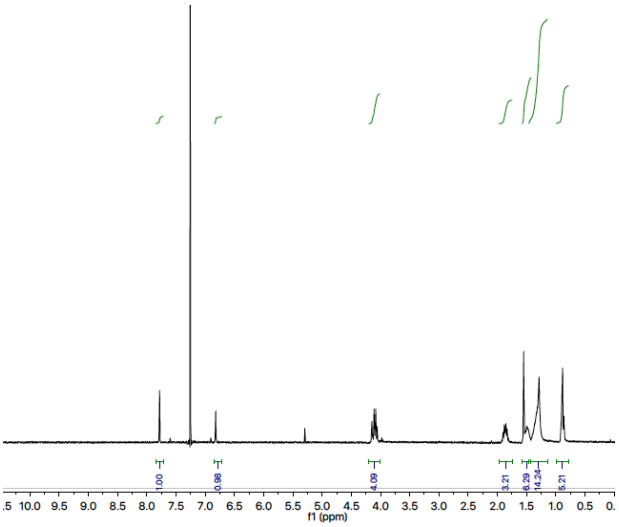

4.5.6 Synthesis of 2,3,6,7- tetraoctyloxyanthracene, 7

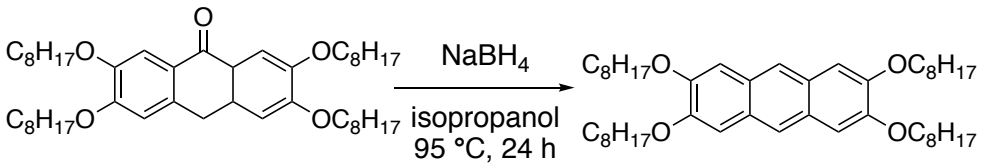

6 **7**

2,3,6,7-Tetraoctyloxy anthrone, 7 (2.0 g, 2.9 mmol), and $NaBH_4$ (0.75 g, 20 mmol) was added to isopropanol (58 mL) and the reaction mixture was refluxed for 24 h under argon. Additional $NaBH_4$ (0.20 g) was added after 2.5 h, followed by an additional 0.35 g aliquat after 12 h to drive the reaction to full conversion. The reaction mixture was poured into 10% hydrogen chloride (60 mL). The resulting precipitate was filtered to isolate 7 as an off-white powder (1.40 g, 72% yield).

^{1}H NMR (300MHz, $CDCl_3$): δ 7.96 (s, 2H, Ar-$H_{9,10}$), 7.10 (s, 4H, Ar-$H_{1,4,5,8}$), 4.10 (t, J = 6 Hz, 8H, Ar-OCH_2), 1.90 (p, J= 6Hz, 8H, β-CH_2), 1.60-1.20 (m, 40 H), 0.90 (t, J = 6Hz, 12 H, -CH_3).

^{1}H NMR of 2,3,6,7-tetraoctyloxyanthracene, 7

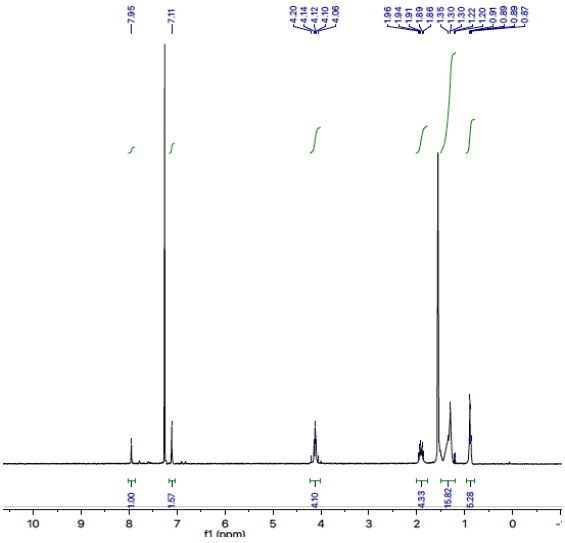

4.5.7 2,3,6,7-Tetraoctyloxy-9,10-dibromoanthracene, 8

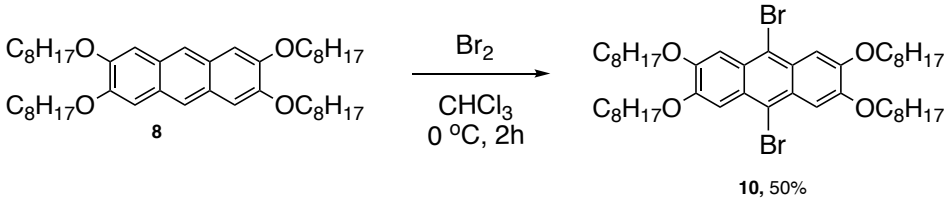

2,3,6,7-Tetraoctyloxyanthracene (0.5 g, 0.7 mmol) and molecular bromine (0.082 mL, 1.6 mmol) were added in chloroform (8 mL) and the mixture was stirred at 0°C for 2 h under air. The solvent was removed under reduced pressure to obtain a green solid. The solid was recrystallized from ethanol to afford 10 as a yellow powder (0.30 g, 50% yield). ^{1}H NMR (300 MHz, $CDCl_3$): δ 7.66 (s, 4H, Ar-$H_{1,4,5,8}$), 4.20 (t, J = 6Hz, 8H, Ar-OCH_2), 1.90 (p, J = 6 Hz, 4H, β-CH_2), 1.40-1.20 (m, 40H), 0.80 (t, J = 6Hz, 12H, -CH_3)

^{1}H NMR of 2,3,6,7-tetraoctyloxy-9,10-dibromoanthracene, ***8***

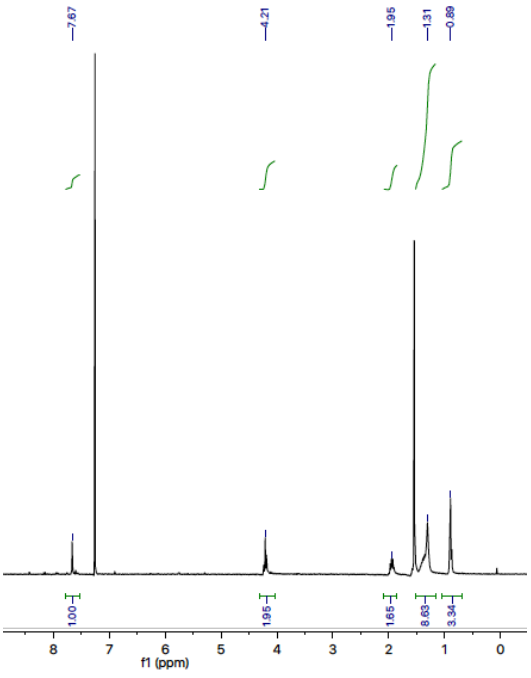

4.5.8 2,3,6,7-Tetrahydroxy-9,10-dimethylanthracene, 10[10]

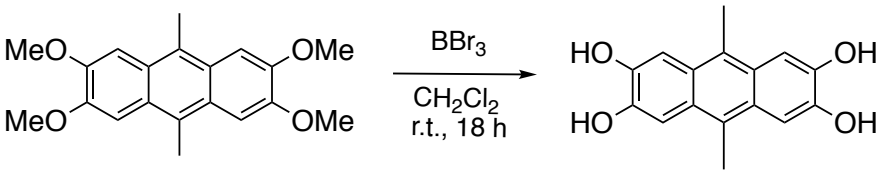

2 **10**, 52 %

2,3,6,7-Tetramethoxy-9,10-dimethylanthracene, 2 (15 g, 45 mmol), was dissolved in a minimum volume of 48% HBr (220 mL) and the solution was heated at reflux for 3 d. After every 8-12 h additional 48% HBr solution (50 mL) was added. After 3 d, the reaction mixture was cooled to room temperature and poured into ice cold water. The resulting suspension was filtered using a fritted funnel. The collected brown solid, was washed with water (300 mL) to remove any traces of HBr to afford 10 as a light brown solid (8.0 g, 52% yield). The product was immediately used in the next step without further purification. ^{1}H-NMR (300 MHz, DMSO-d_6): δ 7.45 (s, 4H, Ar-H), δ 10.42 (s, 4H, Ar-OH)

^{1}H NMR of 2,3,6,7-tetrahydroxy-9,10-dimethylanthracene, ***10***

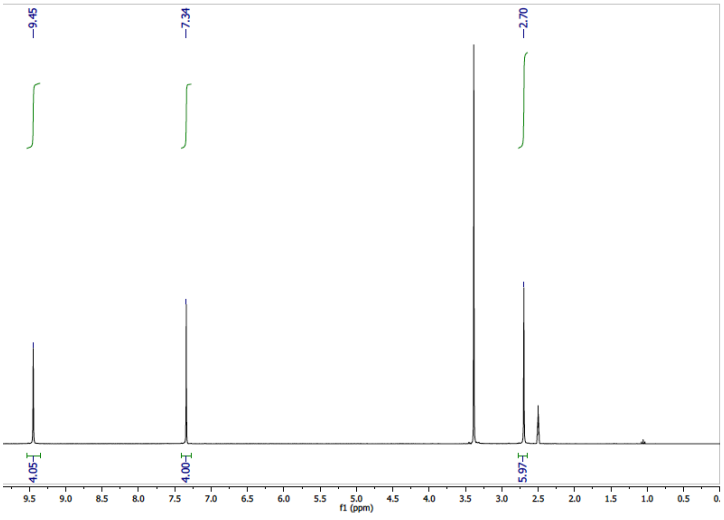

4.5.9 2,3,6,7-Tetraoctyloxy-9,10-dimethylanthracene, 11[10]

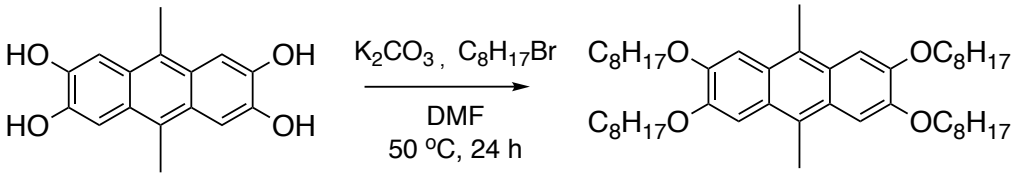

10 **11**, 34 %

2,3,6,7-Tetrahydroxy-(9,10-dimethylanthracene), 10 (1.6 g, 6.0 mmol), was dissolved in 52 mL DMF containing potassium carbonate (6.0 g, 43 mmol) and 1-bromooctane (7.0 mL ,41 mmol) under argon. The mixture was stirred for 90 min and then slowly heated to 60°C for 24 h. Distilled water (30 mL) was added and the mixture was cooled to 0°C and filtered to afford 11 as a brown product (1.5g, 34%). ^{1}H NMR (300MHz, $CDCl_3$): δ 7.4 (s, 4H, Ar-H), δ 4.1 (t, *J* = 6Hz, 8H, Ar-OCH_2), δ 2.9 (s, 6H, Ar-CH_3), δ 1.9 (t, *J* = 6Hz, 8H, Ar-β-CH_2), δ 1.3-1.5(m, 40H), δ 0.9(t, *J*= 6Hz, 12H, -CH_3)

^{1}H NMR of 2,3,6,7-tetraoctyloxy-9,10-dimethyl anthracene, ***11***

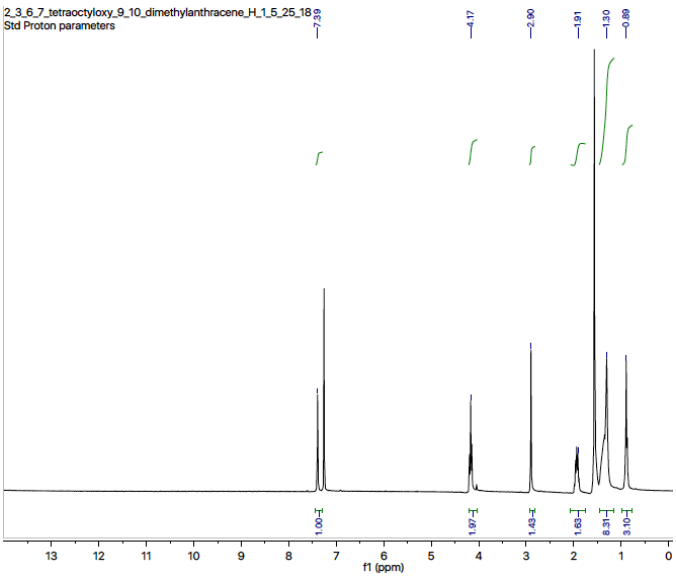

4.5.10 2,3,6,7- Tetramethoxy-9,10-bis(bromomethyl) anthracene, 12

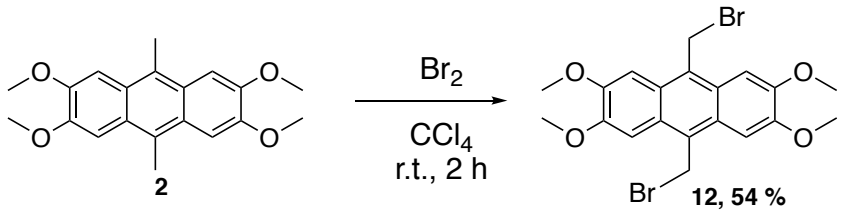

2,3,6,7-Tetramethoxy-9,10-dimethylanthracene (800 mg, 2.4mmol), 2 and bromine (Br_2) (5.8 mmol) were dissolved in CCl_4 (30 mL). The solution was irradiated for 4-5 h under 300W UV lamp. After 5 h, the solution was poured in methanol and a green solid precipitated. The solid was filtered to afford the product as light green powder (200 mg, 17%) which was recrystallized from a 2:3 mixture of chloroform and methanol to afford 12 as a green powder (0.6 g, 50% yield). ^{1}H NMR (300 MHz, $CDCl_3$): δ 7.55 (s, 4H, Ar-H), 5.28 (s, 4H, Ar-CH_2Br), 4.1 (s, 12H, Ar-OCH_3).

^{1}H NMR of 2,3,6,7-tetramethoxy-9,10-bis(bromomethyl)anthracene, ***12***

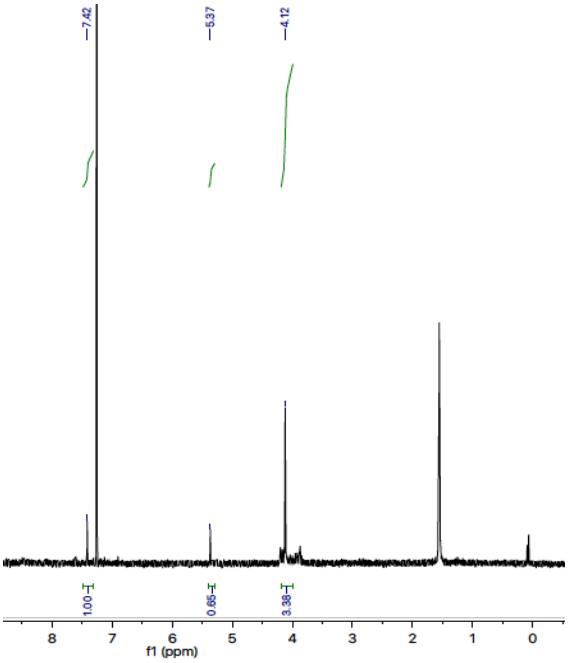

4.5.11 2,3,6,7- Tetraoctyloxy-9,10-bisbromomethyl anthracene, 14[11]

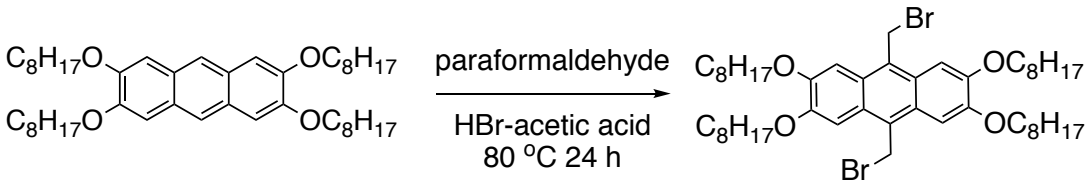

2,3,6,7- Tetraoctlyoxyanthracene (0.3 g, 0.4 mmol), paraformaldehyde (46 mg, 1.5 mmol), and hydrobromic acid (HBr) (0.4 mL) was added to acetic acid (8 mL) and the reaction mixture was refluxed for 24 h at 80 °C . Water (15 mL) was added to the reaction mixture. The resulting precipitate was collected by filtration to afford the crude product. The crude product was recrystallized from chloroform to give a grrenish-yellow product (0.19 g, 50% yield). [1] H-NMR (300 MHz, $CDCl_3$): δ 7.68 (s, 4H, Ar-H), 5.31 (s, 4H, -CH_2Br), 4.21 (t, *J* = 6Hz, 8H, -OCH_2), 1.95 (p, *J* = 6Hz, 8H, Ar-β-CH_2), 1.6-1.3 (m, 40 H), 1.02(t, *J* = 6Hz, -CH_3).

[1]H NMR of 2,3,6,7- Tetraoctyloxy-9,10-bisbromomethyl anthracene

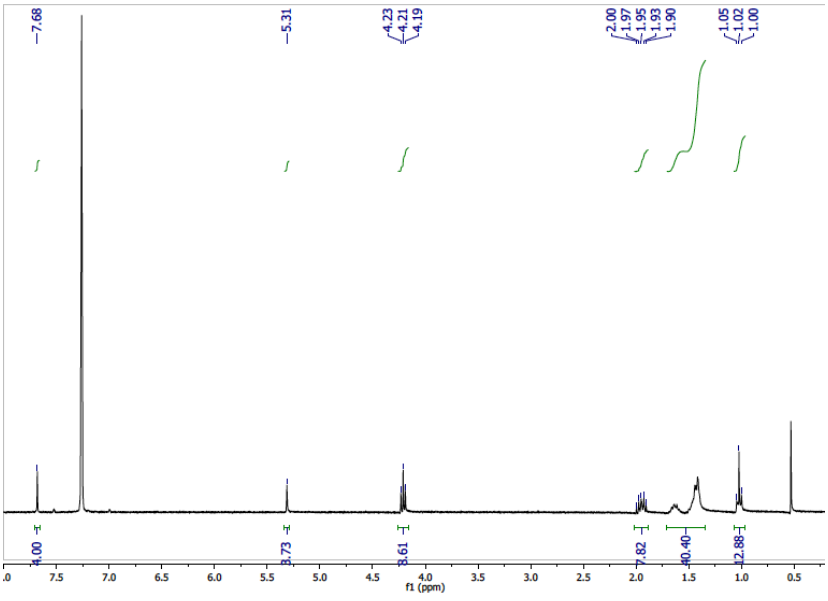

4.6 REFERENCES

1. Junkers, T.; Vandenbergh, J.; Adriaensens, P.; Lutsen, L.; Vanderzande, D., Synthesis of poly (p-phenylene vinylene) materials via the precursor routes. *Polymer Chemistry* **2012,** *3* (2), 275-285.

2. Brabec, C. J.; Sariciftci, N. S.; Hummelen, J. C., Plastic solar cells. *Advanced Functional Materials* **2001,** *11* (1), 15-26.

3. Burrezo, P. M.; Zafra, J. L.; López Navarrete, J. T.; Casado, J., Quinoidal/Aromatic Transformations in π-Conjugated Oligomers: Vibrational Raman studies on the Limits of Rupture for π-Bonds. *Angewandte Chemie International Edition* **2017,** *56* (9), 2250-2259.

4. Brédas, J., Relationship between band gap and bond length alternation in organic conjugated polymers. *The Journal of Chemical Physics* **1985,** *82* (8), 3808-3811.

5. Marrocchi, A.; Silvestri, F.; Seri, M.; Facchetti, A.; Taticchi, A.; Marks, T. J., Conjugated anthracene derivatives as donor materials for bulk heterojunction solar cells: olefinic versus acetylenic spacers. *Chemical Communications* **2009,** (11), 1380-1382.

6. Swager, T. M.; Gil, C. J.; Wrighton, M. S., Fluorescence studies of poly (p-phenyleneethynylene) s: the effect of anthracene substitution. *The Journal of Physical Chemistry* **1995,** *99* (14), 4886-4893.

7. Scherf, U.; Müllen, K., Design and synthesis of extended π-systems: monomers, oligomers, polymers. *Synthesis* **1992,** *1992* (01/02), 23-38.

8. Reich, H. J., Role of organolithium aggregates and mixed aggregates in organolithium mechanisms. *Chemical Reviews* **2013,** *113* (9), 7130-7178.

9. Kulangiappar, K.; Anbu Kulandainathan, M.; Raju, T., Conversion of benzylic bromides to benzaldehydes using sodium nitrate as an oxidant. *Industrial & Engineering Chemistry Research* **2010,** *49* (14), 6670-6673.

10. Balaban T.S., Eichhöfer A., Krische M.J., Lehn J.M., Hierarchic Supramolecular Interactions within Assemblies in Solution and in the Crystal of 2,3,6,7-Tetrasubstituted 5,5'-(Anthracene-9,10-diyl)bis[pyrimidin-2-amines]. Helvetica Chimica Acta **2006**, *89*, 333-351.

11. Zhang C.H., Guo E.Q., Zhang Y.L., Ren H.P., Yang J.W., Donor-Acceptor-Substituted Anthracene-Centered Cruciforms: Synthesis, Enhanced Two-Photon Absorptions, and Spatially Separated Frontier Molecular Orbitals. *Chemistry of Materials* **2009**, *21*, 5125-5135.

CHAPTER 5. CONCLUSION AND FUTURE PERSPECTIVE

5.1 CONCLUSIONS

In this thesis, I have demonstrated the potential of anthracene as a building block in developing low band gap conjugated polymer. The comparative study of the homologous series of phenylene, naphthalene and anthracene containing conjugated polymers in Chapter 2 clearly demonstrated that the fusion a second benzene ring in case of anthracene clearly significantly reduces the band gap of the polymer. Raman spectra indicate more double bond character to the ethynylene linkages in the anthracene containing polymers compared to those containing phenylene and naphthalene.

In Chapter 3, the anthracene, naphthalene monomers were polymerized with naphthalene diimide acceptor. The anthracene containing donor-acceptor polymer **NDIA** by virtue of having two fused benzene rings did significantly destabilize the HOMO of the polymer compared to the phenylene and naphthalene containing polymers **NDIP** and **NDIN** respectively. The naphthalene despite having fused benzene ring was not a better donor than phenylene. The preliminary calculations indicate that the naphthalene HOMO does have node at the carbons fusing the two benzene rings, thus leaving the peripheral π-electrons out of main conjugation along the backbone. The polymers were weakly ordered in solid state as observed from XRD and DSC results.

5.2 FUTURE PERSPECTIVES

The reasons for low absorptivity of charge transfer type transition in **NDIN** can further be theoretically investigated by computing the spatial overlap of ground state and excited states of the polymer. The band gap of anthracene containing donor-acceptor polymer ,**NDIA** is promising for photovoltaic application. The polymer can be blended with electron rich polymers such as polythiophenes to develop polymer/polymer solar cells. In polymer/polymer solar cells, fullerene is replaced with a conjugated polymer that can accept electrons by virtue of having low electron affinity compared to the electron rich polymers. There are some advantages to this. The fullerens being small molecules tend to aggregate in the bulk hetrojunction layers, thus affecting the morphology. Polymer being large in size do not aggregate. Also the polymers can be tuned for optical band gap to enhance the overall light absorption.[1]

An interesting avenue forward is to copolymerize 9,10-diethynyl anthracene with comonomers which also are known to stabilize the quinoidal form in polymers such as thieno[3,4-*b*]pyrazine,[2] thieno[3,4-*b*]thiophene,[2] thienothiadiazoles.[2-3]

Solid-state order is important that would facilitating intramolecular and intermolecular charge transport which is required for performance of organic semiconductors in devices. The orientation of conjugated polymers can be influenced by for example by thermal annealing, blade coating, use of nematic liquid crystalline media,[4] and controlled deposition of polymer from air-water interface.[5] The polymers reported here did not respond well to thermal and blade coating treatments. In this case an alternative is to consider development of amphiphilic anthracene containing poly(arylene-co-phenylene ethynylene)s, that bears hydrophobic and hydrophilic side

chains to assist the self-assembly of polymers at air-water interface and in lyotropic liquid crystals. Such an approach to develop ordered materials would build on studies of poly(phenylene ethynylene)s bearing hydrophobicand hydrophilic side chains at the air-water interface and lyotropic liquid crystals in which polymers adopt a planar conformation in both the environments.[4] This would be advantageous in obtaining face on orientation of polymers deposited from these media on to a solid substrate.

5.3 REFERENCES

1. Nam, S.; Hahm, S. G.; Han, H.; Seo, J.; Kim, C.; Kim, H.; Marder, S. R.; Ree, M.; Kim, Y., All-polymer solar cells with bulk heterojunction films containing electron-accepting triple bond-conjugated perylene diimide polymer. *ACS Sustainable Chemistry & Engineering* **2015,** *4* (3), 767-774.
2. Roncali, J., Molecular engineering of the band gap of π-conjugated systems: Facing technological applications. *Macromolecular Rapid Communications* **2007,** *28* (17), 1761-1775.
3. Bérubé, N.; Gaudreau, J.; Côté, M., Low band gap polymers design approach based on a mix of aromatic and quinoid structures. *Macromolecules* **2013,** *46* (17), 6873-6880.
4. Bouffard, J.; Swager, T. M., Self-assembly of amphiphilic poly (phenylene ethynylene) s in water–potassium dodecanoate–decanol lyotropic liquid crystals. *Chemical Communications* **2008,** (42), 5387-5389.
5. Kim, J.; Swager, T., Control of conformational and interpolymer effects in conjugated polymers. *Nature* **2001,** *411* (6841), 1030.

APPENDIX

Crystal Data of 2,6-(di-(2-ethylhexyl)-9,10-ditrimethylsilyl) anthracene

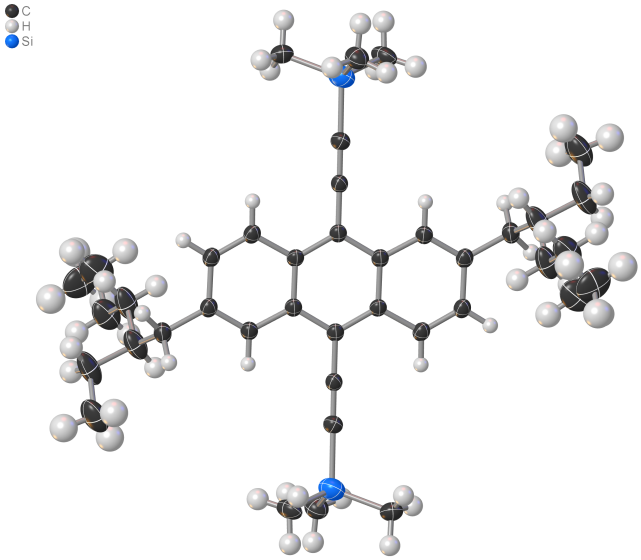

Experimental. Single yellow needle-shaped crystals of **CK-01** were The crystal was chosen from the sample as supplied.. A suitable crystal 0.42×0.12×0.10 mm^3 was selected and mounted on a loop with paratone oil on an XtaLAB Synergy, Dualflex, HyPix diffractometer. The crystal was cooled to T = 99.99(10) K during data collection. The structure was solved with the **ShelXT** (Sheldrick, 2015) structure solution program using the Intrinsic Phasing solution method and by using **Olex2** (Dolomanov et al., 2009) as the graphical interface. The model was refined with version 2017/1 of **ShelXL-2014** (Sheldrick, 2015) using Least Squares minimisation.

Crystal Data. $C_{20}H_{29}Si$, M_r = 297.52, triclinic, P-1 (No. 2), a = 6.3927(6) Å, b = 11.2788(10) Å, c = 13.4718(9) Å, α = 84.705(7)°, β = 88.106(6)°, γ = 84.170(7)°, V = 961.92(14) $Å^3$, T = 99.99(10) K, Z = 2, Z' = 1, $\mu(CuK_\alpha)$ = 0.995 mm^{-1}, 7453 reflections measured, 2726 unique (R_{int} = 0.0409) which were used in all calculations. The final wR_2 was 0.3796 (all data) and R_1 was 0.1211 (I > 2σ(I)).

Compound	**CK-01**
Formula	$C_{20}H_{29}Si$
$D_{calc.}$/ g cm^{-3}	1.027
μ/mm^{-1}	0.995
Formula Weight	297.52
Colour	yellow
Shape	needle
Size/mm^3	0.42×0.12×0.10
T/K	99.99(10)
Crystal System	triclinic
Space Group	P-1
a/Å	6.3927(6)
b/Å	11.2788(10)
c/Å	13.4718(9)
α/°	84.705(7)
β/°	88.106(6)
γ/°	84.170(7)
V/Å^3	961.92(14)
Z	2
Z'	1
Wavelength/Å	1.54184
Radiation type	CuK$_\alpha$
Θ_{min}/°	3.296
Θ_{max}/°	58.897
Measured Refl.	7453
Independent Refl.	2726
Reflections with I	>2172
R_{int}	0.0409
Parameters	195
Restraints	141
Largest Peak	0.874
Deepest Hole	-0.692
GooF	1.638
wR_2 (all data)	0.3796
wR_2	0.3620
R_1 (all data)	0.1360
R_1	0.1211

Table A.1. Structure Quality Indicators

Reflections:	d min (Cu) 0.90	I/σ 14.8	Rint 4.09%	complete at 2θ=118° 99%
Refinement:	Shift 0.000	Max Peak 0.9	Min Peak -0.7	GooF 1.638

A yellow needle-shaped crystal with dimensions 0.42×0.12×0.10 mm^3 was mounted on a loop with paratone oil.

Data were collected using an XtaLAB Synergy, Dualflex, HyPix diffractometer equipped with an Oxford Cryosystems low-temperature device, operating at *T* = 99.99(10) K.

Data were measured using ω scans of 1/2° per frame for s using CuK_α radiation (micro-focus sealed X-ray tube, 50 kV, 1.0 mA). The total number of runs and images was based on the strategy calculation from the program **CrysAlisPro** (Rigaku, V1.171.39.33a, 2017). The maximum resolution that was achieved was Θ = 58.897°.

The diffraction patterns were indexed using **CrysAlisPro** (Rigaku, V1.171.39.33a, 2017) and the unit cells were refined using **CrysAlisPro** (Rigaku, V1.171.39.33a, 2017) on 2671 reflections, 36 % of the observed reflections.

Data reduction, scaling and absorption corrections were performed using **CrysAlisPro** (Rigaku, V1.171.39.33a, 2017) and CrysAlisPro 1.171.39.33a (Rigaku Oxford Diffraction, 2017). A numerical absorption correction based on Gaussian integration over a multifaceted crystal model was applied. An empirical absorption correction using spherical harmonics, implemented in SCALE3 ABSPACK scaling algorithm was also applied. The final completeness is 99% out to 58.897° in Θ. The absorption coefficient μ of this material is 0.995 mm^{-1} at this wavelength (λ = 1.54184Å) and the minimum and maximum transmissions are 0.361 and 1.000.

The structure was solved and the space group *P*-1 (# 2) determined by the **ShelXT** (Sheldrick, 2015) structure solution program using Intrinsic Phasing and refined by Least Squares using version 2017/1 of **ShelXL-2014** (Sheldrick, 2015). All non-hydrogen atoms were refined anisotropically. Hydrogen atom positions were calculated geometrically and refined using the riding model.

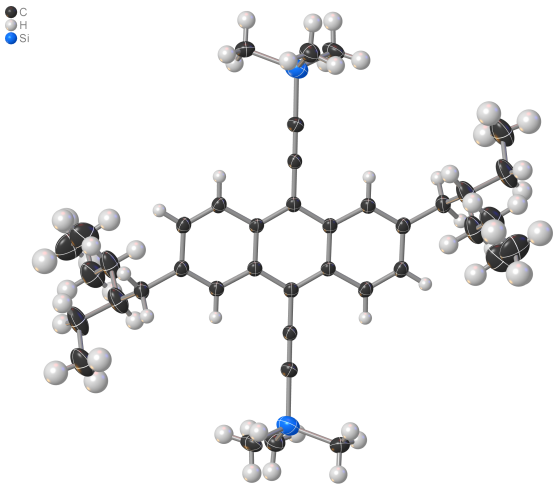

Table A.1. Data Plots: Diffraction Data

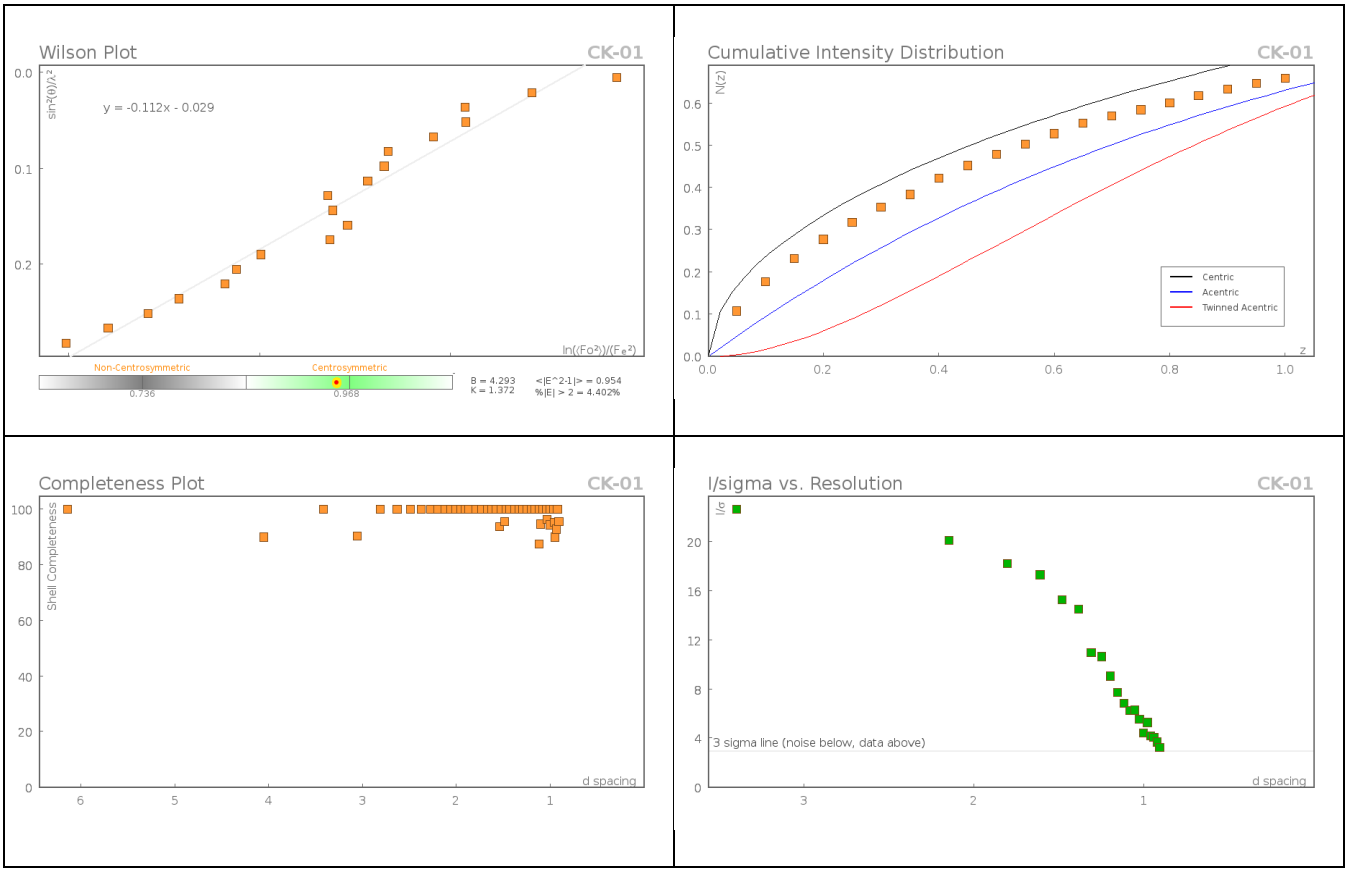

Table A.2. Data Plots: Refinement and Data

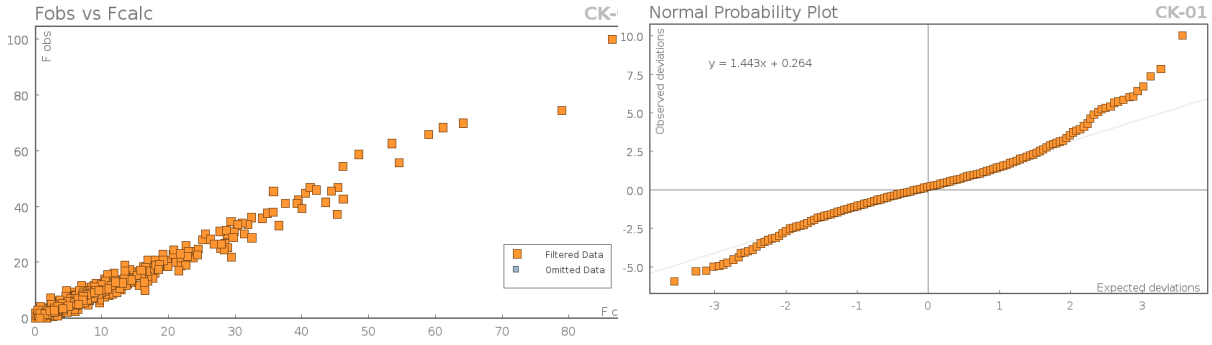

Table A.3. Reflection Statistics

Total reflections (after filtering)	7453	Unique reflections	2726
Completeness	0.99	Mean I/σ	14.75
hkl_{max} collected	(7, 12, 14)	hkl_{min} collected	(-7, -12, -10)
hkl_{max} used	(7, 12, 14)	hkl_{min} used	(-7, -12, 0)
Lim d_{max} collected	100.0	Lim d_{min} collected	0.77
d_{max} used	13.41	d_{min} used	0.9
Friedel pairs	691	Friedel pairs merged	1
Inconsistent equivalents	6	R_{int}	0.0409
R_{sigma}	0.0416	Intensity transformed	0
Omitted reflections	0	Omitted by user (OMIT hkl)	0
Multiplicity	(1260, 1153, 529, 236, 141, 54,	Maximum multiplicity	12
Removed systematic absences	0	Filtered off (Shel/OMIT)	0

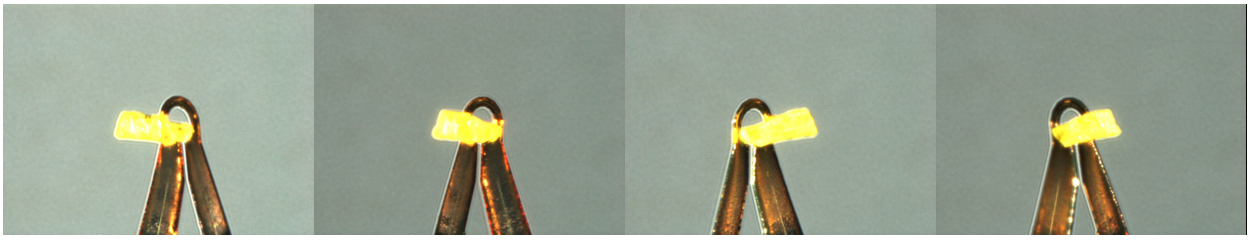

Figure A.1. Images of the Crystal on the Diffractometer

Table A.4.: Fractional Atomic Coordinates ($\times 10^4$) and Equivalent Isotropic Displacement Parameters ($Å^2 \times 10^3$) for **CK-01**.

U_{eq} is defined as 1/3 of the trace of the orthogonalised U_{ij}.

Atom	x	y	z	U_{eq}
Si1	11577(2)	9685.3(13)	-2046.5(11)	58.7(7)
C5	13725(7)	5198(4)	-1203(3)	45.6(11)
C4	11842(7)	5119(4)	-611(3)	43.6(10)
C3	10349(7)	6120(4)	-517(3)	42.7(10)
C7	5188(7)	6874(4)	746(4)	48.4(11)
C6	4801(8)	5750(4)	1282(4)	48.6(11)
C17	8516(7)	5997(4)	79(3)	43.2(10)
C2	10692(7)	7244(4)	-1039(3)	45.4(11)
C8	6920(7)	6986(4)	167(4)	46.5(11)
C1	11020(8)	8210(5)	-1455(4)	55.4(12)
C9	2794(8)	5642(5)	1891(4)	56.0(11)
C18	10064(10)	10859(5)	-1359(4)	70.4(13)
C19	14430(9)	9784(6)	-1946(5)	78.3(15)
C20	10682(10)	9854(6)	-3357(4)	75.1(13)
C10	2915(10)	5735(7)	3005(5)	90.5(14)
C12	4277(15)	6876(7)	4383(4)	112(2)
C11	3820(12)	6842(7)	3289(4)	101.4(19)
C15	773(10)	5657(8)	3511(5)	107.2(19)
C16	-75(15)	4461(8)	3476(7)	129(3)
C13	5077(17)	8041(8)	4589(5)	133(3)
C14	5715(18)	8038(9)	5659(5)	139(4)

Table A.5.: Anisotropic Displacement Parameters ($\times 10^4$) **CK-01**. The anisotropic displacement factor exponent takes the form: $-2\pi^2[h^2a^{*2} \times U_{11} + ... + 2hka^* \times b^* \times U_{12}]$

Atom	U_{11}	U_{22}	U_{33}	U_{23}	U_{13}	U_{12}
Si1	52.4(10)	53.4(10)	69.8(11)	4.4(7)	3.6(7)	-14.3(7)
C5	41.7(17)	44(2)	53(3)	-10.6(18)	2.8(15)	-8.2(14)
C4	40.6(16)	42.0(13)	51(2)	-12.6(13)	1.2(14)	-8.8(11)
C3	40.2(15)	41.3(12)	49(2)	-12.8(11)	0.3(13)	-9.5(9)
C7	44.6(17)	45.3(17)	57(2)	-14.4(15)	2.4(15)	-4.5(12)
C6	46.1(19)	46.1(18)	55(2)	-14.4(15)	3.3(15)	-5.6(14)
C17	40.8(15)	37.9(16)	53(2)	-11.2(13)	2.0(13)	-8.3(11)
C2	41(2)	42.8(12)	54(2)	-10.5(12)	5.6(17)	-7.7(10)
C8	43.4(16)	42.9(17)	55(2)	-12.7(14)	0.4(14)	-4.1(12)
C1	50(2)	47.6(11)	68(2)	-3.3(13)	6.4(19)	-10.6(13)
C9	51.5(19)	59(2)	58.4(17)	-12.5(15)	9.4(13)	-4.9(16)
C18	76(3)	49.3(15)	86(2)	-2(2)	6(2)	-13.2(19)
C19	54.2(12)	77(3)	101(3)	22(3)	-1.2(15)	-21.6(14)
C20	73(3)	79(3)	70.3(14)	6.4(14)	-0.8(15)	-9(3)
C10	80(2)	140(4)	60.8(17)	-30.4(17)	15.0(14)	-39(2)

Atom	U_{11}	U_{22}	U_{33}	U_{23}	U_{13}	U_{12}
C12	127(6)	143(5)	79(2)	-45(3)	14(3)	-53(4)
C11	84(3)	153(4)	79(2)	-54(3)	21(2)	-42(3)
C15	89(3)	177(5)	68(3)	-44(3)	26(2)	-53(3)
C16	90(4)	175(5)	132(7)	-32(4)	27(5)	-56(4)
C13	158(8)	150(5)	108(3)	-49(3)	-14(4)	-60(5)
C14	197(10)	116(6)	115(4)	-58(4)	-32(5)	-19(5)

Table A.6.: Bond Lengths in Å for **CK-01**.

Atom	Atom	Length/Å
Si1	C1	1.841(5)
Si1	C18	1.858(6)
Si1	C19	1.848(6)
Si1	C20	1.862(6)
C5	C4	1.427(6)
C5	C6[1]	1.361(7)
C4	C3	1.415(6)
C4	C17[1]	1.424(6)
C3	C17	1.410(6)
C3	C2	1.425(6)
C7	C6	1.440(7)
C7	C8	1.343(6)
C6	C9	1.509(6)
C17	C8	1.444(6)
C2	C1	1.213(7)
C9	C10	1.519(8)
C10	C11	1.513(4)
C10	C15	1.517(4)
C12	C11	1.516(5)
C12	C13	1.510(3)
C15	C16	1.509(3)
C13	C14	1.510(3)

——[1]2-x,1-y,-z

TableA.7: Bond Angles in ° for **CK-01**.

Atom	Atom	Atom	Angle/°
C1	Si1	C18	108.5(2)
C1	Si1	C19	107.2(3)
C1	Si1	C20	109.4(3)
C18	Si1	C20	108.3(3)
C19	Si1	C18	110.1(3)
C19	Si1	C20	113.2(3)

Atom	Atom	Atom	Angle/°
C6[1]	C5	C4	122.7(4)
C3	C4	C5	122.0(4)
C3	C4	C17[1]	119.1(4)
C17[1]	C4	C5	118.9(4)
C4	C3	C2	119.8(4)
C17	C3	C4	119.9(4)
C17	C3	C2	120.3(4)
C8	C7	C6	121.5(4)
C5[1]	C6	C7	117.8(4)
C5[1]	C6	C9	122.0(4)
C7	C6	C9	120.1(4)
C4[1]	C17	C8	117.4(4)
C3	C17	C4[1]	121.0(4)
C3	C17	C8	121.6(4)
C1	C2	C3	177.8(5)
C7	C8	C17	121.6(4)
C2	C1	Si1	177.8(5)
C6	C9	C10	116.8(4)
C11	C10	C9	115.1(5)
C11	C10	C15	109.0(5)
C15	C10	C9	110.9(5)
C13	C12	C11	112.0(5)
C10	C11	C12	116.5(6)
C16	C15	C10	113.9(6)
C12	C13	C14	112.3(6)

———

[1]2-x,1-y,-

TableA.8.: Torsion Angles in ° for **CK-01**.

Atom	Atom	Atom	Atom	Angle/°
C5	C4	C3	C17	-179.8(4)
C5	C4	C3	C2	1.1(7)
C5[1]	C6	C9	C10	82.9(7)
C4	C3	C17	C4[1]	1.4(7)
C4	C3	C17	C8	-177.9(4)
C4[1]	C17	C8	C7	1.6(7)
C3	C17	C8	C7	-179.1(4)
C7	C6	C9	C10	-98.3(6)
C6[1]	C5	C4	C3	178.5(4)
C6[1]	C5	C4	C17[1]	0.0(7)
C6	C7	C8	C17	-2.1(7)
C6	C9	C10	C11	53.6(8)

Atom	Atom	Atom	Atom	Angle/°
C6	C9	C10	C15	177.9(5)
C17[1]	C4	C3	C17	-1.3(7)
C17[1]	C4	C3	C2	179.5(4)
C2	C3	C17	C4[1]	-179.5(4)
C2	C3	C17	C8	1.2(7)
C8	C7	C6	C5[1]	1.4(7)
C8	C7	C6	C9	-177.4(4)
C9	C10	C11	C12	-170.9(6)
C9	C10	C15	C16	65.3(9)
C11	C10	C15	C16	-167.0(7)
C11	C12	C13	C14	-175.0(8)
C15	C10	C11	C12	63.8(9)
C13	C12	C11	C10	-177.3(8)

[1]2-x,1-y,-z

Table A.8.: Hydrogen Fractional Atomic Coordinates ($\times 10^4$) and Equivalent Isotropic Displacement Parameters ($Å^2 \times 10^3$) for **CK-01**. U_{eq} is defined as 1/3 of the trace of the orthogonalised U_{ij}.

Atom	x	y	z	U_{eq}
H5	13958.42	5943.87	-1555.78	55
H7	4195.01	7551.53	802.9	58
H8	7100.39	7735.04	-192.89	56
H9A	2287.92	4860.95	1792.03	67
H9B	1721.71	6273.42	1619.75	67
H18A	8572.99	10901.08	-1520.36	106
H18B	10594.1	11634.14	-1554.98	106
H18C	10227.03	10660.72	-640.75	106
H19A	14822.79	9633.24	-1245.78	117
H19B	14766.5	10584.94	-2204.52	117
H19C	15211.91	9185.39	-2335.91	117
H20A	11331.03	9182.74	-3709.61	113
H20B	11096.61	10606.86	-3691.66	113
H20C	9148.19	9862.56	-3361.29	113
H10	3854.08	5027.46	3282.7	109
H12A	2975.92	6765.25	4785.13	134
H12B	5339.94	6205.35	4589.32	134
H11A	2825.91	7546.09	3084.03	122
H11B	5145.32	6927.61	2899.86	122
H15A	870.63	5819.54	4217.08	129
H15B	-235.4	6288.56	3188.04	129
H16A	839.42	3839.82	3851.49	193
H16B	-116.97	4274.54	2780.94	193
H16C	-1498.69	4493.31	3771.67	193
H13A	3964.04	8703.57	4438.68	159
H13B	6303.05	8186.23	4142.49	159
H14A	4484.65	7946.98	6102.32	208
H14B	6281.18	8795.06	5751.6	208
H14C	6793.08	7371.75	5816.4	208

REFERENCES

1. CrysAlisPro Software System, Rigaku Oxford Diffraction, (2017).
2. O.V. Dolomanov and L.J. Bourhis and R.J. Gildea and J.A.K. Howard and H. Puschmann, Olex2: A complete structure solution, refinement and analysis program, *J. Appl. Cryst.*, (2009), **42**, 339-341.
3. Sheldrick, G.M., Crystal structure refinement with ShelXL, *Acta Cryst.*, (2015), **C27**, 3-8.
4. Sheldrick, G.M., ShelXT-Integrated space-group and crystal-structure determination, *Acta Cryst.*, (2015), **A71**, 3-8.